Universität Potsdam

Institut für Chemie

Arbeitskreis Angewandte Polymerchemie

Prof. Dr. André Laschewsky

Thermoresponsive Polymers with Co-nonsolvency Behavior

M.Sc. Ing. Cristiane Henschel

Univ.-Diss.

zur Erlangung des akademischen Grades

"doctor rerum naturalium" (Dr. rer. nat.)

in der Wissenschaftsdisziplin "Polymerchemie"

eingereicht an der

Mathematisch-Naturwissenschaftlichen Fakultät

der Universität Potsdam

Tag und Ort der Disputation:

Potsdam, den 16. Dezember 2022

Abstract

Despite the popularity of thermoresponsive polymers, much is still unknown about their behavior, how it is triggered, and what factors influence it, hindering the full exploitation of their potential. One particularly puzzling phenomenon is called co-nonsolvency, in which a polymer is soluble in two individual solvents, but counter-intuitively becomes insoluble in mixtures of both. Despite the innumerous potential applications of such systems, including actuators, viscosity regulators and as carrier structures, this field has not yet been extensively studied apart from the classical example of poly(N-isopropyl acrylamide) (PNIPAM) in mixtures of water and methanol. Therefore, this thesis focuses on evaluating how changes in the chemical structure of the polymers impact the thermoresponsive, aggregation and co-nonsolvency behaviors of both homopolymers and amphiphilic block copolymers. Within this scope, both the synthesis of the polymers and their characterization in solution is investigated. Homopolymers were synthesized by conventional free radical polymerization, whereas block copolymers were synthesized by consecutive reversible addition fragmentation chain transfer (RAFT) polymerizations. The synthesis of the monomers N-isopropyl methacrylamide (NIPMAM) and N-vinyl isobutyramide (NVIBAM), as well as a few chain transfer agents is also covered. Through turbidimetry measurements, the thermoresponsive and co-nonsolvency behavior of PNIPMAM and PNVIBAM homopolymers is then compared to the well-known PNIPAM, in aqueous solutions with 9 different organic co-solvents. Additionally, the effects of end-groups, molar mass, and concentration are investigated. Despite the similarity of their chemical structures, the 3 homopolymers show significant differences in transition temperatures and some divergences in their co-nonsolvency behavior. More complex systems are also evaluated, namely amphiphilic di- and triblock copolymers of PNIPAM and PNIPMAM with polystyrene and poly(methyl methacrylate) hydrophobic blocks. Dynamic light scattering is used to evaluate their aggregation behavior in aqueous and mixed aqueous solutions, and how it is affected by the chemical structure of the blocks, the chain architecture, presence of cosolvents and polymer concentration. The results obtained shed light into the thermoresponsive, co-nonsolvency and aggregation behavior of these polymers in solution, providing valuable information for the design of systems with a desired aggregation behavior, and that generate targeted responses to temperature and solvent mixture changes.

Zusammenfassung

Trotz der Popularität thermoresponsiver Polymere ist noch vieles über ihr Verhalten, sowie dessen Auslöser und Einflüsse darauf unbekannt, was die volle Nutzung ihres Potenzials behindert. Ein besonders ungewöhnliches Phänomen ist die so genannte Co-Nonsolvency, bei der ein Polymer in zwei reinen Lösungsmitteln löslich ist, aber in Mischungen aus beiden unlöslich wird. Trotz der zahlreichen potenziellen Anwendungen solcher Systeme, wie z.B. Aktuatoren, Viskositätsregulatoren und als Transportmedien, ist dieses Feld, abgesehen vom klassischen Beispiel von Poly(*N*-isopropylacrylamid) (PNIPAM) in Mischungen aus Wasser und Methanol, bisher nicht umfassend untersucht worden. Diese Arbeit untersucht daher, welche Auswirkungen die chemische Struktur der Polymere auf das thermoresponsive, Aggregations- und Co-Nonsolvency Verhalten sowohl von Homopolymeren als auch von amphiphilen Blockcopolymeren hat. Dazu wurden sowohl die Synthese der Polymere als auch deren Verhalten in Lösung untersucht. Die Homopolymere wurden durch konventionelle radikalische Polymerisation hergestellt, wogegen die Blockcopolymere durch konsekutive Reversible Addition Fragmentation Chain Transfer Polymerisationen (RAFT) synthetisiert wurden. Die Synthese der Monomere *N*-Isopropylmethacrylamid (NIPMAM) und *N*-Vinylisobutyramid (NVIBAM) sowie einiger Kettenüberträger wird ebenfalls beschrieben. Mittels Trübungs-Messungen wird das thermoresponsive und Co-Nonsolvency Verhalten von PNIPMAM- und PNVIBAM-Homopolymeren mit dem bekannten PNIPAM in wässrigen Lösungen mit 9 verschiedenen organischen Co-Lösungsmitteln verglichen. Außerdem werden die Auswirkungen der Endgruppen, der Molmasse und der Konzentration der Polymere diskutiert. Trotz der Ähnlichkeit ihrer chemischen Strukturen zeigen die drei Homopolymere signifikante Unterschiede bei den Übergangstemperaturen und einige Divergenzen in ihrem Co-Nonsolvency Verhalten. Es wurden auch komplexere Systeme untersucht, nämlich amphiphile Di- und Triblock-Copolymere von PNIPAM und PNIPMAM mit hydrophoben Blöcken aus Polystyrol und Polymethylmethacrylat. Mittels dynamischer Lichtstreuung wird ihr Aggregationsverhalten in wässrigen und gemischten wässrigen Lösungen bewertet und untersucht, wie es von der chemischen Struktur der Blöcke, der Kettenarchitektur, den Co-Lösungsmitteln und der Polymerkonzentration beeinflusst wird. Die Ergebnisse dokumentieren das thermoresponsive, Co-Nonsolvency und Aggregationsverhalten dieser Polymere in Lösung und liefern wertvolle Informationen für die Entwicklung von Systemen mit einem gewünschten Aggregationsverhalten, die gezielt auf Temperatur- und Lösungsmittelgemischänderungen reagieren.

List of Symbols & Abbreviations

A

A	Absorbance
AIBN	2,2′-Azobis(2-methylpropionitrile)
ATRP	Atom transfer radical polymerization

B

BHT	Butylated hydroxytoluene (2,6-Di-tert-butyl-4-methylphenol)

C

c	Molar concentration
CRU	Constitutional repeat unit
CTA	Chain transfer agent

D

d	Length
$Đ$	Dispersity
DCM	Dichloromethane
D_h	Hydrodynamic diameter
DLS	Dynamic light scattering
DMF	N,N-Dimethylformamide
DMSO	Dimethylsulfoxide
DP	Degree of polymerization
DP_n	Number-average degree of polymerization
DSC	Differential scanning calorimetry

E

EA	Elemental analysis
EtOH	Ethanol

F

FRP	Conventional free radical polymerization
FTIR	Fourier transform infrared spectroscopy

G

G	Gibbs free energy

H

H	Enthalpy

I

iPrOH	Isopropanol (2-propanol)
IUPAC	International union of pure and applied chemistry

J

k_B	Boltzmann constant

L

LAM	Less activated monomer
LCST	Lower critical solution temperature

M

m	Mass
MADIX	Macromolecular architecture design by interchange of xanthates
MAIB	Dimethyl-2,2'-azobis(2-methylpropionate)
MAM	More activated monomer
MeOH	Methanol
MMA	Methyl methacrylate
M_n	Number-average molar mass
M_r	Relative molecular mass
MS	Mass spectrometry
M_w	Weight-average molar mass

N

N	Number of molecules
n	Polymer chain length
NIPAM	N-Isopropyl acrylamide
NIPMAM	N-Isopropyl methacrylamide
NMP	N-Methyl-2-pyrrolidone

NMR	Nuclear magnetic resonance
nPrOH	n-Propanol
NVIBAM	*N*-Vinyl isobutyramide
NVF	*N*-vinyl formamide

P

PiPOx	Poly(2-isopropyl-2-oxazoline)
PMMA	Poly(methyl methacrylate)
PNIPAM	Poly(*N*-isopropyl acrylamide)
PNIPMAM	Poly(*N*-isopropyl methacrylamide)
PnPOx	Poly(2-n-propyl-2-oxazoline)
PNVIBAM	Poly(*N*-vinyl isobutyramide)
PS	Polystyrene

R

RAFT	Reversible addition fragmentation chain transfer
RDRP	Reversible-deactivation radical polymerization
R_h	Hydrodynamic radius
RI	Refractive index

S

S	Entropy
SEC	Size exclusion chromatography

T

T	Temperature
T_{CP}	Cloud point temperature
TEMPO	(2,2,6,6-Tetramethylpiperidin-1-yl)oxyl
TFE	2,2,2-Trifluoroethanol
TFT	Trifluorotoluene
T_g	Glass transition temperature
TGA	Thermogravimetric analysis
THF	Tetrahydrofuran

U

UCST	Upper critical solution temperature
UV-vis	Ultraviolet-visible (spectroscopy)

V

V	Volume
VA-044	2,2-Azobis(*N*,*N*-dimethylene-isobutylamidine)dihydrochloride
vol.%	Volume percent
V40	1,1'-Azobis(cyclohexane-1-carbonitrile)
V50	2,2'-Azobis(2-methylpropionamidine) dihydrochloride
V501	4,4'-Azobis(4-cyanovaleric acid)
V70	2,2'-Azobis(4-methoxy-2,4-dimethylvaleronitrile)

W

w_{PNIPAM}	Weight fraction of PNIPAM in the copolymer, obtained from SEC
$w_{PNIPMAM}$	Weight fraction of PNIPMAM in the copolymer, obtained from SEC
wt.%	Weight percent

#

ε	Extinction coefficient
λ_{max}	Wavelength of maximum absorbance
δ	Hildebrand solubility parameter
χ	Flory-Huggins interaction parameter
ϕ	Volume fraction

Polymer Abbreviations used in this Thesis

PX$_n$ Homopolymer of monomer X, with degree of polymerization n, obtained by conventional free radical polymerization. Example: PNIPMAM$_{100}$

PX$_n^R$ Monofunctional homopolymer of monomer X, with degree of polymerization n, obtained by RAFT polymerization using CTA R. Example: PS$_{10}^A$

PX$_n$-b-PX$_n^R$ Bifunctional homopolymer of monomer X, with degree of polymerization n, obtained by RAFT polymerization using CTA R. Example: PS$_{10}$-b-PS$_{10}^F$

PX$_n$-b-PY$_m^R$ Diblock copolymer of monomers X and Y, with degrees of polymerization n and m, obtained by RAFT polymerization with CTA R. Example: PS$_{10}$-b-PNIPAM$_{100}^F$

PX$_n$-b-PY$_m$-b-PX$_n^R$ Triblock copolymer of monomers X and Y, obtained by RAFT polymerization using CTA R. Example: PS$_{10}$-b-PNIPAM$_{100}$-b-PS$_{10}^F$

What each code means:

PX and **PY** are the abbreviation of the chemical constitution of each block:

PS polystyrene
PMMA poly(methyl methacrylate)
PNIPAM poly(*N*-isopropyl acrylamide)
PNIPMAM poly(*N*-isopropyl methacrylamide)
PNVIBAM poly(*N*-vinyl isobutyramide)

n and **m** are the number-average degree of polymerization (DP$_n$) of each block, from SEC analysis
As described in section 6.5, SEC was calibrated using PS or PMMA monodisperse samples. PS calibration was used for all homo- and copolymers containing PS. PMMA calibration was used for all homo- and copolymers containing PMMA, as well as for PNIPMAM and PNVIBAM homopolymers.

R is the code of the RAFT CTA used to obtain the polymer: A, B, C, D, E or F (see section 3.1). If no code is given, polymerization was done by the conventional free radical process.

Table of Contents

1. Introduction & Motivation

Living systems have long served as inspiration for scientific developments. In the field of polymer science, living systems are particularly fascinating for their ability to seamlessly combine sensing of external factors, processing of this information, and autonomous actuation in response. So called "stimuli-responsive polymers" mimic such systems, in a way that the polymeric material shows large reversible changes when subjected to small environmental stimuli. These stimuli may be variations of temperature, pH, electric or magnetic fields, light intensity or wavelength, presence of salts or enzymes, among others. In response, the polymers show drastic responses, for example swelling/collapse, solubilization/precipitation, or shape changes. Hence, in contrast to traditional static polymers, stimuli-responsive polymers are dynamic materials with tunable properties. Such innovative self-adjusting materials have a wide array of potential applications, including autonomous sensors and actuators, self-healing materials, affinity separation systems, minimally invasive medical devices, drug and gene delivery systems, and substrates for cell culture and tissue engineering.[1-3]

Among the various possibilities of environmental stimuli, temperature responsivity is one of the most studied, due to its promising applications, above all in the biomedicine and cosmetics fields. Thermoresponsive polymers show a delicate balance between hydrophobicity and hydrophilicity, which is dependent on the environmental temperature. Hence, with a change of only a few degrees, the polymeric chains may change between soluble (expanded) and insoluble (collapsed) states, thus acting as on/off switches. This may lead to different types of responses, depending on the physical form of the chains. In the case of linear free chains in solution, the system will change between a homogeneous and a phase-separated condition. Most commonly, in aqueous media, polymers will be soluble at low temperatures, but insoluble at high temperatures.[1,2,4,5]

One widely spread approach to make use of such stimuli-responsivity is to incorporate thermoresponsive polymers into block copolymer structures. While homopolymers are composed of a single type of constitutional repeat unit (monomer) throughout the entire chain, copolymers contain at least two types of constitutional repeat units, which may be organized statistically, alternatively, in sections (blocks), as grafts, among others.[6] Copolymers are generally of interest because they enable the macroscopic mixing of incompatible polymers, allow for the combination of the properties from the individual types of constitutional repeat units, and may even lead to amplified properties which exceed the simple combination of the individual materials. Particularly in the case of block copolymers, specific types of self-assembly might occur, especially in solution. Copolymers containing both hydrophobic and hydrophilic blocks are referred to as *amphiphilic*

block copolymers. These amphiphilic block copolymers often take the form of telechelics, with a long hydrophilic middle block with one or more hydrophobic blocks at the chain ends.[7-9] In aqueous environments, such copolymers tend to self-assemble forming a myriad of structures, such as micelles, rods, vesicles and lamellae.[10] When thermoresponsive blocks are present, the balance between hydrophilic and hydrophobic block is changed, and self-assembly undergoes drastic changes in response to the environmental temperature. This specifically occurs at the transition temperature of the polymer. Such responsivity allows such structures to be used as carrier systems, switchable viscosity regulators, cell culture materials, actuators, among several others.[11,12]

Within the realm of thermoresponsive polymers, one particularly puzzling phenomenon is co-nonsolvency, which is the focus of this thesis. The term co-nonsolvency described the unusual behavior where a material is soluble in two pure solvents, for instance DMF and cyclohexane, but counter-intuitively becomes insoluble in certain mixtures of these two solvents.[13] The most well studied example of co-nonsolvency is the polymer poly(*N*-isopropyl acrylamide) (PNIPAM), in mixtures of water and methanol. PNIPAM typically presents a transition temperature around 34°C in pure water (i.e. soluble at room temperature), but the transition temperature is lowered to about -7.5°C in the presence of 55 vol.% of methanol, thus leading to insolubility at room temperature.[14,15] Although co-nonsolvency has already been known for several decades, it is still not understood, and its underlying causes are subject of much debate.[15-22]

Since the currently published studies focus almost solely on homopolymers of PNIPAM in water and methanol, many questions remain unanswered with respect to co-nonsolvency phenomenon on other polymers and polymer architectures. More specifically, it is unclear how the co-nonsolvency behavior of various polymers differs from one another, and how the co-nonsolvency is impacted by the copolymer architecture, namely size and number of blocks, as well as the polarity of the hydrophobic constitutional repeat unit.

For example, poly(2-isopropyl-2-oxazoline) (PiPOx) and poly(2-*n*-propyl-2-oxazoline) (PnPOx), polyleucine and polycaprolactam (Nylon 6) are structural isomers of PNIPAM yet show some considerable differences in their properties.[23] PiPOx also shows LCST-type behavior, with cloud point in pure water around 36°C.[24,25] Although the polymer exhibits co-nonsolvency behavior in water-ethanol mixtures,[26] the phenomenon is not observed in water-methanol mixtures.[25] Moreover, above its transition temperature, PiPOx forms fibrils which irreversibly aggregate into hierarchical structures,[26,27] a behavior which is not seen for PNIPAM. PnPOx, in contrast, shows a cloud point around 21.5°C in pure water and shows co-nonsolvency behavior in both water-methanol[25] as well as water-ethanol mixtures.[26] Meanwhile, polyleucine shows very limited

solubility in water, whereas Nylon 6 is altogether insoluble. These stark differences incite questions regarding the influences that small changes in the chemical structure of the constitutional repeat unit may have on the solubility and thermoresponsive properties of the polymers in question.

Poly(*N*-isopropyl methacrylamide) (PNIPMAM) is an analogous material to PNIPAM, differing chemically solely by the presence of an addition methyl group on the backbone of the polymer. Although this should render the polymer more hydrophobic, thus presenting a lower transition temperature, in reality PNIPMAM shows a transition temperature around 44°C in water, that is, unexpectedly higher than that of PNIPAM.[28] Hence, it is not clear how the chemical structure of the constitutional repeat unit influences the co-nonsolvency and self-assembly behavior, and whether the co-nonsolvency is simply a matter of the chemical functionalities or if it is also impacted by structural isomers. For example, the polymer poly(*N*-vinyl isobutyramide) (PNVIBAM) is a constitutional isomer of PNIPAM, that is, both have almost the same chemical structure, except for the inverted orientation of the amide group. However, PNVIBAM shows a transition temperature around 39°C, that is, about 7°C higher than PNIPAM.[29] In addition, while a brief mention to co-nonsolvency behavior in PNVIBAM can be found in literature,[30] no details have been reported, thus being unclear how the co-nonsolvency behavior of PNVIBAM differs from its structural isomer, PNIPAM.

Furthermore, in the case of amphiphilic block copolymers, it is unclear how the polarity of the hydrophobic constitutional repeat unit impacts the co-nonsolvency behavior. At the starting point of this thesis, the few published reports of co-nonsolvency on block copolymer solutions had solely explored PS-*b*-PNIPAM.[31,32] Given that polystyrene (PS) is a highly hydrophobic polymer, it is an open question whether a more polar (yet still hydrophobic) block, such as poly(methyl methacrylate) (PMMA), can significantly impact the thermoresponsive and co-nonsolvency behavior. PS and PMMA make a particularly interesting choice for comparison, as both polymers are hydrophobic, but exhibit different polarities, while still having similar glass transition temperature (T_g ca. 100°C). This ensure no change on the potential "frozen chain" condition, which should allow a clearer evaluation of the effect of polarity.[12]

Apart from the aspects of thermoresponsivity and co-nonsolvency, the synthesis of such polymers deserves special attention. Based on literature reports on the synthesis of PNIPMAM, this polymer is considerably more complex to polymerize than its acrylamide analog, PNIPAM, and high molar masses are difficult to achieve by free radical polymerization. This complexity is further heightened if copolymer structures are desired. Amphiphilic block copolymers are typically obtained by reversible-deactivation radical polymerization (RDRP) techniques,[33] such as

reversible addition fragmentation chain transfer (RAFT).[34] In contrast to conventional free radical polymerization, RAFT allows polymer chains to be successively reactivated and chain extended, thus allowing the synthesis of multiple blocks. This is achieved using specific chain transfer agents (CTA), which were appropriately designed for degenerative chain transfer, and synthesized to react with the monomers of interest.[35] Since the CTA is incorporated into the polymers as end-groups, certain CTAs may also include additional functionalities, such as UV-vis labels, which e.g. facilitate the characterization and tracking of the formed polymers. However, very few published studies have reported the RAFT polymerization of NIPMAM.[36,37] Furthermore, the RAFT polymerization of NVIBAM poses another challenge. Although it has never been reported before, the activation level of this monomer implies that it would require a different type of RAFT agent (chain transfer agent – CTA) than monomers such as styrene, MMA, NIPAM and NIPMAM.[34,35] Thus, obtaining amphiphilic block copolymers of PNVIBAM with PS or PMMA hydrophobic blocks is expected to be challenging.

Based on these questions and challenges, the overall objective of this doctoral project is to investigate polymeric systems exhibiting co-nonsolvency. In particular, the behavior of systems other than the classical PNIPAM homopolymers and previously reported PS-b-PNIPAM block copolymer is of interest.

Thus, this thesis focuses on two aspects: (1) the synthesis of such polymers, and (2) the study of their thermoresponsive, co-nonsolvency and aggregation behaviors.

In the first part, the objective is to evaluate and optimize the synthesis of PNIPMAM and PNVIBAM homopolymers and amphiphilic block copolymers with PS or PMMA hydrophobic blocks. This is achieved by the evaluation of reaction parameters, such as solvent, initiator, temperature, and chain transfer agent, whenever applicable.

In the second part, the objective is to clarify how the chemical structure of the polymer impacts the thermoresponsivity, co-nonsolvency and self-assembly. This is achieved by comparing the behavior of homopolymers and amphiphilic block copolymers based on constitutional repeat units with a different yet closely related chemical structure: PNIPAM, PNIPMAM and PNVIBAM. In the case of copolymers, the effects of the chain architecture (di- versus triblock) and polarity of the hydrophobic block (PS versus PMMA) are evaluated.

To fulfil these objectives, homopolymers of PNIPAM, PNIPMAM and PNVIBAM were synthesized by conventional free radical polymerization, in a single step. Whenever necessary, non-commercial monomers were also synthesized.

Di- and triblock copolymers with PS or PMMA hydrophobic blocks and PNIPAM, PNIPMAM or PNVIBAM thermoresponsive blocks were synthesized by reversible addition fragmentation chain transfer (RAFT)[38], in two consecutive steps. The assessment of the success of the reactions is done by various molecular characterization techniques, such as nuclear magnetic resonance (NMR), UV-vis spectroscopy, size-exclusion chromatography (SEC), Fourier-transform infrared spectroscopy (FTIR), elemental analysis (EA), differential scanning calorimetry (DSC) and thermogravimetric analysis (TGA). The thermoresponsive, co-nonsolvency and self-assembly behavior of the polymers in aqueous and mixed aqueous/organic solutions is investigated using turbidimetry and dynamic light scattering (DLS), which allow the identification of cloud points and approximate identification of the size and distribution of aggregates.

2. Theoretical Background

This chapter offers the scientific background relevant to the work which will later be presented in this thesis. First, in section 2.1, general concepts of polymer solubility will be clarified, with particular emphasis to the scenario where water is the solvent. Beyond simple homopolymers, the more complex cases of amphiphilic block copolymers and thermoresponsive polymers will also be discussed. Subsequently, in section 2.2, the presence of additional solvents will be discussed, and how polymer solubility is affected in such mixed aqueous solutions. Here, special emphasis will be given to the phenomena of co-nonsolvency, which is the central aspect of this work, including a discussion of polymer/solvent systems known to exhibit the behavior, as well suggested mechanisms. In section 2.3, the synthesis of the previously reviewed polymers will be discussed, with special emphasis on the versatile polymerization method used in this work: Reversible Addition Fragmentation Chain Transfer (RAFT). An overview of the published reports on the polymerization of *N*-isopropyl methacrylamide (NIPMAM) and *N*-vinyl isobutyramide (NVIBAM) will also be presented. Finally, in section 2.4, the most common characterization methods used to study polymer solutions will be introduced.

2.1. Basics of Polymer Solubility

As this thesis is focused on water-soluble polymers, and the atypical solubility phenomenon called co-nonsolvency, it is important to first understand the basics of solubility. The solubility of a given material in a solvent is determined by the Gibbs free energy (G). If the Gibbs free energy of the mixture (G_{12}) is lower than that of the individual components, then solubilization may take place:

$$\Delta G_{\mathrm{m}} = G_{12} - (G_1 + G_2) < 0 \tag{1}$$

Considering that

$$\Delta G_{\mathrm{m}} = \Delta H - T \cdot \Delta S \tag{2}$$

where H is the enthalpy, T is the temperature and S is the entropy, the material will soluble whenever $\Delta H < 0$ and $\Delta S > 0$, and insoluble whenever $\Delta H > 0$ and $\Delta S < 0$. In the cases where both ΔH and ΔS are negative, or both positive, solubility will depend on the temperature of the system.[11]

In ideal systems $\Delta H = 0$, meaning mixing is entropically driven and will occur simply because there are more possible arrangements for a component in the mix than in the separated system.[6] However, a system is considered ideal only when the following criteria are met: the components are small and equally sized, the interactions between components is the same, components show

the same movement before and after mixing, all arrangements have the same energy, and there is no volume change upon mixing. Therefore, polymer solutions are evidently not ideal systems ($\Delta H \neq 0$). In addition, the connectivity between segments drastically limits their arrangement, decreasing entropy. Considering the complexity of the process, the Flory-Huggins Theory has been developed to better describe polymer solubility.[6,39]

Flory-Huggins Theory

The effect of chain segment connectivity on entropy is the topic of the Flory-Huggins Theory. It considers the solution as a lattice, as shown in Figure 1, where each lattice site is occupied either by one solvent molecule or one polymer chain segment. Moreover, given their connectivity, each polymer chain segment can only occupy a lattice site adjacent to its neighboring segments, limiting the entropy (possible arrangements) both for the polymer and for the solvent. Thus, it becomes clear that the entropy of a polymer solution (Figure 1b) is smaller than that of purely low molar mass solutions (Figure 1a). Furthermore, shorter polymer chains and dilute solutions are more favorable to mix since they pose less restrain to the system's arrangement.[6,11,39-41] While the demixed polymer chain (solid state) is fixed to a single possible conformation, the number of possible conformations of the polymer chain in solution is determined by chain flexibility and interactions with the solvent.
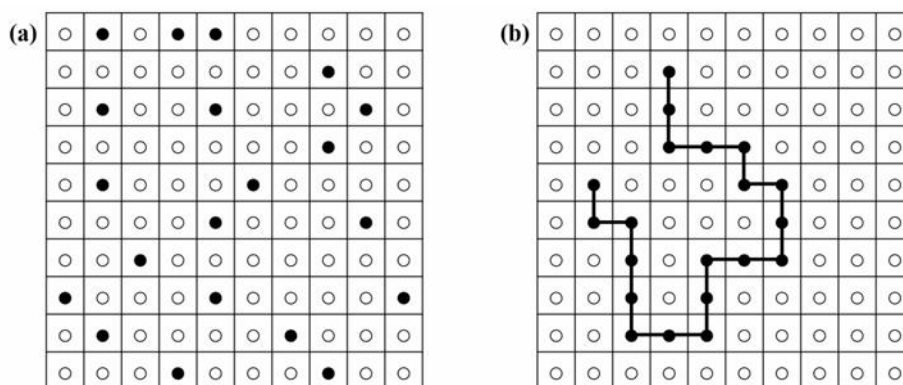

Figure 1. Visual representation of the lattice model for solubility of small molar mass molecules (a) versus polymers (b), where the connectivity between chain segments limits the number of possible arrangements (entropy) of the system (○ = solvent, ● = solute).

These effects become clear when analyzing the expression for the entropy change upon mixing:

$$\Delta S_m = -k_B \left(\frac{\phi_1}{n_1} \cdot \ln \phi_1 + \frac{\phi_2}{n_2} \cdot \ln \phi_2 \right) \tag{3}$$

where k_B is Boltzmann constant, ϕ_1 and ϕ_2 are the solvent and polymer volume fractions, respectively. n_1 and n_2 are the chain length of solvent and polymer molecules, respectively, that is, the number of adjacent lattice sites occupied by each molecule, which would be equivalent to the degree of polymerization of the polymer. Thus, considering the volume fractions will always be values between 0 and 1, the natural logarithms will yield values equal to or lower than zero, leading to a positive entropy of mixing. The magnitude of this entropy change, however, will be strongly dependent on the denominators N_1 and N_2, with larger chain lengths causing a lower entropy of mixing.[6,39,42-44]

Conversely, the mixing enthalpy (ΔH_m) is given by

$$\Delta H_m = k_B \cdot T \cdot N_1 \cdot \phi_2 \cdot \chi \tag{4}$$

where T is the absolute temperature, N_1 is the number of solvent molecules, ϕ_2 is the polymer volume fraction and χ is the Flory-Huggins interaction parameter. This interaction parameter is specific to each polymer/solvent mixture and is a measure of the difference of interaction energies of the demixed and mixed states. In most cases, $\chi > 0$, as interactions of components with themselves tend to be more energetically favorable than interactions with other components. The value of χ is larger than 0.5 for poor solvents, where the polymer molecule is a compact globule, and smaller for good solvents, where the polymer molecule is an expanded coil. Moreover, χ has been shown to be composed of an enthalpic and an entropic component:

$$\chi = \chi_S + \frac{\chi_H}{T} \tag{5}$$

The balance between these enthalpic and entropic contributions, as well as temperature, will determine the miscibility of the polymer in a given solvent.[39,42,44]

Combining the expressions for the entropy and enthalpy of mixing, we can then obtain the Gibbs free energy as:

$$\Delta G_m = k_B \cdot T \left(\frac{\phi_1}{n_1} \cdot \ln \phi_1 + \frac{\phi_2}{n_2} \cdot \ln \phi_2 + \chi \cdot \phi_1 \cdot \phi_2 \right) \tag{6}$$

Although the Flory-Huggins theory and equations derived from it are quite useful for a general representation of polymer solubility, the model is based on certain simplifications and assumptions which usually do not hold true. For example, the concentration, temperature, and molecular weight dependence of the interaction parameter is not taken into account. Changes in chain flexibility in the solid state and solution are also not considered, nor are specific interactions between the polymer and solvent molecules, which may lead to a preferred orientation or organization.

Therefore, the model may leads to considerable deviations from reality, especially when more complex systems are considered.[6,39,41]

Finally, it is also important to highlight that solubilization, particularly in the case of polymers, is not simply a matter of thermodynamics, but also kinetics, and polymer solubilization process will require much more time than typical low molar mass compounds. Factors such as increased molar mass, crystallinity and branching will further slowdown solubilization.[45]

Solubility Parameters

The enthalpic contribution to the Flory-Huggins interaction parameter can be correlated to the Hildebrand solubility parameters of the components (δ_1 and δ_2), as follows:[11,39,46]

$$\chi = \frac{V \cdot (\delta_1 - \delta_2)^2}{k_B \cdot T} \qquad (7)$$

where V is the molar volume of polymer chain segments. Contrary to the Flory-Huggins interaction parameter, the solubility parameter is specific to each polymer or to each solvent alone (not each polymer/solvent pair). It is based on the cohesive energy of the component, that is, the attractive interactions of its molecules with themselves. Solubility is then dependent on the similarity between the component's parameters. Moreover, a combination of solvents might lead to solubility of a certain polymer, even when the individual solvents cannot dissolve it. In this case, if the solubility parameter of one solvent is exceedingly high, while the other is exceedingly low, their combination might give rise to an appropriate solubility parameter for the solubility of the material in question. [41,42]

However, the Hildebrand solubility parameter does not take into account secondary interactions, leading to certain inaccuracies in the results obtained. Thus, the Hansen solubility parameter, or three-dimensional solubility parameter (δ_{3d}), has been created as an extension of the Hildebrand solubility parameter, which focusses on contributions from the dispersion forces (δ_d), dipole forces (δ_p) and hydrogen bonds (δ_h), resulting in:[47]

$$\delta_{3d}^2 = \delta_d^2 + \delta_p^2 + \delta_h^2 \qquad (8)$$

Values of the solubility parameters of a few solvents and polymers are listed Table 1.

Table 1. Hansen and Hildebrand solubility parameters (in MPa$^{0.5}$) of a few solvents and polymers, relevant for this thesis.[48]

Substance	δ	δ$_d$	δ$_p$	δ$_h$
Water	47.9	15.5	16.0	42.4
Methanol	29.7	15.1	12.3	22.3
Ethanol	26.6	15.8	8.8	19.4
Dimethylsulfoxide (DMSO)	26.6	18.4	16.4	10.2
N,N-Dimethylformamide (DMF)	24.8	17.4	13.7	11.3
n-Propanol	24.6	16.0	6.8	17.4
Isopropanol	23.5	15.8	6.1	16.4
1,4-Dioxane	20.5	19.0	1.8	7.4
Acetone	20.1	15.5	10.4	7
Tetrahydrofuran (THF)	19.4	16.8	5.7	8
Poly(*N*-isopropyl acrylamide) (PNIPAM)	23.5	-	-	-
Poly(methyl methacrylate) (PMMA)	22.7	18.6	10.5	7.5
Polystyrene (PS)	22.5	21.3	5.8	4.3

Polymer Interactions in Aqueous Solutions

As presented so far, polymer solubility is less dependent on entropy, and more dependent on enthalpy. Thus, solubilization depends heavily on the substitution of polymer-polymer interactions in favor of polymer-solvent interactions. When the solvent in question is water, the peculiar properties of this solvent must be considered, in particular its high polarity (strong dipole) and ability to form hydrogen bonds, which lead to extraordinarily strong interactions between water molecules and, consequently, a highly ordered and dense structure.[49] Thus, water soluble polymers must present a chemical structure with sufficiently hydrophilic groups, which strongly favors its interaction with water molecules, in the form of hydrogen bonds, ionic interactions and dipolar interactions. Moreover, if hydrophobic groups are present, the impact of hydrophobic interactions must be considered.[11] These interactions originate from the strong attraction between water molecules. If a hydrophobic group is present, the water molecules will then organize in a cage-like fashion around said group, forming a hydration layer which allows for the highest possible density of hydrogen bonds between water molecules. However, this organization evidently causes a decrease of entropy, which outweighs the enthalpy gain, thus disfavoring

11

dissolution of the solute in question. As a result, hydrophobic moieties will generally aggregate, thus reducing the entropy loss of water.[7,11]

However, if both hydrophobic and hydrophilic moieties are present, the hydrophobic/hydrophilic balance of the molecule must be considered, and complex polymer behavior in solution can be achieved by introducing chemical variations within the polymeric chain (for example in the form of copolymers or specific end-groups), or even within each constitutional repeat unit itself.[11]

2.1.1. Amphiphilic Block Copolymers in Aqueous Solutions

Copolymers are polymeric chains containing segments of varying chemical composition, bound together by covalent bonds. These chains may present a variety of architectures, such as linear, branched or star, and the chemically different segments may be organized as alternating or statistically distributed units, or in the form of blocks. In the case of block copolymers, moreover, the number and arrangement of the different blocks may vary greatly, as depicted in Figure 2.[6,10,50-52]
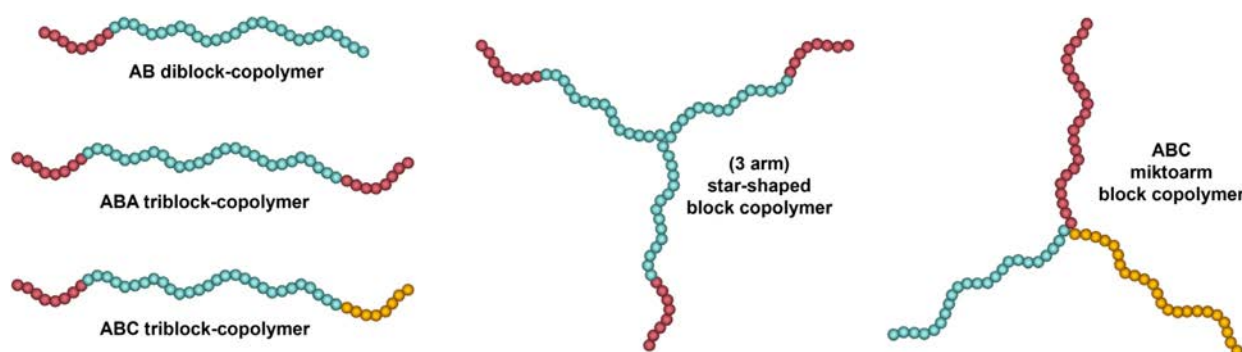
Figure 2. Examples of block-copolymer architectures, where different letters (A, B and C) and differently colored components represent constitutional repeat units with different chemical composition.

The nomenclature of block copolymers follows the guidelines of the International Union of Pure and Applied Chemistry (IUPAC). Diblock copolymers are thus referred to as poly(A)-*block*-poly(B), or PA-*b*-PB, where A and B are the monomers which gave origin to each one of the blocks. Similarly, an ABA triblock copolymer would be PA-*b*-PB-*b*-PA. Moreover, the average degree of polymerization (DP) of each block may be included, such as PA_{DP}-*b*-PB_{DP}.

Copolymers composed of blocks with opposing polarity, that is, at least one hydrophilic and one hydrophobic block, are called amphiphilic block copolymers. Due to the previously discussed polymer interactions in water, in particular hydrophobic interactions, amphiphilic block copolymers tend to self-assemble when in aqueous solution, forming a variety of structures depending on the disposition, size, and nature of the blocks. These structures are formed by the

microphase separation of the hydrophobic and hydrophilic segments of the molecule. As these segments are connected through covalent bonds, several boundaries are formed between the regions where collapsed (globule state) hydrophobic segments are aggregated, and the surrounding regions, where the hydrated (coil state) hydrophilic segments are. To ensure (even if partial) solubility, the hydrophobic/hydrophilic balance must be considered, so amphiphilic block copolymers are typically composed of a long hydrophilic water-soluble block, and one or more short hydrophobic insoluble blocks, since large hydrophobic blocks will typically render the entire molecule insoluble. Hydrophobic interactions will then drive aggregation of the short hydrophobic segments, forming mesoscopic structures such as micelles, rods, vesicles or lamellae, as shown in Figure 3.[7,8,11,12,50,53-55]
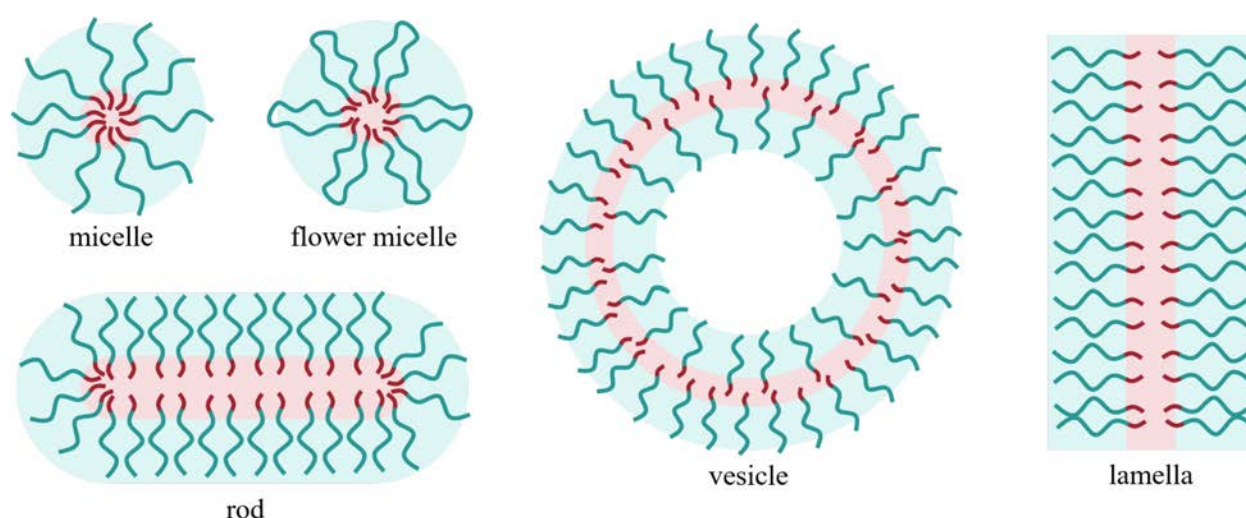
Figure 3. Examples of common mesoscopic structures formed by the self-assembly of amphiphilic block copolymers in aqueous solution. Red segments represent hydrophobic blocks, and turquoise segments represent hydrophilic blocks.

Here it is imperative to point out that, despite the usage of the same name, polymeric micelles differ greatly from the classical micelles composed of small molecule surfactants. Micelles formed by low molecular weight molecules are highly dynamic, with a large number of individual non-aggregated molecules in the solution, and a constant exchange of molecules between aggregates. In the case of large molar masses, the exchange of molecules between aggregates becomes very energetically unfavorable. This leads to a minimal amount of unimers in solution, and mostly kinetically trapped structures, a condition which is exacerbated in case the non-soluble block, typically forming the micellar core, is glassy or semicrystalline, leading to so-called frozen micelles. Besides this increased micellar stability, polymeric amphiphiles also tend to show much lower critical aggregation concentrations (CAC) than the usual critical micelle concentrations

(CMC) of small molecule surfactant. These properties, combined with wide possibilities for tuning chemical composition and molecular architecture, make block-copolymer aggregates extremely useful for a variety of applications, including viscosity modifiers, dispersants, emulsifiers and delivery systems.[12,50,56,57]

2.1.2. Thermoresponsive Polymers

Up to this point, the discussion has focused on polymers and polymer segments which either are soluble or insoluble in water. However, as can be deduced from Equation **(2)**, in the cases where both ΔH and ΔS are negative, or both positive, the signal of ΔG (and therefore the solubility) will depend on the temperature of the system.[11,41] In case ΔH and ΔS are positive (scenario 1), an increase of the temperature will lead to a decrease of ΔG, making the system go from insoluble to soluble at a specific temperature. This is called an upper critical solution temperature (UCST) type behavior. Alternatively, if ΔH and ΔS are both negative (scenario 2), an increase of the temperature will lead to an increase of ΔG and, at a specific temperature, the system will go from soluble to insoluble. This is called a lower critical solution temperature (LCST) type behavior. This type of stimuli-responsive materials, where essential properties (such as solubility) change drastically with small changes in temperature, are called thermoresponsive. The temperature at which this severe change in properties occurs is dependent on concentration, and is given by:

$$T_c = \frac{\Delta H}{\Delta S} \tag{9}$$

As previously discussed, the concentration and molar mass of the polymer typically have a strong influence on the solubility of a polymer, and therefore also on the transition temperature. This influence becomes clear when analyzing the Gibbs free energy as a function of the composition of the mixture, see Figure 4. In the case of curves T_1 and T_2, the Gibbs free energy of the mixture will always be lower than that of the individual components. Hence, the mixture is soluble in all proportions. In the case of curve T_3 and T_4, however, the mixture will be soluble in case the concentration of solute is smaller than x_1 (x_1') or larger than x_4 (x_4'). While if the concentration lies between x_1 and x_2 or between x_3 and x_4, phase separation will occur.[6,58]
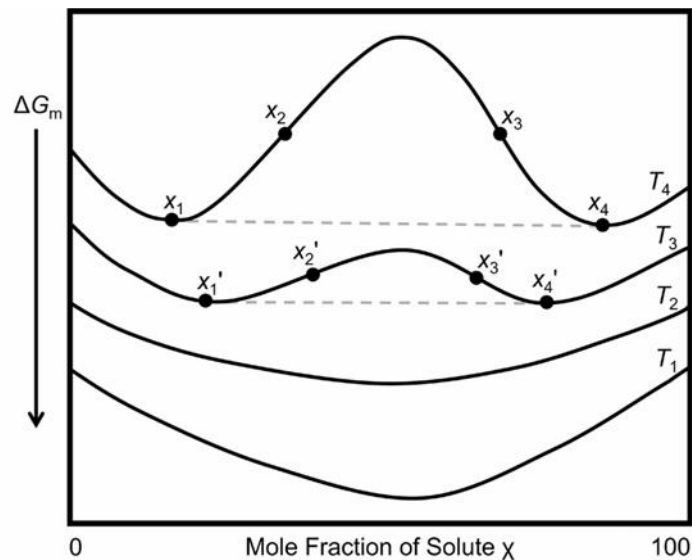
Figure 4. Diagram of the Gibbs free energy as a function of the concentration of polymer in the solution. In the case of temperatures T_1 and T_2, the mixture will be soluble in all compositions. Partially solubility is observed whenever a tangent is able to touch the ΔG_m curve in two points, as is the case for T_3 and T_4, where the common tangent is the gray dashed line.

The composition range in which phase separation occurs is defined by the contact points of the common tangent of the ΔG_m curve, represented in Figure 4 by the gray dashed lines. As can be seen, this range changes with temperature. For UCST-type behavior $T_1 > T_2 > T_3 > T_4$, such that the insoluble range becomes narrower with increasing temperature. The temperature at which the two points x_1 and x_4 converge is the upper critical temperature itself, above which the mixture is soluble in all compositions. For LCST-type behavior, in contrast, $T_1 < T_2 < T_3 < T_4$, such that the insoluble range is larger at high temperatures and narrower at low temperatures. Here, the temperature at which the two points x_1 and x_4 converge is the lower critical temperature, below which the mixture is soluble in all compositions.[6,44,58] If these insolubility ranges are plotted on a graph of temperature versus mole fraction of solute, the phase diagrams shown in Figure 5 would be created. The binodal curve is therefore formed by the points touched by the common tangent of the ΔG_m curve (points x_1 and x_4). Moreover, the so called spinodal curve is created by the inflection points of the ΔG_m curve (points x_2 and x_3 in Figure 4). The area in between the binodal and spinodal curves (that is, between points x_1 and x_2 and between points x_3 and x_4) represents the metastable region.[6,44] In this region, phase separation occurs by nucleation and growth, meaning it will only occur if concentration fluctuations are large enough to overcome the energy barrier. Conversely, in the unstable region, which is the area within the spinodal curve, phase separation occurs as a spinodal decomposition. This process is spontaneous and immediate, with no energy barrier.[6,42,59]
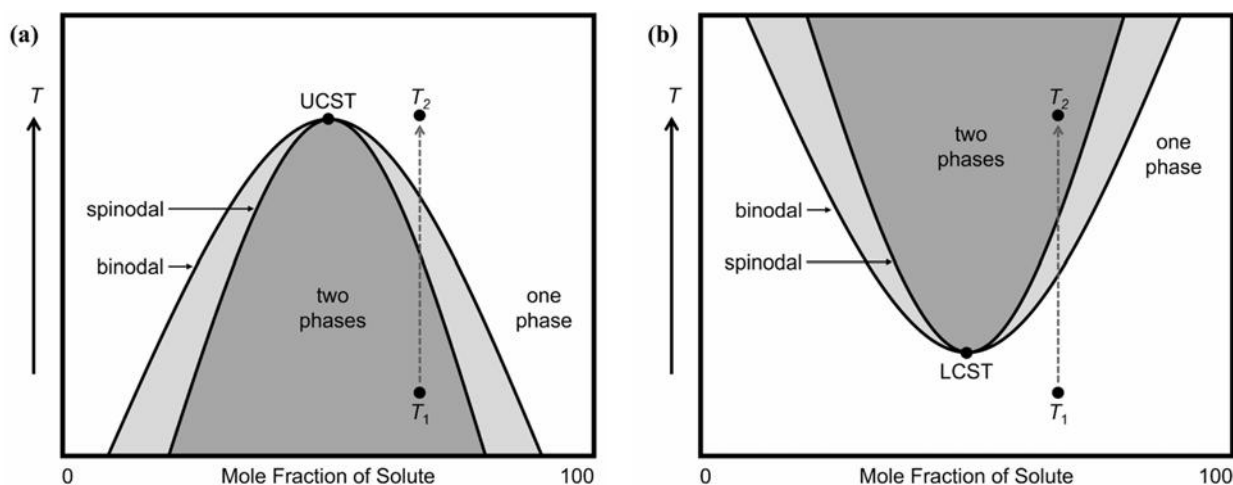
Figure 5. Phase diagram of materials exhibiting UCST (a) and LCST (b) type behavior, with the binodal and spinodal curves delimiting the one-phase stable region, metastable region, and unstable region.

In the first case (a), an increase of the temperature from T_1 to T_2 causes the system to go from an insoluble to a soluble state. The temperature at which the binodal and spinodal curves converge (and highest point of both curves) is the upper critical solution temperature (UCST). In the second case (b), the same increase of temperature causes the system to go from a soluble to an insoluble state. The temperature at which the binodal and spinodal curves converge (and lowest point of both curves) is the lower critical solution temperature (LCST).

Polymeric chain length typically exerts a very strong impact on the transition temperature, with the LCST and UCST being shifted to lower temperatures and lower polymer concentration upon increase of the molar mass. However, for certain materials, this influence is much smaller, and the LCST is hardly affected by chain length. In this case, the material is said to show a LCST type II behavior, as opposed to the typical LCST Type I behavior (Flory-Huggins type behavior). Poly(*N*-isopropyl acrylamide) (PNIPAM) is one of the most well-studied polymers exhibiting LCST Type II. Moreover, a LCST Type III is also possible, in which the material shows a bimodal phase diagram, with Type I behavior at low concentrations and Type II behavior at high polymer concentrations.[12,59]

2.2. Polymer Solubility in Mixed Solvents

As previously discussed, the Hildebrand and Hansen Solubility Parameters are useful to predict the quality of a solvent for a specific material. These parameters may also help estimate the quality of a solvent mixture, through the simple equation[41,60]:

$$\delta_{mix} = \sum \phi_i \cdot \delta_i \tag{10}$$

where δ_{mix} is the solubility parameter of the mixture, ϕ_i is the volume fraction and δ_i is the solubility parameter of each solvent in the mixture. As mentioned before, solubility usually takes place when the value of the solubility parameters of the solvent and the solute are similar. This is colloquially translated as "like dissolves like".

2.2.1. Cosolvency

Through equation **(10)** it becomes evident that mixing a non-solvent with exceedingly high δ with a non-solvent with exceedingly low δ might lead to a mixture with the appropriate δ_{mix} to dissolve the polymer in question. This phenomenon, where a mixture of two non-solvents leads to solubility, is called cosolvency and it is commonly seen in mixtures of solvents at opposite ends of the polarity spectrum. However, despite being a rough guideline, several deviations from the behavior described by equation **(10)** and by the "like dissolves like" rule of thumb can be observed. Certain materials are soluble in a much wider range of solvents (or solvent mixtures) than would be expected by sole evaluation of the solubility parameters, while other times a predicted solubility might not take place in practice. Within these divergences, a few interesting phenomena may be observed.

One example is the unusual behavior shown by poly(methyl methacrylate) (PMMA). The polymer is not readily soluble in pure water, nor in pure alcohols. However, it exhibits a UCST-type behavior in certain water/alcohol mixtures.[61,62] For example, a 28 kg·mol⁻¹ PMMA in aqueous solutions containing about 70 – 82 wt.% ethanol has been shown to present a clearance point (UCST-type transition) upon heating above 25 - 30°C. Moreover, a 14 kg·mol⁻¹ PMMA is reportedly fully soluble in the same solvent composition. Similar behavior could also be seen with methanol and isopropanol as cosolvent.[63] This is a peculiar example of cosolvency behavior for the fact that both water and alcohols are on the same size of the polarity spectrum. The combination of their solubility parameters in fact predicts that water/alcohol mixtures would be less likely to dissolve PMMA than the alcohols alone (see Table 1). This phenomenon was explained by the fact that the alcohol molecules disrupt the structure of water. In large amounts of alcohol, water molecules are not clustered with other water molecules. Without the necessity of breaking the more favorable water-water hydrogen bonds, the ester moiety of the PMMA constitutional repeat unit can in turn be more favorably hydrated by the water molecule, leading to the improved solubility.[11,61,63] UCST cosolvency behavior in mixed aqueous solutions can also be seen on other polymers, including poly(methyl acrylate),[64] poly(2-oxazoline)s,[65-67] and derivatives of poly(ethylene glycol).[62,68]

This cosolvency behavior has been used to produce several copolymers with complex thermoresponsive and self-assembly behavior. For example, formation of micelles has been demonstrated on diblock copolymers of polystyrene and PMMA in aqueous solutions containing 80 wt.% ethanol.[63] UV and temperature responsive behavior has been achieved on azobenzene containing copolymers of PMMA and poly(pentafluorophenyl methacrylate).[62] Similarly, schizophrenic micelles, i.e. micelles with the ability to invert their structure have been obtained from a diblock copolymer of poly(methyl acrylate) and poly(diethylene glycol ethyl ether acrylate), which exhibits both UCST and LCST-type behavior.[69]

2.2.2. Co-nonsolvency

Another puzzling solubility phenomenon in polymers is the so called co-nonsolvency. Contrary to cosolvency, polymers exhibiting co-nonsolvency behavior become insoluble in certain solvent mixtures, despite being fully soluble in each of the solvents individually. This phenomenon is considerably more complex than cosolvency, and is not yet fully understood, despite large number of studies that have focused on its investigation, and the plethora of suggested mechanisms proposed to this date. Although the most well studied co-nonsolvency system is by far poly(N-isopropyl acrylamide) in water/methanol mixtures, the phenomenon has been reported for a number of other cosolvents and polymers.[70] The following sections will summarize the state of the art of co-nonsolvency research in PNIPAM as well as various alternative systems reported to show the phenomenon, and will then discuss the mechanisms that have been suggested to explain the phenomenon.

Classical Co-nonsolvency System: PNIPAM in Mixed Aqueous Solvents

Poly(N-isopropyl acrylamide) (PNIPAM) is certainly the subject of the majority of co-nonsolvency studies found in literature. This may be due to how strongly this polymer exhibits the behavior, as well as the fact that it occurs in a vast number of cosolvents. Although water/methanol mixtures are the most commonly investigated, ethanol, isopropanol, n-propanol, N,N-dimethylformamide (DMF), tetrahydrofuran (THF), dioxane, acetonitrile, acetone, and dimethyl sulfoxide (DMSO) have also been reported to cause co-nonsolvency of PNIPAM when mixed with water.[14,15,71] In all cases, the addition of certain amounts of the cosolvent leads to decrease of the transition temperature, which in many cases drops below room temperature, thus leading to insolubility. When the cosolvent is present in larger amounts, full polymer miscibility is achieved again. Despite this common behavior, each cosolvent leads to somewhat different effects, which becomes clear when plotting the transition temperature against the fraction of cosolvent (whether

molar or volume fraction). As displayed in Figure 6, each cosolvent leads to different curve shapes, with co-nonsolvency taking place in different ranges and with different minima.

In addition to the LCST-type co-nonsolvency of PNIPAM, a UCST-type transition has also been reported. This occurs only for some cosolvents, such as ethanol, isopropanol, n-propanol, DMSO and DMF, and takes place at larger cosolvent fractions than the LCST-type transition.[15]

Co-nonsolvency can be seen not only in dilute solutions of homopolymers, but also in copolymers and various polymer architectures,[31,72-76] as well as in higher concentrations,[77] including hydrogels[14,20,73,76] and polymer films.[78,79] The effects of pressure have also been investigated, yielding the interesting finding that high pressure reverses the co-nonsolvency effect.[80-83]

Alternative Co-nonsolvency Systems

Although many examples of co-nonsolvency are observed in mixed aqueous solutions, several cases of polymers co-nonsolvency in mixed organic solvents can be found in literature. Examples include poly(methyl methacrylate) (PMMA), which shows co-nonsolvency in pyridine/formic acid[84] and in chlorobutane/amyl acetate[85] mixtures, as well as poly(ε-caprolactone) (PCL), which shows co-nonsolvency in pyridine/formic acid and in pyridine/acetic acid mixtures.[84]

Moreover, two types of co-nonsolvency have been reported: mixtures in which the two solvents have a very strong affinity with each other, such as the case of water/methanol, and systems where the miscibility of the two solvents is rather limited. An example of the latter is the system polystyrene in DMF/cyclohexane.[13] The focus of this thesis is the former type, specifically co-nonsolvency occurring in mixed aqueous solutions. Examples of polymers exhibiting this behavior are shown in Figure 7, and will be discussed in the following.
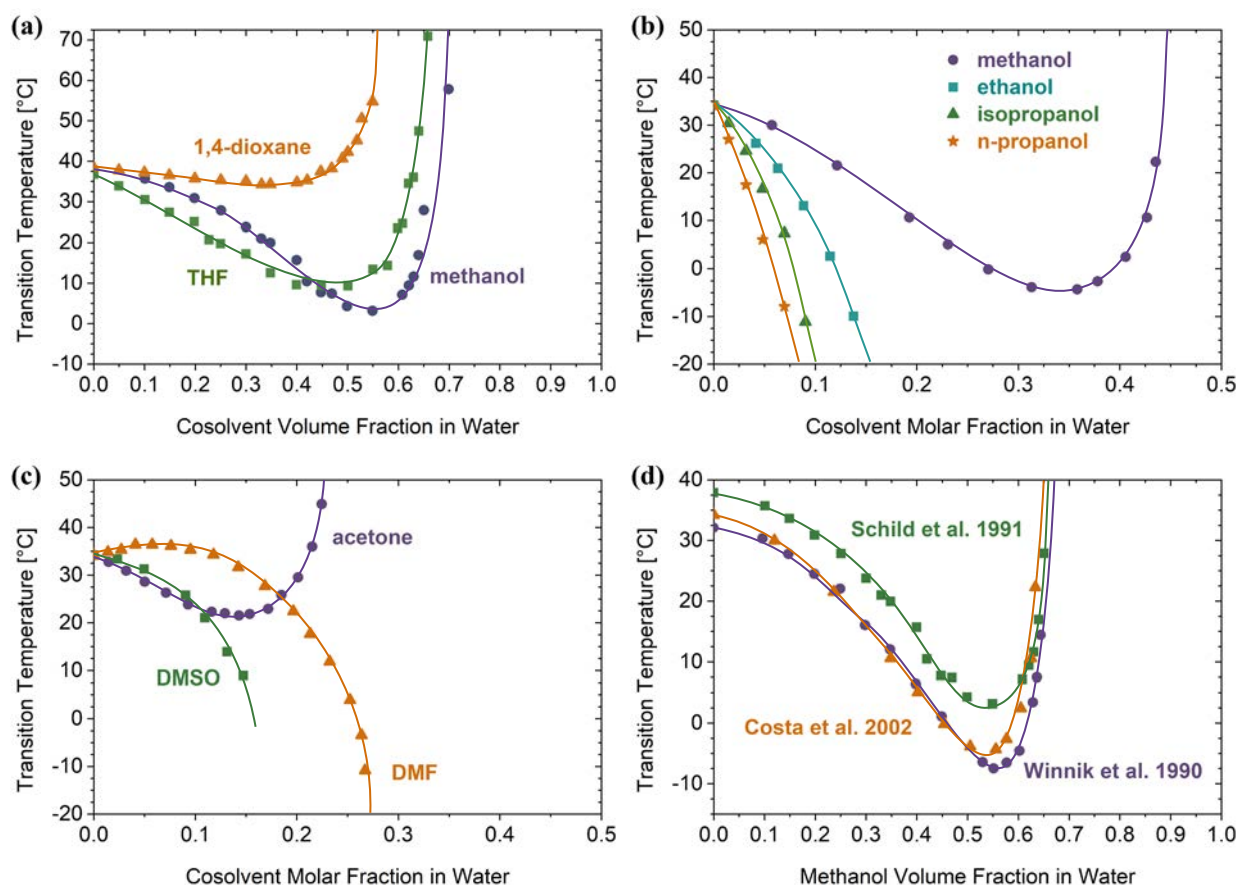
Figure 6. Examples of the co-nonsolvency behavior of linear PNIPAM in mixed aqueous solutions with various cosolvents, redrawn from literature sources: (a) Schild et al.,[14] M_w 160 kg·mol⁻¹, data from cloud point and microcalorimetric measurements at 0.4 g/L. (b)(c) Costa et al.,[15] M_w 120 kg·mol⁻¹, data from cloud point measurements at 1.0 wt.%. (d) Comparison between the phase diagrams in water-methanol, obtained by Schild et al.[*],[14] Costa et al.[†],[15] (as shown on previous figures) and Winnik et al.[‡][86] (M_v 1700 kg·mol⁻¹, data from cloud point measurements at 1.0 g/L). Note that axis units and ranges may vary between graphs. Lines are simply guides for the eye.

---

[*] Reprinted (adapted) with permission from Macromolecules 1991, 24, 4, 948–952, Howard G. Schild, M. Muthukumar, and David A. Tirrell, Cononsolvency in mixed aqueous solutions of poly(*N*-isopropylacrylamide), Copyright (1991) American Chemical Society.
[†] Reprinted (adapted) from Polymer 43, 22, Ricardo O.R. Costa and Roberto F.S. Freitas, Phase behavior of poly(*N*-isopropylacrylamide) in binary aqueous solutions, pages 5879-5885, Copyright (2002), with permission from Elsevier.
[‡] Reprinted (adapted) with permission from Macromolecules 1990, 23, 8, 2415–2416, Francoise M. Winnik, H. Ringsdorf, and J. Venzmer, Methanol-Water as a Co-nonsolvent System for Poly(*N*-isopropylacrylamide), Copyright (1990) American Chemical Society.
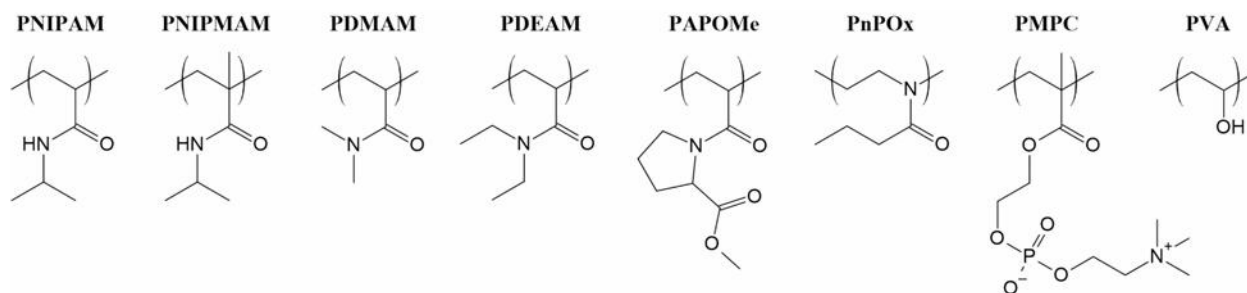
Figure 7. Chemical structure of polymers reported to show co-nonsolvency behavior when exposed to mixed aqueous solvent systems. PNIPAM: poly(*N*-isopropyl acrylamide), PNIPMAM: poly(*N*-isopropyl methacrylamide),[5] PDMAM: poly(*N*,*N*-dimethyl acrylamide),[72,87] PDEAM: poly(*N*,*N*-diethyl acrylamide),[88] PAPOMe: poly(acryloyl-L-proline methyl ester),[89] PnPOx: poly(2-n-propyl-2-oxazoline),[25] PMPC: poly(2-methacroyloxyethyl phosphoryl choline),[90,91] PVA: poly(vinyl alcohol).[92,93]

Poly(*N*-isopropyl methacrylamide), PNIPMAM, has a very similar chemical structure to PNIPAM, differing solely by the presence of an additional methyl side group attached to the backbone of the polymer. Unsurprisingly, PNIPMAM also shows LCST-type thermoresponsive behavior in aqueous media. While the presence of the additional hydrophobic moiety could lead to the expectation that its transition temperature would be lower than for PNIPAM, PNIPMAM in fact has an LCST considerably higher: ca. 44°C in pure water (compared to ca. 32°C of PNIPAM).[28]

Although the transition temperature of PNIPMAM suffers little influence from changes in concentration and molar mass, this influence is nonetheless more pronounced than for PNIPAM, with transition temperatures reportedly varying between 42 and 45°C when concentration is varied between 2 and 150 g·L^{-1}.[28,94] Moreover, the phase transition of PNIPMAM is known to be less well defined than that of PNIPAM, with the transition occurring more slowly and with considerable hysteresis, as opposed to the sharp transition of PNIPAM.[95,96]

PNIPMAM hydrogels have been reported to show co-nonsolvency behavior in water/ethanol mixtures, evidenced by a depression of its degree of swelling (*Q*) at room temperature when ethanol is present in water. In the study performed by Alenichev et al.[97], the authors found that both PNIPAM and PNIPMAM networks showed a minimum *Q* at ethanol volume fractions of ca. 0.33. Similarly, PNIPMAM films have also been reported to show co-nonsolvency behavior upon exposure to mixed water/methanol atmospheres, with a two-step film contraction when exposed to 70/30 water/methanol vapor flow.[5] Co-nonsolvency of PNIPMAM solutions, however, has not been extensively investigated. The few published reports have limited the investigations to water/ethanol mixtures, and have discussed the phenomenon only superficially.[98,99]

Contrary to PNIPAM, the *N,N*-substituted acrylamide poly(*N,N*-dimethylacrylamide) (PDMAM) does not show co-nonsolvency behavior in water-methanol mixtures, but shows UCST-type co-nonsolvency in 45-90 wt.% of 1,4-dioxane or acetone in water.[87] This behavior is interesting for the fact that chain collapse takes place upon cooling (UCST-type), as opposed to heating (LCST-type), as is the case of PNIPAM. Additionally, the effect occurs in cosolvent-rich solutions, as opposed to water-rich solutions in which co-nonsolvency is typically reported to occur for PNIPAM. These differences have been explored by Pagonis et al., who obtained complex behavior in copolymers of PDMAM and PNIPAM, showing either or both LCST- and UCST-type behavior, depending on the composition of the copolymer.[72]

Similarly, the diethyl acrylamide analogue of PDMAM, poly(*N,N*-diethylacrylamide) (PDEAM), does not show co-nonsolvency in water/methanol, but the phenomenon is observed for the polymer in water/ethanol,[100] water/isopropanol and water/n-propanol mixtures.[88] The authors attributed this behavior to fact that the alcohols, particularly those with larger hydrophobic moieties, replace part of the water in forming hydrogen bonds with the polymers, thus rendering the entire gel network more hydrophobic and driving the transition temperature to lower values.[88]

Poly(acryloyl-L-proline methyl ester) (PAPOMe) has also been reported to show co-nonsolvency behavior in aqueous mixtures with methyl, ethyl, propyl, and t-butyl alcohols.[89] For all alcohols, a gradual shrinking of PAPOMe gels can be seen when alcohol content in the solvent mixture is increased from 0 to 20 vol.%. In this range, interestingly, no significant difference can be seen between the various alcohols. Upon further increase of alcohol content, reswelling is seen in the alcohol range of 30 to 43 vol.%. Finally, in the range of 80 to 100 vol.% of alcohol, a partial shrinking is recorded. Differently from the low alcohol content range, within 30 to 100 vol.% of alcohol, significant variances can be seen between the investigated alcohols, which can be plausibly correlated to the hydrophobicity of the solvents.

Pooch et al.[25] investigated the potential co-nonsolvency behavior in aqueous methanol of poly(2-cyclopropyl-2-oxazoline) (PcyPOx) and two structural isomers of PNIPAM: poly(2-isopropyl-2-oxazoline) (PiPOx) and poly(2-*n*-propyl-2-oxazoline) (PnPOx). While no co-nonsolvency behavior was identified in PcyPOx and PiPOx, PnPOx did show a decrease of its transition temperature upon increase of methanol content in water from 0 to 35 vol.%, in a quite similar fashion as is observed for PNIPAM. The fact that one structural isomer of PNIPAM shows co-nonsolvency (PnPOx), while another one does not (PiPOx) was explained by the authors as a result of the degree of freedom of the polymer chains, which is much larger for PnPOx than PiPOx.

These results provide interesting insights regarding the influence of chemical structure on co-nonsolvency behavior and raise the question about the type of effects that could be achieved through other structural variations on the constitutional repeat unit. For example, another PNIPAM structural isomer, poly(*N*-vinyl isobutyramide) (PNVIBAM), also shows thermoresponsivity in water, although with LCST somewhat higher than PNIPAM (ca. 39°C), despite the presence of the same chemical moieties.[29] While Akashi and coworkers have briefly mentioned the co-nonsolvency behavior of PNVIBAM in water/ethanol mixtures,[30,101] no details have been published.

Besides the several examples of co-nonsolvency in mixed aqueous solutions from polymers exhibiting LCST-type thermoresponsivity, the behavior has also been reported for UCST-type thermoresponsive polymers. Examples include the polyzwitterions poly(2-methacroyloxyethyl phosphoryl choline) (PMPC), which shows UCST co-nonsolvency in aqueous solutions with 35-80% alcohol,[90,91,102] and poly[3-((2-(methacryloyloxy)ethyl)dimethylammonio) propane-1-sulfonate] (PSPE), which shows UCST co-nonsolency in water/methanol mixtures.[5] Moreover, poly(vinyl alcohol) (PVA) also shows UCST co-nonsolvency in water/DMSO mixtures, with maximum gelation and phase separation at 60 vol.% of DMSO.[92]

Suggested Mechanisms

Despite the numerous of studies that have investigated the co-nonsolvency phenomenon of polymers in mixed aqueous solutions, its underlying causes, and the mechanism through which it occurs is still very much under debate. Various research groups have proposed theories based on theoretical calculations, molecular simulations, and experimental findings, but none has been awarded general acceptance.

Through microcalorimetric studies, Schild et al. (1991) found that the addition of the cosolvent reduces the enthalpy of the phase transition endotherm, indicating that the number and/or strength of polymer-water contacts are reduced.[14] Based on the three-component solubility parameters, Mukae et al. (1994) found that the swelling degree of PNIPAM gels is consistent with the magnitude of the hydrogen bonding component of the solubility parameter of the organic solvent (comparing acetonitrile, dioxane, THF and DMSO). Thus, it seems hydrogen bonding is a predominant interaction defining the solubility of the polymer in said organic solvents. These differences, combined with the specific interactions between water and each cosolvent, may lead to the different co-nonsolvency behaviors found in each solvent mixture.[71]

Water - Cosolvent Complexes

Zhang et al. (2001) studies in extremely dilute solutions suggested that co-nonsolvency is a result of the formation of water-methanol complexes, which are stronger than interactions of the individual solvents with the polymer, thus making the mixture a poor solvent for PNIPAM.[103] Young and Chuang (2002) suggested a similar explanation for the co-nonsolvency of PVA in water-DMSO.[93] Pang et al. (2010) reinforced this claim with molecular dynamics simulations, showing that water-methanol clusters are most abundant in the mixture compositions at which co-nonsolvency of PNIPAM takes place.[17] Bischofberger et al. (2014) proposed a similar theory, claiming that the cosolvents act as kosmotropes, strengthening the hydrogen bonded water network, which is unfavorable to the hydration of the hydrophobic moieties of the polymer.[104]

Competitive Binding

In 2005, Okada and Tanaka concluded that the phase behavior of PNIPAM in water is a result of sequential polymer-water hydrogen bonds along the polymer chain, termed cooperative hydration.[105] The group then later (2008-2011) asserted that co-nonsolvency is originated by a competition between water and cosolvent on forming hydrogen-bonds with the polymer. This was based on a statistical-mechanical model which showed that co-nonsolvency takes place at the same methanol fraction where a depression on the number of hydrogen bonds along the polymer chain occurs.[18,106,107] A similar theory has been proposed by Pica and Graziano (2016), who specified that the competition between water and cosolvent on forming attractive interactions with the polymer reduces the overall attractive energy due to basic geometric limitations.[108] Similarly, Dalgicdir et al. (2017) claimed that the interactions between methanol and the isopropyl group of PNIPAM geometrically hinders the hydrogen-bonds between water and the amide of the polymer.[109] According to the authors, configurational entropy further contributes to the co-nonsolvency effect, given that methanol-enriched polymer globules have an increased configurational entropy compared to the polymer globules in pure water. In turn, lower temperatures suffice to overcome the energy of polymer-solvent interactions (achieving $\Delta G_m < 0$), lowering the transition temperature.[110] In 2020, Tavagnacco et al.[111] provided further support to the competitive interaction hypothesis, through atomistic molecular dynamics simulations.

Also in 2020, Grinberg et al.[112] suggested an extension to the Okada and Tanaka theory, combining features of competitive binding, water-solvent complexes and typical Flory-Huggins interaction parameter behavior.[105,106] The authors claimed that in the low methanol content range

phase transition is caused by the melting of the water-polymer cooperative hydration, which intensifies with increasing methanol fraction, due to the formation of water-methanol complexes. Beyond a critical methanol content (where the T_{CP} of PNIPAM reaches its minimum), phase separation then follows the typical Flory-Huggins interaction parameter behavior, where solvent quality decreases with temperature, as is usual for polymer solutions in organic solvents.

Preferential Adsorption, Forming a Hydrophobic Shell

In a contrasting mechanism, Walter et al. (2012) proposed that the formation of strong hydrogen-bonds between the polymer and the cosolvent (preferential adsorption) are in fact responsible for the co-nonsolvency effect.[20] The authors argued that, since hydrogen bonds occur between the polar moieties of the polymer and the cosolvent, this would result in the cosolvent molecules being oriented such that the nonpolar moieties (specifically the methyl group of methanol) are facing outwards. Therefore, the system polymer + cosolvent shell appears rather hydrophobic, thus driving the chain collapse.

Preferential Adsorption, Leading to Bridging

The concept that preferential adsorption may be responsible for the chain collapse has further been supported by Heyda et al. (2013).[113] From theoretical models the authors determined that strong polymer-cosolvent interactions induce the collapse of the chains. However, instead of the formation of a hydrophobic shell, they suggested that the polymer coil collapse is a result of cross-linking-like bridging effects of the polymer by the cosolvent, a model which has been supported by some research groups,[114-117] albeit rebutted by others.[118]

2.3. Synthesis of Polymers Exhibiting Co-nonsolvency Behavior

Synthesis of homopolymers exhibiting co-nonsolvency behavior can be done in a variety of ways, including step-growth polymerizations (such as polycondensation and polyaddition) as well as chain-growth polymerizations (such as free-radical or ionic polymerizations), depending on the monomer to be polymerized. However, given that factors such as molar mass, molar mass distribution and end-groups can impart a strong influence over the behavior of the polymer in solution,[59,119] it is often important to hold some level of control over the polymerization and reduce side reactions, thus providing known end-groups, narrower molar mass distribution, and controllable molar masses. For this end, living ionic polymerizations and controlled radical polymerizations tend to offer best results.[120]

Although living anionic polymerization works very well for non-polar monomers (e.g., styrene), it is more difficult on polar monomers, such as *N*-isopropyl acrylamide and most other monomers which generate thermoresponsive polymers. To allow this type of polymerization, protection of the acidic amide proton[121,122], careful solvent selection, and thorough elimination of impurities is required. Because of these challenges, radical polymerization has been a popular method for the synthesis of thermoresponsive polymers, as it is a less sensitive and less selective method, allowing the polymerization of a wider range of monomers and is especially suited for the monomers studied in this thesis: styrene, methyl methacrylate (MMA), *N*-isopropyl acrylamide (NIPAM), *N*-isopropyl methacrylamide (NIPMAM), and *N*-vinyl isobutyramide (NVIBAM). Moreover, through variations of the free radical polymerization method, namely controlled radical polymerizations (e.g., RAFT, ATRP, NMP), it is possible to achieve a level of control over the molar mass, molar mass distribution and control of side reactions comparable to those of living ionic polymerizations, with the added benefit of facile synthesis of copolymers.

Thus, the following sections are focused on describing the two methods utilized for the synthesis and of homo- and copolymers studied in this thesis: free radical polymerization and a type of Reversible-Deactivation Radical Polymerization (RDRP) method called Reversible Addition Fragmentation Chain Transfer (RAFT).

2.3.1. Free Radical Polymerization – FRP

Free radical polymerization is a chain growth polymerization method, where the constitutional repeat units are consecutively incorporated to a growing chain through addition reactions, leading to long polymer molecules, depending on the reactivity of the monomer. Differently from the highly selective anionic and cationic polymerizations, radical polymerization can be applied to almost any monomer containing a double bond, while simultaneously being less sensitive to the choice of solvent and to the presence of trace impurities.[123]

The conventional free radical polymerization method is composed of three steps: initiation, propagation, and termination. During initiation, a free radical first needs to be generated. This is often achieved by homolytic dissociation of an initiating species (initiator), which may be done by thermal, photochemical, or redox means, being thermal the most common. Among the known free radical initiators, peroxides and azo compounds, more specifically dialkyldiazenes, alkyl derivatives of diazene, are the most widely used. Depending on the variations on their chemical structure, these initiators offer a wide selection of dissociation rates and, consequently, activation temperatures. This, combined with their relatively high stability for storage, are the factors contributing to their high popularity.[39,124] The category of azo initiators includes the ones used in

this thesis: 2,2′-azobis(2-methylpropionitrile) (AIBN), dimethyl-2,2'-azobis(2-methylpropionate) (MAIB), 1,1'-azobis(cyclohexane-1-carbonitrile) (V40), 2,2'-azobis(2-methylpropionamidine)dihydrochloride (V50), and 2,2'-azobis(4-methoxy-2,4-dimethylvaleronitrile) (V70). Their homolytic dissociation reaction and 10 h half-life decomposition temperatures are shown in Figure 8.[125-129] Alternative to the use of an external initiator, a few monomers offer the possibility of self-initiation. The most well-stablished case for this is styrene, where self-initiation occurs thermally, through the formation of a Diels-Alder dimer, with subsequent transfer of one of its hydrogens to another styrene molecule.[130-132] After formation of the initiating species, a polymer chain is then initiated, in which the initiating species I* adds to the π bond of the monomer to form a new radical.

In the second step of the free radical polymerization, propagation, new constitutional repeat units are repeatedly added to the growing chain. One of the advantages of radical polymerization is that propagation rate constants, that is, the speed at which the growth of the polymer chain occurs, are typically much larger than those of step growth polymerization.[124]

Polymer chains typically grow for about 5 to 10 seconds before terminating,[133] which constitutes the third step of the free radical polymerization process. Termination may occur in various ways, depending on the type of radical and on the reaction conditions. Recombination is the most common termination method, and the almost exclusive termination process for monomers such as styrene, for example. During recombination, as the name implies, two polymeric chains with active radical species are combined, resulting in one chain with larger molar mass. The second most common termination method is called disproportionation. Here, a hydrogen radical which is beta to the radical center is transferred to a radical center of another growing chain, annihilating both radicals and resulting in 2 chains, one of which is saturated. Disproportionation is particularly favoured when there is steric hindrance, for example in the polymerization of methyl methacrylate (MMA), and also upon increase of reaction temperature.[124]

Although termination rates are typically much higher than propagation rates, since the concentration of radicals is quite low (steady state around 10^{-7} M), the formation of long polymer chains is still possible. Moreover, since termination requires two active chains to occur, the polymerization rate is dependent on the square root of the termination rate constant.[133]
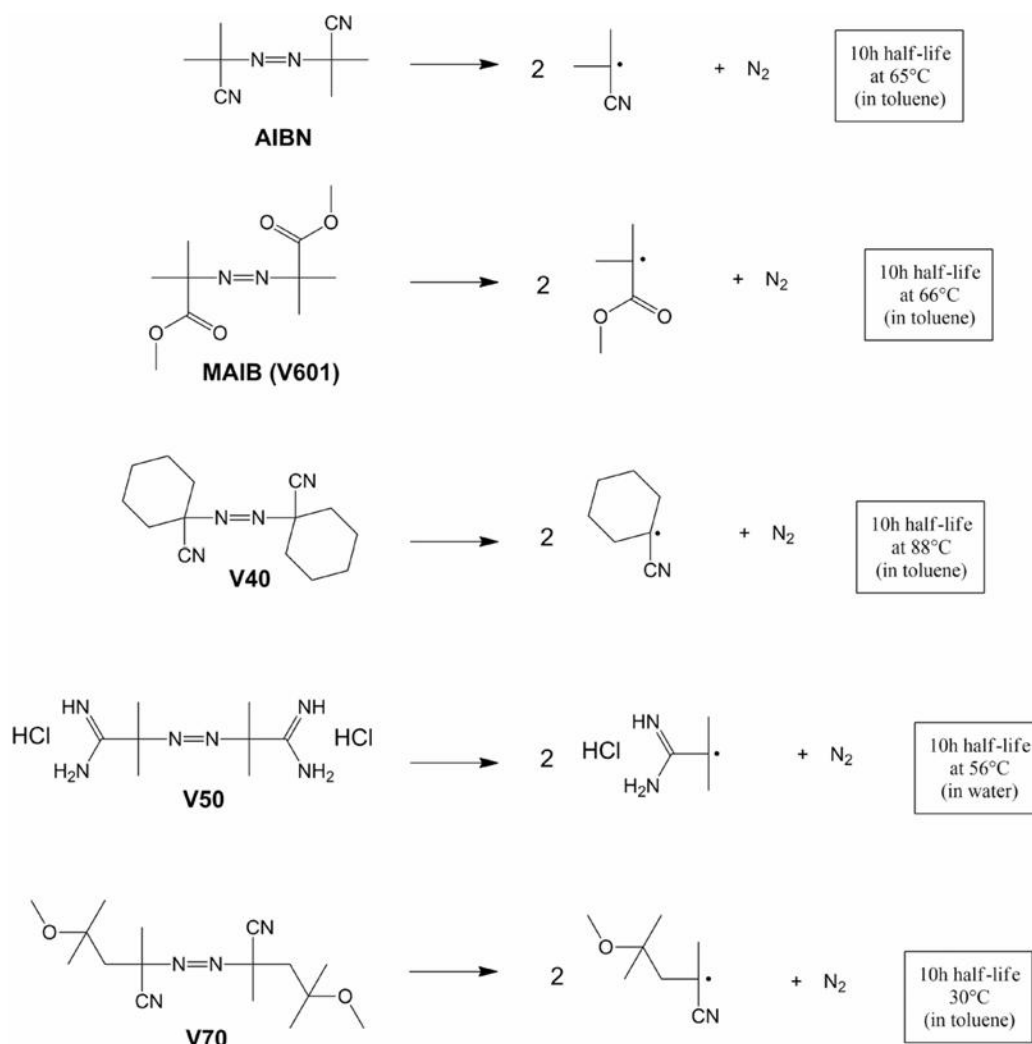
Figure 8. Homolytic dissociation and half-life of the dialkyldiazenes (azo) initiators used in this thesis.

Conventional free radical polymerizations typically lead to molar mass distributions ($Đ = M_w \cdot M_n^{-1}$) considerably broader than those of ionic polymerizations, with $Đ$ above 1.5 or even 2.0. This is a result of the aforementioned termination processes (absent in ionic polymerizations), as well as a number of possible side reactions and monomer depletion effects. Monomer depletion, that is, the reduction of monomer concentration over the course of the polymerization reaction, causes a considerable variation in molar mass of the formed chains, with the first polymer molecules having significantly larger molar masses than the last.[133]

One of the most common unwanted reactions occurring during free radical polymerization are chain transfer reactions. Here, the radical center is transferred to monomer, solvent, initiator, impurities or even to another polymer chain (leading to branching). Due to the potential detriment in polymer architecture, as well as molar mass and molar mass distribution, minimization of chain transfer reactions is an important factor when choosing the solvent for a radical polymerization: solvents such as benzene, for example, show some of the lowest chain transfer constants.

Inhibition and retardation may also occur when undesired substances are present, as these may react with the active radical species and supress the polymerization. Since oxygen is one of the most common inhibitors, radical polymerizations are typically conducted under inert gases such as nitrogen and argon or under vacuum.[133]

Depolymerization is also an important process to consider. While polymerization is strongly favoured at low temperatures, depolymerization becomes more prominent at higher temperatures, eventually reaching a so-called ceiling temperature, where the polymerization-depolymerization processes are in equilibrium, and above which the depolymerization is favoured. For styrene, for example, this the ceiling temperature is 310°C, while for MMA it is 220°C. However, for some monomers, this temperature may be so low, that their polymerization is practically impossible.

Despite its various hurdles, free radical polymerization is the most industrially relevant polymerization technique and is also still widely used in academia. It allows the facile synthesis of homopolymers, and may produce alternating, statistical, or random copolymers, depending on the copolymerization parameters of the monomers.[134] Also block copolymers structures may be obtained through more complex processes, for example through chain extension of a homopolymer with functional end-groups (where the first homopolymer acts as a macroinitiator) or reacting functional end-groups of two homopolymers.

2.3.2. Reversible-Deactivation Radical Polymerization – RDRP

Reversible-deactivation radical polymerizations (RDRP) or controlled radical polymerizations are processes based on conventional free radical polymerization. However, RDRP facilitate the synthesis of polymers with more complex molecular architecture, provide increased level of control over molar mass, and allow narrower molar mass distributions, which may be as low as Đ 1.1. To achieve this, RDRP relies on an equilibrium between a small number of active growing chains and a large number of dormant or deactivated chains, which cannot propagate, but also not terminate. Since the chains are constantly and quickly switching between the two states (quicker than the lifetime of the radical), the growth of most chains occurs in parallel, instead of one chain being initiated, growing and terminating, before other chains have even been initiated. With this, all chains have statistically equal chances to grow (leading to low Đ), and molar masses increase linearly with conversion, which allows control over the desired molar mass.[133]

Moreover, these methods often reduce the effect of bimolecular termination reactions, since the concentration of active radicals is much smaller than the concentration of growing chains in RDRP, in contrast to conventional free radical polymerization.[123] Because of this, RDRP processes are often attributed the label "living radical polymerization". However, this label is incorrect because,

differently from ionic polymerization, bimolecular chain termination still occurs, even if less prominently noted.

Another benefit of RDRPs is that, after the polymerization is stopped, the dormant chains can be reactivated to continue polymerizing. This can be exploited to perform multiple consecutive polymerizations, that is, the polymer chains obtained from one monomer can be chain-extended with another monomer to obtain block copolymers.[34]

Within RDRP, three methods stand out: ATRP, NMP, and RAFT, which differ in the way the reversible deactivation is achieved.

In atom transfer radical polymerization (ATRP), an alkyl halide-based initiator and a redox-active transition metal catalyst, often Cu(I), are used. Here, atom transfer is responsible for the reversible deactivation of propagating radicals. This method offers relatively broad applicability, in that it can be performed on various types of monomers. However, there are some limitations on monomers with hydrophilic functional groups, as well as limitations in solvents. Moreover, the transition metal catalysts used in ATRP typically need to be removed post-polymerization, due to their toxicity.[135]

Nitroxide mediated polymerization (NMP), in contrast, makes use of stable nitroxyl radicals, such as TEMPO, with radical-radical reaction leading to the deactivation of the growing chain. This process, also often called stable free radical polymerization (SFRP), is particularly useful for the polymerization of styrene, although not optimal for other monomers, such as methacrylates, and vinyl acetate.[135]

Finally, in reversible addition fragmentation chain transfer (RAFT) the growing chain is deactivated through degenerative chain transfer of its active radical to a dithioester chain transfer agent, and subsequently to another polymer chain. RAFT offers the broadest applicability, being viable for monomers with a wide range of functional groups, at various temperatures and in various solvents.[135] RAFT is the process which was used to obtain the block copolymers discussed in this thesis, and will therefore be covered in more detail in the following section.

2.3.3. Reversible Addition Fragmentation Chain Transfer – RAFT

Reversible addition fragmentation chain transfer (RAFT) polymerization was developed in 1998 by Ezio Rizzardo, Graeme Moad, San H. Thang and coworkers from the Commonwealth Scientific and Industrial Research Organisation (CSIRO) in Australia.[136] RAFT is a type of reversible-deactivation radical polymerization (RDRP) in which a dithioester chain transfer agent (CTA or RAFT agent) is added to a traditional free radical polymerization monomer and initiator system.[137] With this, chain transfer reactions, which typically occur but are unwanted during

conventional free radical polymerization can be exploited, yet made reversible. With this, a large portion of the chains are kept in a dormant state, with rapid equilibrium between the active and dormant states. As a consequence, molar mass increases linearly with conversion, and it is therefore possible to predict the number-average degree of polymerization (DP_n) based on the monomer conversion (C), and the initial concentrations of monomer $[M]_0$ and CTA $[CTA]$ in the system:[124]

$$DP_n = C \cdot \frac{[M]_0}{[CTA]} \tag{11}$$

The RAFT method stands out among all RDRP because of its versatility. The CTA contains an initiating R-group and a reactivity-modifying Z-group, which may be designed to control the polymerization of a very wide variety of monomers and may also be used to introduce specific functionalities as end-groups on the polymer chains. Additionally, it is very tolerant to unprotected functionalities in the monomer and solvent, may be performed in the presence of Lewis acids and may even be performed in water, as long as a hydrolytically stable CTA is chosen.[133]

As a caveat, however, RAFT inherently leads to lower molar masses than the conventional free radical process, with maximum M_n around 80~100 kg/mol).[59,138]

RAFT Mechanism

During RAFT polymerization, the same initiation, propagation, and termination processes occur as in conventional free radical polymerization. However, in addition to these, a pre-equilibrium and main equilibrium processes take place, as shown in Figure 9.

First, initiation takes place the same way as in a conventional radical polymerization process: by formation of the initiating species and polymer chain initiation. The RAFT pre-equilibrium process can then occur, in which the radical from the growing polymer chain ($P_n\bullet$) is transferred to the CTA. With this, the intermediate radical structure is formed (Figure 9), where the radical cannot propagate. Ideally, the radical is then transferred to the CTA's R-group, the so-called initiating group, which fragments and can start a new polymer chain. The original polymer chain then stays dormant.[34,133]

In the RAFT main equilibrium, this chain transfer continues to occur, with the active radical center being constantly transferred to another polymer chain. This causes all polymer chains to continuously and rapidly change between active and dormant states. Here, it is important that the rate of addition and fragmentation reactions be higher than the rate of propagation. This provides equal probability for all polymer chains to propagate, leading to low molar mass distributions.[138]

As shown in Figure 9, all addition and fragmentation reactions are reversible, and the likelihood of the reaction following the desired route, as opposed to the undesired reverse route, is determined by suitability of the CTA's R and Z groups with respect to the monomer being polymerized.[34] Ideally, at the end of the reaction (upon quenching or full consumption of monomer) all polymer chains retain a CTA molecule as end-group, remaining as dormant polymer chains (Figure 9). These can then be reactivated for chain extension, for example, with a different monomer, yielding block copolymers. If the dithioester end-groups are undesired in the end product, a number of methods have been described for its removal.[139,140]
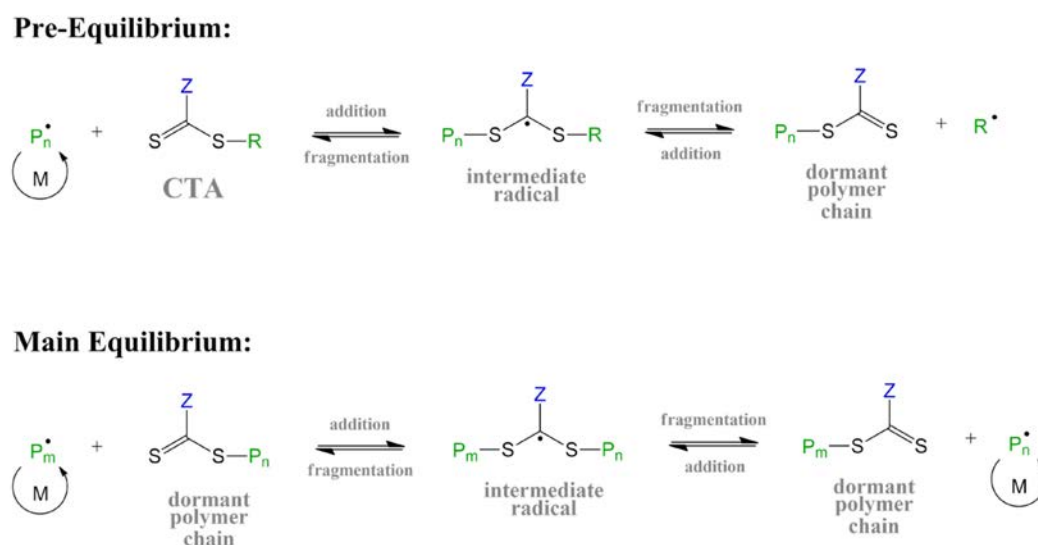
Figure 9. Mechanism of RAFT polymerization (adapted from Moad et al.[133]*).

Although the CTA's R group is an initiating group, in RAFT it is necessary that an active radical first be formed externally, so it can then react with the CTA and release the R-group, which will initiate more chains. This means addition of a radical initiator is still necessary. However, since the CTA also gives functional end-groups, it is important to use as little initiator as possible, to avoid chains which do not contain the CTAs end-groups. Thus, the proper balance must be found. [133]

Similarly, it is important to keep in mind that while some time is necessary for the RAFT process to start and achieve the main equilibrium, prolonged reaction times may however lead to loss of end-groups.[133]

---

* Used with permission of CSIRO Publishing, from "Living Radical Polymerization by the RAFT Process", Graeme Moad, Ezio Rizzardo and San H. Thang, 58, 6, 2005; permission conveyed through Copyright Clearance Center, Inc.

Monomer Activity Level: MAMs and LAMs

One of the most important factors to consider when planning a RAFT polymerization is the reactivity of the monomer to be polymerized, which will determine the choice of CTA to be used. To facilitate this task, monomers are typically divided into two groups: more activated monomers (MAMs) and less activated monomers (LAMs).

On MAMs, an electron withdrawing group or other stabilizing moiety is conjugated to the double bond.[138] In turn, these form more stable radicals, and therefore good leaving groups, leading to generally low rates of addition and high rates of fragmentation on the RAFT process. To compensate these characteristics, MAMs require more active CTAs, which increase the rates of addition and decrease the rate of fragmentation. If the CTA is chosen poorly, MAMs may polymerize without enough interaction with the CTA, providing some level of control over the molar mass, but little to no control over the molar mass distribution.[35] This class of monomers is by far the most reported for RAFT, and includes acrylics, methacrylics, styrenes, acrylamide, methacrylamide and acrylonitrile, thus comprising most of the monomers discussed in this thesis: styrene, methyl methacrylate (MMA), *N*-isopropyl acrylamide (NIPAM), and *N*-isopropyl methacrylamide (NIPMAM).

On LAMs, however, the double bond is adjacent to an electron donating group, such as an oxygen or nitrogen with lone pairs, or a saturated carbon. In turn, these are very reactive radicals, and bad leaving groups.[138] This causes high rates of addition and low rates of fragmentation on the RAFT process. To counterbalance these effects, LAMs require less active CTAs, which will cause the radicals to be added to the CTA less quickly and promote its more frequent fragmentation. A poor CTA might in turn lead to inhibition of the polymerization, as the radical (growing chain) would be added to the CTA and possibly never fragment again, hindering propagation of the polymerization.[35] This family of monomers includes vinyl esters and vinyl amides, as is the case of the monomer *N*-vinyl isobutyramide (NVIBAM), which is extensively discussed in this thesis. Besides guiding the choice of RAFT agent, the monomers' activity level also determines the sequence in which different monomers should be copolymerized: more activated monomers should always be polymerized first, and less activated monomers last. Since MAMs are better leaving groups, when the new monomer (LAM) is added, the poly(MAM) will easily fragment from the CTA and allow re-initiation of the polymerization. Whereas if LAMs were to be polymerized first, the poly(LAM) would be less prone to fragment from the CTA, remaining in the dormant state while the polymerization of the MAM monomer occurs without any interaction with the CTA (homopolymerization as opposed to copolymerization).[34,35]

Here it is important to highlight that despite the classification of monomers in these two distinct families, monomer activity level is not a "black or white", "all or nothing" classification, but rather a gradient. That is, some MAMs will be considerably more active than others, just as some LAMs will be considerably less active than others, and some monomers will inevitably lie close to the middle of the separation between MAMs and LAMs. Thus, the polymerization sequence (more activated monomers first and less activated monomers last) must be chosen correctly not only in the case of copolymerization between MAM and LAM monomers, but also when both monomers are MAMs, or both monomers are LAMs. Although in these cases an incorrect polymerization sequence might be less critical than in the case of a poly(MAM)-*b*-poly(LAM), there is still a higher chance of success if the slightly more active monomer is polymerized before the slightly less active monomer. [34,35]

Chain Transfer Agent Design

As mentioned before, the versatility of the RAFT process, and the fact that it can be applied to a wide range of monomers with different activity levels can be attributed to the flexibility of choosing a CTA with correspondingly adequate activity level. The effectiveness of a CTA in controlling the polymerization of a particular monomer is determined by the CTA's R-group (the initiating group) and Z-group (the reactivity-modifying group). Vast literature is available to assist on this selection,[34,35,133,138,141-143] as well as commercially available CTAs suitable for a variety of monomers in both MAM and LAM categories.[35,138]

The Reactivity-Modifying Z-Group

While the RAFT process is made possible by the reactive C=S bond on the dithioester of the CTA, the selection of Z-group allows tuning this reactivity, modifying the addition and fragmentation rates to suit the levels required for the monomer which will be polymerized. Stabilizing Z-groups promote chain addition (formation of intermediate radical), but an intermediate radical which is too stable might cause retardation.[35] Some of the most common types of Z-groups used for RAFT polymerization are dithiobenzoates, trithiocarbonates, dithiocarbamates, and xanthates, as shown in Figure 10.
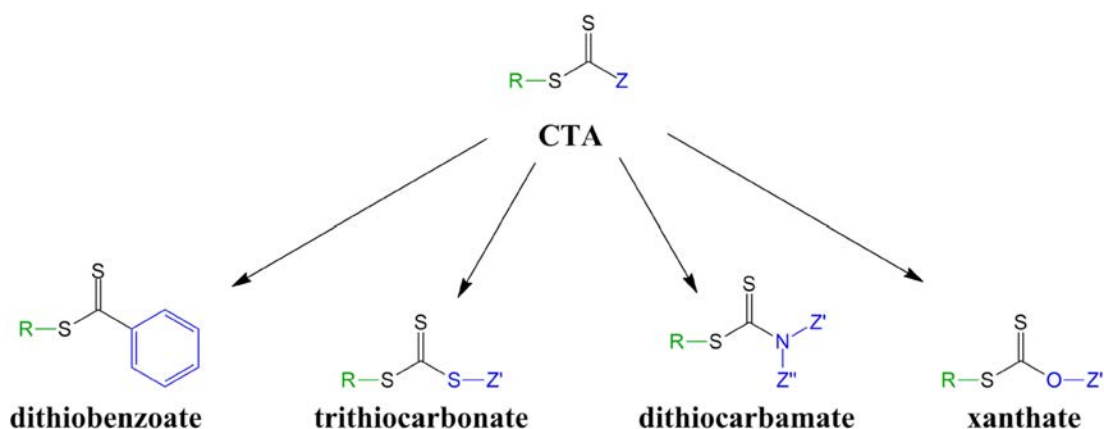
Figure 10. Some of the most common types of RAFT agents, based on the Z-group (in blue).[138]

Dithiobenzoates are some of the most well-known Z-groups, with typical use on the polymerization of very activated monomers, such as methacrylate and methacrylamide monomers. These CTAs generally have very high transfer constants, are prone to hydrolysis and show a bright pink color. Due to the high stability of the intermediate species, these CTAs often act as "radical sinks", causing retardation when present in high concentrations.[138,144]

Trithiocarbonates also lead to high transfer constants, although slightly lower than dithiobenzoates, while being slightly more hydrolytically stable and causing less retardation. For these reasons, trithiocarbonates are the most common type of Z-groups. These CTAs show a bright yellow color, and are commonly used in the polymerization of styrenes, acrylates, and acrylamides (i.e., MAMs).[138,144]

Dithiocarbamate Z-groups, in turn, lead to CTAs which are often colorless and have generally lower activity levels, resulting in their common use for the polymerization of electron rich monomers, that is, LAMs. However, the activity level of dithiocarbamate CTAs may vary widely depending on the substituents on the nitrogen.[145] A similar activity level (and tunability thereof) is achieved with xanthate CTAs. The RAFT process in which the dithioester is a xanthate is termed macromolecular architecture design by interchange of xanthates (MADIX). Such xanthate CTAs are typically colorless and have lower transfer constants, being suitable for the polymerization of LAMs. However, similarly as for dithiocarbamates, the activity levels of xanthates may be increased considerably by introduction of electron withdrawing substitutes.[146] An overview of the activity level of various Z-groups which are frequently reported in literature is depicted in Figure 11.
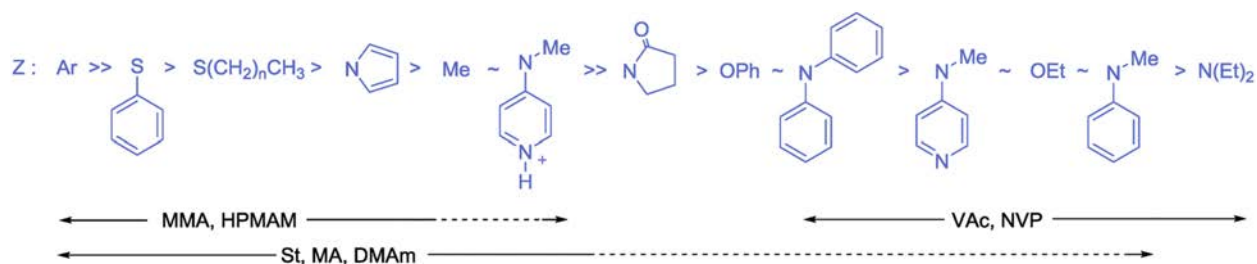
Figure 11. Suggested suitability of various Z-groups for the controlled polymerization of different monomers, by Daniel J. Keddie.[34]* Solid lines represent good control and dashed lines represent poor control, leading to potentially broader molar mass distributions of the MAMs. MMA: methyl methacrylate, HPMAM: *N*-(2-hydroxypropyl) methacrylamide, St: styrene, MA: methyl acrylate, DMAm: *N,N*-dimethylacrylamide, VAc: vinyl acetate, NVP: *N*-vinyl pyrrolidone.

The typically low activity level of dithiocarbamates and xanthates, and the reason why these are generally more suited to control the polymerization of LAMs, lies on the zwitterionic canonical forms of their structures, reducing the reactivity of the CTA towards radical addition (Figure 12). However, this can be avoided whenever the lone electron pairs on the N and O are prevented from delocalizing with the C=S double bond, for example, in the cases where the nitrogen or oxygen are part of an aromatic ring or if the substituents are electron withdrawing moieties, e.g., if a carbonyl group alpha to the nitrogen.
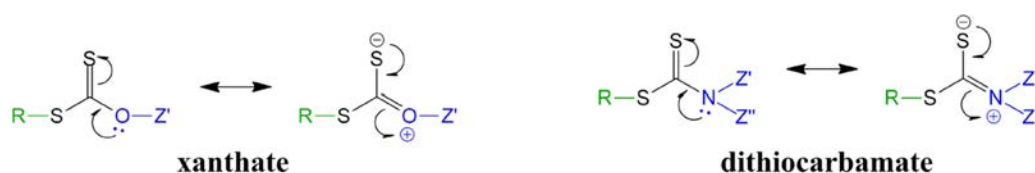
Figure 12. Zwitterionic canonical forms of chain transfer agents with a lone electron pair adjacent to the thiocarbonyl group (adapted from Daniel J. Keddie [34]*).

Through this type of tuning, one could achieve a dithiocarbamate CTA which is best suited to the control of the polymerization of MAMs than that of LAMs, or achieve a CTA that is "universal", with broad applicability, offering acceptable control over the polymerization of both MAMs as well as LAMs, although with somewhat limited efficiency in one or both cases.[133,145-149] Such CTAs are of great interest since they allow synthesis of poly(MAM)-*b*-poly(LAM) copolymers,

---

which would otherwise be impossible to achieve through purely MAM or purely LAM CTAs. Some of the most promising examples of such "universal" CTAs are those containing 3,5-dimethylpyrazole Z-groups, or derivatives thereof where an halogen substituent (electron withdrawing) is introduced in the 4 position of the pyrazole ring.[145,150,151] An overview of various dithiocarbamate Z-groups reported in literature, and their respective activity levels is depicted in Figure 13.[150,151]
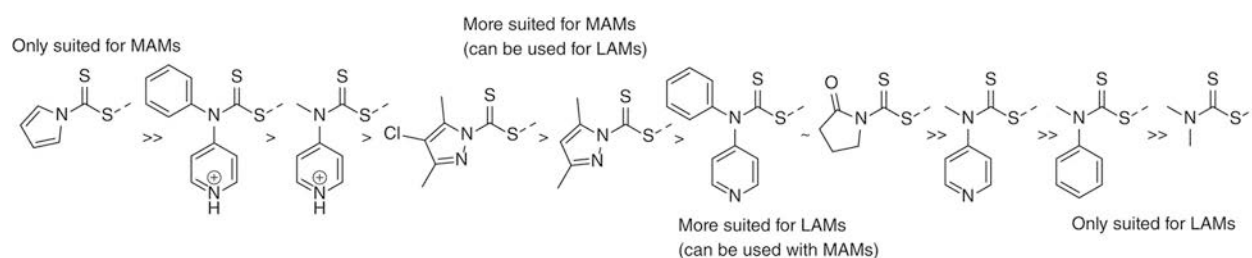
Figure 13. Suitability of dithiocarbamate Z-groups for the controlled polymerization of more activated monomers (MAMs) and less activated monomers (LAMs), from Gardiner et al.[151]*

Another possibility for controlling the polymerization of both MAMs and LAMs, thus obtaining poly(MAM)-*b*-poly(LAM)s, are switchable CTAs, which is usually achieved through protonation and deprotonation of the Z group. The most common example thereof is the pH-switchable *N*-aryl-*N*-(4-pyridinyl)dithiocarbamate, which offers acceptable control over the polymerization of MAMs when protonated, and is suitable to polymerize LAMs in their deprotonated state, as shown both in Figure 11 and Figure 13.[35,138]

The Initiating R-Group

Despite the immense impact of the Z-group on the effectiveness of a CTA for the control of the polymerization of a particular monomer, the R-group is also relevant in this regard. The R–S is a weak single bond, and once cleaved, the R-group must be able to initiate the polymerization of the monomer in question. Very importantly, the R-group must be a good homolytic leaving group in comparison to the growing polymer chain, to ensure its fragmentation from the intermediate radical is favored over the fragmentation of the growing chain. As for any leaving group, the fragmentation tendency of R is improved in the order primary < secondary < tertiary radical center.[35] Thus, as illustrated in Figure 14, it is not enough for R to be a monomeric equivalent of

the propagating chain. This is especially unfavorable in case the radical is on a tertiary carbon in the growing chain, whereas its monomeric equivalent R-group would generate a secondary radical, less prone to fragmentation. Additionally, penultimate unit effects may also disfavor the fragmentation of a monomeric equivalent R-group with respect to the polymeric chain. Thus, small R groups are generally less prone to fragmentation than their polymeric equivalents.[34,35,133]

If chosen poorly, the R-group may lead to broad molar mass dispersities on MAMs due to inferior homolytic leaving group ability, or retardation due to slow re-initiation of polymerization in the case of LAMs.[34] One common approach for the selection of R-group is to use the initiating species of a suitable initiator. Thus, some of the most common R groups are based on cumyl and cyanoisopropyl moieties.[137]
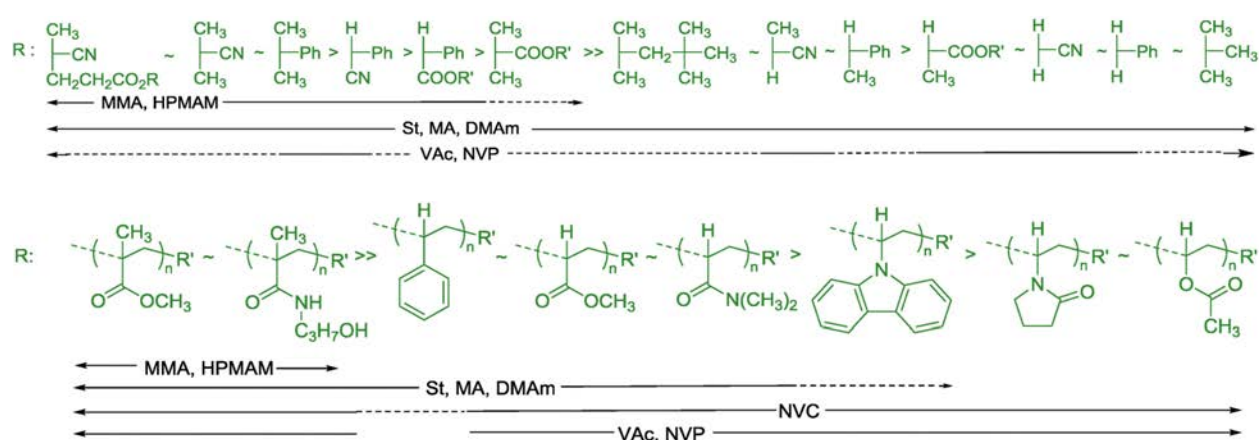
Figure 14. Suggested suitability of various low molar mass R-groups (top) and polymeric-R-groups (bottom) for the controlled polymerization of different monomers, by Daniel J. Keddie.[34]* Solid lines represent good control and dashed lines represent poor control, leading to potentially broader molar mass distributions of MAMs or retardation of the polymerization of LAMs. MMA: methyl methacrylate, HPMAM: *N*-(2-hydroxypropyl) methacrylamide, St: styrene, MA: methyl acrylate, DMAm: *N,N*-dimethylacrylamide, NVC: *N*-vinyl carbazole, VAc: vinyl acetate, NVP: *N*-vinyl pyrrolidone.

Multifunctionality

One of the biggest advantages of RAFT (and other RDRP methods) over conventional free radical polymerization is the ease in obtaining complex polymer structures, such as di-, tri- or multi- block copolymers, multi-arm polymers, polymer brushes, etc. For the straightforward case of AB or ABC block copolymers (where A, B, and C are different polymer blocks), simple monofunctional

---

CTAs can be used. Monomer A is polymerized first, and the obtained polymer is used as a macro-CTA for the polymerization of B (and so subsequently for the polymerization of more blocks). However, when ABA or multi-arm (co)polymers are desired, this may more easily be achieved with multifunctional CTAs. In this case, the CTA contains not one but 2 or more dithioester moieties, connected in one of two possible ways, as depicted in Figure 15. In the Z-approach, the Z-group is in the core or the CTA, and the subsequent polymerization of multiple monomers occurs from the chain ends inwards. This means that the first block to be polymerized will be located at the chain ends, while the last block to be polymerized will be in the middle of the chain. Conversely, in the R-approach, the R group is in the core, and polymerization occurs from the middle of the chain outwards. An example of both cases is shown in Figure 15. Here, ABA or BAB copolymers may be obtained after only two polymerization steps. Symmetrical copolymers containing more than 2 different monomers can also be synthesized this way, and the same concept applies to CTAs with 3 or more functionalities, which yield star-shaped polymers with 3 or more arms, where each arm may be composed of multiple polymeric blocks.[152-155]

The selection between the Z-approach and R-approach should be guided by the degree of activation of the monomers that will be polymerized. This is because the polymerization should be done in a decreasing order of monomer activity level: most activated monomers first and least activated monomers last.[34]
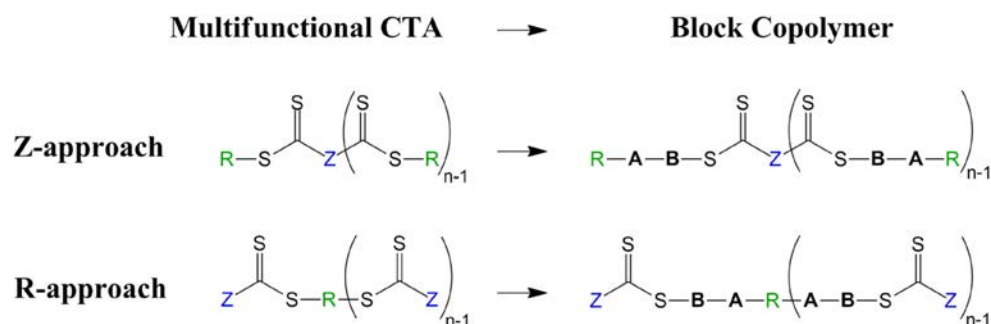
Figure 15. Multifunctional CTAs through Z- and R-approaches, and corresponding obtained block copolymers after two polymerization steps, where n is the CTA's functionality, A is the first polymer block to be polymerized and B is the second polymer block to be polymerized.

Intrinsic and Additional Functionalities

One intrinsic characteristic of RAFT processes is that the CTA is (ideally) incorporated in the majority of the chains as end-groups, opening up various possibilities of characterization and functionalization. Through ^{1}H NMR spectroscopy, it is often possible to compare the ratio of R and Z group signals, each of which would be on one end of the polymer chain, thus determining

the level of loss of end-groups and the "livingness" of the system.[133,138] Moreover, the dithioester moiety itself is a chromophore, serving as label on UV-vis spectroscopy, and allowing facile molar mass determination even at very high molar masses.[156]

The chain transfer agents may also be functionalized beyond simply offering appropriate Z- and R-groups, and instead include any number of labels,[36,157] or even groups which allow subsequent polymerizations through other methods, such as ATRP.[158-160] Such incorporation of additional functionalities is generally done through the R-group, due to the lability of the C-S bond.[35,140] However, this lability may also be explored to achieve functionalization after the polymerization. This can be achieved, for example, through the reaction of the dithioesters with amines or hydroxides to achieve thiols. Alternatively, thermolysis and radical-induced reactions are popular methods for removal of the dithioester moieties.[35,140]

2.3.4. Polymerization of *N*-isopropyl methacrylamide – NIPMAM

Differently from PNIPAM, whose straightforward synthesis has been deeply studied and reported, PNIPMAM has received a minute fraction of the attention. Of the publications reporting the polymerization of NIPMAM, this is mostly performed by conventional free radical polymerization[28,94,96,161-181] and only in a couple of cases by RAFT.[36,37]

In the majority of the cases, the characterization of the obtained polymer is extremely scarce, and often very little information is provided about the polymerization parameters. Based on the information available, only a handful of initiators have ever been used for the polymerization of NIPMAM: AIBN being by far the most common,[28,94,96,161,163,164,166,169,170,174-176] with V501 as second most popular choice,[36,165,167,168,172,180,181] followed by a variety of persulfates.[171,178,179] Accordingly, reactions are generally performed at 60°C,[28,94,96,163,169,172,175,178,179] 65°C,[161,164,166,181] 70°C,[167,179,180] or 75°C.[36,170,174] Reaction times are typically long, mostly ≥ 20 h[37,96,162,167,169,171,175,176,180,181] and up to 2 days.[164] Reported solvents include ethanol (or ethanol/water mixtures),[94,96,161,165,167,168,172,180,181] water,[171,178,179] methanol,[94,163,169] DMF,[162,175] THF,[28,164] acetone,[166,176] isopropanol,[174] and chloroform.[170]

In the publications where molar masses are described, these are generally low, mostly ≤ 20 kg·mol^{-1}.[28,36,37,161,162,166,169,175] One rare exception is a PNIPMAM with M_w 160 kg·mol^{-1} and Đ 1.2, obtained by Ruiz-Rubio et al. by free radical polymerization with ammonium peroxodisulfate as redox initiator and sodium disulfate as accelerator, at 30°C in water for 20 h.[171] Additionally, Netopilík et al. reported a PNIPMAM with M_n 57 kg·mol^{-1}, M_w 96 kg·mol^{-1} and Đ 1.7, obtained with AIBN in ethanol at 60°C for 24 h.[96] In the remaining cases where larger average molar masses are reported, these typically show very high molar mass dispersities (e.g.,

M_w 136 kg·mol^{-1} with $Đ$ 3.67[172]), or are obtained through fractionation[173,175,178], dialysis[163] or gel filtration[177] of a reaction product with broad molar mass distribution.

NIPMAM is also often copolymerized with other monomers[37,161,162,164,166,176,179,180] and/or crosslinkers.[180,181]

So far, only two authors have reported the RAFT polymerization of NIPMAM. Liu et al.[37] copolymerized NIPMAM with (Z)-4-(1-cyano-2-(4-(dimethylamino) phenyl)vinyl)phenylmethylacrylate, using cumyl dithiobenzoate as CTA. The polymerization was performed in NMP at 70°C for 36 h with AIBN as initiator, to give a copolymer with M_n 12 kg·mol^{-1} and $Đ$ 1.23. Meanwhile, Viet Hildebrand[36] homopolymerized NIPMAM in TFE at 75°C for 16 h, using V501 as initiator and a fluorophore-labeled trithiocarbonate RAFT agent (the same as CTA **B**, in this thesis). The author obtained a PNIPMAM of M_n 20 kg·mol^{-1} and $Đ$ 1.3.

Apart from NIPMAM, the polymerization of methacrylamide and *N*-substituted and *N,N*-disubstituted methacrylamides has been vastly reported to present more challenges than their acrylamide analogues. Several authors have attributed this to steric hindrance caused by the additional methyl group adjacent to the double bond.[182-184] However, others have pointed out that anionic polymerization of these monomers is considerably more facile than their radical polymerization. Thus, the difficulties may be more related to the conformation of the C=C bond with respect to the C=O bond, rather than steric hindrance. While acrylates predominantly adopt a s-cis conformation, methacrylamides typically adopt a s-trans conformation.[185-188]

2.3.5. Polymerization of *N*-vinyl isobutyramide – NVIBAM

While literature reports on PNIPMAM are scarce, those discussing poly(*N*-vinyl isobutyramide), PNVIBAM, are yet rarer. The available publications originate almost exclusively from one single research group: since the early 90's Akashi et al. have published a series of papers covering the evolution of their work with PNVIBAM (and other vinyl amides).[29,30,101,189-205] The group first reported the synthesis of PNVIBAM through a series of post-polymerization modifications starting from poly(*N*-vinyl acetamide), PNVAM, which was first converted into poly(vinylamine), PVAM, and finally into PNVIBAM.[189] However, the group later acknowledged that the resulting polymer likely contained unreacted amino groups (PVAM), thus impacting the measured properties (e.g., T_{CP}).[29] As a comparison, the authors then synthesized the NVIBAM monomer, and evaluated its conventional free radical polymerization using a series of solvents and initiators. A summary of the results obtained is shown in Table 2. On subsequent publications from the group, the polymerization of NVIBAM was performed with AIBN initiator, at 60°C for 24 h, with

ethanol,[30,190,191,202] methanol,[194,196] or DMF[195,198] as solvent. With this, the authors obtained, for example, yields around 85 to 85% , M_n of 10 to 22 kg·mol^{-1} and Đ around 2.3[190,195]

Table 2. NVIBAM polymerization parameters and obtained results, by Suwa et al. Reaction products were purified by dialysis in water using a membrane with cutoff molar mass 1000 g·mol^{-1}.[29]

Run	Solvent	Initiator	Temperature [°C]	Reaction Time [h]	Yield [%]	M_n [kg·mol^{-1}]
1	Water	K$_2$S$_2$O$_8$	4	12	2.0	21.0
2	Water	VA-044	60	12	58.9	13.1
3	Ethanol	Benzoyl peroxide	60	12	9.8	2.3
4	Ethanol	AIBN	60	12	84.0	7.9
5	DMF	AIBN	60	12	61.0	3.7
6	Dioxane	AIBN	60	12	61.0	10.0
7	Benzene	AIBN	60	12	85.0	18.2

Additionally, the group of Hiroharu Ajiro, who previously worked with Akashi, recently produced poly(*N*-vinyl isobutyramide) gels in water at 70°C, with V50 as initiator.[206] Other authors reporting studies with PNVIBAM[171,207] have obtained the polymer commercially from the Canadian company Polymer Source Inc., who offers PNVIBAM with M_n ranging from 7 to 20 kg·mol^{-1} (Đ 3.0 ~ 1.22).[208]

Although the RAFT polymerization of NVIBAM has never been shown, its vinyl amide structure would classify it as a less activated monomer (LAM).

2.4. Characterization of Thermoresponsive and Associative Polymers

In this thesis, the characterization of the synthesized polymers relied heavily on two methods: turbidimetry, which provided information regarding the thermoresponsivity of the polymers in solution, and dynamic light scattering (DLS), which provided information regarding the aggregation of the polymers. In the following sections, these two methods will be presented in detail. Subsequently, a few alternative characterization methods will be briefly discussed.

2.4.1. Turbidimetry

Turbidimetry is one of the simplest methods to probe thermoresponsive polymers in solution and is based on the change in the solution's turbidity when the polymer changes between the dissolved (one-phase solution) and undissolved (two-phase solution) states. The turbidity is quantified by

measuring the light transmittance through the solution (typically in a cuvette) over a defined temperature range which encompasses the phase transition. This temperature range is typically selected so that the measurement starts with the polymer in its soluble state, where the solution is clearer, and the temperature is then gradually changed until reaching the polymer's insoluble state, where the solution becomes more turbid. The cloud point temperature (T_{CP}) is then identified as the temperature at which the light transmittance shows an abrupt drop. From this point, another measurement is often performed, in which the temperature returns to the polymer's soluble range. In the case of polymers exhibiting lower critical solution temperature (LCST) behavior, this means a heating curve, where the polymer goes from coil to globule, will be measured first and a cooling curve, polymer goes from globule to coil, will be measured second. In the case of polymers exhibiting lower critical solution temperature (UCST), the cooling curve is typically measured first and the heating curve second. The reason for this sequence is that the kinetics of the aggregation are typically faster than for the re-dissolution, yielding more accurate transition temperatures. The globule to coil transition can then be measured to assess the hysteresis of the phase transition process.[209]

Although turbidimetry is a quick, simple, and thus invaluable technique, it is important to keep in mind what is actually being measured. Recalling section 2.1.2, where the nature of the phase transition and the definitions of binodal and spinodal were presented, one could expect the onset of the transition identified by turbidimetry to coincide with the spinodal. However, in practice demixing will usually occur not via spinodal decomposition, but by nucleation and growth at the metastable region between the binodal and spinodal. Moreover, detection of the process by turbidimetry depends on the formed aggregate reaching a critical size that affects the visual properties of the solution. Here, faster heating or cooling rates lead to further discrepancies, as the temperature may change faster than the kinetics of the aggregation, leading to delayed identification of the T_{CP}.[59] For these reasons, it is recommended that the transition identified by turbidimetry be coined cloud point temperature (T_{CP}) or demixing temperature (T_{dem}), rather than phase transition temperature or, even more inaccurately, LCST and UCST.[59,209]

Finally, it is important to consider and explicitly inform readers about what point of the turbidity over temperature curve has been taken as the cloud point, since innumerous different conventions exist, and values obtained through different procedures may not be directly comparable. Typically, the T_{CP} is either taken to be the point where the normalized transmittance falls below an arbitrary amount, e.g., 50%,[209-212] 90%,[210,213] 95%,[214] or 98%,[215,216] or the onset of the transmittance drop.[217,218] In this thesis, the latter approach was chosen, as it is more representative of the start of the demixing process.

2.4.2. Dynamic Light Scattering (DLS)

A relatively simple yet exceptionally useful technique to characterize solutions of self-assembling polymers is dynamic light scattering (DLS), which allows the estimation of the size and size distribution of the particles in the solution. In the case of polymer solutions, these particles may be unimers (single dispersed molecules), polymer micelles, and other well-ordered self-assembled structures (e.g., rods or vesicles), fractal aggregates or unorganized clusters.[209] DLS is based on Brownian motion, that is, the natural motion that all particles exhibit in solution, and the concept that larger particles move slower than smaller particles. Thus, using the Stokes-Einstein equation, one can estimate the hydrodynamic radius R_h of the particles:

$$R_h = \frac{k \cdot T}{6 \cdot \pi \cdot \eta \cdot D_0} \tag{12}$$

where k is the Boltzmann constant, T is the temperature, η is the viscosity of the solvent, and D_0 is the translational diffusion coefficient extrapolated to infinite dilution.[50,219]

It is important to highlight, however, that the values obtained for polymers may not always perfectly represent the real dimensions of the unimers, micelles, or aggregates, since the hydrodynamic radius (R_h) or hydrodynamic diameter (D_h) obtained from DLS measurements is the size of a hypothetical sphere with the same diffusion coefficient as the particle being measured.[219] Moreover, it must be noted that there is still much discussion regarding the origin of the slow and fast relaxation modes, and whether these are attributed to differently sized particles (unimers, micelles, aggregates, clusters, etc.), or rather to anisotropic particles.[220-226]

To perform the measurement, the sample is exposed to a light beam and the scattered light suffers constructive and destructive interference to create a unique signal which is measured at a specific angle θ. More specifically, the device evaluates the variation in detected light intensity (I) over a period of delay times (τ), and quantifies how correlated this intensity is with the scattered light intensity at an earlier time (t). This correlation represented graphically in the form of relaxation curves (correlograms), which is a plot of the second order autocorrelation function

$$g_2(\tau) = \frac{\langle I(\tau) \cdot I(t + \tau) \rangle}{\langle I(t)^2 \rangle} \tag{13}$$

over the delay time.[219,227,228]

On the one hand, solutions containing only small particles, which show fast Brownian motion, will cause the intensity of the scattered light to become uncorrelated with the original signal rather fast.

As a result, the autocorrelation function will decay at short delay times. The signal from a solution containing simply larger particles, on the other hand, will remain similar to the original signal for a longer period of time, due to the slower movement of the particles in solution. This will, therefore, generate a delayed autocorrelation function decay. Consequently, mixtures of particles with various sizes, that is, with a broad size distribution, will show a broader decay, as shown in Figure 16b.[228]
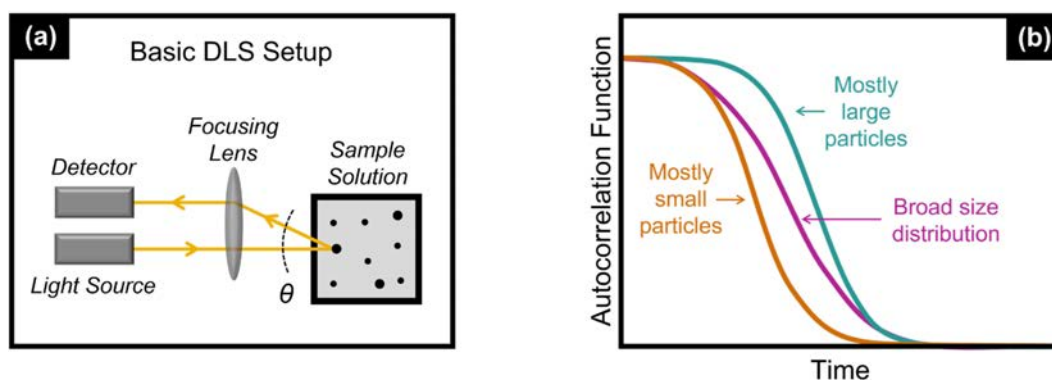
Figure 16. Basic DLS Setup with for backscattering detection, where $\theta = 173°$ (a). Example autocorrelation curves for solutions containing particles of different sizes and size distributions (b).

The angle at which the measurement is done (θ) also plays an important role on the results obtained, with most common angles being 90° and 173°C. The latter one, represented in Figure 16a, is referred to as backscattering detection and typically offers the advantage of reduction of multiple scattering effects, allowing measurement of solutions with higher concentrations. Moreover, this method suffers less impact from the presence of dust or other large contaminants in the solution. This advantage can be attributed to the fact that such contaminations are typically large particles, which tend to scatter the light forward, as opposed to backwards. Naturally, the backscattering detection will also impose a limitation on the resolution offered by the DLS to measure solutions with large particles.[229]

2.4.3. Other Common Characterization Techniques

Besides turbidimetry and dynamic light scattering, a variety of other characterization methods also offer the possibility of characterizing solutions of thermoresponsive and amphiphilic, self-assembling polymers.

The coil to globule transition of thermoresponsive polymers is an endothermic process because energy is required to undo the hydrogen bonds which exist between the polymer and the solvent

in the dissolved state. Therefore, the transition may be probed with calorimetry methods, such as **differential scanning calorimetry (DSC)** with sufficient sensitivity. For the measurement, the difference in heat capacity between the sample and a reference is measured over a temperature range, and endothermic processes can be identified by a peak in the heat capacity. Besides allowing the identification of the demixing temperature of thermoresponsive polymers, the integral of the endotherm represents the enthalpy of the transition, providing information on the amount of hydrogen bonds dissolved during the coil to globule transition.[59,209] Several authors have evaluated the comparability of the demixing temperatures obtained by turbidimetry and DSC.[211-213,215,218,230] The results obtained seem to be deeply depended on the method used to define T_{dem}, that is, which point in the light transmittance curve and DSC endotherm is chosen to represent the T_{dem}, similar as was discussed in section 2.4.1 for the turbidimetry method.

Another characterization method often used to characterize thermoresponsive polymers is liquid-state **proton nuclear magnetic resonance (^{1}H NMR)**, in which an external magnetic field is applied to a polymer solution, causing the nuclei of the polymers atoms to be excited into a higher energy spin state. The spin will then return to its equilibrium state in what is called a relaxation process. The identification of the coil to globule transition relies on the fact that dissolved (hydrated) polymer chains are more mobile and show slow relaxation, thus being identifiable by sharp chemical shift peaks. Dehydrated polymer chains, however, have limited mobility and show fast relaxation, leading to broader or altogether absent peaks, similar to solid-state systems.[231,232] As downsides of the method, it is important to remember that ^{1}H NMR spectra must be collected in deuterated solvents, and the transition temperature in D_2O may vary from that in H_2O. Moreover, it is a costly method and may not offer high temperature resolution for the identification of the transition temperature. However, it is advantageous for being readily available to most polymer chemists and providing information about local segmental mobility in the globular state. That is, if certain functional groups in the polymer chain retain water molecules in the globular state, their mobility will not be so strongly decreased and they will, in turn, remain more sharp and identifiable in the ^{1}H NMR spectrum.[68]

Rheology is a field which allows not only the investigation of thermoresponsive polymers in solution, but also the characterization of associative (self-assembling) polymers. Simply put, the different structures in which amphiphilic polymers assemble may lead to different impacts on the viscosity of the system. For example, copolymers with multiple associative blocks will typically lead to bridging by physical cross-linking of the self-assembled structures, thus causing a starker

increase in the viscosity of the system compared to polymers with a single associative block. Exactly because of these influences and tunability, one of the most common applications of associative polymers is as rheology modifiers (e.g., thickeners). Thus it is natural that rheological techniques have found vast application for the characterization of such materials, providing information about the type of self-assembled structure as well as its dependence on factors such as chain size, blocks length, branching, temperature, and concentration.[57]

Finally, some of the most insightful methods for the elucidation of the structures formed by associative polymers in solution are scattering techniques, such as **X-ray** and **neutron scattering**. This field naturally also encompasses light scattering methods, as is the case of DLS, which is discussed in the previous section. Scattering techniques are based on the scattering intensity upon subjecting the sample to a beam, either light, X-rays or neutrons. One of the main differences between X-ray and neutron scattering methods in comparison to light scattering is the wavelength of the applied radiation, which allows probing considerably smaller structures. Another difference is that the distinction between phases (e.g., solvent and polymer phase) in light scattering methods is the difference between refractive indices. In the case of X-ray scattering, in contrast, atomic number determines differentiation, whereas for neutron scattering distinction is dependent on coherent scattering length of the atom's nucleus. The coherent scattering length is notably different for D and H, thus permitting the successful characterization of chains and structures in solutions when using deuterated solvents. Small-angle neutron scattering (SANS) is a particularly powerful method for the characterization of associating polymers, and may provide vast information about the structure, size, and hydration of self-assembled structures.[4,233]

3. Synthesis of Polymers Exhibiting Co-nonsolvency

As discussed in details in section 2.2.2, the co-nonsolvency effect has been extensively studied in poly(*N*-isopropyl acrylamide) (PNIPAM). Although other polymers have been reported to show such a behavior, their characterization has not been nearly as deep. In this work, to better elucidate the impacts of chemical structure on co-nonsolvency, the phenomenon is investigated on alternative polymers with chemical structure analogous to PNIPAM: PNIPMAM (poly(*N*-isopropyl methacrylamide)) and PNVIBAM (poly(*N*-vinyl isobutyramide)). The similarity of their chemical structure to the well-known PNIPAM allows a more objective investigation of the effects of small changes on the chemical structure upon the co-nonsolvency behavior. Specifically, PNIPMAM varies from PNIPAM by the presence of an additional methyl group attached to the backbone, whereas an inverted position of the amide group differentiates PNVIBAM from PNIPAM. To add an additional level of complexity to the systems, these materials are compared not only in the form of homopolymers, but also as amphiphilic di- and triblock copolymers. These are composed of short hydrophobic blocks of polystyrene (PS) or poly(methyl methacrylate) (PMMA) and long thermoresponsive blocks of PNIPAM, PNIPMAM and PNVIBAM.

This chapter focuses on the synthesis of these little studied polymers. Most homopolymers were synthesized by conventional free radical polymerization (FRP), while copolymers were synthesized by Reversible Additional Fragmentation Chain Transfer (RAFT) radical polymerization. Therefore, the first section (3.1) focuses on the selection and synthesis of the chain transfer agents used for the RAFT polymerizations. Subsequently, the synthesis of monomers, homopolymers and block copolymers of PNIPAM (section 3.2), PNIPMAM (section 3.2.1) and PNVIBAM (section 3.2.2) is discussed in details.

Following, in chapter 0, the co-nonsolvency behavior of each of these materials is investigated in detail, and the results are discussed in the context of their differing chemical structures.

3.1. Chain Transfer Agents

A variety of chain transfer agents (CTAs) were used in this thesis, with the purpose to (1) evaluate the polymerization of monomers with different reactivities and (2) obtain block copolymers with different architectures, namely di- and triblock copolymers. Although some of these CTAs are available commercially, a few others had to be synthesized to meet specific requirements. In total, six chain transfer agents (CTAs) were used, and their chemical structures are depicted in Figure 17. Table 3 provides an overview of their main characteristics, as well as which polymerizations each CTA was used for.
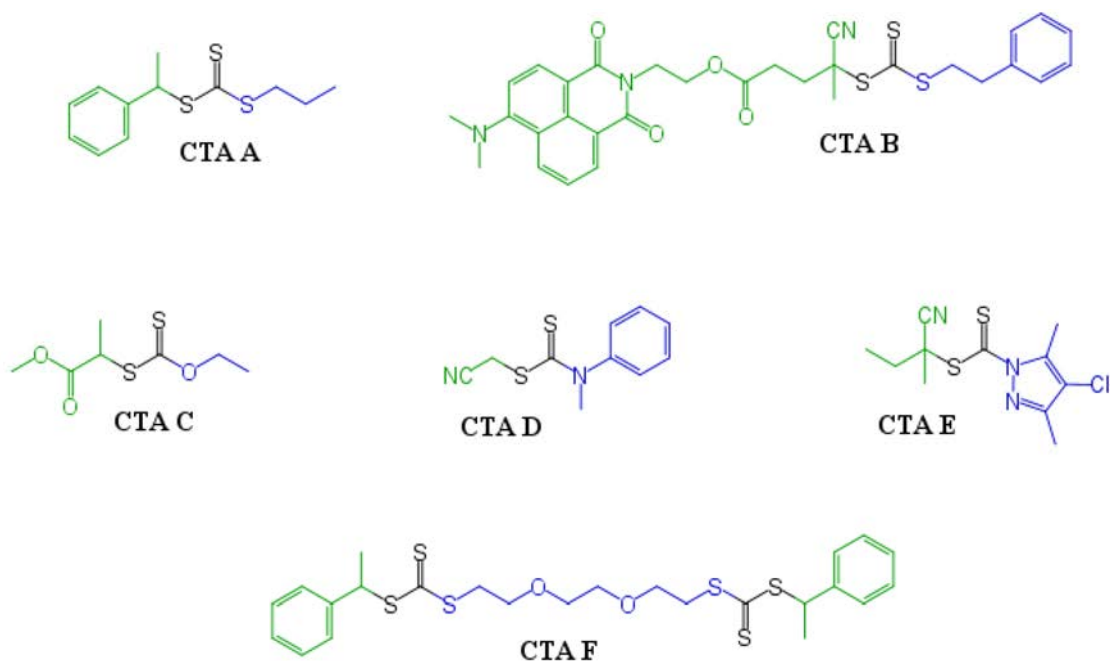
Figure 17. Chemical structure of the Chain Transfer Agents (CTAs) used in this thesis. R-groups (leaving groups) are shown in green, while Z-groups (reactivity modifying groups) are shown in blue.

3.1.1. CTA Selection

CTAs referred to as monofunctional (CTAs **A** to **E**) are those containing a single thiocarbonylthio moiety, and a single R-group (i.e., one addition/fragmentation point). These CTAs were used to synthesize diblock copolymers, and a few homopolymers. Bifunctional CTA **F**, in contrast, contains two thiocarbonylthio moieties, joined together by the Z-group. This CTA contains two identical R-groups, and hence two addition/fragmentation points, allowing the synthesis of triblock copolymers with PA-*b*-PB-*b*-PA architecture.

As shown, all chain transfer agents contain at least one thiocarbonylthio moiety. This moiety may undergo a π- π* electronic transition, which leads to a strong absorption band in the UV range, thus enabling its use as an end-group label for the characterization of the polymers. To further apply UV-vis spectroscopy for polymer characterization, the R-group of CTA **B** is functionalized with a UV-vis label, which is consequently incorporated into the polymers as an end-group. This allows for molar mass estimation through the R group, thus avoiding that Z end-group losses give rise to calculated molar masses which are larger than the reality.[157]

Table 3. Main characteristics of the Chain Transfer Agents (CTAs) used in this thesis.

	Description	Functionality*	UV-vis label	Used / tested for				
				PS	PMMA	PNIPAM	PNIPMAM	PNVIBAM
CTA A	1-phenylethyl propyl carbonotrithioate	1		✓		✓		
CTA B	2-(6-(dimethylamino)-1,3-dioxo-1H-benzo[de]isoquinolin-2(3H)-yl) ethyl 4-cyano-4-(((phenethyl-thio)carbonothioyl)thio)pentanoate	1	✓		✓	✓	✓	
CTA C	methyl 2-((ethoxycarbonothioyl)thio)propanoate	1			✓	✓			✓
CTA D	cyanomethyl methyl(phenyl)carbamodithioate	1			✓	✓			✓
CTA E	2-cyanobutan-2-yl 4-chloro-3,5-dimethyl-1H-pyrazole-1-carbodithioate	1			✓	✓			✓
CTA F	(ethane-1,2-diylbis(oxy))bis(ethane-2,1-diyl) bis(1-phenylethyl) bis(carbonotrithioate)	2			✓		✓		

* "Functionality" refers to the number of addition/fragmentation points in the chain transfer agent.

The abovementioned CTAs were used to synthesize thermoresponsive amphiphilic di- and triblock copolymers by Reversible Addition Fragmentation Chain Transfer (RAFT) polymerization. This was done in two steps, starting with the polymerization of the short hydrophobic blocks (either polystyrene (PS) or poly(methyl methacrylate) (PMMA)) in the presence of an adequate CTA. The produced oligomer was then used as a macro-CTA for the polymerization of the long thermoresponsive block: either poly(*N*-isopropyl acrylamide) (PNIPAM), poly(*N*-isopropyl methacrylamide) (PNIPMAM) or poly(*N*-vinyl isobutyramide) (PNVIBAM). This synthesis sequence was chosen to facilitate characterization and to increase the reliability of the RAFT processes.

Loss of CTA end-groups leads to "dead" polymer chains, which cannot be subsequently reactivated for chain extension. This can occur in several ways, both during as well as after polymerization. Common processes include hydrolysis, thermal degradation or termination reactions. As the polymerization reaction proceeds and monomer concentration is reduced, the continuously formed initiator radicals have a higher chance of causing terminations. To avoid this effect, it is generally recommended that RAFT polymerizations be conducted only up to

conversions around 70%.[34] Therefore, to preserve CTA end-groups and allow the synthesis of block copolymers, is advantageous to first synthesize the blocks which require shorter reaction times and lower monomer conversions.

Moreover, short oligomers facilitate characterization by end-group analysis, given that lower molar masses imply a higher proportion of end-groups. Since signals from the end-groups are used as reference for molar mass calculation by NMR and UV-vis, their visibility in the spectrum is vital for the accuracy of the calculation. In the case of the high molar masses of the thermoresponsive block, the signals of the polymer's constitutional repeat units completely overwhelm those of the end-groups. Consequently, using the more prominent signals of the previously characterized hydrophobic block as a reference instead gives more accurate results.

Furthermore, self-assembly of amphiphilic block copolymers is quite sensitive to even small changes in the length of the hydrophobic block, whereas small differences in length of the hydrophilic block are less critical. For this reason, if different hydrophilic blocks are to be compared, it is important that their hydrophobic blocks be identical in both structure and length, ensuring comparability. Thus, synthesizing the hydrophobic block first allows the use of this same precursor for the chain extension with different comonomers and/or with hydrophilic block different lengths.

Given the different reactivities of each of the monomers, the chain transfer agents had to be selected accordingly, and the sequence of which monomers would be polymerized first and second needed to be considered, while certain combinations of hydrophobic/thermoresponsive polymers were not possible. In the synthesis of block copolymers by RAFT, monomers must always be polymerized in an order of decreasing activity level (see Figure 18). This is necessary since otherwise the first monomer (less activated) will be too poor of a leaving group to efficiently fragment from the CTA and allow the chain extension with the more activated (second) monomer. Therefore, as evidenced in Figure 18, the chain extension of PS with PNIPMAM was not possible, as NIPMAM is more activated than styrene.
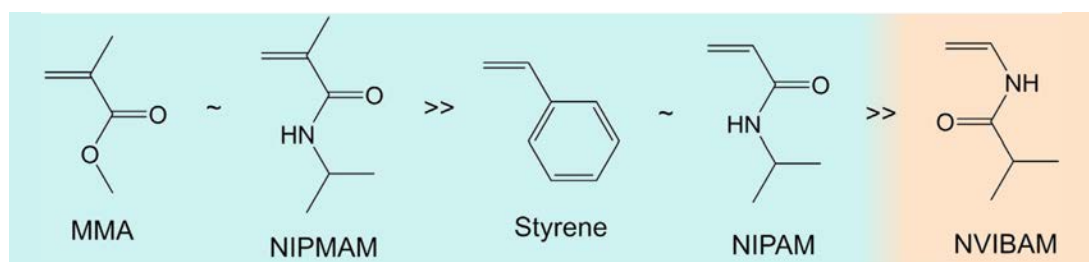
Figure 18. Monomers used in this thesis, from left to right, in decreasing order of activity levels. More activated monomers (MAMs) are shown in turquoise, less activated monomer (LAM) is shown in orange.

In the more extreme case of NVIBAM, which is a LAM (less activated monomer), its polymerization not only needs to take place after the polymerization of the more activated monomers (MAMs) styrene and methyl methacrylate, but special CTAs are necessary. Styrene, MMA, NIPAM and NIPMAM are all MAMs, and generally CTAs with the same reactivity modifying Z-groups may be used for all (although different initiating R-groups might still be needed). Thus, trithiocarbonate CTAs **A**, **B** and **F** were selected to obtain these polymers, as they have been shown to successfully control the polymerization of MAMs. For styrene, R-groups with secondary or even primary radical centers could be used (CTAs **A** and **F**), whereas for MMA, R-groups with more stable radical centers were necessary to ensure high enough fragmentation rates to promote control over the polymerization.[35]

NVIBAM, conversely, requires less active CTAs (lower rates of addition and higher rates of fragmentation) to compensate for the poor leaving group capabilities of this monomer. This is usually achieved using *O*-alkyl-xanthate or *N*-alkyl-*N*-aryl-dithiocarbamate CTAs, as opposed to the dithioesters and trithiocarbonates typically used for more activated monomers. Therefore, the selection of a CTA which allows both the polymerization the first block (MAM) and second block (LAM) is not a trivial task. Three CTAs were tested for this end, namely an *O*-alkyl-xanthate (CTA **C**), a *N*-alkyl-*N*-aryl-dithiocarbamate (CTA **D**) and a pyrazole-based dithiocarbamate (CTA **E**). While CTAs **C** and **D** are more suitable for the polymerization of LAMs, they may offer partial control over the polymerization of some MAMs, such as styrene.[35] CTA **E**, however, is a chain transfer agent with intermediate activity levels, which has been shown to satisfactorily control the polymerization of MAMs (styrene and MMA), as well as a less activated monomer (vinyl acetate).[150]

3.1.2. Synthesis & Characterization of the CTAs

Of the abovementioned chain transfer agents, CTAs **A**, **C** and **F** were synthesized within the scope of this work, while CTA **B** was kindly provided by a former colleague, Viet Hildebrand,[36,157] and CTAs **D** and **E** were obtained commercially.

The synthesis of CTA **A** and CTA **F** was done through deprotonation of a thiol precursor (which formed the Z group) by triethylamine, followed by reaction of the thiolate with CS_2 to form a trithiocarbonate anion, which was subsequently reacted with a bromide precursor (which formed the R group), to give the desired CTA. The synthesis and purification of this CTA was straightforward, yielding 95% of pure product, as evidenced by ^1H (Figure 19a) and ^{13}C nuclear magnetic resonance, thin layer chromatography, elemental analysis, Fourier-transform infrared spectroscopy and UV-vis spectroscopy. In the case of CTA **F**, a dithiol precursor was used, leading

to a bifunctional CTA. Similar to CTA **A**, the synthesis of CTA **F** was rather straightforward, although its purification proved more challenging, requiring 2 subsequent purifications by column chromatography as well as several washing steps. Despite the extensive purification procedure, a high yield of 94% was achieved, with satisfactory purity which was evaluated by several characterization methods, as already described by CTA **A**. The ^{1}H NMR spectrum of CTA **F** is depicted in Figure 19c.

The synthesis of CTA **C** followed a similar procedure as for CTAs **A** and **F**, but an alcohol was used as precursor instead of a thiol. Since alcohols have a lower acidity than thiols, a stronger deprotonating agent was necessary. Consequently, sodium hydroxide was used instead of triethylamine. The synthesis and purification of this CTA was remarkably easy, and the obtained product (91% yield) showed high purity. As for the other CTAs, the obtained product was extensively characterized, and its ^{1}H NMR spectrum is shown in Figure 19b.

^{1}H NMR spectra of the remaining CTAs, as well as ^{13}C NMR, UV-vis and FTIR spectra of all CTAs are provided in Annexes 7.1, 7.2 and 0. The maximum absorption wavelength and extinction coefficient data obtained from the UV-vis measurements of all CTAs is summarized in Table 4. This data was used to calculate the molar mass of the polymers synthesized using each of the CTAs.

Table 4. Maximum absorption wavelength (λ_{max}) and extinction coefficient (ε) at λ_{max} of the Chain Transfer Agents (CTAs) used in this thesis, measured by UV-vis spectroscopy, in ethyl acetate.

	Molar mass [g·mol^{-1}]	Functionality	λ_{max} [nm]	ε [L·mol^{-1}·cm^{-1}]
CTA A	256.44	1	310	16300
CTA B	605.79	1	409	9800
CTA C	208.29	1	278	10400
CTA D	222.33	1	277	8300
CTA E	287.83	1	312	15600
CTA F	542.86	2	310	36700
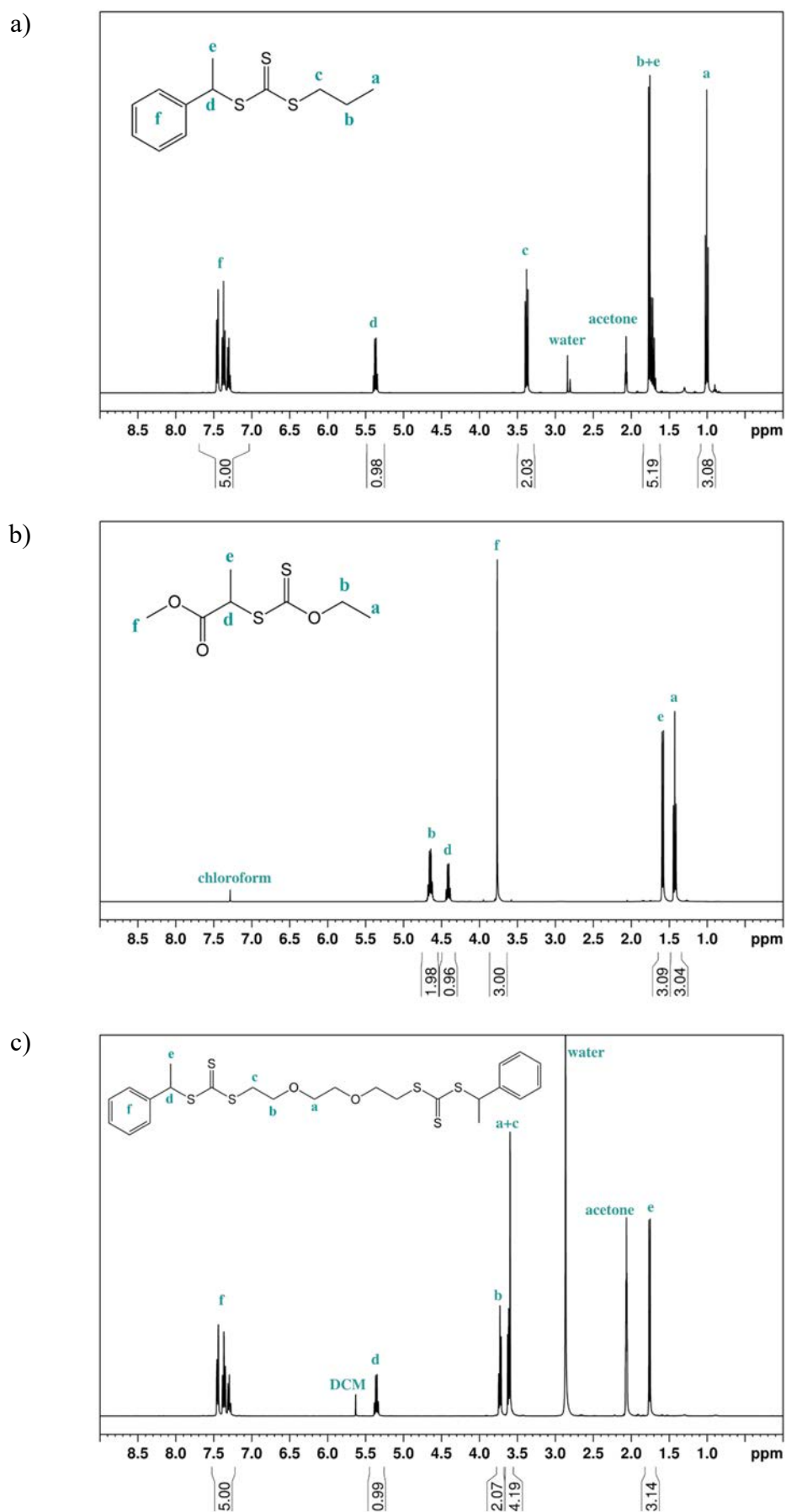
Figure 19. ^{1}H NMR of CTA A in acetone-d_6 (a), of CTA C in CDCl$_3$ (b) and of CTA F in acetone-d_6 (c).

For CTAs **A** and **F**, the absorption band used as reference is the π- π^* transition of the C=S bond on the trithiocarbonate moiety at around 310, which explains the similarity in maximum absorption wavelength and extinction coefficient for these CTAs. As two trithiocarbonate moieties are present in each molecule of CTA **F**, the extinction coefficient for this molecule is about 2 times higher.

The π- π^* transition of the C=S bond was also used as reference for CTA **C** (xanthate moiety) and CTAs **D** and **E** (dithiocarbamate moiety). Here, the impact of the different substitution patterns of each CTA becomes clear with the variations of maximum absorption wavelength and extinction coefficient for trithiocarbonates, xanthate and dithiocarbamates.

In the case of CTA **B**, although a trithiocarbonate group is also present, the CTA possesses a naphthalimide moiety in its R-group, which acts as a UV-vis label due to the π- π^* transition from the conjugated segment, absorbing at around 409 nm.[36,234] This allows for molar mass estimation through the R group, thus avoiding that Z end-group losses give rise to calculated molar masses which are larger than the reality.[157] Since the absorption bands of the naphthalimide moiety partially overlap the π- π^* band of the trithiocarbonate, only the naphthalimide band could be used for molar mass determinations.

3.2. Synthesis of Polymers based on PNIPAM

Although the thermoresponsivity and co-nonsolvency behavior of PNIPAM has been extensively studied, only a limited number of studies have focused on the properties of copolymers of PNIPAM, and particularly of amphiphilic block copolymers (see section 2.2.2).

In order to shine some light into the thermoresponsive and co-nonsolvency behavior of these structures, a series of thermoresponsive amphiphilic di- and triblock copolymers based on PNIPAM were synthesized. This was achieved through reversible addition fragmentation chain transfer (RAFT) polymerization, in two steps. First, the short hydrophobic block was synthesized. Two polymers were compared for this end: polystyrene (PS) and poly(methyl methacrylate) (PMMA). These so-called macro-CTAs were then chain extended with poly(*N*-isopropyl acrylamide) (PNIPAM). The following sections describes in detail these two synthetic steps. The reasons for the choice of PS and PMMA as hydrophobic blocks, as well as the comparison between the obtained copolymers is discussed in detail in section 4.2.2 (page 126).

3.2.1. Synthesis of PS and PMMA Precursors for Amphiphilic Block Copolymers

Monofunctional and bifunctional polystyrene (PS) macro-CTAs were synthesized using CTAs **A** and **F**, respectively. Both PS syntheses were done in bulk at 110°C, with self-initiation,[131,132] that

is, without the addition of an initiator. Degrees of polymerization were kept rather low, as otherwise the block copolymers cannot be dissolved in water.[9]

Monofunctional poly(methyl methacrylate) (PMMA) macro-CTAs were synthesized using CTA **B**. Polymerizations were done in benzene at 65°C, with AIBN as radical initiator. Initiator amounts were kept as low as possible, to ensure that only a minimal number of chains is initiated by the initiator, and the functional end-group (CTA) is therefore present on almost all chains. Various chain lengths were compared, with degrees of polymerization ranging between 17 and 75. For both PS and PMMA, the monomer/CTA ratio and the reaction time were specifically selected to obtain the desired conversion and degree of polymerization. A list of the synthesized hydrophobic macro-CTAs and main characterization results is provided in Table 5. The results obtained are within what is expected for these systems. The molar mass results from the various characterization methods are in good accordance with each other, and Z/R ratios (the ratio between the molar masses obtained by NMR via the Z and R groups) are virtually 1, evidencing the success of the RAFT process with minimal loss of end-groups.

For all reactions, NMR analysis shows the expected reduction of intensity of signals from the double bond, as well as the typical broadening of the signals upon polymerization, indicating the successful conversion of the monomer into polymer.

Moreover, in the case of PS, the signal of the CTA's alpha position to the trithiocarbonate group (signal d, Figure 19a) disappears upon polymerization, and signals from the constitutional repeat unit at the alpha position appears (Figure 20, signal q_1, at 4.7 – 5.2 ppm), evidencing the successful attachment of the growing chain to the CTA. Conversion was calculated from the crude reaction mixture (see example in Figure 20a) by comparing the signal intensities of the protons on the terminal alkene carbon (signals cis p* and trans p*, at 5.2 – 5.9 ppm) with the signals of the aromatic moieties (signal f+r+r*, at 6.9 – 7.6 ppm), thus obtaining the fraction of residual monomer and, reciprocally, the fraction of converted monomer units.

For monofunctional PS_{10}^A (done with CTA **A**), molar mass calculations through Z end-group were done after purification (Figure 20b) by comparing the relative signal intensities of the aromatic moieties (signal f+r, at 6.9 – 7.6 ppm) with the signal of the constitutional repeat unit on the alpha position to the trithiocarbonate (signal q_1, at 4.7 – 5.2 ppm). Molar mass calculations through R end-group, in contrast, were done using end-group signal 3 (at ca. 0.95 ppm). For bifunctional PS_{10}-*b*-PS_{10}^F (done with CTA **F**, Figure 21), Z end-group signals a+b+c, (at 3.4 – 3.7 ppm) and R end-group signal e, (at 0.9 – 1.2 ppm) were used.

Table 5. Main characterization results for PS and PMMA macro-CTAs. Both PS reactions done in bulk, at 110°C with self-initiation. The monofunctional PS sample was prepared with CTA A, while the bifunctional PS-*b*-PS was prepared with CTA F. All PMMA reactions were done with CTA B and AIBN initiator, in benzene (50 wt.%) at 65°C.

Index	Product	Conversion [%]	M_n [kg·mol^{-1}]							$Đ^{SEC}$	Ratio M_n Z/R (NMR)
			Theor. (b)	NMR R-group	NMR Z-group	UV-vis	EA C/N ratio	EA C/S ratio	SEC		
1	**PS$_{10}$^{A}**	62	1.3	1.3	1.3	1.3	-	1.2	1.1 (c)	1.21	1.05
2	**PS$_{10}$-*b*-PS$_{10}$^{F}**	62	2.9	2.6	2.7	3.0	-	2.6	2.1 (c)	1.20	1.01
3[*]	**PMMA$_{17}$^{B}**	40 (a)	*2.2* (a)	2.7	2.7	3.5	-	-	2.3 (d)	1.38	1.00
4	**PMMA$_{20}$^{B}**	82 (a)	*3.9* (a)	3.4	3.0	2.9	3.2	3.0	2.6 (d)	1.60	0.87
5	**PMMA$_{24}$^{B}**	63	3.2	3.6	3.6	3.1	3.4	4.3	3.0 (d)	1.41	0.98
6	**PMMA$_{27}$^{B}**	83 (a)	*3.9* (a)	3.3	3.4	3.0	3.3	2.8	3.3 (d)	1.36	1.03
7	**PMMA$_{41}$^{B}**	85	6.1	4.9	4.9	4.6	4.7	3.9	4.7 (d)	1.32	1.00
8[†]	**PMMA$_{75}$^{B}**	63 (a)	*5.9* (a)	8.4	8.5	8.3	6.6	9.7	8.1 (d)	1.22	1.02

(a) Yield is given in lieu of conversion when the latter is not available. Resulting $M_n^{theor.}$ are provided tentatively.

(b) Theoretical molar mass, calculated from the conversion (or yield) and monomer/CTA ratio.

SEC measured in NMP and calibrated using PS (c) or PMMA (d) standards.

---

[*] I kindly thank Dr. Dirk Schanzenbach for performing this polymerization.
[†] I kindly thank Ekin Sehit and Dr. Dirk Schanzenbach for performing this polymerization.
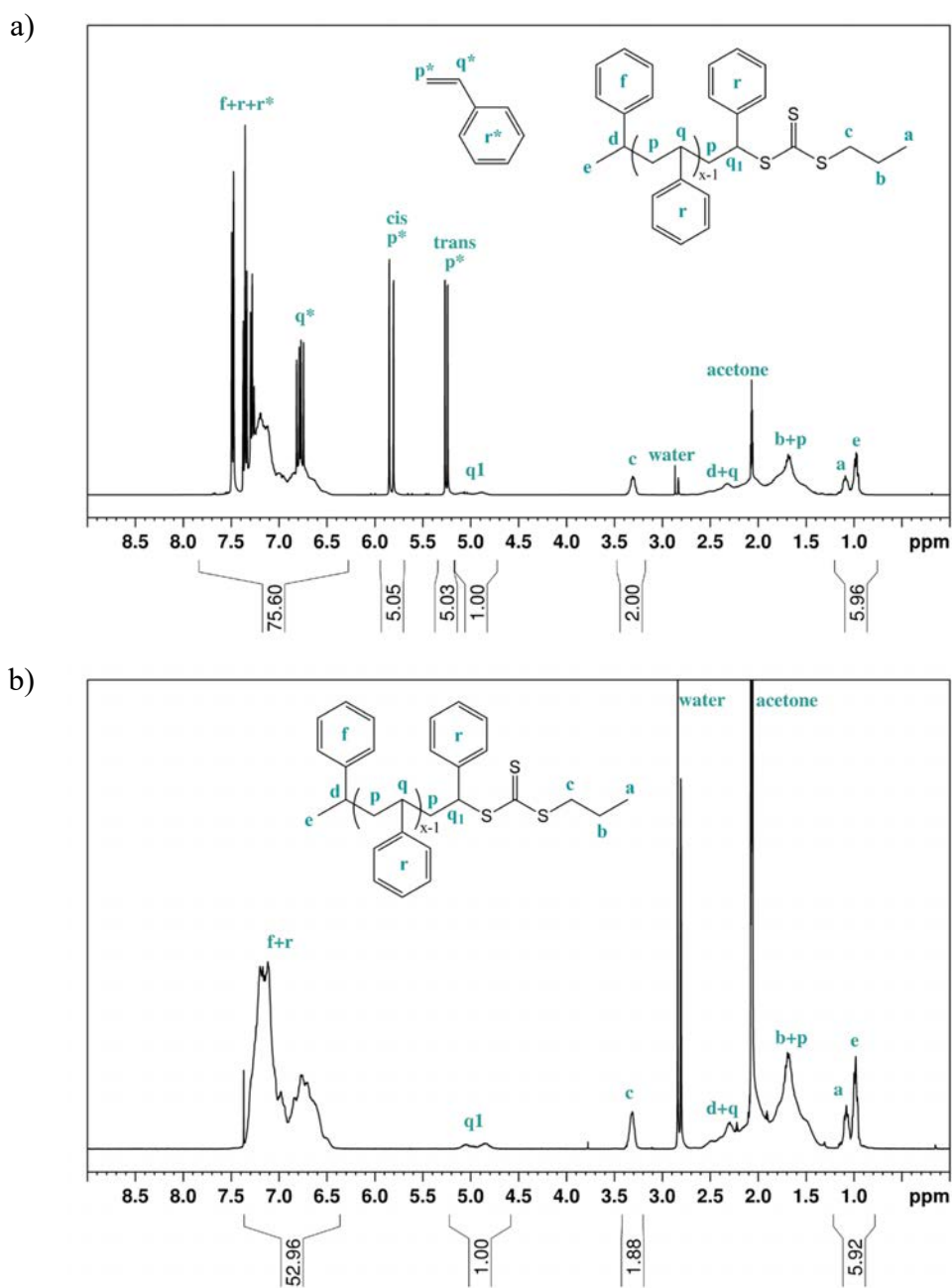
Figure 20. ^{1}H NMR spectra of PS_{10}^{A} (reaction index 1, in acetone-d_6), crude reaction mixture (a) and after purification (b).
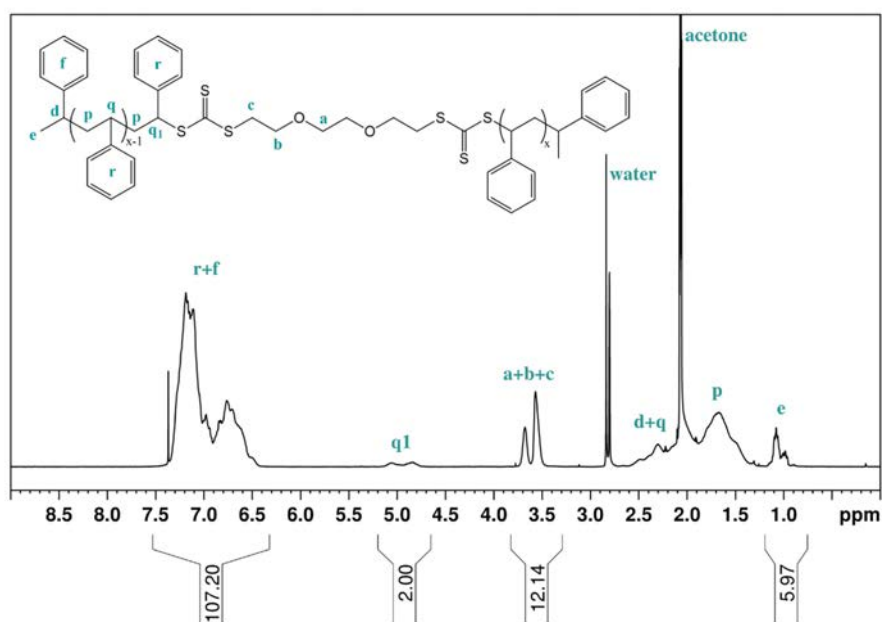
Figure 21. ^{1}H NMR spectrum of PS$_{10}$-b-PS$_{10}^F$ (reaction index 2, in acetone-d$_6$), after purification.

In the case of PMMA (example shown in Figure 22), molar mass calculations through Z end-group were done by comparing the relative signal intensities of the constitutional repeat unit (signal r, at 3.6 ppm) with end-group signal c at 2.9 ppm. Additionally, molar mass calculations through R end-group were done using signals i+k+m and l at 7.6 – 8.7 ppm.
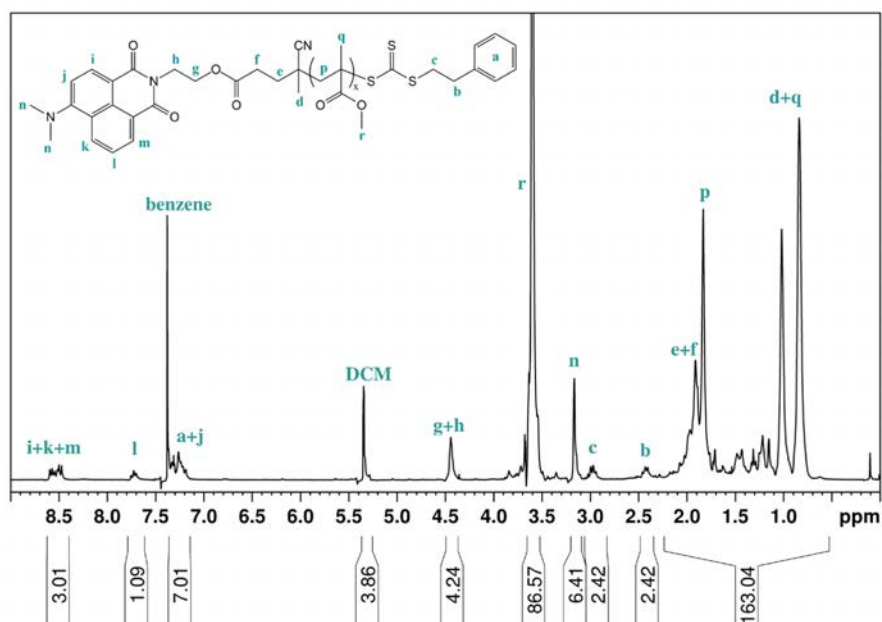
Figure 22. ^{1}H NMR spectrum of PMMA$_{20}^B$ (reaction index 4, in DCM-d$_2$), after purification.

The successful preparation of the various macro-CTAs was further corroborated by UV-vis, SEC, EA, FTIR, DSC and TGA, as listed in Table 5 and shown in the annexes.

3.2.2. RAFT Polymerization of NIPAM to Obtain Amphiphilic Block Copolymers

The previously synthesized PS and PMMA oligomers were used as macro-CTAs for the polymerization of NIPAM (and some also for NIPMAM, as described in section 3.3.3). RAFT polymerizations of NIPAM were performed in benzene, with a monomer concentration of 30 wt.%. All reactions were done at 65°C and allowed to proceed overnight. Monomer / macro-CTA ratios were accordingly chosen to obtain a long PNIPAM block, in contrast to the short PS and PMMA blocks (large w_{PNIPAM}), thus ensuring solubility of the copolymers in water. The success of the polymerization was confirmed by ^{1}H NMR, SEC, UV-vis, FTIR, EA, DSC, and TGA (see annexes). The main results of the various characterization techniques are listed in Table 6.

All reactions exhibit close to quantitative conversion, and no impact from the type or size of macro-CTA on the course of the polymerization of NIPAM could be identified. The molar mass values calculated from the different characterization techniques are mostly in accordance with each other, which is particularly positive given that the different methods measure the molar mass in different ways: by end-group analysis (UV-vis), by the hydrodynamic radius of the chains (SEC), and by the ratio of chemical moieties from each block (NMR and elemental analysis).

NMR spectra from PS-*b*-PNIPAM, PS-*b*-PNIPAM-*b*-PS and PMMA-*b*-PNIPAM polymers, both before and after purification are exemplified in Figure 23, Figure 24, and Figure 25, respectively. In the case of PS-based copolymers, the signal of the aromatic moieties (ca. 6 – 8 ppm in Figure 23 and Figure 24) is overlapped with the signal of the amide proton from the NIPAM monomer and PNIPAM polymer, which hinders the calculation of the degree of polymerization of the PNIPAM block (DP_n^{PNIPAM}) by evaluation of the block size ratio. Therefore, the calculation of DP_n^{PNIPAM} was done by comparison of the signal from the constitutional repeat unit of PNIPAM (signal v, at 4.0 ppm in Figure 23b and Figure 24) with the signal from the R-groups of the CTA. For the diblock copolymer (Figure 23b), the signal c at 3.4 ppm was taken as R-group reference. For the triblock copolymer (Figure 24), signal a+b+c at 3.5 – 3.8 ppm was used.

In the case of PMMA-based copolymers, the degree of polymerization of the PNIPAM block could be calculated more reliably through the comparison of the signals of the PS or PMMA constitutional repeat units, to reduce s from the low signal intensities of the end-groups. Therefore, the relative signal intensities of the constitutional repeat unit of PMMA (Figure 25, signal r, at 3.6 ppm) and constitutional repeat unit of PNIPAM (signal v, at 4.0 ppm) were compared, assuming that the block size of PS and PMMA is the same on the macro-CTA and on the final block copolymers.

Number-average molar masses were also calculated by end-group analysis using UV-vis, as listed in Table 6, and examples shown in Annex 7.2. The results obtained by UV-vis are in generally good accordance with those from ^{1}H NMR, which is to be expected, given that both methods are based on end-group analysis.

Further evaluations were also performed by SEC. SEC elugrams of all PNIPAM amphiphilic block copolymers are shown in Figure 26. For all PNIPAM copolymers, comparisons of SEC elugrams before and after chain extension are shown in Annex 7.3 - Figure A 55 (copolymers based on PS) and Figure A 56 (copolymers based on PMMA).

Table 6. Main characterization results for thermoresponsive amphiphilic block copolymers based on PNIPAM, with PS or PMMA hydrophobic blocks.

| Index | Product | Precursor Index | Conversion [%] | M_n [kg·mol^{-1}] | | | | | $Đ^{SEC}$ | w_{PNIPAM}^{SEC} |
				Theor. [b]	NMR	UV-vis	EA C/N	SEC		
9	PS$_{10}$-*b*-PNIPAM$_{65}$^{A}	1	97	13	16	15	12	8.5 [c]	1.41	0.87
10	PS$_{10}$-*b*-PNIPAM$_{85}$^{A}	1	99	16	13	12	11	11 [c]	1.28	0.90
11	PS$_{10}$-*b*-PNIPAM$_{180}$-*b*-PS$_{10}$^{F}	2	95	25	20	28	25	23 [c]	1.23	0.91
12	PS$_{10}$-*b*-PNIPAM$_{250}$-*b*-PS$_{10}$^{F}	2	98	34	37	39	26	31 [c]	1.25	0.93
13	PMMA$_{17}$-*b*-PNIPAM$_{337}$^{B}	3	92 [a]	28 [a]	35	36	29	40 [d]	1.39	0.94
14	PMMA$_{20}$-*b*-PNIPAM$_{554}$^{B}	4	98	33	60	57	39	65 [d]	1.37	0.95
15	PMMA$_{24}$-*b*-PNIPAM$_{379}$^{B}	5	99	31	32	40	24	46 [d]	1.37	0.93
16	PMMA$_{27}$-*b*-PNIPAM$_{802}$^{B}	6	98	65	63	79	56	94 [d]	1.27	0.96
17	PMMA$_{41}$-*b*-PNIPAM$_{456}$^{B}	7	96	41	42	46	40	56 [d]	1.18	0.92
18	PMMA$_{75}$-*b*-PNIPAM$_{366}$^{B}	8	98	34	43	38	39	50 [d]	1.41	0.84

(a) Yield is used in lieu of conversion when the latter is not available. Resulting $M_n^{theor.}$ is provided tentatively.

(b) Theoretical molar mass, calculated from the conversion (or yield) and monomer/CTA ratio.

SEC measured in NMP and calibrated using PS (c) or PMMA (d) standards.
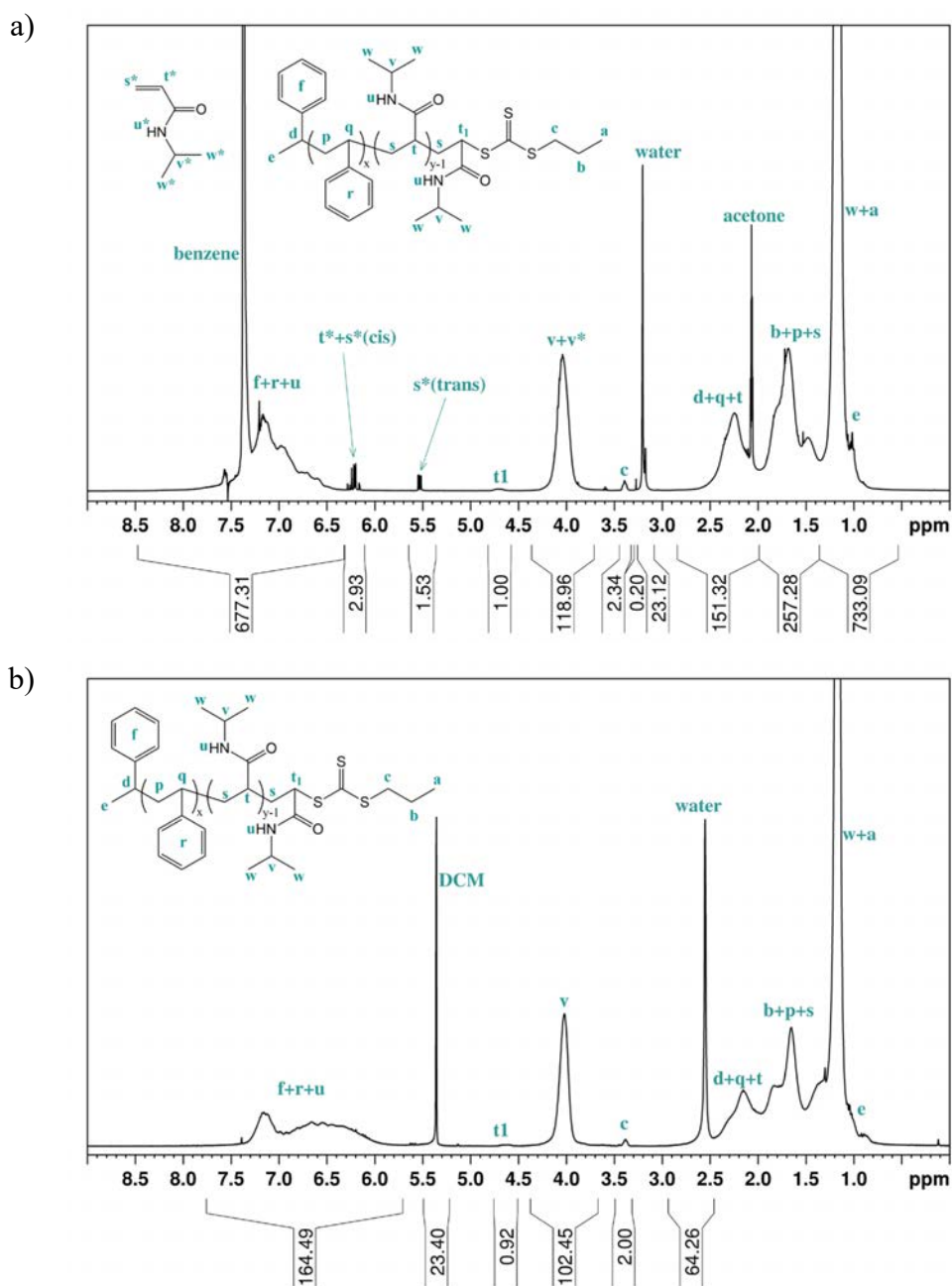
Figure 23. ^{1}H NMR spectra of PS_{10}-b-$PNIPAM_{85}^A$ (reaction index 10), crude reaction mixture (a, in acetone-d_6) and after purification (b, in DCM-d_2).
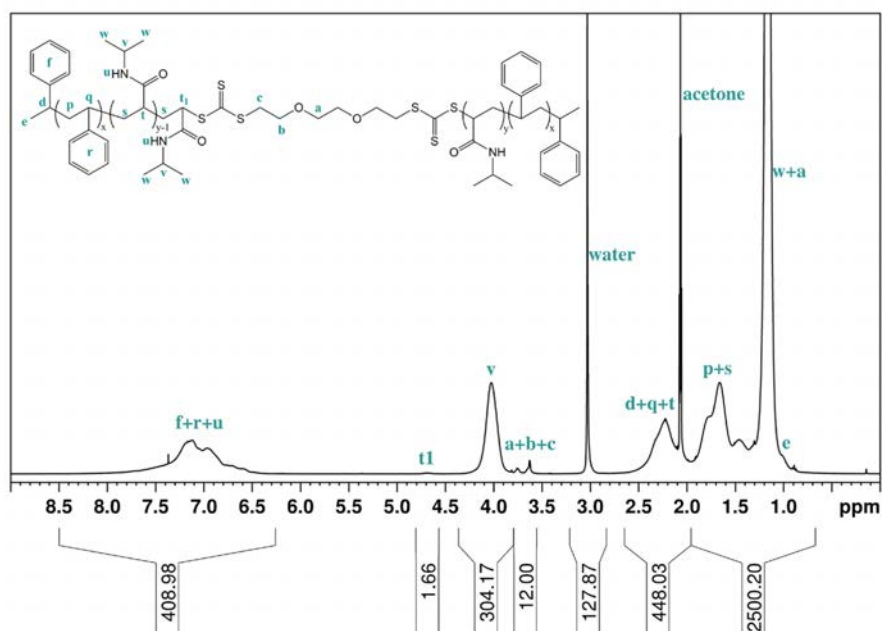
Figure 24. ^{1}H NMR spectra of PS$_{10}$-*b*-PNIPAM$_{250}$-*b*-PS$_{10}^F$ (reaction index 12, in acetone-d$_6$).
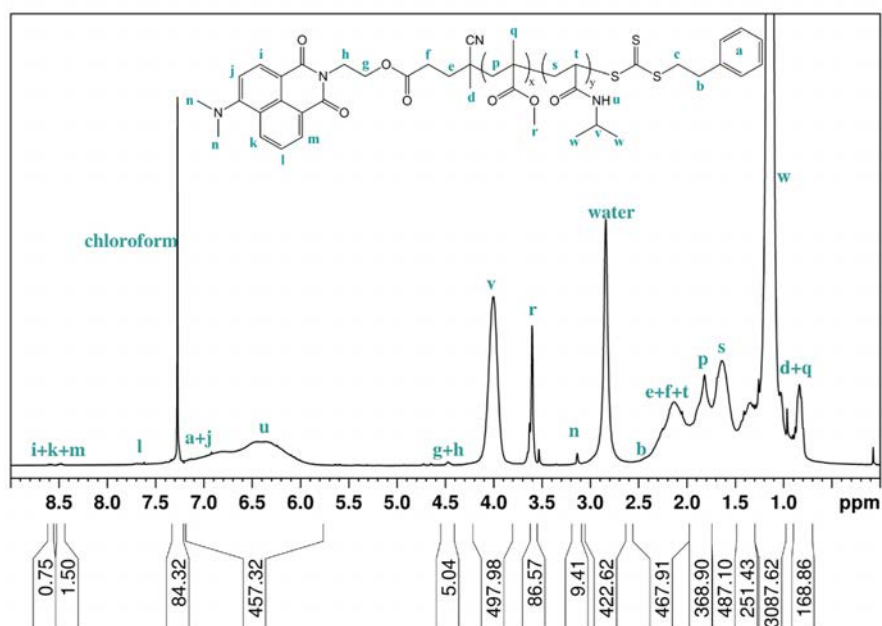
Figure 25. ^{1}H NMR spectra of PMMA$_{20}$-*b*-PNIPAM$_{554}^B$ (reaction index 14, in CDCl$_3$).
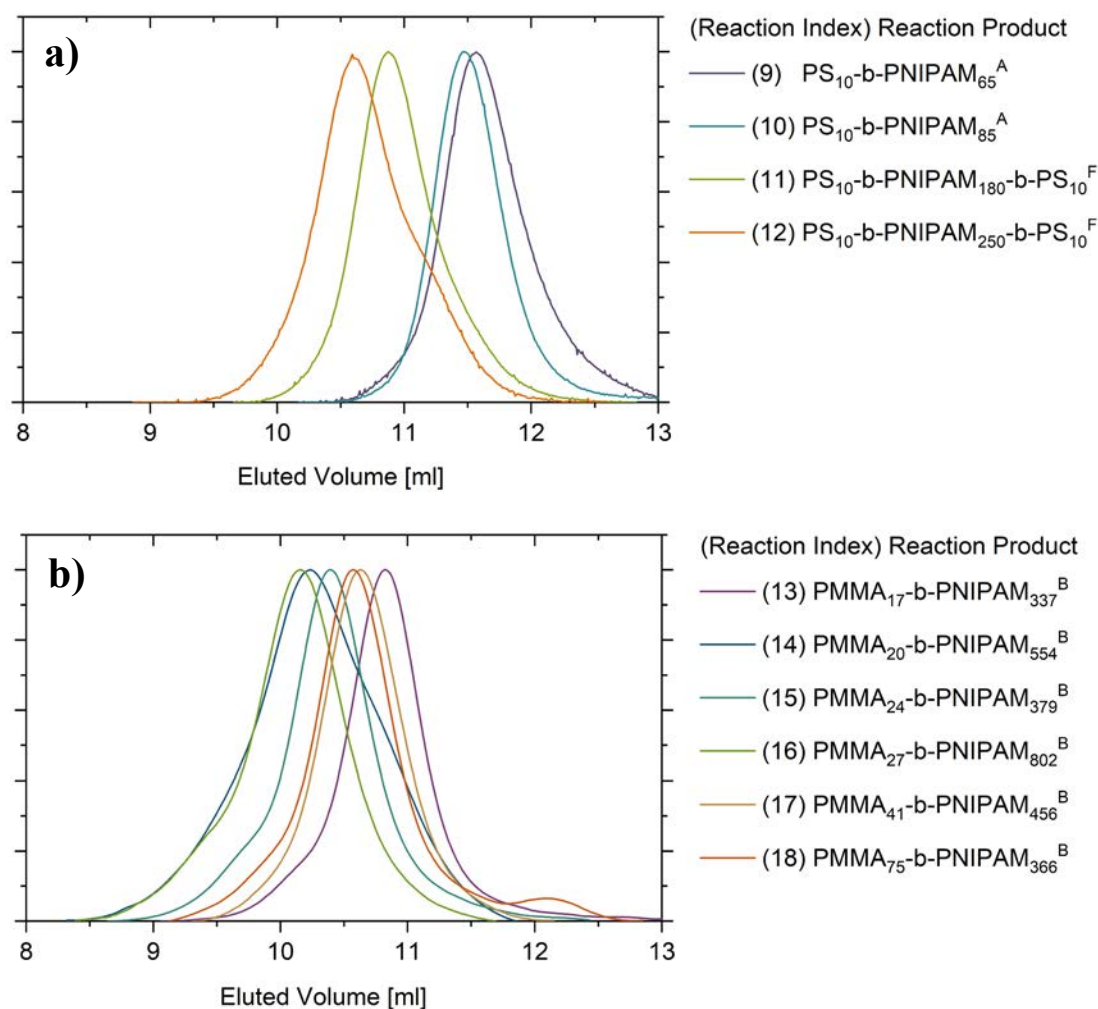
Figure 26. SEC elugrams of all PNIPAM block copolymers. (a) Diblock and triblock copolymers based on PS. (b) Diblock copolymers based on PMMA. All SEC measured in NMP. The curves have been smoothed and normalized.

The SEC results allow an evaluation of the success of the polymerizations based on the shift towards larger molar masses (earlier elution) after chain extension, shape of the molar mass distributions (monomodal or multimodal), and dispersity indices.

For all chain extension reactions, a strong shift to larger molar masses could be seen. However, while some reactions yielded narrow monomodal distributions (e.g., reactions 10, 11, 16, and 17), others led to a bimodal molar mass distribution. In some cases (e.g., reaction 18), this bimodality seems clearly caused by an incomplete reaction of the macro-CTA precursor. This is likely due to loss of end-groups during the polymerization of the first block, hindering the reactivation of the chains for chain extension. As previously mentioned, this is a common concern in the synthesis of block copolymers, particularly when synthesizing long blocks, or applying long reaction times.

In other cases, both populations show molar mass larger than the precursor (e.g., reactions 12 and 14), indicating that reactivation of the macro-CTA did occur. In this case, the existence of a

population with lower molar masses could indicate loss of end-groups during the progress of the chain extension (NIPAM polymerization) reaction. This loss of end-groups may have occurred after some NIPAM units had already been added to the macro-CTA, but before the end of the reaction, capping the obtained molar masses, while the remaining chains could react further.

Thermal analysis of the dry diblock copolymers by differential scanning calorimetry (DSC) revealed only one glass transition, which occurs at temperatures ranging from 123 to 136 °C, as shown in Table 7 and Annex 0. This T_g agrees with the T_g of high-molar-mass PNIPAM homopolymers (ca. 130 °C, depending on molar mass, tacticity and water content),[235,236] which could indicate a microphase separation of the hydrophobic (PS or PMMA) and the PNIPAM blocks in the bulk. Although such microphase separation is known to occur in PMMA-b-PNIPAM copolymers where the PMMA and PNIPAM blocks have similar sizes,[235] it may not be the case here. Firstly, because the glass transition of PS (about 47 to 62 °C) or PMMA (about 73 to 81 °C) could not be seen in the thermograms of any of the copolymers. Moreover, copolymers with very short PNIPAM segments (particularly PS$_{10}$-b-PNIPAM$_{65}$^{A}, see Figure A 67) showed slightly lower T_g than the remaining copolymers, which would be further evidence indicating a mixture of the PS and PNIPAM blocks in dry bulk.

Table 7. Glass transition temperature of the PNIPAM copolymers and their macro-CTA precursors.

Copolymer Index	Copolymer	Precursor (macro-CTA) Index	T_g Macro-CTA [°C]	T_g Copolymer [°C]
9	PS$_{10}$-b-PNIPAM$_{65}$^{A}	1	47	123
10	PS$_{10}$-b-PNIPAM$_{85}$^{A}	1	47	126
11	PS$_{10}$-b-PNIPAM$_{180}$-b-PS$_{10}$^{F}	2	62	129
12	PS$_{10}$-b-PNIPAM$_{250}$-b-PS$_{10}$^{F}	2	62	131
13	PMMA$_{17}$-b-PNIPAM$_{337}$^{B}	3	-	134
14	PMMA$_{20}$-b-PNIPAM$_{554}$^{B}	4	59	134
15	PMMA$_{24}$-b-PNIPAM$_{379}$^{B}	5	75	129
16	PMMA$_{27}$-b-PNIPAM$_{802}$^{B}	6	73	134
17	PMMA$_{41}$-b-PNIPAM$_{456}$^{B}	7	81	136
18	PMMA$_{75}$-b-PNIPAM$_{366}$^{B}	8	91	131

3.3. Synthesis of Polymers based on PNIPMAM

Poly(*N*-isopropyl methacrylamide) (PNIPMAM) is a thermoresponsive polymer with chemical structure very similar to that of PNIPAM, except for the presence of an additional methyl group on the backbone. Although this would expectedly render the material more hydrophobic, thus causing a decrease of the transition temperature, PNIPAM has been reported to show T_{CP} around 44°C, that is, considerably higher than PNIPAM (ca. 32°C).[28]

Contrary to the plethora of studies focused on PNIPAM, very few have investigated its methacrylamide analog, and the few published reports on its co-nonsolvency properties have focused solely on water/ethanol systems.[97-99] This scarcity may be, at least in part, for the fact that the polymerization of NIPMAM is more challenging, especially when using reversible addition fragmentation chain transfer - RAFT, and high molar masses with low dispersity seem difficult to attain. Therefore, one goal of this thesis was to more closely investigate the polymerization of NIPMAM, potentially identifying critical aspects and improvement potentials. For this, both homopolymers and amphiphilic block copolymers were synthesized, for subsequent characterization of its thermoresponsive and aggregation behaviors.

Although the *N*-isopropyl methacrylamide – NIPMAM monomer is available commercially, the available purity level is low, and extensive purification is necessary before polymerization. Thus, one of the first aspects which were investigated (and described here in section 3.3.1) was the synthetic and purification procedure of the monomer, and its impact on the obtained polymer. Subsequently, the focus was given to the polymerization reaction parameters. Here, several initiators, solvents and temperatures were evaluated using conventional free radical polymerization (section 3.3.2). Finally, the RAFT polymerization of NIPAM was studied, through which both homopolymers as well as amphiphilic block copolymers were obtained (section 3.3.3).

3.3.1. Evaluation of Monomer Synthesis & Purification Methods

Synthesis of *N*-isopropyl methacrylamide – NIPMAM monomer was done through reaction of isopropylamine with methacryloyl chloride, in the presence of NaOH. The monomer which resulted from this procedure is coded **S-NIPMAM-R** (S standing for self-synthesized, and R standing for purification by recrystallization). The ^{1}H NMR spectrum of the resulting material (Annex 7.1, Figure A 7) is in accordance with that of purified commercial NIPMAM, evidencing the success of the synthesis.

Although no contamination could be identified in the monomer at this stage, neither by NMR spectroscopy nor by thin layer chromatography, it is possible that trace amounts of *N*-oxides formed from the degradation of the monomer are present. These could act as inhibitors to the subsequent polymerization, even if only present in small quantities. Thus, part of the monomer was subjected to additional purification, for which it was dissolved in dichloromethane (DCM) and washed against a 0.1 N aqueous solution of NaOH. The monomer which was subjected to this additional step is coded **S-NIPMAM-RW** (where W stands for washing against NaOH(aq.)). As a comparison, commercially obtained monomer was subjected to the same two purification procedures, yielding **C-NIPMAM-R** and **C-NIPMAM-RW** (C standing for commercial).

These monomer samples were then polymerized through conventional free radical polymerization, to evaluate the impact of impurities on the polymerization, compare the efficacy of the different purification procedures, and to compare the quality of the commercially obtained monomer and the synthesized monomer. All polymerizations were done under the same conditions, using AIBN as initiator (monomer:AIBN ratio ca. 610:1) and benzene as solvent (25 wt.% monomer concentration of reactants in mixture). Reactions were performed at 65°C for 24h. Conversion was calculated from ^{1}H NMR spectra of the crude reaction mixture, through comparison of the relative signal intensity of the double bond of the monomer with that of the CH on the isopropyl group. Workup was done by solubilization in acetone and precipitation in 2:1 diethyl ether / pentane mixtures. All the reactions were carried out simultaneously. Listed in Table 8 are the conversion and molar mass results obtained from each sample. The SEC elugrams of the samples are shown in Figure 27 and the coloration of the crude reaction mixtures is depicted in Figure 28. Apart from the difference in coloration and achieved conversions, the results obtained from the five reactions are very similar with respect to the obtained molar masses and polymer dispersities *Đ*.

Table 8. Main results of the polymerization of NIPMAM, where the monomer was obtained and purified by different methods. Polymerizations performed using ca. 0.164 mol.% of AIBN in benzene (monomer concentration 25 wt.%) at 65°C for 24 h.

Index	Reaction Product	Monomer Code	Conversion	SEC		
				M_n [kg·mol^{-1}]	M_w [kg·mol^{-1}]	$Đ^{SEC}$
19	PNIPMAM$_{264}$	C-NIPMAM-R	57%	34	69	2.1
20	PNIPMAM$_{301}$	C-NIPMAM-RW	65%	38	79	2.1
21	PNIPMAM$_{305}$	S-NIPMAM-R	60%	39	78	2.0
22	PNIPMAM$_{295}$	S-NIPMAM-RW	74%	37	81	2.2
23	PNIPMAM$_{339}$	S-NIPMAM-RW [*]	72%	43	89	2.1

Monomer code legend: C stands for monomer obtained commercially, S stands for synthesized monomer, R stands for purification by recrystallization 2 times from n-hexane, W stands for purification by washing against NaOH(aq.). (*) To evaluate reproducibility, two reactions were performed with the same monomer sample, namely the synthesized monomer purified by recrystallization and subsequent washing against NaOH(aq.).

SEC measured in NMP and calibrated using PMMA standards.
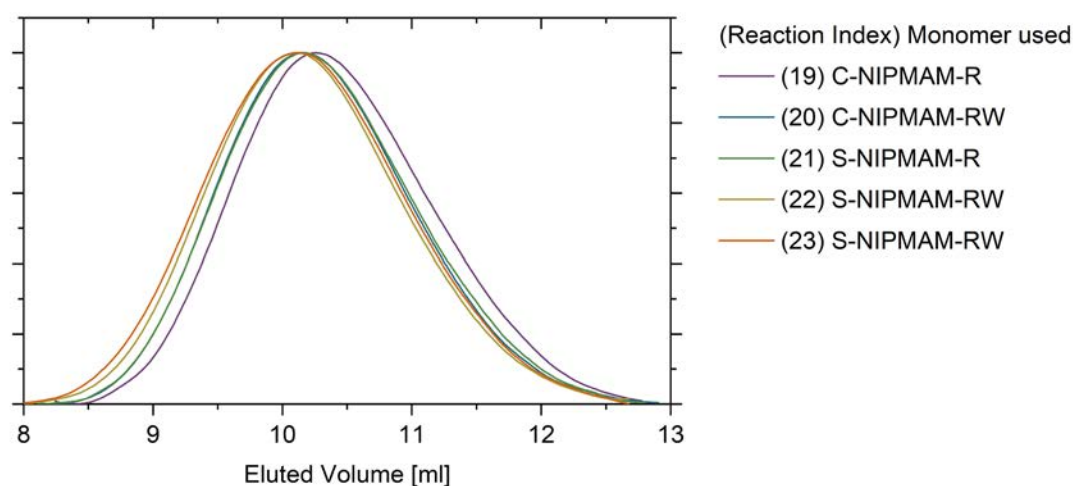
Figure 27. SEC elugrams of PNIPMAM (measured in NMP), where the monomer used for each reaction was obtained and purified by different methods (samples listed in Table 8).
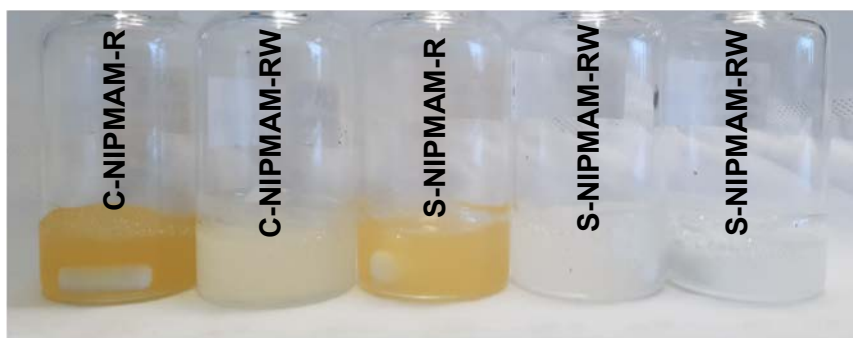
Figure 28. Crude reaction mixture of the polymerization of NIPMAM synthesized and obtained commercially; purified by recrystallization or recrystallization followed by washing against NaOH(aq.).

Possibly, slightly better results are obtained for the synthesized monomer in comparison to the commercially obtained one, and when applying the more extensive purification procedure than simple recrystallization. These measures at least clearly improve coloration and seem to have some impact over conversion. Nonetheless, analysis of the SEC elugrams (Figure 27), reveals that the variation of conversions and molar mass results are not significant enough to attribute the overall difficulties on the polymerization of NIPMAM to the factors evaluated here (synthesis and purification method), especially when considering the reproducibility of the results and error margin of the characterization methods.

3.3.2. Screening of Initiators, Solvents and Temperatures

In order to find the best possible system (solvent, initiator, temperature) to polymerize NIPMAM, and to exclude issues of solubility, as well as to evaluate reproducibility, several screening conventional free radical polymerization (FRP) reactions were performed with various initiators, temperatures and solvents. The tested initiators were 2,2′-azobis(2-methylpropionitrile) (AIBN), dimethyl-2,2'-azobis(2-methylpropionate) (MAIB), 1,1'-azobis(cyclohexane-1-carbonitrile) (V40), 2,2'-azobis(2-methylpropionamidine)dihydrochloride (V50), and 2,2'-azobis(4-methoxy-2,4-dimethylvaleronitrile) (V70). Their chemical structure is depicted in Figure 29. These initiators were chosen to cover a wide range of polarity and bulkiness, thus allowing an evaluation of the influence of these factors on the polymerization of NIPMAM.
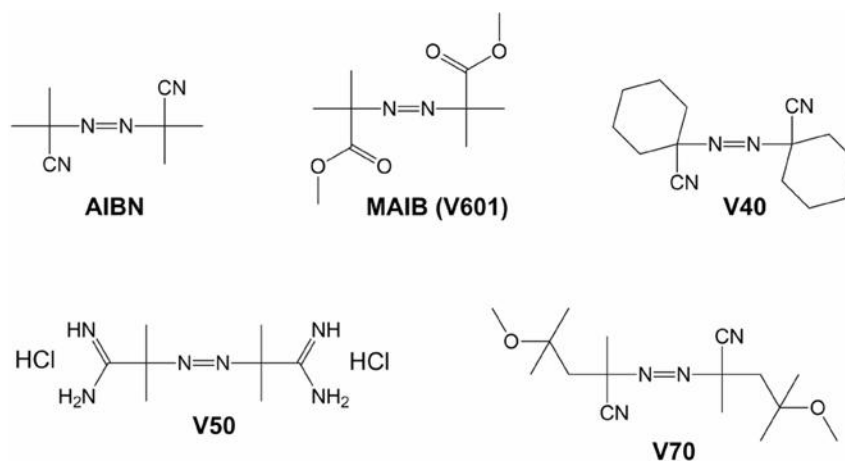
Figure 29. Chemical structure of the initiators assessed for the polymerization of NIPMAM.

Analogously, the choice of solvents was based on the solubility of both the monomer and the initiator, with the aim of covering a broad range of polarities, from benzene (nonpolar), via trifluorotoluene - TFT and ethanol to 2,2,2-trifluoroethanol - TFE (highly polar). Other than a few exceptions, the temperature chosen for each reaction was that of the 10 h half-life of the initiator. To evaluate reproducibility, certain reactions were repeated multiple times. Conversion was calculated from ^{1}H NMR spectra of the crude reaction mixture, through comparison of the relative signal intensity of the double bond of the monomer with that of the CH on the isopropyl group. The complete list of reactions and results obtained is compiled in Table 9. A typical ^{1}H NMR spectrum of a homopolymer PNIPMAM obtained by conventional free radical polymerization is shown in Annex 7.1 - Figure A 36.

Analyzing the outcome from the various reactions, one of the most striking aspects is the poor reproducibility of the results. Even using the same system, and under the same reaction conditions, the course of the reactions varied enormously (see for example reactions 1-5, 9-13, 17-21 and 23-26. This variability of results can be clearly visualized in Figure 30, which shows the range (whiskers), median (circle) as well as individual data points (diamonds) of monomer conversion and dispersity obtained from each of the four main systems evaluated here.

Table 9. Polymerizations of NIPMAM using various initiators, solvents, and temperatures. All reactions were done with a monomer / initiator ratio of ca. 1200 and concentration of ca. 30 wt.%, for about 18 h.

Index	Product	Initiator	Solvent	Temperature [°C]	Conversion [%]	$M_n^{SEC\,(*)}$ [kg·mol^{-1}]	$M_w^{SEC\,(*)}$ [kg·mol^{-1}]	$Đ^{SEC\,(*)}$
24	PNIPMAM$_{390}$	AIBN	benzene	65	26	50	95	1.9
25	PNIPMAM$_{445}$	AIBN	benzene	65	46	57	119	2.1
26	PNIPMAM$_{393}$	AIBN	benzene	65	63	50	138	2.8
27	PNIPMAM$_{776}$	AIBN	benzene	65	89	99	276	2.8
28	PNIPMAM$_{956}$	AIBN	benzene	65	96	122	366	3.0
29	PNIPMAM$_{469}$	AIBN	benzene	72	79	60	153	2.6
30	PNIPMAM$_{424}$	AIBN	benzene	72	41	54	112	2.1
31	PNIPMAM$_{241}$	AIBN	TFE	65	89	31	86	2.8
32	-	MAIB	benzene	66	6	-	-	-
33	-	MAIB	benzene	66	7	-	-	-
34	-	MAIB	benzene	66	9	-	-	-
35	PNIPMAM$_{426}$	MAIB	benzene	66	51	54	133	2.5
36	PNIPMAM$_{936}$	MAIB	benzene	66	54	110	322	2.7
37	-	V40	benzene	88	0	-	-	-
38	PNIPMAM$_{1154}$	V50	TFE	56	52	147	293	2.0
39	PNIPMAM$_{810}$	V50	TFE	56	66	103	187	1.8
40	PNIPMAM$_{895}$	V50	TFE	56	85	114	226	2.0
41	PNIPMAM$_{201}$	V50	TFE	56	91	26	58	2.3
42	-	V70	benzene	30	0	-	-	-
43	PNIPMAM$_{381}$	V70	EtOH	30	21	48	95	2.0
44	PNIPMAM$_{219}$	V70	EtOH	30	31	28	89	3.2
45	PNIPMAM$_{682}$	V70	EtOH	30	35	87	173	2.0
46	PNIPMAM$_{689}$	V70	EtOH	30	63	88	159	1.8
47	-	V70	TFT	30	0	-	-	-

TFT: trifluorotoluene, TFE: 2,2,2-trifluoroethanol, EtOH: ethanol.

(*) SEC measured in NMP and calibrated using PMMA standards.
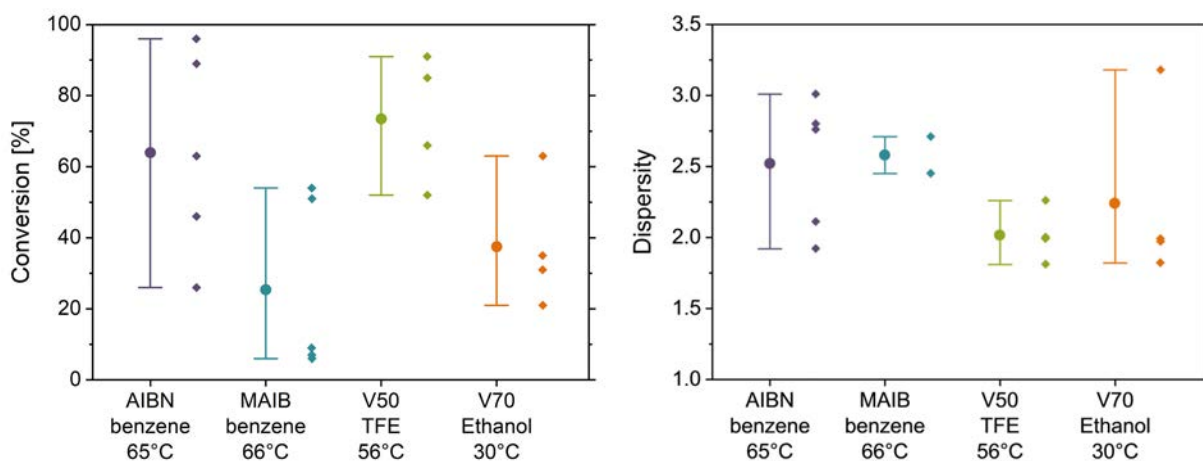
Figure 30. Monomer conversion (left) and dispersity (right) results obtained from the polymerization of NIPMAM using the four main systems (initiator / solvent / reaction temperature) investigated in this study. Whiskers represent the range (minimum – maximum), circles represent the mean and diamonds represent the individual datapoints for each system.

Still, through these plots, a general trend can be seen, where systems AIBN / benzene / 65°C and V50 / TFE / 56°C tend to yield higher conversions than MAIB / benzene / 66°C and V70 / ethanol / 30°C. This indicates that the difficulties in polymerizing NIPMAM are unlikely to be related to a low-lying ceiling temperature. Moreover, poor monomer solubility does not seem to be responsible for the issues either. Although NIPMAM is not soluble in benzene at room temperature, which might lead to questions regarding its solubility at higher temperatures, the monomer is readily soluble in TFE. Nonetheless, the results obtained from TFE do not show any significant and systematic superiority with respect to those obtained from benzene. This implies also that the solvent polarity is not a decisive factor. However, it is important to highlight that a larger number of reactions would have to be performed with each system to obtain more reliable statistics and draw more accurate conclusions.

The lack of reproducibility on the results seems to indicate that NIPMAM's polymerization issues are governed by some (highly variable) external factor, rather than intrinsic characteristics of the system (initiator / solvent / temperature) used. However, in this study, the variations could not be directly correlated to any external aspects involving weather conditions, monomer/initiator/solvent batch, degassing gas and duration, reaction volume, nor cleaning procedure for the reaction flask. It is important to remark, however, that the monomer / initiator ratio used in the reactions discussed in this section were extremely high (1200 : 1). In contrast, the monomer / initiator ratio applied in the previous section (3.3.1- Evaluation of Monomer Synthesis & Purification Methods) was only 610 : 1. The high monomer / initiator ratio used here was chosen to increase the monomer

concentration in the reaction mixture, and reduce potential monomer depletion effects. However, this also leads to a small concentration of radicals in the reaction mixture, which makes the systems particularly sensitive to trace impurities and trace side-reactions which consume initiator radicals and/or propagating radicals.

3.3.3. RAFT Polymerization of NIPMAM

Based on the results obtained from the screening described on the previous section, two systems were chosen for evaluation under reversible addition fragmentation chain transfer (RAFT) polymerization: AIBN / benzene / 65°C and V50 / TFE / 56°C. Given the interest in obtaining amphiphilic block copolymers based on PNIPMAM, for characterization of their co-nonsolvency and self-assembly behavior, PMMA macro-CTAs were used rather than the pure CTA (except for reaction index 59, which will be discussed in subsequent paragraphs). The same PMMA macro-CTAs were used as for the polymerization of NIPAM (see section 3.2.1, Table 5). As previously described, these macro-CTAs were polymerized using the dye-labelled CTA **B**, due to the possibility of more accurately characterizing the obtained polymers by end-group analysis.

Table 10 presents a list of the polymerizations performed with the two abovementioned systems. The most striking result of these tests is that the RAFT polymerization of NIPMAM simply did not occur when TFE was used as a solvent, despite the relative success that the V50/TFE system produced on conventional free radical polymerizations. Moreover, the RAFT polymerization of NIPMAM in TFE, using this same CTA **B** (albeit without the PMMA block) has been shown before, using V501 (4,4'-azobis(4-cyanovaleric acid)) as initiator.[5,237] The thiocarbonate moiety of the CTA is prone to hydrolysis, generating H_2S, which acts as a strong inhibitor for radical polymerizations. Although the same batch and bottle of high purity TFE solvent was used for both the conventional free radical polymerizations and RAFT reactions shown in this thesis, it is plausible that the solvent indeed contained a residual amount of water, which caused partial degradation of the CTA, and inhibition of the RAFT reactions. This may have occurred in very small amounts, such that no discoloration could be visually detected, but even trace amounts of inhibitor could have a significant effect on the polymerization. Based on the results at hand, it is not possible to draw concrete conclusions and more experiments are recommended, particularly with evaluation of the water content of the TFE solvent.

Table 10. Reaction conditions and obtained monomer conversion of the RAFT polymerizations of NIPMAM aiming the comparison of V50 and AIBN as initiator, as well as TFE and benzene as solvent. All reactions listed in this table were performed using concentration of ca. 30 wt.%, for about 18 h. All precursors were PMMA macro-CTAs.

Index	Product	Precursor Index	Initiator	Monomer : Macro-CTA : Initiator Ratio	Solvent	Temperature [°C]	Conversion [%]
48	-	5	V50	610 : 1 : 0.18	TFE	56	0
49	-	5	V50	625 : 1 : 0.18	TFE	56	0
50	-	5	V50	638 : 1 : 0.18	TFE	56	0
51	-	4	AIBN	624 : 1 : 0.18	TFE	65	0
52	PMMA$_{17}$-*b*-PNIPMAM$_{145}$[B]	3	AIBN	551 : 1 : 0.20	benzene	65	97 [a]
53	PMMA$_{20}$-*b*-PNIPMAM$_{146}$[B]	4	AIBN	327 : 1 : 0.12	benzene	72	56
54	PMMA$_{20}$-*b*-PNIPMAM$_{242}$[B]	4	AIBN	507 : 1 : 0.18	benzene	71	51
55	PMMA$_{24}$-*b*-PNIPMAM$_{443}$[B]	5	AIBN	632 : 1 : 0.18	benzene	72	44
56	PMMA$_{27}$-*b*-PNIPMAM$_{248}$[B]	6	AIBN	592 : 1 : 0.20	benzene	71	78
57	PMMA$_{41}$-*b*-PNIPMAM$_{153}$[B]	7	AIBN	611 : 1 : 0.22	benzene	71	30
58	-	8	AIBN	302 : 1 : 0.13	benzene	65	28
59	PNIPMAM$_{146}$[B]	CTA B	AIBN	271 : 1 : 0.10	benzene	71	58

TFE: 2,2,2-trifluoroethanol.

(a) Yield is used in lieu of conversion when the latter is not available.

Meanwhile, the polymerizations using AIBN and benzene yielded conversion values (and variability) in accordance with those observed in conventional free radical polymerization of NIPMAM. The detailed molar mass characterization results of the products of these reactions are listed in Table 11. As mentioned before, reaction index 59 was performed using the pure CTA, as opposed to PMMA macro-CTAs, which was the case of the other RAFT polymerizations of NIPMAM. This was done to assess the influence of the pre-existing PMMA block attached to the CTA, in comparison to the use of the CTA alone.

Table 11. Molar mass characterization results for the RAFT polymerizations of NIPMAM, using AIBN as initiator, benzene as solvent and concentration of ca. 30 wt.%, for about 18 h.

Index	Product	Conversion [%]	M_n [kg·mol^{-1}] Theor. [b]	NMR	UV-vis	EA $^{C/N}$	SEC [c]	M_w^{SEC} [kg·mol^{-1}] [c]	$Đ^{SEC}$ [c]	$w_{PNIPMAM}$ (from SEC)
52	PMMA$_{17}$-*b*-PNIPMAM$_{145}$^{B}	97 [a]	*70* [a]	81	87	81	21	44	2.1	0.89
53	PMMA$_{20}$-*b*-PNIPMAM$_{146}$^{B}	56	27	55	44	51	21	46	2.2	0.88
54	PMMA$_{20}$-*b*-PNIPMAM$_{242}$^{B}	51	37	62	67	55	33	66	2.0	0.92
55	PMMA$_{24}$-*b*-PNIPMAM$_{443}$^{B}	44	38	115	-	-	59	141	2.4	0.95
56	PMMA$_{27}$-*b*-PNIPMAM$_{248}$^{B}	78	63	78	79	64	35	107	3.1	0.90
57	PMMA$_{41}$-*b*-PNIPMAM$_{153}$^{B}	30	29	38	44	38	24	46	1.9	0.80
59	PNIPMAM$_{146}$^{B}	58	21	23	23	-	19	35	1.8	0.97

(a) Yield is used in lieu of conversion when the latter is not available. Resulting $M_n^{theor.}$ is provided tentatively.

(b) Calculated from the conversion (or yield) and monomer / CTA ratio.

(c) SEC measured in NMP and calibrated using PMMA standards.

As the results listed in Table 11 indicate, the RAFT polymerization of NIPMAM poses an even bigger challenge than its free radical polymerization. This is evidenced by the variability in the achieved monomer conversion and high molar mass dispersities.

Although no reaction provided results typically expected for RAFT polymerizations, it seems that increasing the size of the pre-existing PMMA block leads to negative effect on the conversion. Nonetheless, this does not seem to directly correlate to the dispersity of the obtained products.

The elevated dispersity of the reaction products raises the question whether the polymerization of NIPMAM was indeed controlled, or whether the monomer mostly homopolymerized without interaction with the chain transfer agent and, therefore, without promoting the chain extension of the existing PMMA block. In this case, a closer analysis of the results, and particularly of the molar mass dispersion curves from SEC may provide further information.

Comparing the molar mass values obtained from the various characterization methods for each of the reaction products, it is striking the variability between the results. This can be better understood when evaluating how each method works and what it measures. Molar masses obtained from both NMR and UV-vis are number-average values, based on end-group analysis. Thus, loss of end-groups leads to incorrectly large molar mass results, as the proportional amount of Z end-groups

in the system is reduced. As a result, it is possible to see that, in most cases, there some consistency between the molar masses obtained by NMR and UV-vis, and the variations seen for a few of the polymers could potentially be attributed to inaccuracies on sample preparation and evaluation / calculation of the results. This includes possible variations while weighing the samples, diluting the UV-vis solutions, baseline correction of the NMR spectrum or integral range selection on NMR.

Molar masses obtained from elemental analysis were calculated based on the carbon/nitrogen ratio of the MMA and NIPMAM constitutional repeat units. This method was used to avoid errors caused by the residual water content of the copolymer, which cannot be neglected, given the highly hygroscopic nature of the PNIPMAM block. Therefore, somewhat similarly to NMR and UV-vis, elemental analysis in this case yields molar mass values based on the overall proportion between PMMA and PNIPMAM and will produce erroneous values if homopolymer PNIPMAM chains are present in the system, e.g., in case NIPMAM homopolymerizes instead of chain extending the existing PMMA macro-CTAs. Accordingly, M_n^{NMR}, M_n^{Vis} and M_n^{EA} are in rough accordance with each other, and variations can be plausibly attributed to measurement imprecisions.

SEC measurements, in contrast, depends on the hydrodynamic diameter of the polymer chains, which determines the elution time of each molecule. A refractive index detector was used to identify the concentration of polymer being eluted over time, and comparison against a calibration standard (in this case, PMMA) yielded the concrete molar mass values. Given that the polymers under evaluation here are not fully composed of PMMA, a certain error in the molar mass results is expected by default. Nonetheless, SEC is valuable for providing information based on the actual size of each chain (in case there are no specific interactions with the column material). This excludes, for example, the abovementioned errors due to loss of end-groups, when using end-group analysis. Moreover, SEC offers the benefit of revealing the shape of the molar mass distribution, even if the absolute molar mass values are somewhat misleading. The elugrams of all the polymers listed in Table 11 are depicted in Figure 31. Comparisons between the elugrams of the PMMA macro-CTAs and obtained PMMA-*b*-PNIPMAM copolymers are available in Figure A 57, in the annexes.
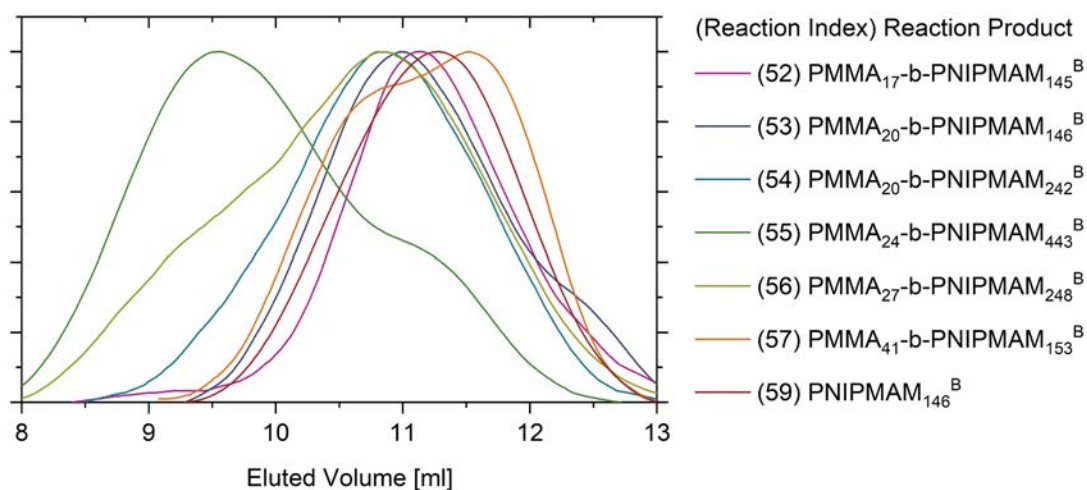
Figure 31. SEC elugrams of PNIPMAM homo- and copolymers obtained by RAFT polymerization. All SEC measured in NMP. The curves have been smoothed and normalized.

A bimodal molar mass distribution is evidenced by the elugrams of reactions indices 53 and 55, where shoulder at long elution times indicates a shoulder at low molar masses. Similarly, reactions indices 56 and 57 show a shoulder at early elution times, indicating that the molar mass distribution shows a shoulder at high molar masses. These bimodal distributions could be a result of homopolymerization taking place in parallel to chain extension of the PMMA block, premature termination reactions, undesired chain transfer reactions (e.g., to monomer or to polymer) or recombination reactions. Still, a seemingly monomodal distribution does not exclude the possibility that early termination or homopolymerization took place, as the bimodal distribution might not always be clearly identifiable depending on the overlap between the two populations. Because of this, the question remains whether loss of end-groups and homopolymerization of NIPMAM took place, for example, in the case of reactions indices 52, 54 and 59, which appear monomodal.

To clarify this doubt, additional SEC measurements were performed, using a combination of the reflective index (RI) detector with a visible-ultraviolet (UV) detector measuring the absorption at a wavelength of 409 nm. This is the maximum absorption wavelength of the chromophore on the R-group of CTA **B** and could, therefore, provide information regarding the amount of R end-groups being eluted. Given that the PMMA block is attached to the R-group of the CTA, this would also indicate the amount of PMMA blocks being eluted. The refractive index detector, in contrast, provides information on the proportion of polymer in the eluting solution, that is, the mass of

polymer being eluted at each time.[(* see footnote)] By comparison of the results from the RI and UV detectors, one can to evaluate whether the proportion of PMMA blocks (R-groups) to polymeric mass throughout elution fits the expected ratio for each molar mass (according to the calibration). With this, it is possible to identify whether PMMA blocks are (partially) absent at certain molar masses, that is, whether NIPMAM homopolymerized. Two polymers were selected for this evaluation, namely PMMA$_{20}$-b-PNIPMAM$_{242}$^{B} (reaction index 54) and PMMA$_{41}$-b-PNIPMAM$_{153}$^{B} (reaction index 57).

For a clearer comparison between the results of the two detectors, it is helpful to multiply the intensity of the UV signal by the molar mass. This is necessary because the distribution obtained from the RI detector is given with respect to mass, while the distribution obtained from the UV detector is given with respect to number of labelled chains. This means that, as the molar mass increases, the proportion of end-groups decreases, leading to a reduced UV signal at higher molar masses, even if the same mass of polymer is being eluted and all chains contain the R end-groups. In contrast, the RI signal is directly proportional to the polymeric mass and will not suffer such reduction. Thus, the multiplication of the UV signal by the molar mass allows the direct comparison between the UV and RI signals.

The molar mass distributions obtained with the RI detector, as well as the corrected distribution obtained with the UV detector are illustrated in Figure 32a for PMMA$_{20}$-b-PNIPMAM$_{242}$^{B} - reaction index 54 and in Figure 32b for PMMA$_{41}$-b-PNIPMAM$_{153}$^{B} - reaction index 57. Figure 32c and Figure 32d show the ratio between the RI and (corrected) UV signals for each polymer. In an ideal case, where all polymer chains contain an R end-group (and assumingly a PMMA block), this ratio would be equal to 1 over the entire molar mass range. In case of partial homopolymerization, where some chains do not contain an R group (and PMMA block), the ratio would be >1, given that the RI signal (proportional to polymeric mass) would remain unchanged,

---

* It must be noted that the refractive index of a copolymer or polymer mixture depends on the refractive index of the individual polymers, being slightly different for PMMA and PNIPMAM. Here, the ratio between the sizes of the PNIPMAM and PMMA blocks are not constant throughout the entire molar mass range, changing considerably as the PNIPMAM block size increases. Therefore, the refractive index of the copolymer is also not constant, leading to some inaccuracies in the results obtained. However, these inaccuracies are not being considered here, as the PNIPMAM block size is expected to be much larger than the PMMA block size, thus the refractive index variation is assumed to be small.
Another aspect that must be considered, for both refractive index as well as UV detection methods, is the potentially misleading information obtained by SEC. In the present study, all polymer chains are considered to be linear, containing either one or no R-group. However, in reality, a number of side-reactions and terminations may occur during polymerization, potentially leading to more complex chain structures (e.g., branching) or existence of two R-groups in the same chain (e.g., if chain transfer to polymer occurs). Since the molar mass obtained by SEC is based on the hydrodynamic radius, a branched architecture would be identified by SEC as having a much smaller molar mass (smaller hydrodynamic radius) than a liner chain of same (real) molar mass.

but the (corrected) UV signal would be reduced, given the partial absence of R end-groups. Moreover, it is important to highlight that the quality and accuracy of the signals are proportional to the amount of material being detected (whether polymeric mass or end-groups). Thus, larger imprecisions are expected at the edges of the molar mass distribution (very low and very high molar masses), given the lower quantity of material to be detected. Furthermore, in the case of the corrected UV signal, any signal noise is amplified in the large molar mass range, given the multiplication by the molar mass.

With this in mind, it becomes clear that on PMMA$_{20}$-b-PNIPMAM$_{242}$^{B} (reaction index 54), the copolymerization was rather satisfactory, despite its wide molar mass distribution for a RAFT polymerization ($Đ$ 1.99, see Table 11). This is evidenced by the good accordance between the distribution curves obtained from the two detectors, as well as the ratio between the signals, which is quite close to 1 in the molar mass range where most of the molecules are found, indicating the presence of R end-groups. Thus, it is likely that most chains do indeed contain a PMMA block.

Sample PMMA$_{41}$-b-PNIPMAM$_{153}$^{B} (reaction index 57), on the contrary, shows adequate presence of R end-groups only in the range around 8 to 11 kg·mol^{-1}, a very small fraction of its distribution. Instead, the sample shows extreme absence of R end-groups at high molar masses. Most striking is the mostly monomodal character of the distribution detected by UV, whereas the distribution detected by RI is clearly bimodal. Thus, two polymer populations seem to be present: one with lower molar masses, which chain extended the existing PMMA block, and another population with much larger molar masses, lacking the RAFT CTA's R end-groups, and consequently the PMMA block. This hints that undesired reactions took place in parallel with the normal course of the polymerization. One possibility is that conventional free radical polymerization (population of higher molar mass) took place in parallel to the RAFT process (population of lower molas mass), given that RAFT polymerization typically leads to lower molar masses than the conventional free radical process.[59,138] Alternatively (or additionally), chain transfer to monomer may have occurred.
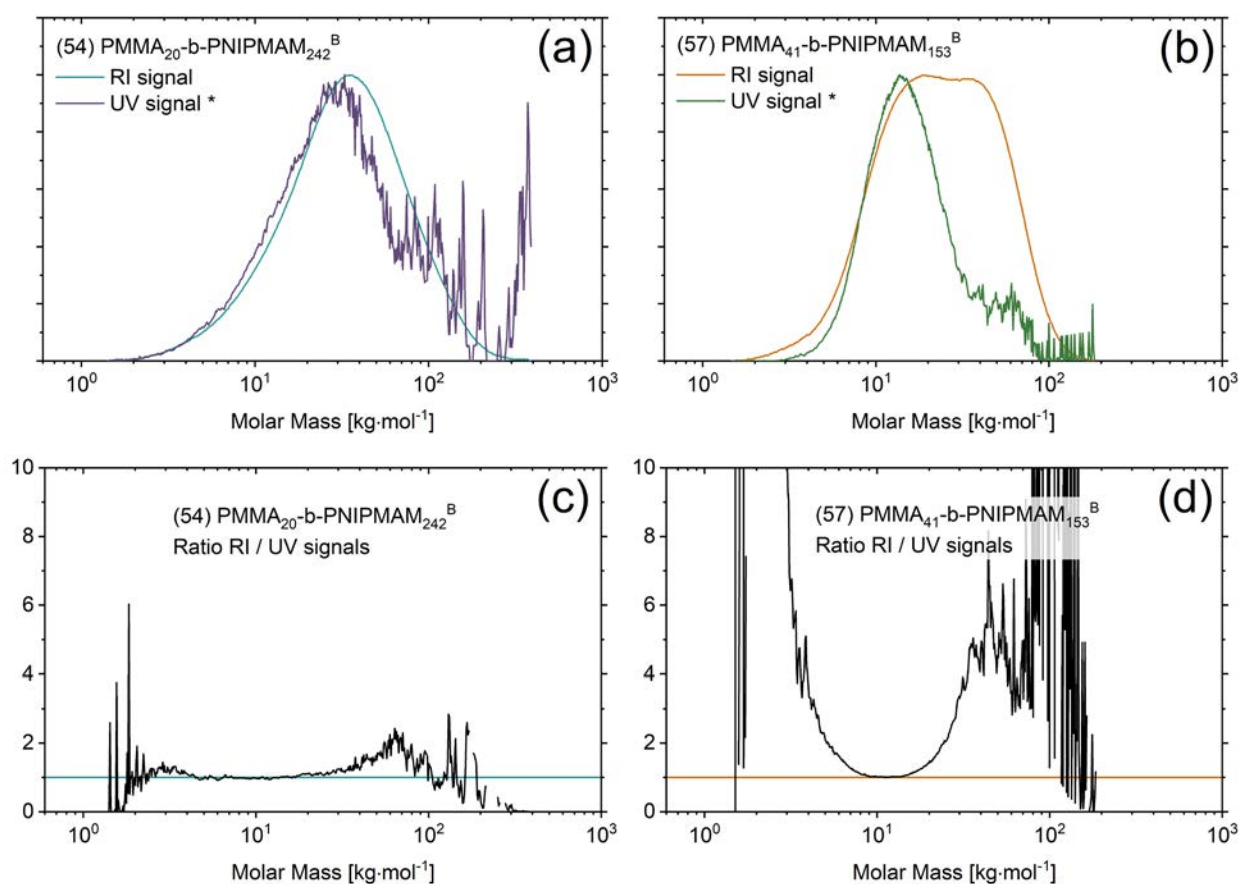
Figure 32. SEC molar mass distribution of (a) PMMA$_{20}$-*b*-PNIPMAM$_{242}$^{B} (reaction index 54) and (b) PMMA$_{41}$-*b*-PNIPMAM$_{153}$^{B} (reaction index 57), obtained both with RI and UV detectors (* the UV signals have been corrected by multiplication by the molar mass). All SEC measured in THF and calibrated using PMMA standards. The ratio between the signal intensity from RI and (corrected) UV is shown in (c) for reaction index 54 and (d) for reaction index 57.

The results obtained from reaction index 54 (PMMA$_{20}$-*b*-PNIPMAM$_{242}$^{B}) suggest that the initiation of the polymerization occurred, as expected, mostly by the CTA's R-group. However, the broad distribution suggests RAFT kinetics were not sufficiently fast. More specifically, the rate of addition seems to have been insufficient with respect to the rate of propagation. It cannot be ruled out, however, that chain transfer to polymer may have occurred, leading to the formation of a population of branched polymer chains, with a considerably larger perceived molar mass.

In contrast, in reaction index 57 (PMMA$_{41}$-*b*-PNIPMAM$_{153}$^{B}) initiation occurred only partially by the CTA's R-group. This also clarifies the lower conversion obtained in this reaction, considering that amount of initiator (AIBN) in the reaction is much smaller than CTA. The results obtained from this reaction suggest that either the rate of fragmentation of the macro-CTA was insufficient, or the rate of initiation of NIPMAM by the PMMA macro radical was insufficient. Since the same macro-CTA (reaction index 7) was used to initiate a polymerization of NIPAM (reaction index

17), where no significant issues were detected, a poor rate of initiation of NIPMAM by the PMMA macro radical seems a more likely scenario.

With this, the difference of outcomes obtained from reactions indices 54 and 57 suggest that the size of the PMMA sequence on the macro-CTA might impact the rate of initiation of NIPMAM by the PMMA macro radical.

In any case, the issues in the polymerization of NIPMAM are not exclusively present in RAFT, but also affect the conventional free radical polymerization of NIPAM, although it is considerably exacerbated in the RAFT process.

3.4. Synthesis of Polymers based on PNVIBAM

Poly(N-vinyl isobutyramide) (PNVIBAM) is another analog to poly(N-isopropyl acrylamide), which contains exactly the same chemical functionalities, but the position of the amide group is inverted, i.e. it is a constitutional position isomer of PNIPAM. Although the presence of the same chemical moieties would formally lead to the same hydrophilic/hydrophobic balance, and thus expectedly to the same transition temperature, PNVIBAM has been reported to show a T_{CP} around 39°C, that is, about 7°C higher than PNIPAM.[29]

PNVIBAM has only scarcely been studied in the literature. Its thermoresponsive properties have been investigated in the presence of salt,[193] in correlation to pressure,[192] and in the presence of comonomers.[29,190,195,197] However, most studies focused on chemically crosslinked hydrogels and its co-nonsolvency behavior has not been reported upon in details.[30]

The lack of reports on PNVIBAM might be partially because obtaining both its monomer, as well as the polymer requires special consideration. The NVIBAM monomer is not commercially available, and its synthesis is less well stablished than, for example, NIPAM and NIPMAM. Being a vinylamide, NVIBAM cannot be synthesized directly by reaction of the amine with the acid chloride, as is common practice for the acrylamides NIPAM and NIPMAM. Thus, PNVIBAM has been reportedly obtained by post polymerization modification of poly(N-vinyl acetamide) into poly(vinyl amide) and finally into poly(N-vinyl isobutyramide). However, qualitative conversion could not be achieved and the residual amino side groups may affect the properties of the obtained PNVIBAM.[189] Alternatively, the synthesis of NVIBAM monomer has been reported through pyrolysis of (N-α-isopropoxyethyl)isobutyramide, a method that is laborious, requires special equipment and generates low yield.[29] Other reported methods include the reaction of isobutyraldehyde with a vinyl azide generated *in situ*.[238] Most recently, the reaction of N-vinyl formamide with isobutyryl chloride was reported, simplifying the access considerably.[239,240]

In addition to the challenges of monomer synthesis, the controlled radical polymerization of NVIBAM to obtain well-defined homo- and copolymers has not been reported yet and cannot be expected to be straightforward. Being a vinyl amide monomer, thus representing a LAM, as opposed to the acrylamides NIPAM and NIPMAM, the control of its polymerization through RAFT generally requires different types of chain transfer agents, to compensate for the lower activation level.[34]

In the next sections, the synthesis of the NVIBAM monomer and its polymerization, both by conventional free radical polymerization and RAFT polymerization, will be described.

3.4.1. Synthesis of NVIBAM Monomer

The synthesis of the *N*-vinyl isobutyramide – NVIBAM monomer was done through *N*-acylation of *N*-vinyl formamide with isobutyryl chloride in the presence of triethylamine, and subsequent removal of the formyl group by selective hydrolysis using sodium hydroxide.[239] The synthesis was performed twice, generating about 10 g and 25 g batches (43% and 55% yield) of pure NVIBAM monomer, as evidenced by ^{1}H NMR (Figure 33), ^{13}C NMR (Annex 7.1 - Figure A 8), elemental analysis and FTIR (Annex 0 - Figure A 63).
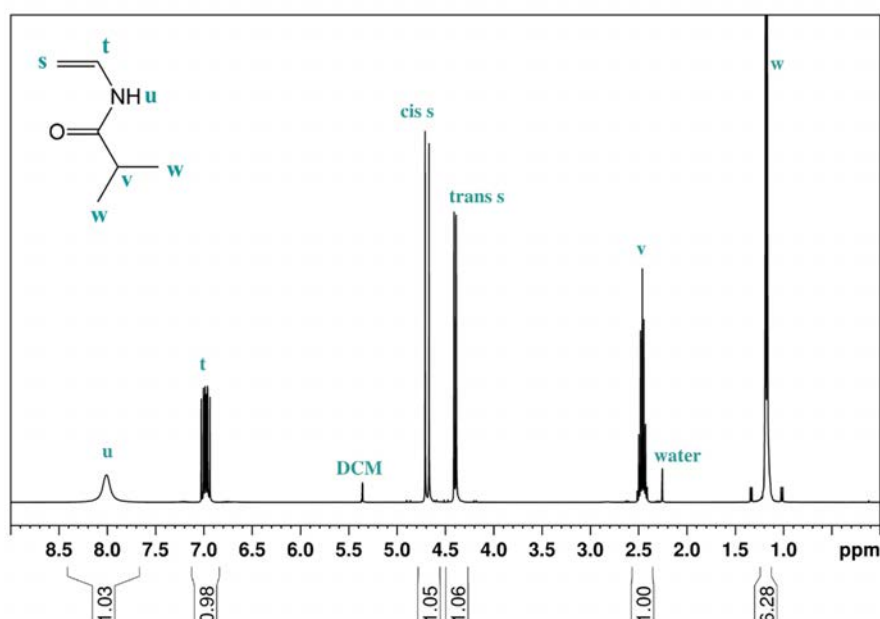
Figure 33. ^{1}H NMR spectrum of NVIBAM monomer in CDCl$_3$.

The success of the reaction, and obtained yield, is strongly related to the purity of the reagents, particularly *N*-vinyl formamide (NVF). NVF is remarkably challenging to purify and the addition of chasers (e.g., formamide) to aid distillation is a common practice.[241] However, since the

reactants used on the synthesis of NVIBAM are of relatively low cost, and the reaction can be scaled up or repeated rather easily, a compromise on the obtained yield for a reduced effort invested in the purification of NVF proved advantageous. Nonetheless, it is strongly recommended that NVF be freshly purified before its use.

3.4.2. Conventional Free Radical Polymerization of NVIBAM

Suwa et al. has compared the efficacy of various solvents and initiators for the conventional free radical polymerization of NVIBAM.[29] Based on their findings, two initiators were chosen here for evaluation: AIBN and MAIB, both using benzene as solvent, in a monomer concentration of 30 wt.%. Temperatures of 65°C were used for AIBN and 66°C for MAIB. A complete list of the reactions, including main parameters and results is given in Table 12. Typical ^{1}H and ^{13}C NMR spectra of a homopolymer PNVIBAM obtained by conventional free radical polymerization are shown in Annex 7.1 - Figure A 44 and Figure A 45, respectively. SEC elugrams for the polymers are shown in Annex 7.3 - Figure A 59.

Table 12. Conventional free radical polymerizations of NVIBAM. All reactions were done in benzene, with monomer concentration of ca. 30 wt.%.

Index	Product	Initiator	Monomer / Initiator Ratio	Temperature [°C]	Reaction Time [h]	Conversion [%]	M_n^{SEC} [kg·mol^{-1}] (b)	M_w^{SEC} [kg·mol^{-1}] (b)	$Đ^{SEC}$ (b)
60	PNVIBAM$_{377}$	AIBN	600 : 1	65	5:00	80	43	90	2.12
61	PNVIBAM$_{303}$	AIBN	599 : 1	65	3:30	62	34	68	1.99
62	PNVIBAM$_{340}$	MAIB	845 : 1	66	5:20	56	39	72	1.87
63	PNVIBAM$_{287}$	MAIB	838 : 1	66	4:00	42	32	56	1.74
64	PNVIBAM$_{1069}$	MAIB	800 : 1	66	1:45	78 (a)	121	347	2.87

(a) Yield is given in lieu of conversion when the latter is not available.

(b) SEC measured in NMP and calibrated using PMMA standards.

Although Suwa et al.[29] allowed the reactions to proceed for 12 h, considerably lower reaction times were used here, because very high viscosities hindered stirring of the reaction mixtures at these time points. As evidenced by the obtained conversions, and the fact that the polymers could be easily dissolved in a variety of solvents, no significant crosslinking had occurred. Therefore, a

lower concentration, or a better solvent for the polymer might be preferable, allowing longer reaction times and higher monomer conversion.

The molar masses and dispersities obtained are mostly within expected values for conventional free radical polymerization, with exception of reaction index 64, where a higher dispersity was obtained. This reaction also produced much larger molar masses in considerably less time than the remaining reactions. It is unclear what caused these differences, but it may be related to a different level of impurities in the reaction mixture. A larger number of reactions and, optimally, kinetics evaluations thereof would be recommended to evaluate the polymerizations in more details and draw solid conclusions about the results obtained with the two initiators.

Independent from the potential differences between AIBN and MAIB, the kinetics of NVIBAM FRP reactions is clearly faster than that of NIPMAM polymerizations under the same reaction conditions, which was to be expected, given the higher reactivity of vinyl monomers in comparison to methacrylamide monomers.[35]

3.4.3. RAFT Polymerization to Obtain PNVIBAM Homo- and Copolymers

In order to obtain amphiphilic block copolymers based on PNVIBAM, reversible addition fragmentation chain transfer (RAFT) radical polymerization was used. Similar to the previously discussed PNIPAM and PNIPMAM based copolymers, styrene and methyl methacrylate (MMA) were selected as hydrophobic comonomers. Given that styrene and MMA are more activated monomers (MAMs) and NVIBAM is a less activated monomer (LAM), the obtained block copolymers would have the general constitution P(MAM)-*b*-P(LAM). However, the RAFT polymerization of MAMs and LAMs generally requires chain transfer agents (CTAs) with different activity levels, which can compensate for the typically poor addition rates of MAMs (due to the high stability of the radicals from these monomers), and for the poor leaving group characteristic of LAMs (due to the higher reactivity of the radical from these monomers). Therefore, to polymerize both MAMs and LAMs, the selected CTAs needed to offer relatively intermediate activity levels. Thus, three CTAs were selected for evaluation: CTAs **C**, **D** and **E**. CTAs **C** and **D** are typically more appropriate for the polymerization of LAMs, however, they may offer partial control over the polymerization of MAMs.[35] Meanwhile, CTA **E** reportedly offers truly intermediate activity levels, being capable of controlling the polymerization of both MAMs and LAMs.[150]

The following section describes the attempts on the polymerization of styrene and MMA with the three selected CTAs, while the subsequent section discusses the preliminary evaluations of the

polymerization of NVIBAM with the pure CTAs, as well as with the obtained PS and PMMA macro-CTAs.

Synthesis of PS and PMMA Precursors for Chain Extension with PNVIBAM

Both styrene and methyl methacrylate polymerizations were attempted using CTAs **C**, **D** and **E**. In the case of styrene, all reactions were conducted in bulk (no solvent), at 110°C, with self-initiation, that is, the reaction is started by the monomer itself, without addition of an initiator. MMA polymerizations were done in benzene, with a concentration of 50 wt.%, at 65°C using initiator AIBN. Similar to the reactions performed with CTA **B**, the CTA / initiator ratios used here were as small as possible, to maximize the amount of polymer chains with CTA end-groups. Table 13 lists the main results obtained from all PS and PMMA reactions done using CTAs **C**, **D** and **E**. SEC elugrams are available in Annex 7.3 - Figure A 60.

Molar masses from elemental analysis were obtained through the ratio of carbon/sulfur in the samples. In the case of macro-CTAs synthesized with CTAs **D** and **E**, calculations were also be done with the carbon/nitrogen content. For all polymers, the molar masses from both methods were in good accordance with each other.

Polymerization of Styrene with CTAs C, D and E

In the case of 65, 66 and 67, the maximum absorbance wavelength (λ_{max}) measured by UV-vis considerably shifted after polymerization (see Annex 7.2 - Figure A 50), which is known to occur on solvatochromic chromophores, whenever there is a strong change in the chemical constitution (particularly polarity) of the environment. Given the sharp shape of the absorbance peak, the shift of only 6 nm causes the absorbance at the original position (278 nm) to significantly vary from λ_{max}, now shifted to 284 nm. It is known that the absorbances of the polymer should ideally be obtained at the same wavelength that is used to measure the extinction coefficient of the pure CTA. However, in this case using the peak absorbance of the macro-CTA (λ_{max} 284 nm) and the extinction coefficient from peak position of the pure CTA (λ_{max} 278 nm) provided results most in accordance with those of the other characterization methods.

For PS polymerized with CTA **C** (reactions 65, 66, and 67), conversion was calculated from ^{1}H NMR spectra of the crude reaction mixture (see example in Figure 34a) by comparing the signal intensities of the proton on the terminal alkene carbon of the monomer (signal cis p* at ca. 5.8 ppm) with the signals of the aromatic moieties (signals r and r* at 6.4 – 7.8 ppm). For this, the intensity of the overlapped signal q* was deducted from the integral of the aromatic moieties, assuming that the intensity of q* is the same as that of cis p*. Molar mass calculation through R

end-group were done after purification (Figure 34b) by comparing the relative signal intensities of the aromatic moieties (signal r, at 6.3 – 7.5 ppm) with end-group signal f (at 3.3 – 3.6 ppm). Meanwhile, molar mass calculation through Z end-group were done using end-group signal b (at 4.5 – 4.6 ppm).

Table 13. Main characterization results for PS and PMMA macro-CTAs obtained by RAFT using CTAs designed for the polymerization of less activated monomers (LAMs). PS reactions done in bulk, at 110°C with self-initiation. PMMA reactions done with AIBN initiator, in benzene (50 wt.%) at 65°C. Polymerization details are listed in section 6.4.2, Table 22 and Table 23.

Index	Product	CTA	Conversion [%]	M_n [kg·mol^{-1}] Theor. (a)	NMR R-group	NMR Z-group	UV-vis	SEC (b)	EA (c)	$Đ^{SEC}$ (b)	Ratio M_n Z/R (NMR)
65 [*]	PS$_{13}$^{C}	C	38	0.6	1.7	1.5	1.6 (d)	1.6	1.7	1.49	0.89
66 [*]	PS$_{17}$^{C}	C	34	0.6	2.3	2.0	1.8 (d)	2.0	2.1	1.56	0.86
67	PS$_{28}$^{C}	C	63	1.3	3.7	3.1	3.3 (d)	3.2	3.9	1.50	0.84
68 [†]	PS$_{20}$^{D}	D	82	0.8	1.3	1.3	0.5	2.3	0.8	1.69	1.00
69 [†]	PS$_{28}$^{D}	D	80	1.0	1.7	1.7	0.8	3.1	1.1	1.84	0.98
70	PS$_2$^{E}	E	63	0.9	0.5	0.7	0.5	0.5	0.7	1.18	1.30
71 [*]	PMMA$_{279}$^{C}	C	97	2.7	-	-	1.5	28	-	2.51	-
72 [†]	PMMA$_{180}$^{D}	D	99	2.3	-	-	1.0	18	-	2.30	-
73 [†]	PMMA$_{19}$^{E}	E	99	2.7	1.8		1.6	2.2	1.8	1.70	-

(a) Theoretical molar mass, calculated from the conversion and monomer/CTA ratio.

(b) SEC measured in NMP and calibrated using PS or PMMA standards, according to the sample.

(c) Calculated using the carbon/sulfur ratio.

(d) λ_{max} strongly shifted after polymerization. The absorbance values of the macro-CTA were obtained from the new peak position (284 nm), but the extinction coefficient was obtained from the original peak position (278 nm).

For these polymers it is important to highlight that signals of the unreacted CTA are still visible by ^{1}H NMR after polymerization (signals a*, b*, d*, e* and f*), along with signals of CTA in the

polymer. This indicates that only part of the CTA was involved in the polymerization, while another part remained inactive. Comparing the intensity of signals f and f* provides a value for "CTA conversion", which was of 28% for reactions 65 and 66, and 53% for reaction 67. The fact that only a fraction of the CTA took part in the polymerization also explains why the molar mass of these polymers obtained by ^{1}H NMR, UV-vis, SEC and EA is so high in comparison to the theoretical molar mass, since $M_n^{Theor.}$ is calculated from the monomer conversion versus the monomer/CTA ratio used in the reaction. For a deeper evaluation of this hypothesis, a couple of samples were collected during the course of reaction index 67. From these samples, the conversion of the monomer and the CTA were calculated by ^{1}H NMR. The values obtained, as well as the data points of all other PS reactions shown in this section, is shown in Figure 37, as a function of reaction time. With these results, the gradual activation of the CTA during the reaction is clearly visible, which follows a similar trend as the monomer conversion itself. Based on this, it seems that CTA **C** is a bit too inactive, i.e., its rate of addition is too low, and its rate of fragmentation is too high for the proper control of the polymerization of styrene. This low activity level is to be expected, given the lone electron pair on the oxygen of the xanthate, combined with an electron donating group (ethyl). As a result, the growing polymer chains are not effectively added to the CTA, leading to some control over the molar mass, but poor control over the molar mass dispersity, which is a typical consequence of using LAM CTAs for the polymerization of MAMs.[35,242]

For PS polymerized with CTA **D** (reactions 68 and 69), conversion was calculated from the ^{1}H NMR spectra of the crude reaction mixture (see example in Figure 35a) by comparing the signal intensities of the proton on the terminal alkene carbon of the monomer (signal cis p* at ca. 5.8 ppm) with the signals of the aromatic moieties (signals r and r* at 6.3 – 7.8 ppm). Thus, the intensity of the overlapped signal a* was deduced from the integral of the aromatic moieties, assuming that the intensity of each proton on a* is the same as that of each proton on d*.

Molar mass of these polymers was calculated from the ^{1}H NMR spectra of the end-product (see example in Figure 35b) by comparing the signal intensities of the aromatic moieties (signal r, at 6.3 to 7.8 ppm) with the R end-group (signal d, at 4.1 ppm) and Z end-group (signal b, at 4.8 ppm). However, it is possible that the CTA was not properly involved in the polymerization of styrene in these reactions. This conclusion is based on the fact that the signal of the CH_2 on the alpha position to the dithiocarbamate did not change intensity or position after polymerization (^{1}H NMR spectrum of the pure CTA is provided in Annex 7.1 - Figure A 4). The hypothesis is further supported by the broad molar mass distribution measured for these polymers, which is even higher than those obtained with the xanthate CTA. These results come as no surprise, given that the activity level of the *N*-alkyl-*N*-aryl dithiocarbamate is even lower than that of the *O*-ethyl xanthate.

Similar to the xanthate, the lone electron pair on the nitrogen decreases the CTAs activity, an effect which is only exacerbated by the substituents on the nitrogen. In addition, the CTA's R-group most likely also played a big role in the results obtained, given that the primary carbon is a very poor homolytic leaving group with respect to styrene. Although the R-group radical stability is slightly improved by the cyano group, it is far from enough to generate stability levels comparable to that of the (poly)styrene radical.[35,145]
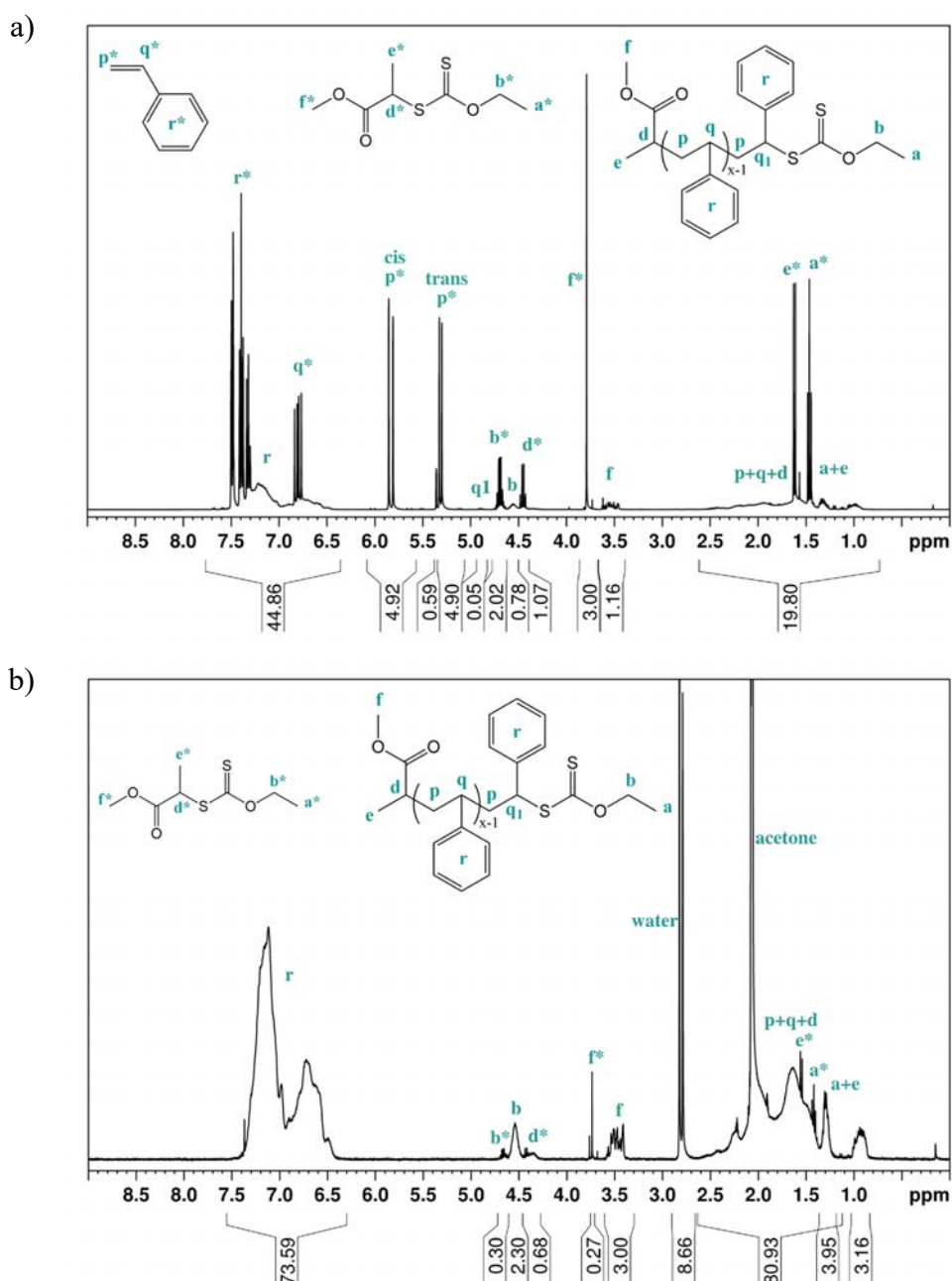
Figure 34. ^{1}H NMR spectra of PS$_{13}$[C] (reaction index 65), crude reaction mixture (a) in DCM-d$_2$, and after purification (b) in acetone-d$_6$.
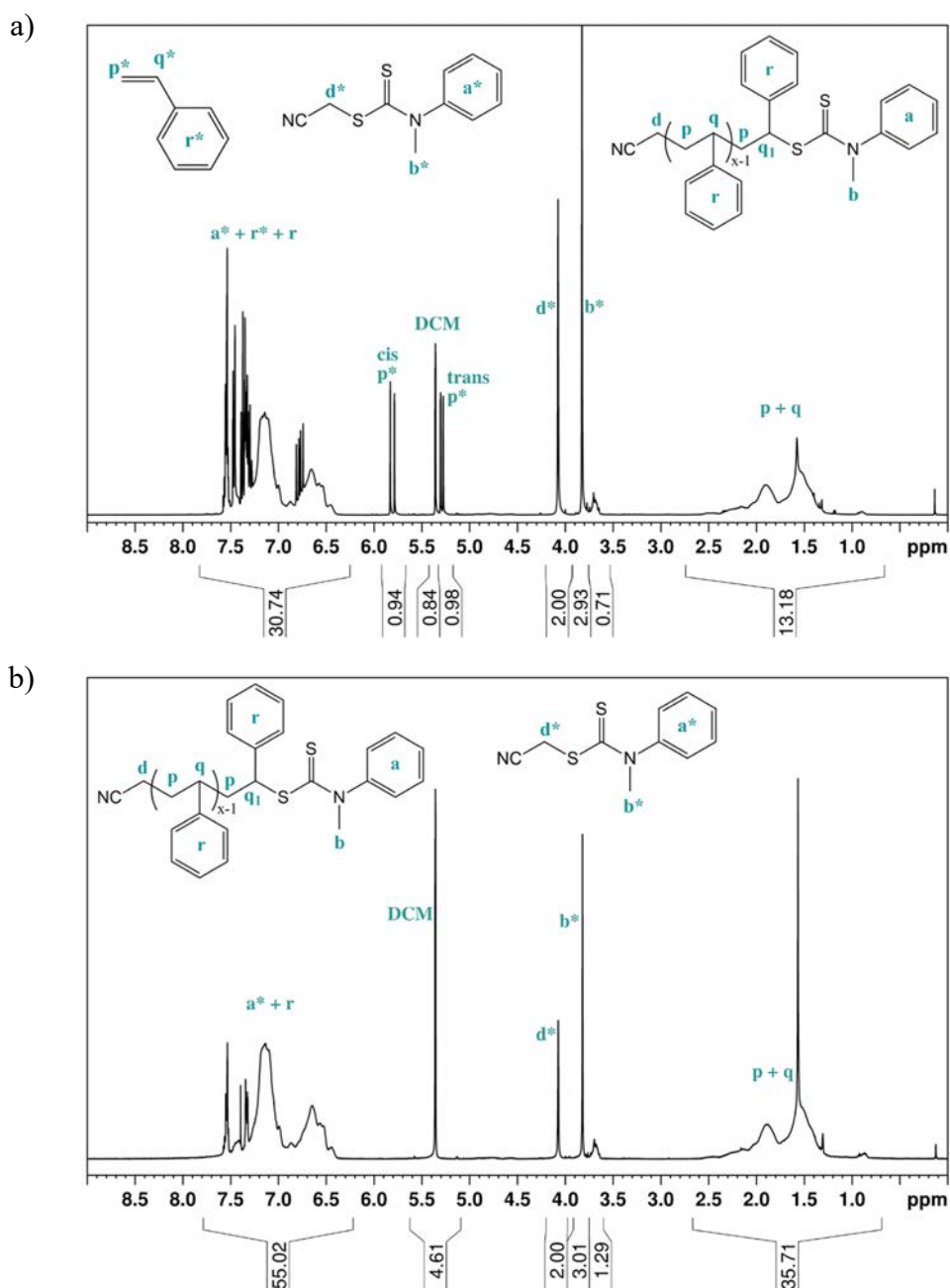
Figure 35. ^{1}H NMR spectra of PS$_{20}{}^D$ (reaction index 68), crude reaction mixture (a) in DCM-d$_2$, and after purification (b) in acetone-d$_6$.

For PS$_2{}^E$ (reaction 70), conversion was calculated from the crude reaction mixture (Figure 36) by comparing the signal intensities of the protons on the terminal alkene carbon of the monomer (signals cis p* and trans p* at 5.1 – 6.0 ppm) with the signal of the aromatic moieties (signal r, at 6.6 – 7.7 ppm), thus obtaining the fraction of residual monomer and, reciprocally, the fraction of converted monomer units. Molar mass calculations for this polymer were done through Z end-group after purification (Annex 7.1 - Figure A 22) by comparing the relative signal intensities of the aromatic moieties (signal r, at 6.5 – 7.5 ppm) with the signal of the constitutional repeat unit on the alpha position to the trithiocarbonate (signal q$_1$, at 4.4 – 4.8 ppm). Molar mass calculations

through R end-group were done using signals a and b, at 2.65 and 2.16 ppm, respectively. For this, the intensity of the overlapped signals d, e, f, p and q were deduced from the integral, assuming that the intensity of each proton of d, e and f is the same as that of q1, and that the intensity of each proton of p and q is the same as the intensity of each proton on r.

As described in Table 13, extremely low molar masses were obtained for the polymerization of styrene with CTA **E**, although a satisfactory molar mass dispersity was achieved. This indicates that CTA **E** is indeed capable of controlling the polymerization of styrene, but some retardation may take place.
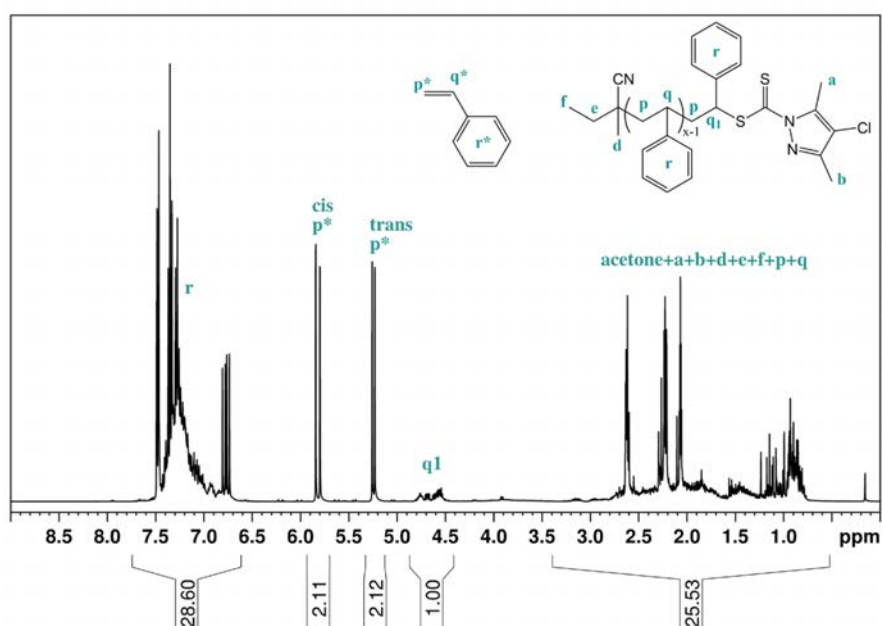
Figure 36. ^{1}H NMR spectra of PS$_2^E$ (reaction 70), in acetone-d$_6$, before purification.
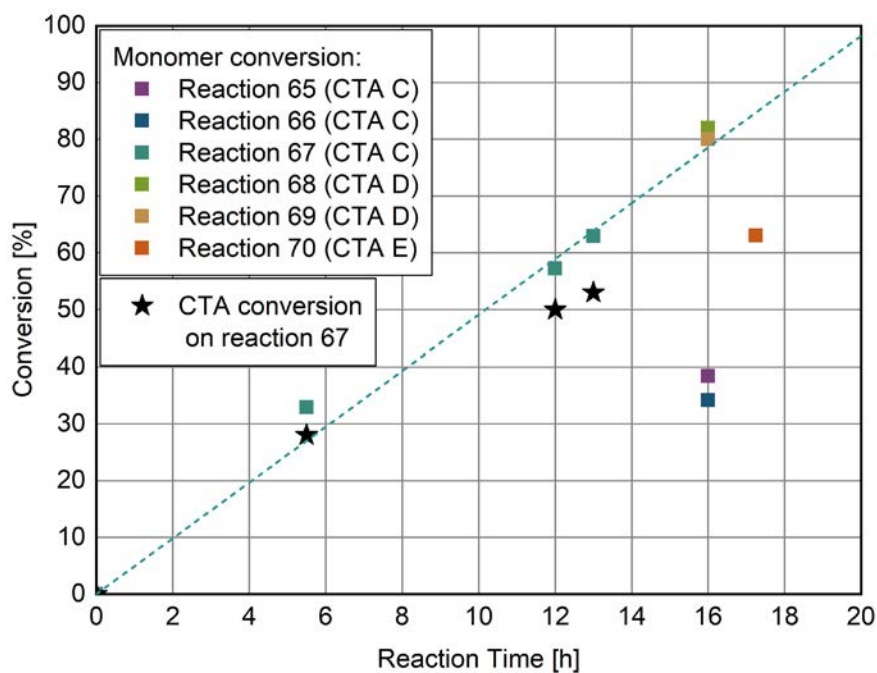
Figure 37. Monomer conversion of the polymerizations of styrene using CTAs C, D and E, as well as CTA conversion on reaction 67, plotted against rection time. Dashed line is a guide to the eye.

Polymerization of MMA with CTAs C, D and E

Conversion of the PMMA macro-CTAs (reactions 71, 72 and 73) was calculated from the crude reaction mixtures (see example in Figure 38a) by comparing the relative signal intensities of the protons on the terminal alkene carbon of the monomer (at ca. 5.60 and 6.15 ppm) with the signal of the methyl group attached to the ester on the side group of the polymer (at ca. 3.64 ppm).

In the ^{1}H NMR spectrum of PMMA$_{279}$^{C} (reaction 71, Annex 7.1 – Figure A 23) and PMMA$_{180}$^{D} (reaction 72, Annex 7.1 – Figure A 24), the signals of pure CTA are still visible after polymerization and there is no (or very little) sign of reacted CTA signals. This strongly indicates that polymerization occurred by conventional free radical polymerization, as opposed to RAFT. This conclusion is corroborated by the polymers' high molar masses and broad molar mass distributions, obtained by SEC. Based on this, it is clear that the xanthate and dithiocarbamate CTAs (CTA **C** and CTA **D**) are exceedingly inactive for the control of the polymerization of MMA. The reasons for this are the same as previously described for styrene, but in the case of MMA the mismatch of activity level of CTA and monomer is stronger yet, given the higher activation level of this monomer. For example, while the primary carbon R-group of CTA **D** was still marginally suitable for the polymerization of styrene, its radical stability is fully insufficient to compete with the high stability of the tertiary carbon radical of the growing PMMA chain.[35,243,244] Therefore, the intermediate species (R-S-C•(Z)-S-P$_n$) will overbearingly cleave on the methacrylate (forming P$_n$•) as opposed to the cyanomethyl (which would form R•).
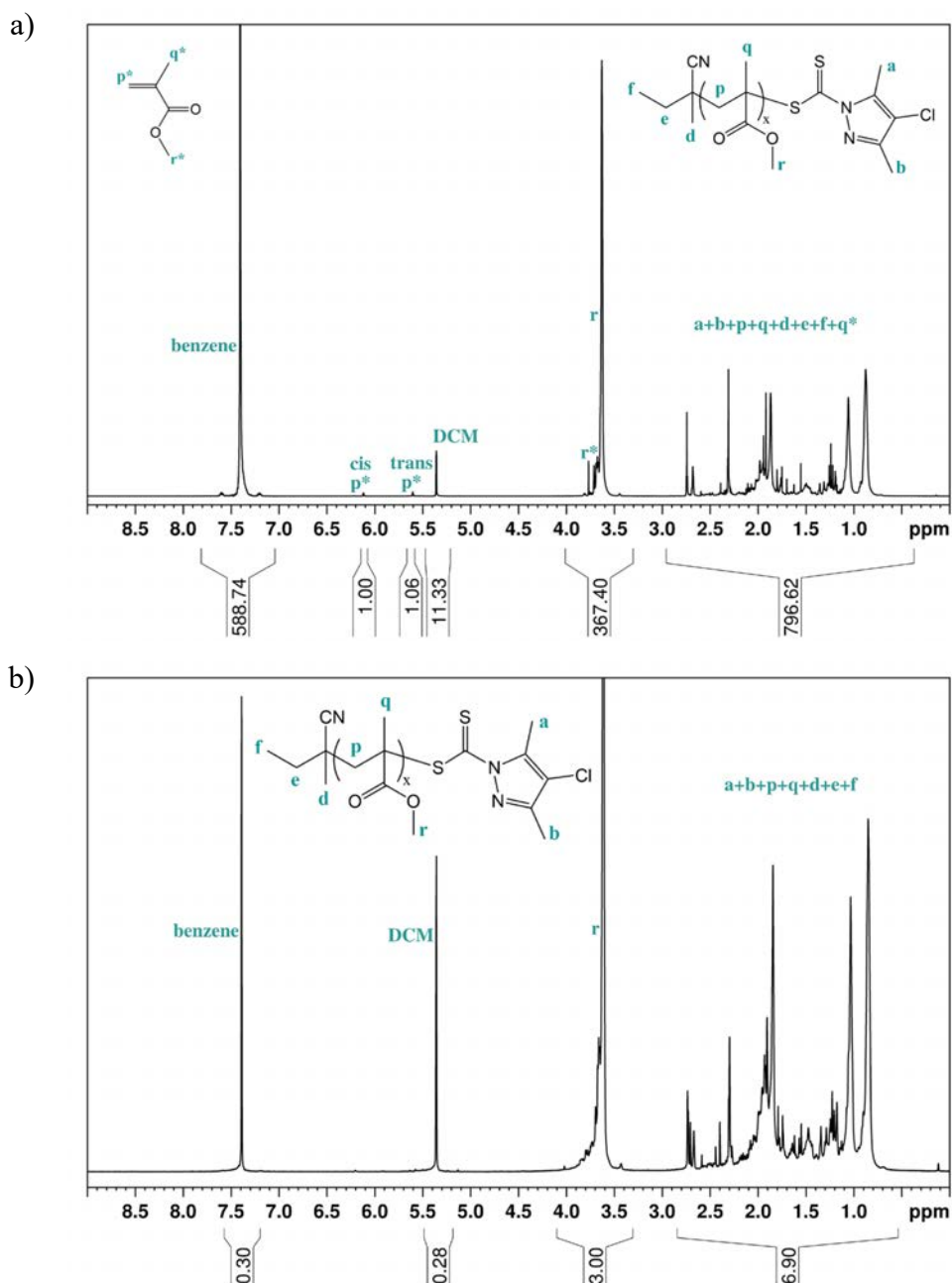
Figure 38. ^{1}H NMR spectra of PMMA$_{19}$^{E} (reaction 73) crude reaction mixture (a) and after purification (b), in DCM-d$_2$.

For PMMA$_{19}$^{E} (reaction 73), M_n^{NMR} was calculated by comparing the signal intensities of the methyl group attached to the ester on the side group of the polymer (Figure 38b - signal r, at 3.62 ppm) with the signal of the combined R and Z end-groups (signals a, b, d, e and f, at 0.5 – 3.0 ppm). For this, the intensity of the overlapped signals p and q and q were deduced from the integral, assuming that the intensity of each proton of p and q is the same as the intensity of each proton on r. The results obtained confirm that CTA **E** offers marginal control of the polymerization of MMA, with some control over the molar mass but poor control over the dispersity, as could have been

expected from the intermediate activity levels of the CTA, resulting from the attenuated effect of the lone electron pair of N due to the electron withdrawing halogen on the pyrazole ring system.[150]

RAFT Polymerization of NVIBAM

Preliminary evaluation of the polymerization of NVIBAM were perform by RAFT with the goal of obtaining both PNVIBAM homopolymers, as well as amphiphilic block copolymers. For the former, CTAs **C**, **D** and **E** were evaluated. For the latter, a few PS and PMMA macro-CTAs were selected from the reactions described in the previous subsection, namely PS_{13}^C (reaction 65), PS_{20}^D (reaction 68) and $PMMA_{19}^E$ (reaction 73). Table 14 provides a concise overview of all the reactions performed with CTAs **C**, **D** and **E**.

Table 14. Overview of RAFT polymerizations aimed at evaluating the synthesis of P(MAM)-*b*-P(LAM)s. Reaction indices are given in parenthesis, followed by reaction product. Columns in turquoise list the polymerizations of MAMs, to obtain macro-CTAs. Columns in orange list the polymerizations of the LAM NVIBAM, either with the pure CTA to obtain a homopolymer, or with a macro-CTA to obtain a copolymer.

	PS	PMMA	PNVIBAM	PS-*b*-PNVIBAM	PMMA-*b*-PNVIBAM
CTA C	(65) PS_{13}^C (66) PS_{17}^C (67) PS_{28}^C	(71) $PMMA_{279}^C$	(74) $PNVIBAM_{0'}^C$ (75) $PNVIBAM_{0''}^C$	(78) PS_{13}-*b*-$PNVIBAM_{44}^C$	-
CTA D	(68) PS_{20}^D (69) PS_{28}^D	(72) $PMMA_{180}^D$	(76) $PNVIBAM_{81}^D$	(79) PS_{20}-*b*-$PNVIBAM_0^D$	-
CTA E	(70) PS_2^E	(73) $PMMA_{19}^E$	(77) $PNVIBAM_{336}^E$	-	(80) $PMMA_{19}$-*b*-$PNVIBAM_0^E$

The results obtained from the homopolymerizations of NVIBAM using CTAs **C**, **D** and **E** are summarized in Table 15. As shown, the use of CTA **C** did not yield any polymer, while the use of CTAs **D** and **E** produced relatively low conversions (especially CTA **D**) and broad molar mass distributions (especially CTA **E**).

Table 15. Molar mass characterization results for the RAFT homopolymerizations of NVIBAM. All reactions were performed with AIBN initiator, with a concentration of ca. 30 wt.% in benzene, for about 16 h. The monomer / CTA / initiator ratio was about 270 : 1 : 0.10, for all reactions.

Index	Product	CTA	Conversion [%]	Molar Mass [kg·mol^{-1}]				
				$M_n^{Theor.\,(a)}$	$M_n^{EA\,(b)}$	$M_n^{SEC\,(c)}$	$M_w^{SEC\,(c)}$	$Đ^{SEC\,(c)}$
74	PNVIBAM$_0$,^{C}	C	0	-	-	-	-	-
75	PNVIBAM$_0$,,^{C}	C	0	-	-	-	-	-
76	PNVIBAM$_{81}^D$	D	10	3.2	-	9.3	15	1.58
77	PNVIBAM$_{336}^E$	E	35	11	39	38	71	1.84

(a) Calculated from the conversion and monomer / CTA ratio.

(b) Calculated from the carbon/sulfur ratio.

(c) SEC measured in NMP and calibrated using PMMA standards.

Calculation of conversion of sample PNVIBAM$_{81}^D$ (reaction 76) was done through ^{1}H NMR (Figure 39a) by comparing the relative signal intensities of the proton on the terminal alkene carbon of the monomer (signals cis s* and trans s* at 4.5 and 4.8 ppm) with the signal of the CH on the isopropyl group (signal v + v* at 2.6 ppm).

Calculation of conversion of sample PNVIBAM$_{336}^E$ (reaction 77, Figure 39b) was done using the signal of the proton on the terminal alkene carbon of the monomer (s*) with the signal of the CH on the backbone of the polymer (signal t at 4.05 ppm).

For both samples, calculation of the molar mass by ^{1}H NMR was not possible due to overlap of the signals from the CTA's end-groups with signals of the constitutional repeat unit of PNVIBAM. In the case of PNVIBAM$_{81}^D$, the signals of the aromatic end-groups are overlapped by the signal of the amide proton and the signals of the aliphatic end-groups are overlapped by the signals of the CH on the backbone of the polymer. In the case of PNVIBAM$_{336}^E$, the end-groups are overlapped by signals of the backbone as well as methyl side groups.
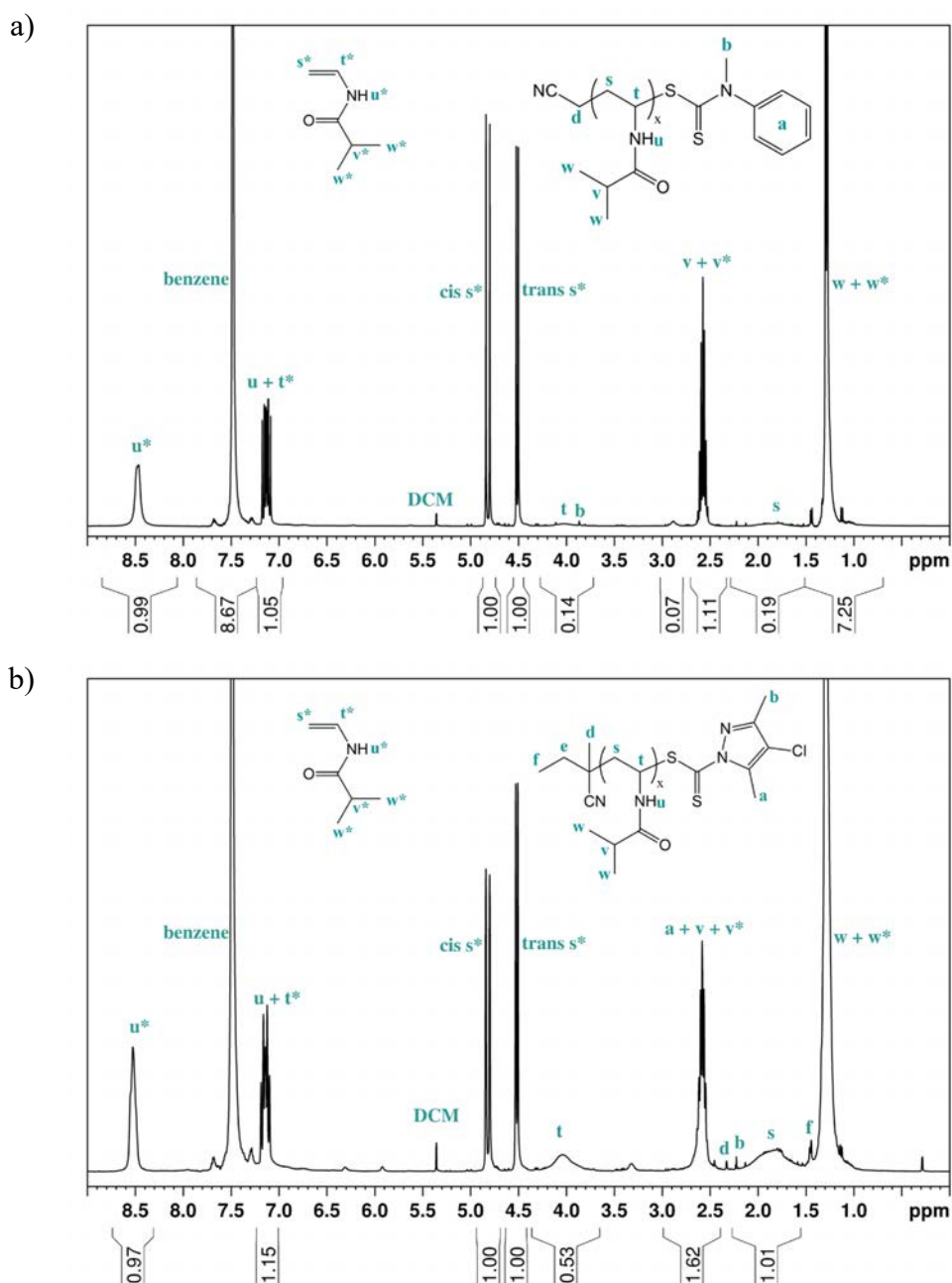
Figure 39. ^{1}H NMR spectra of (a) PNVIBAM$_{81}^{D}$ (reaction 76) and (b) PNVIBAM$_{336}^{E}$ (reaction 77), in DCM-d$_2$, before purification.

In addition to the homopolymerization of NVIBAM using CTAs **C**, **D** and **E**, a few preliminary experiments were performed using these CTAs in the form of a macro-CTA. In this case, the CTA's Z-group is the same as the virgin CTA, but the R-group is substituted with a preexisting short PS or PMMA block. These preliminary evaluations were performed with the goal of obtaining amphiphilic block copolymers of a more activated monomer (MAM) and a less activated monomer (LAM), i.e., P(MAM)-*b*-P(LAM)s. For this end, three of the macro-CTAs described in the previous sub-section were selected for chain extension with NVIBAM. The results of these polymerizations are listed in Table 16.

Table 16. Molar mass characterization results for the RAFT polymerizations of NVIBAM using PS or PMMA macro-CTAs (monomer / CTA / initiator ratio of ca. 270 : 1 : 0.13). All reactions were performed with AIBN initiator, with a monomer concentration of ca. 30 wt.% in benzene, for about 18 h.

Index	Product	Conversion [%]	Molar Mass [kg·mol⁻¹]					W_{NVIBAM} (from SEC)
			$M_n^{Theor. (a)}$	$M_n^{EA (b)}$	$M_n^{SEC (c)}$	$M_w^{SEC (c)}$	$Đ^{SEC (c)}$	
78	PS₁₃-*b*-PNVIBAM₄₄[C]	10	4.6	23	6.6	9.3	1.42	0.76
79	PS₂₀-*b*-PNVIBAM₀[D]	0	-	-	-	-	-	-
80	PMMA₁₉-*b*-PNVIBAM₀[E]	0	-	-	-	-	-	-

(a) Calculated from the conversion and monomer / CTA ratio.

(b) Calculated from the carbon / nitrogen ratio.

(c) SEC measured in NMP and calibrated using PMMA standards.

Calculation of conversion of sample PS₁₃-*b*-PNVIBAM₄₄[C] (reaction 78) was done through ^{1}H NMR of the crude reaction mixture (Figure 40) by comparing the signal of the proton on the terminal alkene carbon of the monomer (signals cis s* and trans s* at 4.3 and 4.7 ppm) with the signal of the methyl side groups of both the monomer and polymer (signal w + w* at 1.1 ppm). Calculation of the molar mass by ^{1}H NMR was not possible due to overlap of the signals from the macro-CTA with signals of the constitutional repeat unit of PNVIBAM. Elemental analysis did not detect any sulfur in the sample.

Based on the results obtained from the preliminary experiments of NVIBAM polymerization with LAM CTAs and macro-CTAs, no clear and conclusive trend can be identified.

It would be expected that the xanthate CTA **C** effectively control the polymerization of LAM NVIBAM, given its R and Z groups. Yet, while polymerization using the macro-CTA PS₁₃[C] seems to have generated a small amount of copolymer with some level of control over dispersity, the homopolymerization using CTA **C** produced no polymer whatsoever.

According to the theory and published studies on the RAFT polymerization of LAMs,[34,35,145,245] CTA **D** should be ideal for the controlled synthesis of PNVIBAM, offering even better control than xanthates. Although the results obtained in the homopolymerization of NVIBAM with CTA **D** were slightly better than those with CTA **C**, the chain extension of the macro-CTA PS₂₀[D] did not produce any conversion of NVIBAM monomer. This could be attributed to the poor ability of the PS radical of reinitiating a PNVIBAM chain, and its better leaving group ability compared to

NVIBAM. Meanwhile the cyanomethyl moiety might be a more appropriate choice of R-group for the polymerization of NVIBAM. However, the question remains of why the chain extension with PS$_{13}$^{C} yielded better results than the PS$_{20}$^{D}.
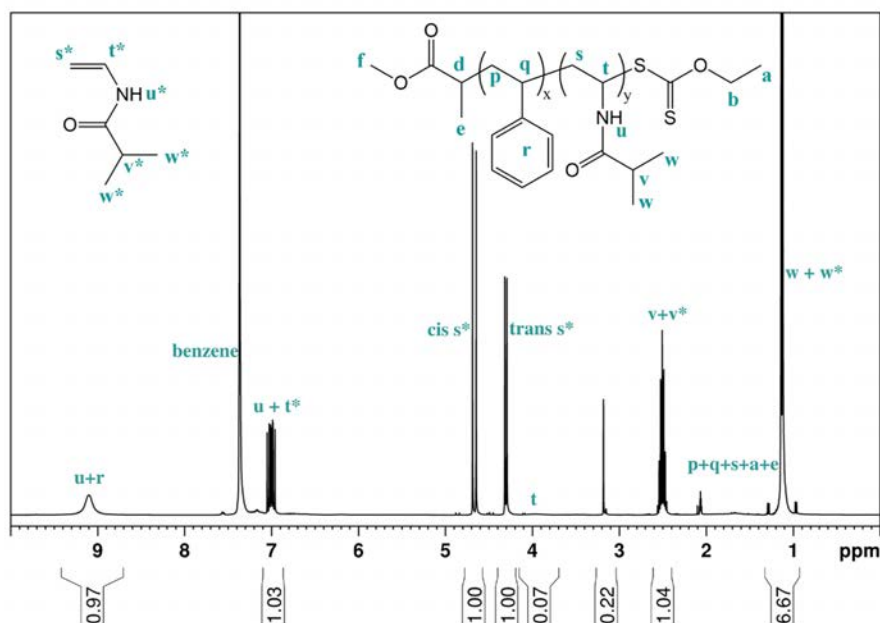
Figure 40. ^{1}H NMR spectra of PS$_{13}$-*b*-PNVIBAM$_{44}$^{C} (reaction 78) before purification, in acetone-d$_6$.

Finally, in the case of CTA **E**, homopolymerization of NVIBAM led to rather broad molar mass distributions, despite the slightly higher conversion compared to the reactions with CTAs **C** and **D**. Chain extension of the PMMA$_{19}$^{E} macro-CTA, however, yielded no copolymer at all, which again could be attributed to the poor ability of the tertiary C of the PMMA to reinitiate the growing NVIBAM chain.

Although it is not possible to affirm the reasons for the discrepancies in the results obtained in the RAFT polymerizations of NVIBAM, it is possible that degradation products, either of the CTAs or of the monomer itself have caused inhibition of some reactions. Benzene was chosen as solvent due to its high stability against side reactions, and the moisture and impurities level was controlled to be minimal, so hydrolysis due to residual water in the solvent is unlikely. However, if moisture was anyway present in the system, for example from the monomer, a degradation of the CTA could occur, generating H$_2$S, which would strongly inhibit the polymerization. Similarly, the NVIBAM monomer itself is considerably more prone to degradation than the MAMs discussed in this thesis, and the generated degradation products, such as acetaldehyde, could act as inhibitors.

Although the preliminary experiments described in this section provide some hints to the potential synthesis of P(MAM)-*b*-(LAM)s based on PNVIBAM, further studies are definitely needed for

more conclusive affirmations. It is important to highlight that, differently from the RAFT polymerization of MAMs, the RAFT (or MADIX) polymerization of LAMs is not nearly as widely studied and reported upon. Moreover, the majority of the studies available focus on vinyl acetate, *N*-vinyl pyrrolidone or *N*-vinyl caprolactam.[245,246] Although these studies provide valuable information, the RAFT polymerization of LAMs is generally a very sensitive system, where small changes on the chemical structures or reaction setup may have large impacts on the results obtained. It is not sufficient that the used CTA have a sufficiently low activity level. An optimal balance must be met, and the leeway for these systems is typically very narrow.

This may mean that a single CTA is not sufficient for the synthesis of P(MAM)-*b*-(LAM)s based on PNVIBAM, but a switchable CTA, for example, could provide more successful results, as recently shown by Pan et al.[247]

4.   Aggregation and Co-nonsolvency

The behavior of solutions from the polymers described on chapter 0 was studied using turbidimetry and dynamic light scattering (DLS). On the one hand, analyzing the light transmittance of polymer solutions over a temperature range (turbidimetry), allowed precise identification of the cloud point temperatures of the homo- and copolymers. Moreover, upon comparison of the results obtained in various mixed solvents, the co-nonsolvency behavior of the sample was delineated. Similarly, this method allowed for the study of the effects of molar mass and concentration on the transition temperatures. DLS, on the other hand, provided important information on the aggregation of amphiphilic block copolymers, namely the hydrodynamic diameters and size distribution of the aggregates, and how these properties change with temperature and presence of co-solvents.

The results of these investigations are presented and discussed in the following sections, starting (section 4.1) by the behavior of the homopolymers PNIPMAM and PNVIBAM, and how it compares to the well-studied PNIPAM. The thermoresponsive and co-nonsolvency behavior of each of these polymers is mapped out, not only in the typical water-methanol solvent system, but for an exceptionally wide variety of co-solvents.

Subsequently, in section 4.2, the aggregation and co-nonsolvency behavior of amphiphilic block copolymers is discussed. Here, the behavior of these polymers in solution is evaluated, along with the influences from chain architecture (homopolymer versus di- and triblock copolymers), block sizes, type of cosolvent, concentration, and chemical composition of both the hydrophobic (PS versus PMMA) and thermoresponsive blocks (PNIPAM versus PNIPMAM). Lastly, chapter 0 presents a summary of the main conclusions drawn from the results of this thesis.

4.1. Behavior of PNIPMAM and PNVIBAM Homopolymers in Solution

As previously discussed, the behavior of poly(*N*-isopropyl acrylamide) (PNIPAM) in solution has been the subject of numerous publications. The impact on the transition temperature has been studied for a plethora of aspects, including molar mass, concentration, pressure, presence of co-monomers, co-solvents, salts, etc.[12,59] Meanwhile, analogous polymers such as poly(*N*-isopropyl methacrylamide) (PNIPMAM) or poly(*N*-vinyl isobutyramide) (PNVIBAM) have only scarcely been studied, despite the valuable insights that their behavior could potentially provide with respect to the influence of small changes on the chemical structure of the polymer. With this purpose, aqueous solutions of PNIPMAM and PNVIBAM homopolymers were prepared and extensively studied by turbidimetry (light transmittance), as shown on the following sections.

4.1.1. Thermoresponsivity: Effect of End-groups, Molar Mass, and Concentration

As described in section 2.1.2, PNIPAM differs from many other thermoresponsive polymers by showing an LCST type II behavior, that is, its transition temperature shows exceptionally little dependence on molar mass and concentration. Thus, one important question to be answered for PNIPMAM and PNVIBAM is whether these show the same type of behavior.

End-Group and Molar Mass Effects

To evaluate the influence of molar mass on the thermoresponsive behavior of PNIPMAM and PNVIBAM, several homopolymers of varying chain lengths were synthesized (see chapter 0), and their aqueous solutions were subjected to turbidimetry characterization.

The cloud point temperatures (T_{CP}) of PNIPMAM samples with various number-average molar masses (M_n^{SEC} = 17 to 147 kg·mol^{-1}) are plotted in Figure 41. The individual transmittance curves are available in Annex 7.6 - Figure A 74. Table 17 lists the main polymerization parameters and molar mass results from each of the evaluated samples. On both the Figure and Table, a few data points from the literature are included, for reference. The data for PNVIBAM, and graphical representation thereof, is provided in Table 18 and Figure 42, whereas the individual transmittance curves are shown in Annex 7.6 - Figure A 75. The chemical structure of the initiators used is depicted in Figure 29 (page 71), and the SEC molar mass distribution curves of these PNIPMAM and PNVIBAM polymers is provided in Annex 7.3 - Figure A 58 and Figure A 59, respectively.

The measured T_{CP} of PNIPMAM was between 40.9 and 45.4°C. The notable variation of the results is not a big surprise, given that PNIPMAM has been repeatedly reported to show a broader phase transition compared to PNIPAM.[12,28,95,96] The range of T_{CP} values measured is in general accordance with the reports found in literature.[28,95,173] Despite the wide T_{CP} range, no clear trend of dependence on molar mass can be seen. However, when identifying the data points according to the end-group of the polymers (Figure 41), a correlation between the end-groups of the polymer and the transition temperature becomes visible. For example, polymers containing CTA **B** or initiator V70 as end-groups show considerably lower T_{CP}, which can be plausibly correlated with the hydrophobicity of the end-group moieties. Meanwhile, the highest transition temperatures measured are those of polymers synthesized with initiators V50, MAIB and AIBN, which are more polar groups and/or less bulky, inducing a more limited effect on the behavior of the polymer chain. Although these samples are also the ones with the highest molar mass, it is possible that the lower hydrophobicity of the initiator (incorporated in the polymer as end-group) is at least partially responsible for the increased T_{CP}. In contrast, when solely samples containing the same end-groups

are compared (e.g., AIBN), only small differences in T_{CP} are seen for the various molar masses. Given that these differences are within the precision of the characterization method, no direct correlation between the molar mass and transition temperature can be drawn. This behavior is in good accordance with the reported behavior of PNIPAM, which shows small effects of molar mass on the T_{CP}, while end-groups have a much more significant effect.[59,248,249] For example, the presence of hydrophobic end-groups has been shown to lead to lower T_{CP} of PNIPAM at low molar masses. That is because the proportion of end-groups to constitutional repeat units of polymer is much higher for shorter chain lengths.[212]

Alternatively, the turbidity curves of PNIPAM have also been shown to be affected by the polymerization conditions of the sample under investigation.[59] For example, polymerization of NIPAM in methanol and *tert*-butanol has been shown to produce polymers with higher cloud points than polymerization in benzene and 1,4-dioxane, even though the samples showed similar molar masses, end-groups and stereochemical composition. This has been attributed to the quality of the solvent, which may lead the growing chain to adopt a more compact structure (in a poorer solvent), thus leading to a higher chance of branching, and in turn lower T_{CP}.[210] Here, the sample polymerized in ethanol at 30°C showed a considerably lower T_{CP} than those polymerized in benzene and TFE at 56 to 72°C. In that case, other than the solvent, it might be that the reaction temperature has led to different chain architectures (branching), variations in tacticity (isotactic, syndiotactic, atactic), or even changes in the ratio between chains terminated by disproportionation and recombination, which affects the percentage of chains containing initiator-derived end-groups.

Table 17. Main polymerization conditions, molar mass results and cloud point temperature of PNIPMAM samples. Samples PNIPMAM$_{146}$^{B} and PNIPMAM$_{195}$^{B} were obtained by RAFT, using CTA B. All other samples were obtained by conventional free radical polymerization. Samples from the literature are included for comparison, and their reference number is given in brackets, in place of the reaction index.

Index	Sample	Solvent	Conc. [wt.%]	Temp. [°C]	Time [h:m]	Initiator	M_n^{SEC} [kg·mol^{-1}]	$Đ^{SEC}$	T_{CP} [°C]
[28]	PNIPMAM$_{133}$	THF	15	60	18:00	AIBN	17	1.74	44.0
59	PNIPMAM$_{146}$^{B}	Benzene	30	71	18:00	AIBN	19	1.84	41.0
[36]	PNIPMAM$_{195}$^{B}	TFE	29	75	16:00	V501	20	1.3	41.0
44	PNIPMAM$_{219}$	EtOH	30	30	17:50	V70	28	3.18	40.9
31	PNIPMAM$_{241}$	TFE	20	65	18:00	AIBN	31	2.80	45.4
21	PNIPMAM$_{305}$	Benzene	25	65	24:00	AIBN	39	2.01	44.2
23	PNIPMAM$_{339}$	Benzene	25	65	24:00	AIBN	43	2.07	44.0
43	PNIPMAM$_{381}$	EtOH	30	30	18:15	V70	48	1.97	41.5
30	PNIPMAM$_{424}$	Benzene	34	72	18:30	AIBN	54	2.07	43.7
35	PNIPMAM$_{426}$	Benzene	25	66	18:00	MAIB	54	2.45	44.9
81	PNIPMAM$_{492}$	Benzene	30	65	18:00	AIBN	63	2.56	43.8
45	PNIPMAM$_{682}$	EtOH	30	30	17:55	V70	87	1.99	40.9
27	PNIPMAM$_{776}$	Benzene	30	65	18:05	AIBN	99	2.80	44.4
40	PNIPMAM$_{895}$	TFE	30	56	18:00	V50	114	1.99	44.4
36	PNIPMAM$_{936}$	Benzene	29	66	18:20	MAIB	119	2.71	44.6
28	PNIPMAM$_{956}$	Benzene	30	65	18:05	AIBN	122	3.01	44.4
38	PNIPMAM$_{1154}$	TFE	30	56	17:50	V50	147	2.00	44.9
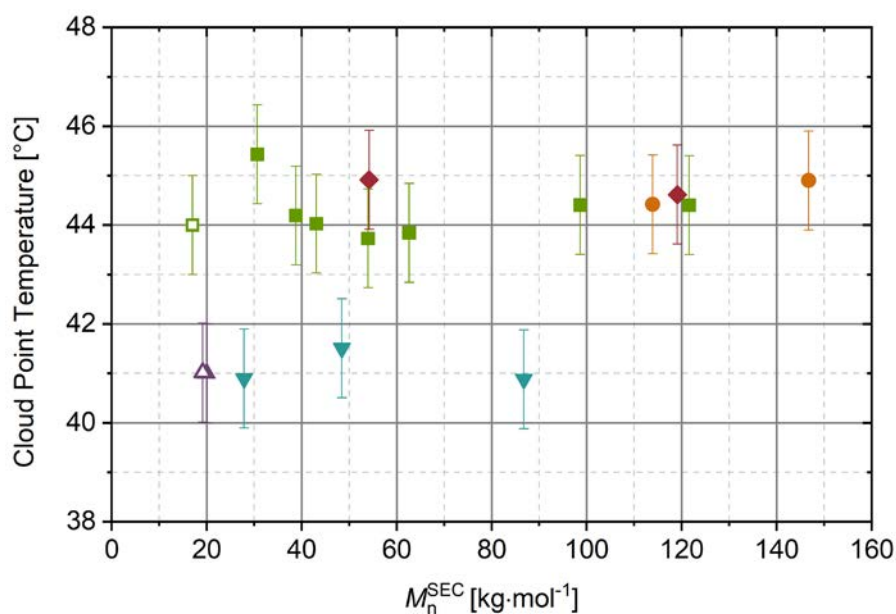
Figure 41. Cloud point temperature (±1°C) as a function of the number-average molar mass of PNIPMAM in water with concentration of 10 g·L^{-1}. Closed symbols represent original data, and open symbols represent data points from literature (see Table 17). The symbol's shape and color represent the polymer's various end-groups: green squares for **AIBN**, red diamonds for **MAIB**, orange circles for **V50**, purple upturned triangles stand for **CTA B**, and turquoise downturned triangle for **V70**.

Differently from PNIPMAM, PNVIBAM showed much less variation in its T_{CP}, which was found to be between 38.6 and 39.3°C. This confirms the few reports in literature, which place its transition temperature at about 39°C. [29,190,195] Similarly as for PNIPMAM, the transition temperatures obtained within the molar mass range of 9.3 to 121 kg·mol^{-1} (Figure 41) were virtually the same, considering the precision of the method. In fact, when comparing solely samples with the same end-groups, there seems to be a small increase in the T_{CP} with increasing molar mass. For PNIPAM, in contrast, numerous studies have reported its transition temperature to exponentially decay with increasing molar masses, thus leading to a steeper T_{CP} decrease at the low molar mass range, but with T_{CP} remaining virtually unaltered for high molar masses.[59,95,119,211,212,250-253] In contrast, the behavior seen here for PNVIBAM could, as explained before, be related to a more pronounced effect of the end-groups at lower molar masses, where they represent a higher proportion of the polymer chains. Nonetheless, the detected variability in the results of PNVIBAM is considerably small ($\Delta T_{CP} \sim 0.7$°C) and might well be within the margin of error of the analytical method.

Table 18. Main polymerization conditions, molar mass results and cloud point temperature of PNVIBAM samples. All samples were polymerized in benzene, with a concentration of 30 wt.%.

Index	Sample	CTA	Temp. [°C]	Time [h:m]	Initiator	M_n^{SEC} [kg·mol^{-1}]	$Đ^{SEC}$	T_{CP} [°C]
76	PNVIBAM$_{81}^D$	D	65	16:00	AIBN	9.3	1.58	39.3
63	PNVIBAM$_{287}$	none	66	4:00	MAIB	32	1.74	38.9
61	PNVIBAM$_{303}$	none	65	3:30	AIBN	34	1.99	38.9
77	PNVIBAM$_{336}^E$	E	65	16:00	AIBN	38	1.84	38.6
62	PNVIBAM$_{340}$	none	66	5:20	MAIB	39	1.87	39.0
60	PNVIBAM$_{377}$	none	65	5:00	AIBN	43	2.12	38.9
64	PNVIBAM$_{1069}$	none	65	1:45	MAIB	121	2.87	39.2
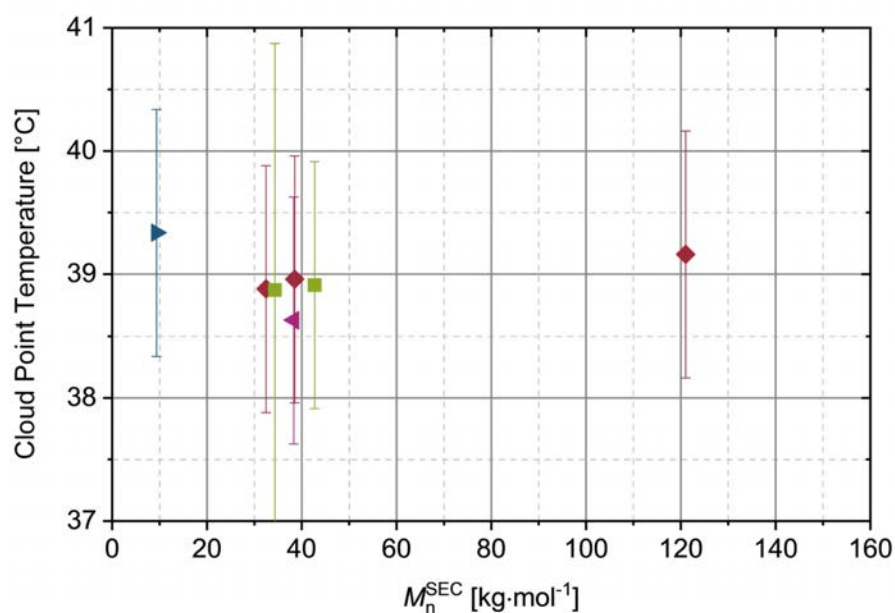
Figure 42. Cloud point temperature (±1°C) as a function of the number-average molar mass of PNVIBAM in water with concentration of 10 g·L^{-1}. The symbol's shape and color represent the polymer's various end-groups: blue tringle pointing to the right represent **CTA D**, red diamonds for **MAIB**, green squares for **AIBN**, and pink triangle pointing to the left for **CTA E**.

Concentration Effects

The effect of polymer concentration in aqueous solution was investigated for both PNIPMAM and PNVIBAM. For each polymer, a sample with lower molar mass (M_n^{SEC} 43 kg·mol^{-1}) and a sample with higher molar mass (M_n^{SEC} ca. 122 kg·mol^{-1}) was compared. It is important to point out that

while all four samples were polymerized in benzene at ca. 65°C, sample PNVIBAM$_{1069}$ was synthesized using MAIB initiator, whereas all other samples were synthesized using AIBN initiator. However, based on the results presented in the previous section of this thesis, this difference is not expected to lead to great variation in the obtained cloud point temperatures.

As shown in Figure 43 (for PNIPMAM) and Figure 44 (for PNVIBAM), the T_{CP} of both polymers clearly follows an apparently exponential decay with increasing concentration, regardless of molar mass. PNIPAM has also been reported to show an exponential decay of T_{CP} upon increase of concentration, with $\Delta T_{CP} = 1.5°C$ on a concentration range of $0.3 \sim 50$ g·L^{-1}.[254] Such behavior can be explained by the closer range contact between chains at higher concentrations, and propensity for polymer-polymer interactions as opposed to polymer-solvent interactions.

Moreover, as discussed on the previous section, the T_{CP} of PNIPAM is reportedly higher for lower molar mass polymers, where the magnitude of the exponential decay of T_{CP} is also larger.[119] This can be attributed to the higher relative content of end-groups on polymers of lower molar mass, which leads to stronger deviations from the inherent behavior of the polymer.[59,119,248]

This effect also seems to impact the results obtained here for both PNVIBAM and PNIPMAM, given that the T_{CP} of the samples with higher molar mass varies much less with concentration than the T_{CP} of the samples with lower molar mass. The cloud point variation between the concentrations of 0.5 and 50 g·L^{-1} is 2.2°C for PNVIBAM$_{377}$ versus 1.0°C for PNVIBAM$_{1069}$, and 1.4°C for PNIPMAM$_{339}$ versus 0.9°C for PNIPMAM$_{956}$.
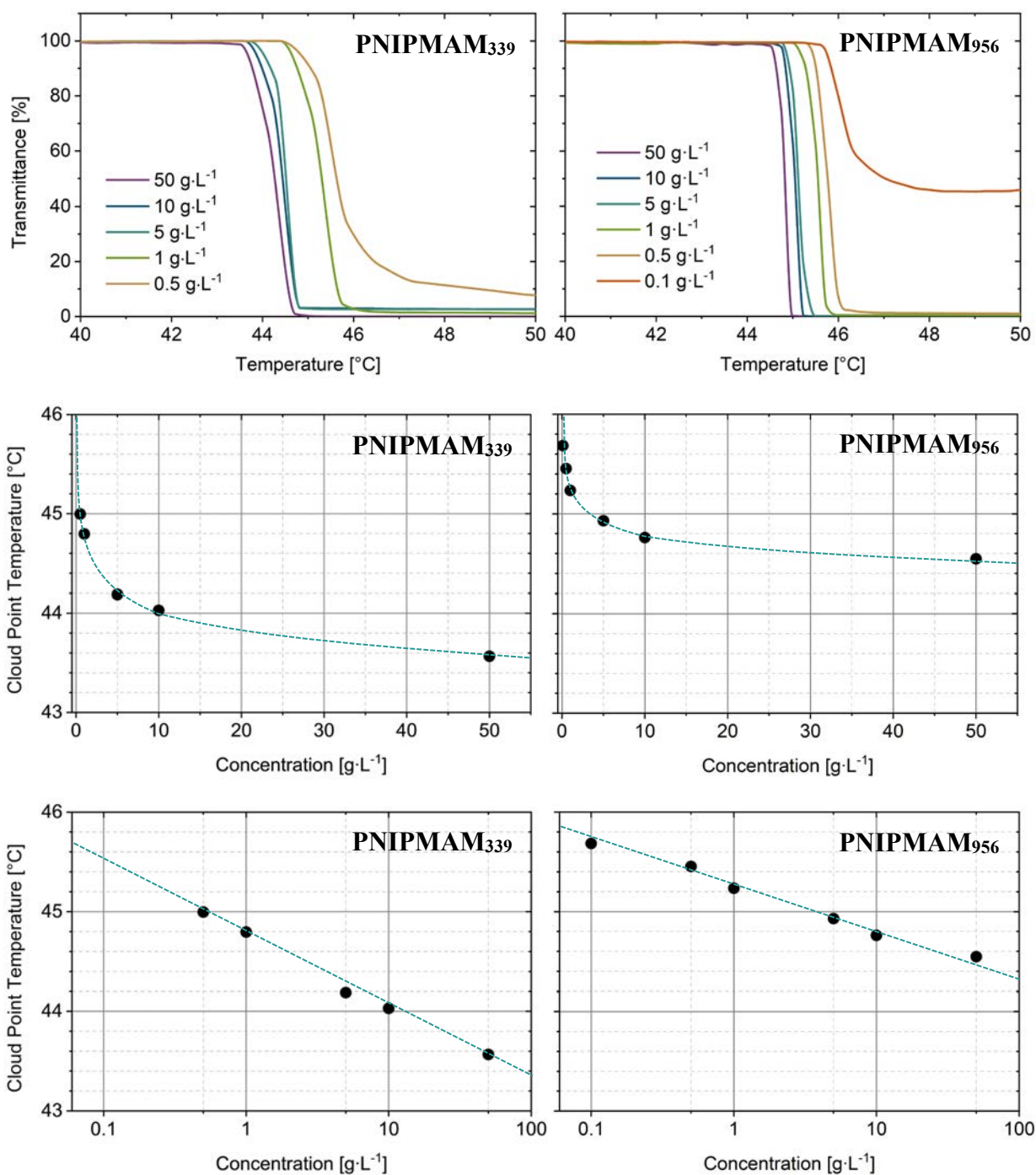
Figure 43. Turbidimetry heating curves (top), and cloud point temperature (±1°C) as a function of polymer concentration in water in linear (middle) and logarithmic (bottom) scale, for PNIPMAM$_{339}$ (on the left-hand side, reaction 23, M_n^{SEC} 43 kg·mol^{-1}) and for PNIPMAM$_{956}$ (on the right-hand side, reaction 28, M_n^{SEC} 122 kg·mol^{-1}). Dashed lines are guides for the eye.
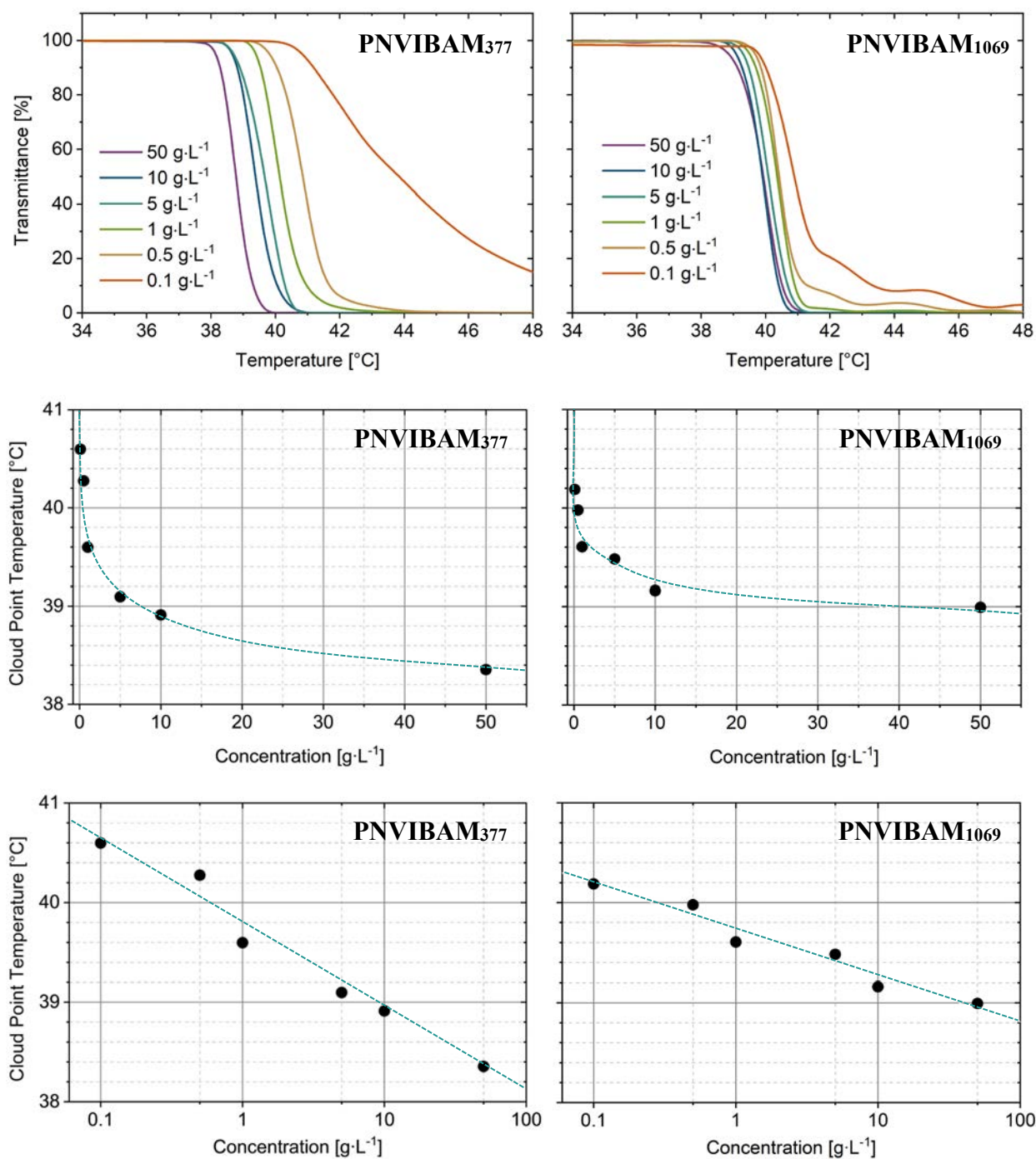
Figure 44. Turbidimetry heating curves (top), and cloud point temperature ($\pm 1°C$) as a function of polymer concentration in water in linear (middle) and logarithmic (bottom) scale, for PNVIBAM$_{377}$ (on the left-hand side, reaction 60, M_n^{SEC} 43 kg·mol^{-1}) and PNVIBAM$_{1069}$ (on the right-hand side, reaction 64, M_n^{SEC} 121 kg·mol^{-1}). Dashed lines are guides for the eye.

4.1.2. Co-nonsolvency: Comparison of Co-solvents

The co-nonsolvency of PNIPAM has been the focus of several publications. Although most studies have focused solely on water-methanol solvent systems, a few authors have reported the co-nonsolvency behavior also for other organic cosolvents. Many of the proposed mechanisms to

explain why co-nonsolvency occurs focus solely on PNIPAM in water-methanol mixtures and disregard the fact that the phenomenon is also seen for a variety of different polymers and cosolvents. Moreover, it is currently debated whether or not co-nonsolvency is a generic phenomenon, which does not depend on the specific interactions between the components of the system.[114,118] Thus, the existence of experimental data on co-nonsolvency in a wide array of systems could be of great value for the development and proofing of theoretical models that may explain the phenomenon.

In this regard, one of the most comprehensive studies of co-nonsolvency in various cosolvents is that published by Costa and Freitas, where co-nonsolvency of PNIPAM with cosolvents methanol, ethanol, isopropanol, n-propanol, acetone, DMSO and DMF were compared.[15] Additionally, acetonitrile, THF and 1,4-dioxane have also been reported to lead to co-nonsolvency on PNIPAM.[14,71] With base on these studies, the co-nonsolvency behavior of PNIPMAM and PNVIBAM in the presence of a variety of cosolvents was investigated here, and their behaviors compared to that of PNIPAM.

Figure 45, Figure 46 and Figure 47 illustrate the effect of various co-solvents on the cloud point temperature of PNIPMAM and PNVIBAM. The data of PNIPAM, from Costa and Freitas,[15] is included for comparison.
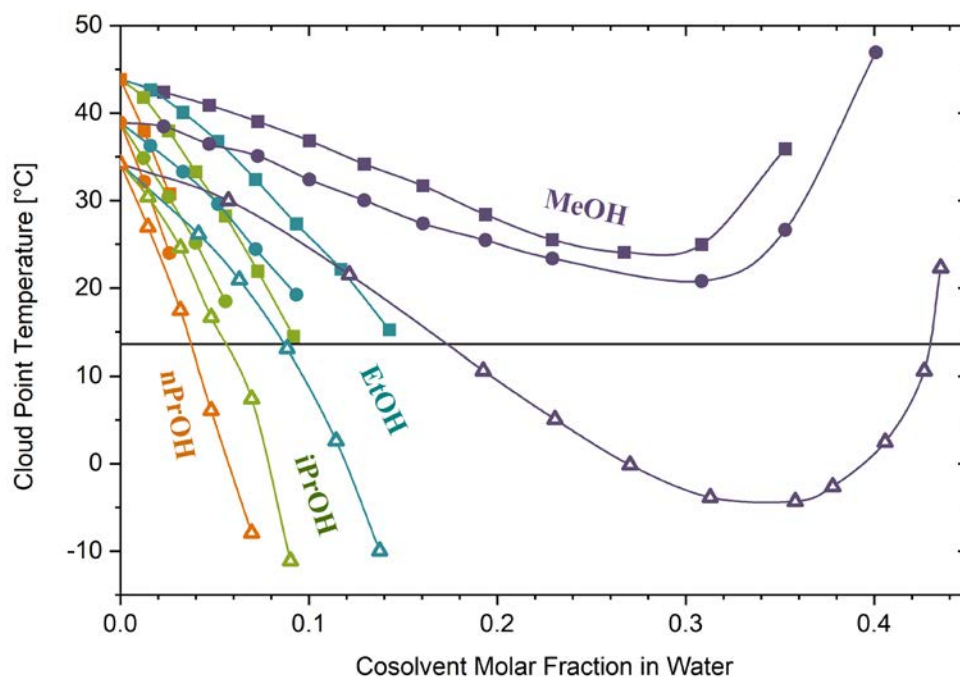
Figure 45. Cloud point temperatures (±1°C) of PNIPMAM$_{492}$ (■, reaction 81), PNVIBAM$_{377}$ (●, reaction 60), and PNIPAM$_{1060}$ (△, redrawn from Costa and Freitas[*][15]) in aqueous solutions containing varying fractions of alcohols: methanol (MeOH), ethanol (EtOH), isopropanol (iPrOH), and n-propanol (nPrOH) (concentration 10 g·L^{-1}). The horizontal line at ca. 14°C illustrates the lower temperature limit of the experimental setup used in this study.

All three polymers show the same behavior in water-alcohol mixtures (Figure 45), with PNIPMAM consistently showing the highest transition temperatures, followed by PNVIBAM and lastly PNIPAM. The polarity of the alcohol determines the intensity of the co-nonsolvency effect (T_{CP} decrease), with methanol leading to the mildest effects and n-propanol leading to the strongest ones. In the case of methanol, the presence of up to about 30 mol.% of co-solvent in water decreases the transition temperature. When more methanol is present, T_{CP} increases again, eventually exceeding that of pure aqueous solution. In the case of ethanol, isopropanol and n-propanol, such increase of T_{CP} at intermediate alcohol content could not be measured, probably because the increase is extremely sharp. Nonetheless all three polymers become soluble at room temperature in alcohol-rich aqueous solutions.

---

[*] Reprinted (adapted) from Polymer 43, 22, Ricardo O.R. Costa and Roberto F.S. Freitas, Phase behavior of poly(*N*-isopropylacrylamide) in binary aqueous solutions, pages 5879-5885, Copyright (2002), with permission from Elsevier.
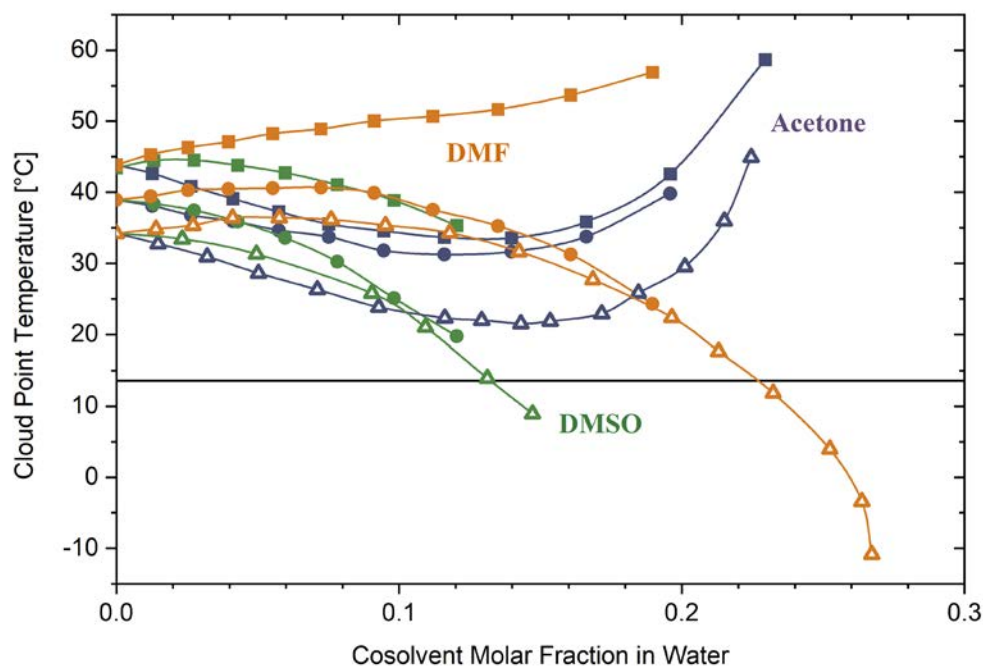
Figure 46. Cloud point temperatures (±1°C) of PNIPMAM$_{492}$ (■, reaction 81), PNVIBAM$_{377}$ (●, reaction 60), and PNIPAM$_{1060}$ (△, redrawn from Costa and Freitas[*][15]) in aqueous solutions containing varying fractions of organic cosolvents: acetone, dimethyl sulfoxide (DMSO), and dimethyl formamide (DMF) (solution concentration 10 g·L^{-1}). The horizontal line at ca. 14°C illustrates the lower temperature limit of the experimental setup used in this study.

Acetone (Figure 46) imparts on both PNIPMAM and PNVIBAM a similar behavior as methanol, albeit with a more pronounced effect on T_{CP} (shift to lower temperatures). For PNVIBAM, DMSO and DMF have similar influence on the transition temperatures as what has been shown for PNIPAM. DMSO shows little impact when present in low fractions but causes T_{CP} to drop more strongly as the fraction of co-solvent is increased. The effect of DMF is similar, although low fractions of the co-solvent indeed cause a slight increase of T_{CP}, before its shift to lower temperatures.

DMSO fractions in water leads to increase of the transition temperature of PNIPMAM up to molar fraction of ca. 0.15, after which the T_{CP} decreases, in typical co-nonsolvency fashion. DMF, however, has a considerably different effect on PNIPMAM than on PNVIBAM and PNIPAM. Here, T_{CP} increases continuously, with no signs of co-nonsolvency behavior.

[*] Reprinted (adapted) from Polymer 43, 22, Ricardo O.R. Costa and Roberto F.S. Freitas, Phase behavior of poly(*N*-isopropylacrylamide) in binary aqueous solutions, pages 5879-5885, Copyright (2002), with permission from Elsevier.
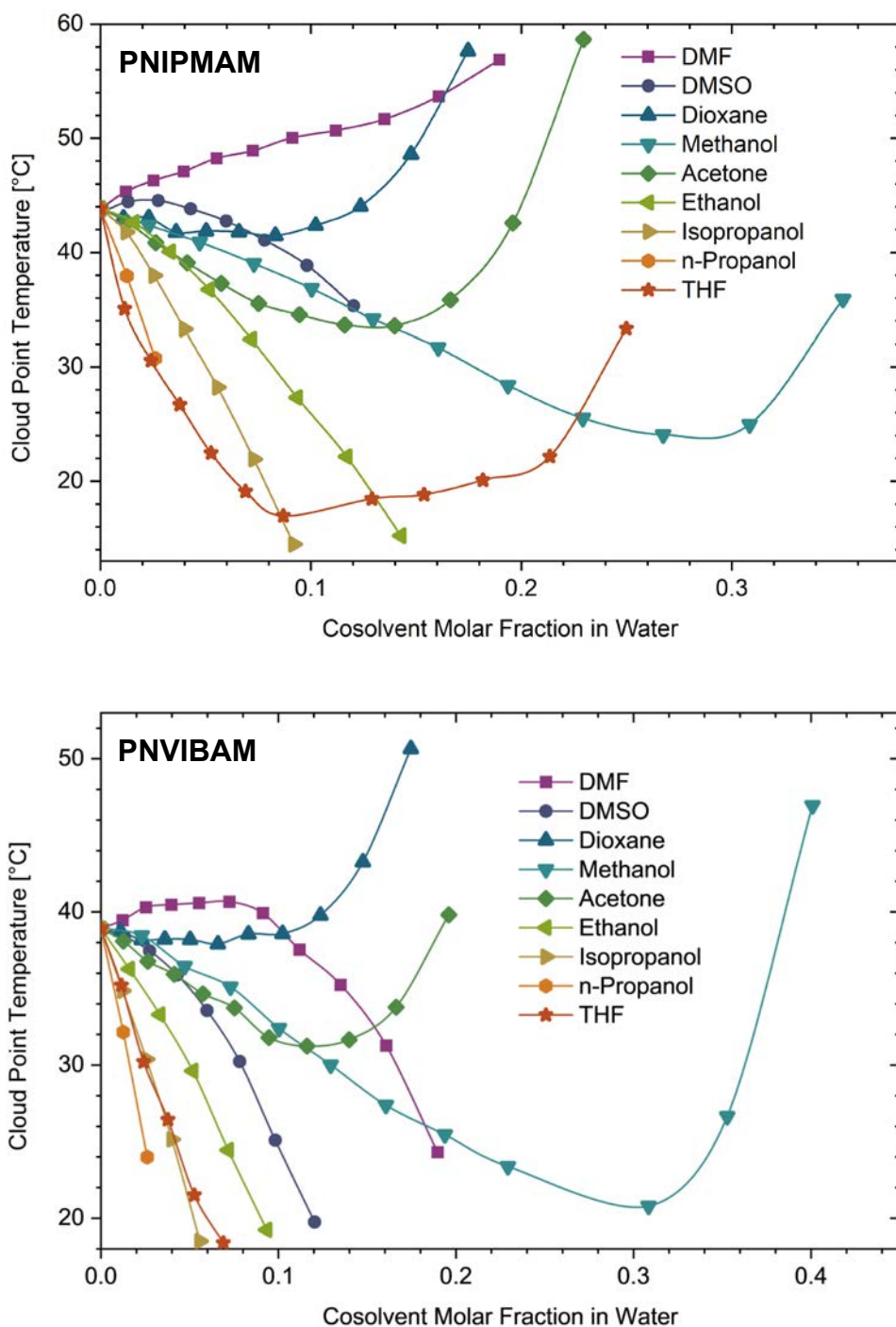
Figure 47. Cloud point temperatures (±1°C) of PNIPMAM$_{492}$ (top, reaction 81) and PNVIBAM$_{377}$ (bottom, reaction 60) in aqueous solutions with varying fractions of co-solvents (solution concentration 10 g·L^{-1}).

For both PNIPAM and PNVIBAM, small THF contents in water causes a very sharp decay of the transition temperature (Figure 47). For PNIPMAM, an increase of T_{CP} is then recorded when THF molar fraction is higher than 0.1. This behavior could not be identified for PNVIBAM, most likely due to its lower transition temperatures, outside the capability of the analytical setup.

Finally, co-nonsolvency of PNIPMAM and PNVIBAM in water-dioxane was also evaluated. Although a faint decay of T_{CP} can be seen in dioxane molar fractions below 0.1 (particularly in the case of PNIPMAM), this effect is considerably limited when compared to the other cosolvents, and a drastic increase of T_{CP} can be seen for both polymers when the molar fraction of dioxane is further increased.

Overall, the co-nonsolvency behavior of PNIPMAM and PNVIBAM is comparable to that of PNIPAM, with transition temperatures consistently following the trend of PNIPAM < PNVIBAM < PNIPMAM. However, a few exceptions were identified, most remarkable of which is the fact that DMF does not cause co-nonsolvency in PNIPMAM, contrarily to the very pronounced co-nonsolvency effect seen in PNIPAM and PNVIBAM.

4.2. Behavior of Amphiphilic Block Copolymers in Solution

Self-assembled polymeric structures in solution can be achieved through amphiphilic block copolymer architectures. When thermoresponsive polymers are incorporated into such copolymers, one can profit from their unique properties to develop active nanoscopic systems capable of performing functions such as macro-surfactants, viscosity control, drug delivery, nano-actuators, among many others, which can be control externally by changes in temperature.[7,10] Analogously, the same applies for the co-nonsolvency behavior, enabling responsivity of said systems to an additional stimulus: the presence and concentration of a cosolvent. Besides enabling the numerous potential applications of these systems, studying their thermoresponsivity, aggregation or self-assembly and co-nonsolvency behaviors provides valuable information that may shed extra light on mechanisms that lead to these responses, and that are to date not fully understood.

For this end, amphiphilic block copolymers containing a hydrophobic and a thermoresponsive block were synthesized, in which the thermoresponsive block exhibits co-nonsolvency behavior. These polymers were studied in aqueous and mixed aqueous solutions, to evaluate how the co-nonsolvency effect influences the aggregation of said copolymers, and vice-versa.

As for the previous section, turbidimetry was extensively used to characterize the thermoresponsive behavior of the polymers, by determining the transition temperature (cloud point) of their solutions in pure water and mixtures of water with a cosolvent. To characterize the aggregation of these polymers below the cloud point, dynamic light scattering (DLS) was employed, which provides information regarding the hydrodynamic diameter of particles, whether unimers or clusters, in solution over a broad temperature range. Above T_{CP}, however, DLS

characterization is no longer possible, due to the high turbidity of the system. The relaxation curves obtained from the DLS measurements, that is, the intensity autocorrelation function over time (correlograms), was fitted by the program to obtain the average hydrodynamic diameter (D_h) of the particles (unimers, organized self-assembled structures or irregular aggregates). The quality of the fit was inspected, and the calculated average diameters were considered only in the case of very good accordance between the collected data and the fitted data. In case a satisfactory fit could not achieved, only the raw correlograms were qualitatively evaluated. Before discussing the results obtained from DLS, it is important to point out the limitations of the method itself, and the limitations of the setup used in this study. As reviewed in section 2.4.2, the sizes of polymer structures obtained from DLS must be considered with care, as they do not necessarily represent the real size of the aggregated, but the size of a hypothetical sphere with the same diffusion coefficient as the particle being measured (hydrodynamic diameter, D_h). Additionally, one must remember that the results obtained relay heavily on the refractive indices of the components in the system. Here, the refractive index of each system is considered here to be ideally uniform. However, in mixed systems, as the ones investigated here, the refractive index is unlikely to be uniform, and determination of local refractive indices would be necessary to obtain more reliable results. Another notable limitation is that the device employed in these studies allows measurements in a single scattering angle: 173°C. Despite the advantages of this angle, the so-called backscattering detection mode, an evaluation of various scattering angles would be essential to obtain a more encompassing picture of the system. Finally, as previously mentioned, the device and software used do not allow any control over the fitting of the results, often leading to poor fit qualities in complex systems. Notwithstanding these limitations, the method may provide invaluable preliminary information about the systems and allow comparative evaluations of the effects from factors such as chemical structure, polymer architecture, molar mass, cosolvents, and concentration.

A final note must also be made about terminology related to aggregation of polymers in solution. While some amphiphilic block-copolymers may self-assemble into organized structures (such as micelles, rods, vesicles, etc.), others may simply aggregate into irregular clusters. Due to lack of information about the internal organization of the "particles" detected, the DLS setup used here naturally does not allow for a differentiation between irregular clusters or organized structures. Although in some cases assumptions are made based on the characteristics of the system, the hydrodynamic diameters and typical behaviors reported in literature, any differentiation between these two scenarios is purely hypothetical.

4.2.1. Homopolymers versus Amphiphilic Block Copolymers

Thermoresponsivity and Co-nonsolvency

Turbidimetry measurements were performed to characterize the thermoresponsive and co-nonsolvency behavior of the amphiphilic diblock copolymers discussed in this thesis. Figure 48 shows the change in the cloud point temperature of PMMA-*b*-PNIPAM and PMMA-*b*-PNIPMAM with increasing amounts of methanol. Example curves of analogous homopolymers are included for reference. The individual light transmittance curves are shown in Figure 59 (reaction indices 13 and 54) and in Annex 7.6 – Figure A 76 (reaction index 81).

As for the homopolymers, the copolymers clearly show co-nonsolvency behavior, with a decrease of the cloud point temperatures upon addition of small fractions of methanol. For both PNIPMAM and PMMA-*b*-PNIPMAM, a minimum in the T_{CP} can be seen at around 55 vol.% methanol, beyond which the cloud point increases again.
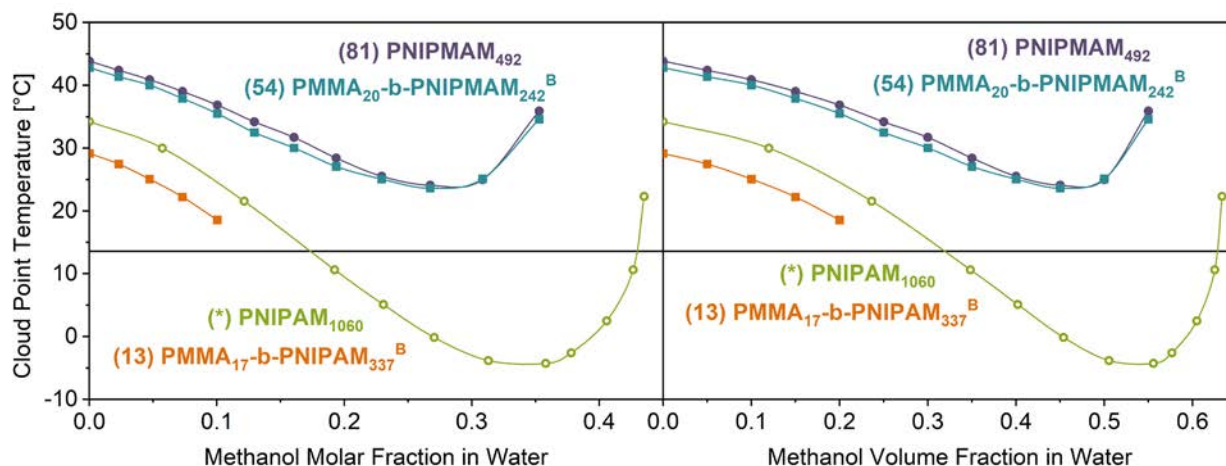
Figure 48. Cloud point temperatures (±1°C) in dependency of methanol fraction in water (molar fraction is shown on the left, volume fraction on the right), for PNIPAM and PNIPMAM homopolymers (●) and amphiphilic block copolymers (■). Measurements performed with solution concentration of 10 g·L^{-1}. Reaction indices are given in parenthesis before the sample's name. (*) Data of PNIPAM$_{1060}$ (open symbols) was redrawn from Costa and Freitas*.[15] The horizontal line at ca. 14°C illustrates the lower temperature limit of the experimental setup used in this study.

A striking behavior seen in Figure 48 is that the presence of a hydrophobic polymer block seems to affect PNIPAM very differently than PNIPMAM. The amphiphilic block copolymer

---

* Reprinted (adapted) from Polymer 43, 22, Ricardo O.R. Costa and Roberto F.S. Freitas, Phase behavior of poly(N-isopropylacrylamide) in binary aqueous solutions, pages 5879-5885, Copyright (2002), with permission from Elsevier.

PMMA-*b*-PNIPAM shows significantly lower transition temperatures than the homopolymer PNIPAM. This well-known behavior[31,255] is to be expected from the change in the overall hydrophilic/hydrophobic balance of the system, which is shifted towards a more hydrophobic average. Conversely, the homopolymer PNIPMAM and copolymer PMMA-*b*-PNIPMAM show essentially the same transition temperatures throughout the entire methanol fraction range evaluated. This difference in behavior becomes remarkably evident in Table 19 and Figure 49, where the cloud points of several PNIPAM and PNIPMAM homopolymers and copolymers in water are shown (T_{CP} versus methanol content curves are depicted in Figure 58).

While a variation of T_{CP} of almost 9°C can be seen for PNIPAM, depending on the presence, type, and size of the hydrophobic block, PNIPMAM shows no significant difference between the cloud points of homopolymers and copolymers of various block sizes. In fact, the variations in T_{CP} seen between PNIPMAM homopolymers and copolymers are smaller than the variations seen in the homopolymer alone, as a result of factors such as molar mass, end-groups and concentration (see discussion in Section 4.1.1). This is particularly puzzling, given that CTA **B** or V70 initiator end-groups imparted a decrease of about 3°C in the T_{CP} of the PNIPMAM homopolymer compared to homopolymers with AIBN, V50 or MAIB end-groups. Meanwhile, the same CTA **B** end-groups combined with a PMMA block seems to lead to a decrease of barely 1°C compared to homopolymers with AIBN, V50 or MAIB end-groups.

To further characterize the behavior of these polymers in solution, and to better identify the differences between the homo- and copolymers, dynamic light scattering (DLS) measurements were performed in solutions containing various methanol fractions. The results are presented and discussed in the following section.

Table 19. Cloud point temperatures of PNIPAM and PNIPMAM homopolymers and copolymers in pure water. Polymer concentration in the solution is given, as well as well as the weight fraction of the thermoresponsive block in the copolymers (w_{PNIP}, obtained from SEC). (*) For comparison, values from the literature are included, and their reference numbers are given in brackets, in place of the reaction index.

Index	Homopolymer	Conc. [wt.%]	T_{CP} [°C]
59	PNIPMAM$_{146}$[B]	10	41.0
44	PNIPMAM$_{219}$	10	40.9
31	PNIPMAM$_{241}$	10	45.4
21	PNIPMAM$_{305}$	10	44.2
23	PNIPMAM$_{339}$	10	44.0
43	PNIPMAM$_{381}$	10	41.5
30	PNIPMAM$_{424}$	10	43.7
35	PNIPMAM$_{426}$	10	44.9
81	PNIPMAM$_{492}$	10	43.8
45	PNIPMAM$_{682}$	10	40.9
27	PNIPMAM$_{776}$	10	44.4
40	PNIPMAM$_{895}$	10	44.4
36	PNIPMAM$_{936}$	10	44.6
28	PNIPMAM$_{956}$	10	44.4
38	PNIPMAM$_{1154}$	10	44.9
[31]*	PNIPAM$_{200}$	20	32.3
[15]*	PNIPAM$_{1060}$	10	34.2

Index	Copolymer	w_{PNIP}	Conc. [wt.%]	T_{CP} [°C]
52	PMMA$_{17}$-*b*-PNIPMAM$_{145}$[B]	0.89	10	42.9
56	PMMA$_{27}$-*b*-PNIPMAM$_{248}$[B]	0.90	10	42.4
54	PMMA$_{20}$-*b*-PNIPMAM$_{242}$[B]	0.92	10	42.8
55	PMMA$_{24}$-*b*-PNIPMAM$_{443}$[B]	0.95	10	44.1
9	PS$_{10}$-*b*-PNIPAM$_{65}$[B]	0.87	10	25.5
13	PMMA$_{17}$-*b*-PNIPAM$_{337}$[B]	0.94	10	29.1
13	PMMA$_{17}$-*b*-PNIPAM$_{337}$[B]	0.94	20	28.8
[31]*	PS$_{14}$-*b*-PNIPAM$_{310}$[B]	0.95	20	29.5
16	PMMA$_{27}$-*b*-PNIPAM$_{802}$[B]	0.96	10	29.4
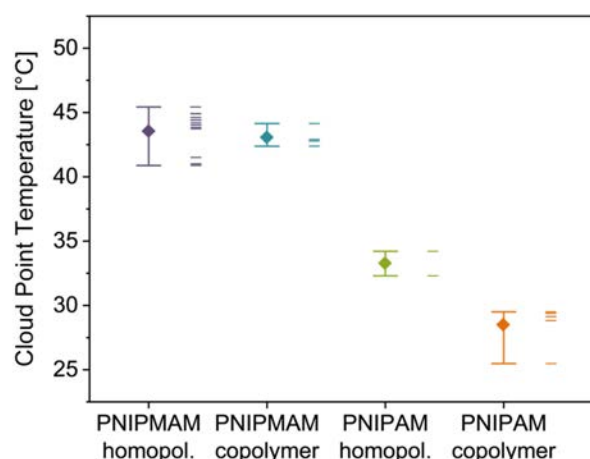
Figure 49. Cloud point temperatures of PNIPAM and PNIPMAM homopolymers and copolymers in pure water. Whiskers represent the range (minimum – maximum), diamonds represent the mean and lines represent the individual T_{CP}'s of each system. See Table 19 for detailed sample information. See Figure 58 for T_{CP} in water + methanol solutions. Measurement precision ±1°C.

Aggregation and Self-Assembly

One striking difference between thermoresponsive homopolymers and their amphiphilic block copolymer analogues is the possibility for self-assembly in solution. While the homopolymers may be dispersed in water below T_{CP} in the form of unimers (single molecule coils), amphiphilic block

copolymers may self-assemble into organized structures, due to hydrophobic interactions within the hydrophobic block. Through self-assembly, ordered structures such as micelles, rods, vesicles and lamellae may the formed, depending on the macromolecular architecture, as well as size and nature of the blocks.[11,12] One of the most commonly studied structures are core-shell micelles, often seen for linear copolymers composed of a short hydrophobic block and a long hydrophilic block.[135] This design was chosen for the copolymer discussed in this section, in which the hydrophilic block is composed of a polymer exhibiting co-nonsolvency behavior: poly(N-isopropyl methacrylamide). Its aggregation in mixed aqueous solutions was then compared to a corresponding homopolymer analogue.

Figure 50 shows the results obtained by DLS from the homopolymer poly(N-isopropyl methacrylamide) (PNIPMAM$_{492}$, reaction index 81) and the amphiphilic block copolymer poly(methyl methacrylate)-co-poly(N-isopropyl methacrylamide) (PMMA-b-PNIPMAM, reaction index 54) in water/methanol mixtures with increasing methanol volume fraction. For clarity of visualization, the relaxation curves are shown in the form of the range between the curve at 15°C (at longest relaxation times) and the curve immediately before the transition temperature of each sample (at shortest relaxation times). The temperature range shown for each sample is noted in the respective plots. For all samples, the relaxation continuously shifts to shorter times with increasing temperature (see Annex 7.7 – Figure A 78 and Figure A 79 for the individual curves), indicating a decrease of hydrodynamic diameter with increasing temperature. This can be attributed to the thermoresponsive behavior of the polymer, in which even below the transition temperature the solvent quality decreases as the temperature increases, causing the polymer chains to adopt a more compact conformation. This behavior has been widely reported for both PNIPAM[95,256-259] and PNIPMAM[173] homopolymers.

The multimodal nature of the relaxation of the homopolymer indicates the presence of some large particles, alongside small ones. To clarify the discussion, these two populations will be subsequently referred to as population S (homopolymer particles of smaller D_h) and population L (homopolymer particles of larger D_h). In contrast to the homopolymer, the copolymer shows a considerably narrower and more monomodal D_h distribution. This could, in part, be a result of the larger dispersity of the homopolymer ($Đ$ = 2.56) with respect to the copolymer ($Đ$ = 1.99). However, given the existence of two well marked homopolymer populations, with a pronounced difference in relaxation times (rather than simply one broad population, as is the molar mass distribution of PNIPMAM$_{492}$, see Figure A 58), it is likely that the homopolymer is dispersed partially in the form of single molecule coils (population S = unimers) and partially as multi-molecule aggregates (population L = clusters). Such coexistence of unimers and clusters in

aqueous solutions of PNIPMAM homopolymer below T_{CP} has recently been shown by Ko et al., using small angle neutron scattering (SANS).[28]

At low methanol fractions (0 to 20 vol.%), the homopolymer population S is clearly smaller than the copolymer particles, despite the fact that the molar mass of the homopolymer is much larger than that of the copolymer. Thus, these results corroborate the hypothesis that the homopolymer is dispersed in the form of unimer coils, while the copolymer tends to aggregate or self-assemble, likely in the form of micelles with a hydrophobic (PMMA) core and a hydrophilic (PNIPMAM) shell, as has been reported for amphiphilic diblock copolymers based on PNIPAM, for example.[31,260]

Conversely, the homopolymer population L is markedly larger than said copolymer micelles, further supporting the assumption that part of the homopolymer chains is aggregated into multi-molecule clusters.

From the DLS results shown in Figure 50, it is also possible to see that with increasing methanol fraction, the separation of the homopolymer chains into two populations is attenuated, as the hydrodynamic diameter of the population S increases and merges with the population L. Consequently, at 60:40 and 50:50 water / methanol solutions, the particles from the homopolymer and copolymer seem to have a very similar D_h. This evolution becomes particularly clear when analyzing the average hydrodynamic diameter with increasing volume fraction of methanol from 20 to 50 vol.% (Figure 51). Due to their strongly multimodal character, the data of the homopolymer in pure water and in 90:10 (vol.) water / methanol could not be fitted by the program and is not shown. Here it is important to highlight that the values shown in Figure 51 for the remaining solvent compositions must be considered with caution. This is firstly due to the inherently limited accuracy of the method, and the assumptions that are made to obtain the hydrodynamic diameters, which may not translate directly into the real unimers or aggregate diameters. Secondly, as the data of the homopolymer in these solvent compositions still showed a slightly multimodal distribution, the simple fit offered by the program cannot provide accurate hydrodynamic diameters. Nonetheless, keeping these considerations in mind, and evaluating the hydrodynamic diameter results along with the raw relaxation curves, allows the identification of certain trends that provide valuable information about the system. For this end, the reader is referred to Annex 7.7, where one can find a direct comparison of the relaxation curves with increasing amounts of methanol, for both the homopolymer (Figure A 80a) and copolymer (Figure A 80b), all at 25°C (below the cloud point of the systems).
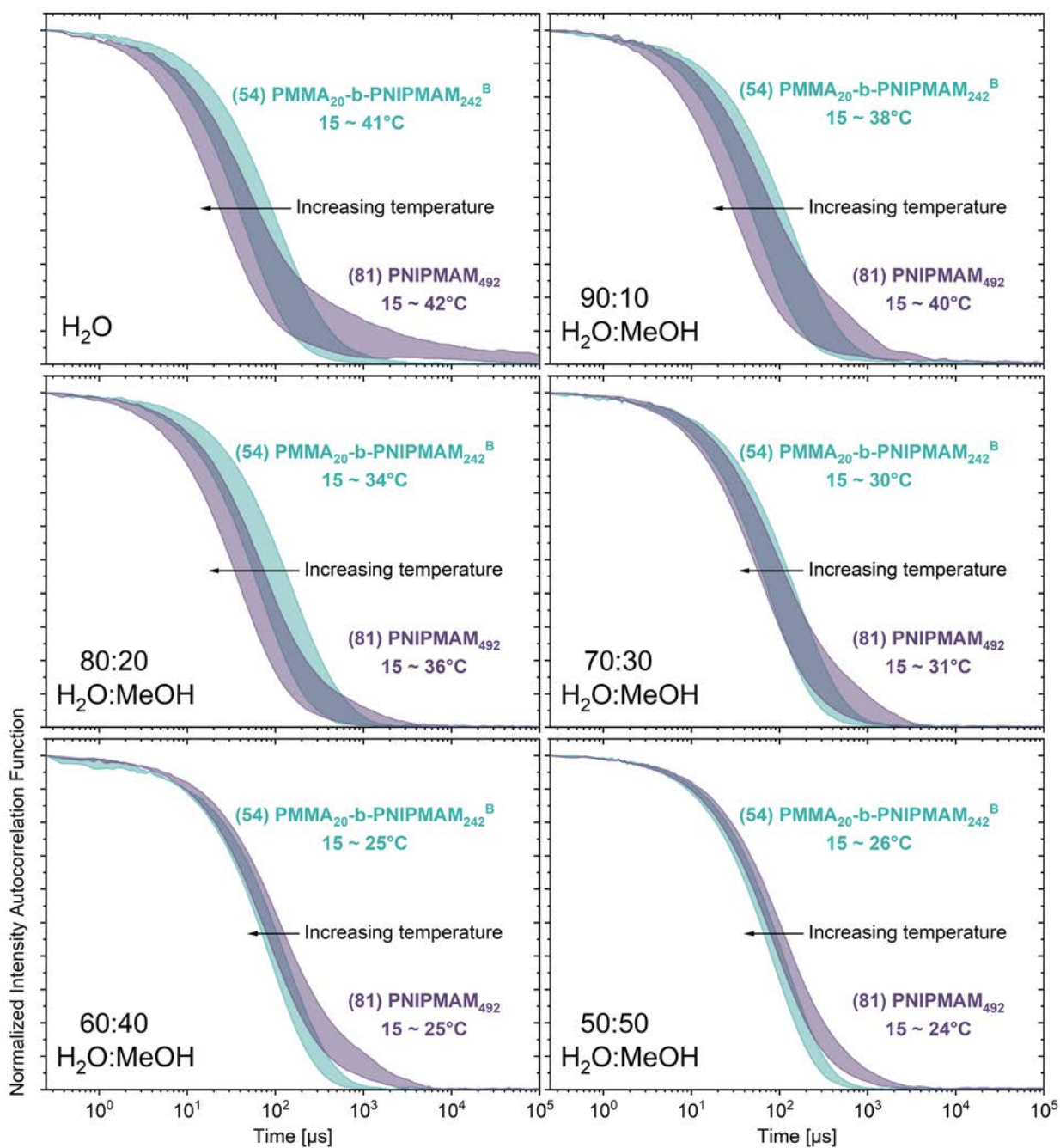
Figure 50. Effect of temperature on the intensity autocorrelation function of homopolymer PNIPMAM$_{492}$ (reaction index 81) and amphiphilic block copolymer PMMA$_{20}$-*b*-PNIPMAM$_{242}$^{B} (reaction index 54) in water/methanol solutions with varying volume fractions of methanol, from 15°C until immediately below the transition temperature of each sample. Results obtained by DLS, with concentration of 10 g·L^{-1}. Reaction indices are given in parenthesis before the sample's name.

The results shown in Figure 50, Figure 51, and Figure A 80 suggest that the increased methanol content from 20 to 50 vol.% promotes the formation of homopolymer clusters, driven by the reduction of the solvent quality as is typical of the co-nonsolvency phenomenon, even below T_{CP}. Interestingly, a different behavior is seen for the copolymer, where the samples in 20 to 50 vol.%

methanol show a tendency of slightly decreased hydrodynamic diameter (shorter relaxation times) with increase in methanol content. As a result, at 20 vol.% methanol, the D_h of the homopolymer particles is about half of the D_h of the copolymer particles, at 40 vol.% the diameters are essentially identical, and finally, at 50 vol.% the homopolymer actually shows larger hydrodynamic diameters than the copolymer. The contraction of the polymer chains with increasing methanol fraction is to be expected from the worsening of solvent quality.[77,261] However, along with this contraction, the homopolymer seems to be driven to aggregate with other chains, whereas the copolymer seems to contract and simply maintain the micellar structures, without being driven to a second level of aggregation.

Once the temperature (or methanol content) is increased above a critical level, however, intense clustering takes place both in the homopolymers and copolymers, and the systems undergo phase separation.
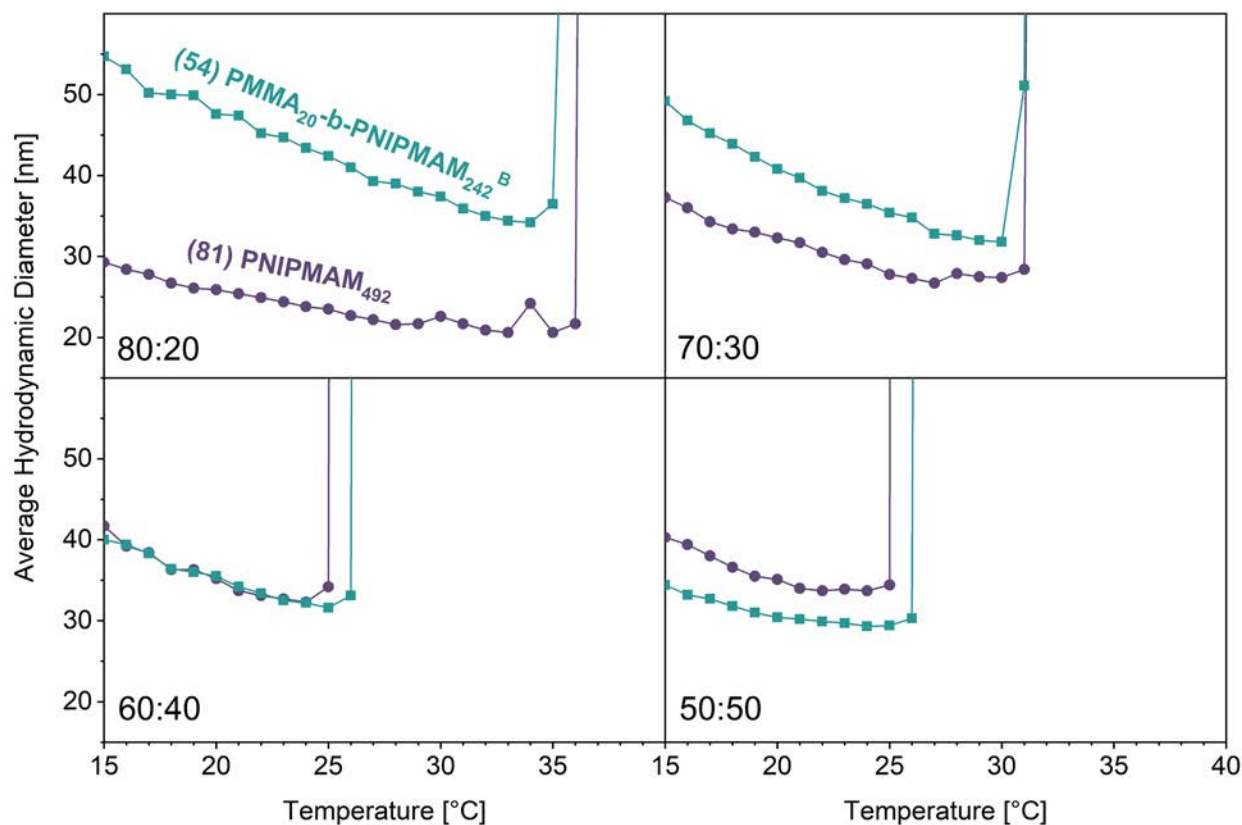
Figure 51. Average hydrodynamic diameter of homopolymer PNIPMAM$_{492}$ (● reaction index 81) and amphiphilic block copolymer PMMA$_{20}$-*b*-PNIPMAM$_{242}$^{B} (■ reaction index 54) in water/methanol solutions with 0.2 to 0.5 volume fraction of methanol, at 15 to 40°C (across the T_{CP} of the samples). Results obtained by DLS, with concentration of 10 g·L^{-1}. Reaction indices are given in parenthesis before the sample's name.

It is unclear what is the cause for such differences in behavior below T_{CP}. One may speculate that it is related to the ease by which homopolymer unimers and copolymer micelles can aggregate: while homopolymer single molecules (unimers) have a higher level of freedom, allowing an easy stacking over other molecules, the aggregation of two micelles requires that the polymer chains of one micelle penetrate the already dense corona of another micelle, which becomes even denser once the chains start contracting due to presence of methanol. A visual representation of this hypothesis is depicted in Figure 52. This effect is particularly exacerbated for PNIPMAM, in comparison to PNIPAM, due to the additional methyl group, which further limits the freedom of the molecule and increases the steric hindrance to the aggregation with other chains. Thus, below T_{CP}, it is more advantageous for the contracted micelles to remain in their colloidal state, in which they are sterically stabilized. The steric hindrance caused by the methyl group, and consequently weaker intramolecular interactions between the amide groups has been suggested as an explanation for the higher T_{CP} of PNIPMAM versus PNIPAM, despite the presence of the additional hydrophobic moiety.[165,262] This has also been shown to lead to larger and more hydrated aggregates in the two-phase state of PNIPMAM compared to PNIPAM.[28]

This hypothesis could potentially also help explain the puzzling similarity between the transition temperatures of PNIPMAM homopolymers and PMMA-*b*-PNIPMAM amphiphilic block copolymers (see results from turbidimetry in the previous section). It may be that the effect of steric hindrance caused by methyl group (driving T_{CP} to higher temperatures) supersedes the effect of the hydrophobic block (which would be expected to drive T_{CP} to lower temperatures).
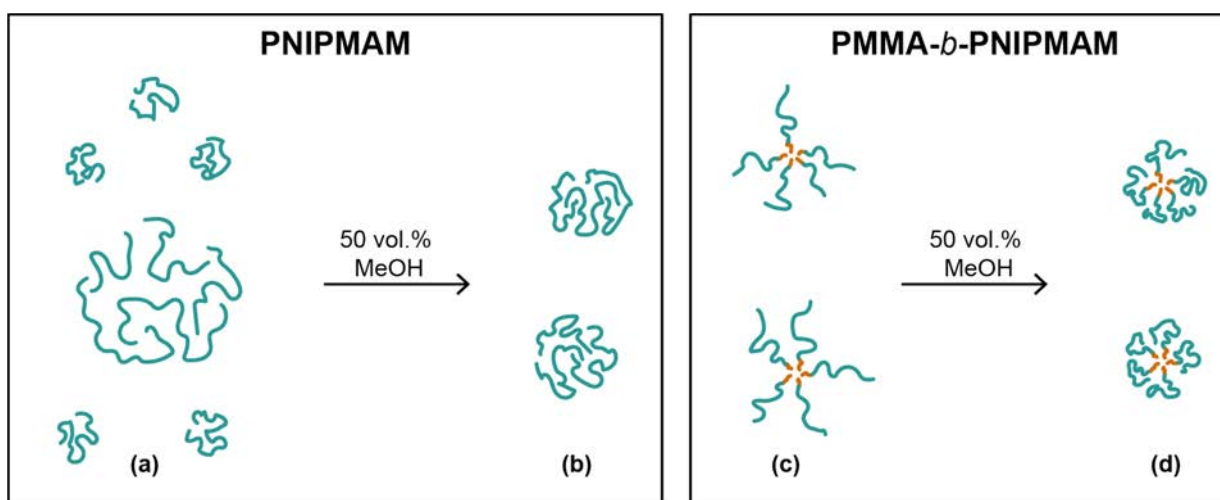
Figure 52. Visual representation of the hypothetical effect of methanol cosolvent on the aggregation of PNIPMAM$_{492}$ and PMMA$_{20}$-*b*-PNIPMAM$_{242}$[B]. In pure water, the homopolymer (a) is dissolved as a mixture of unimers and aggregates, whereas the copolymer (c) is self-assembled into micelles. When methanol is present in the aqueous solution, the PNIPMAM segments in both the homopolymer and the copolymer slightly shrink due to lower solvent quality. In the case of the homopolymer (b), this process is accompanied by aggregation of the unimers into aggregates, leading to a single population of multi-molecule aggregates. The size of the copolymer micelles (d), in contrast, simply reduces due to the shrinking. These scenarios are based on the DLS results at a temperature of about 20°C (below the T_{CP}), and a 10 g·L^{-1} concentration. Sizes are not to scale.

4.2.2. Factors Influencing the Behavior of Amphiphilic Diblock Copolymers

Chemical Structure of the Thermoresponsive Block: PNIPMAM versus PNIPAM

In the previous section, the aggregation and self-assembly of PNIPMAM homopolymers and copolymers was compared in depth, and the transition temperature of various PNIPAM and PNIPMAM amphiphilic block copolymers was briefly discussed (see Table 19 and Figure 49). Here, the behavior of these samples is evaluated in more detail, with emphasis on the differences seen between the self-assembly of copolymers based on PNIPMAM versus PNIPAM.

The effect of temperature and presence of methanol on the hydrodynamic diameter of PMMA$_{17}$-*b*-PNIPAM$_{337}$[B] (reaction index 13) and PMMA$_{20}$-*b*-PNIPMAM$_{242}$[B] (reaction index 54) below T_{CP} is illustrated in Figure 53, while the individual relaxation curves are available in Annex 7.7 – Figure A 79 and Figure A 81.

In pure water, PMMA-*b*-PNIPAM is known to form core-shell micelles with a PMMA core and a PNIPAM shell.[260,263,264] Here, at 15 to 25°C (i.e., well below T_{CP} in pure water), the sample shows very little hydrodynamic diameter variation. Above this range, and up to the transition temperature, a slight increase in D_h is seen. This may be a result of aggregation of micelles at temperatures

immediately below the transition temperature, due to a decrease of the solvent quality.[260] In contrast, the particles of PMMA-*b*-PNIPMAM tend to steadily decrease in D_h upon increase of the temperature from 15 to 36°C, as discussed in the previous section. Besides this difference in behavior, the hydrodynamic diameters seen for the acrylamide copolymer are considerably smaller than those of the methacrylamide analog, despite the larger molar mass of the former. This could possibly be related to the additional methyl moiety in PNIPMAM, which decreases the mobility of the chain as well as increases its bulkiness, leading to more stretched thermoresponsive segments and, therefore to a larger micelle corona.

The presence of methanol in water also seems to affect the two samples differently: PMMA-*b*-PNIPMAM shows some decrease in hydrodynamic diameter upon addition of 10 or 20 vol.% of methanol in water, whereas PMMA-*b*-PNIPAM shows a marked increase in D_h, especially at lower temperatures. This may indicate that the acrylamide copolymer micelles aggregate upon addition of methanol, similarly to what was previously seen for PNIPMAM homopolymers. Alternatively, it may be that the aggregation number, that is, the number of molecules per micelle, increases with increasing amounts of methanol, leading the chains to adopt a slightly more stretched conformation due to the denser packing. This scenario could in fact be enhanced by the cosolvency effect of the PMMA block, which would reduce its insolubility in the solvent mixture, facilitating the mobility of chains between micelles.[265] The methacrylamide copolymer, in contrast, seems to show simple contraction of its micelles upon addition of methanol, despite also containing a PMMA block prone to cosolvency behavior. In the previous section, it was speculated that the tendency of PNIPMAM to aggregate, while the PMMA-*b*-PNIPMAM micelles shrank, could be related to the ease in which homopolymer unimers and copolymer micelles can aggregate. Here, once again, this hypothesis may apply, given the increased mobility and reduced bulkiness of PNIPAM chain segments compared to the PNIPMAM in the copolymer, facilitating intermolecular association, even between micelles. This hypothesis is schematized in Figure 54.
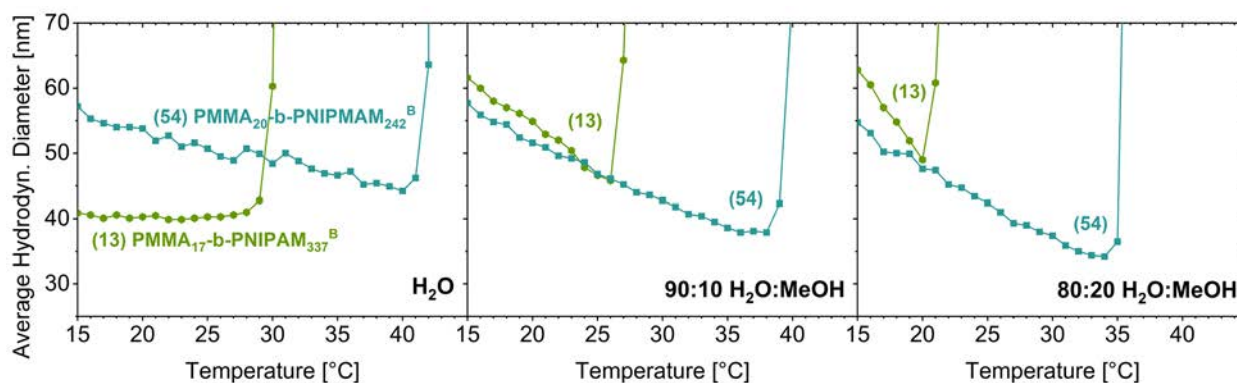
Figure 53. Average hydrodynamic diameter of PMMA$_{17}$-*b*-PNIPAM$_{337}$^{B} (● reaction index 13, w_{PNIPAM}^{SEC} 0.94) and PMMA$_{20}$-*b*-PNIPMAM$_{242}$^{B} (■ reaction index 54, $w_{PNIPMAM}^{SEC}$ 0.92) from left to right in pure water, 90:10 and 80:20 water/methanol (vol.) solutions below the transition temperature. Results obtained by DLS, with concentration of 10 g·L^{-1}.
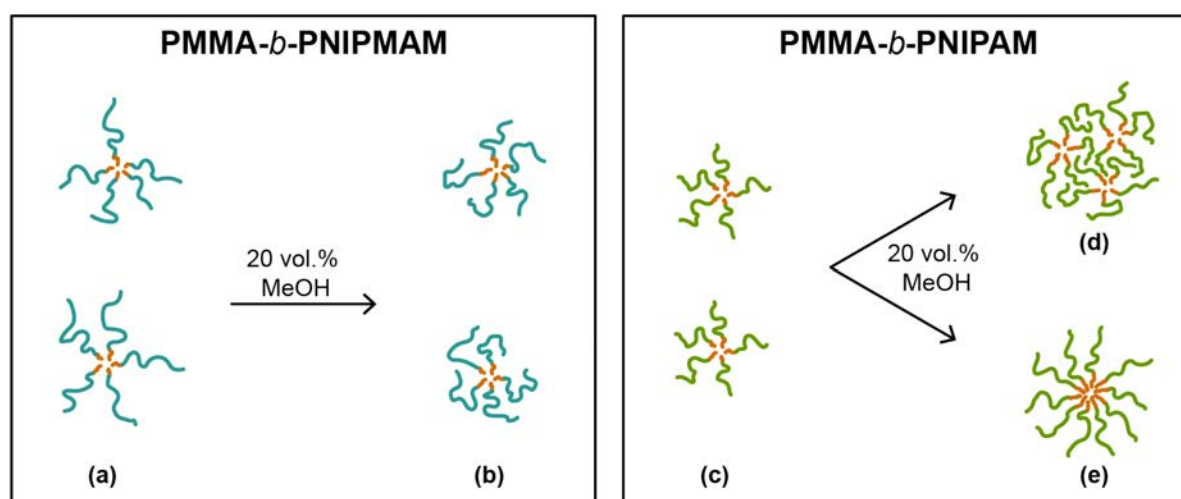
Figure 54. Visual representation of the hypothetical effect of methanol cosolvent on the aggregation of PMMA$_{20}$-*b*-PNIPMAM$_{242}$^{B} and PMMA$_{17}$-*b*-PNIPAM$_{337}$^{B}. In pure water, both copolymers (a, c) are self-assembled into micelles. When methanol is present in the aqueous solution, the thermoresponsive segments slightly shrink due to lower solvent quality. For the PNIPMAM copolymer (b), this leads to decrease in micelle size. In the case of the PNIPAM copolymer, increase of aggregate size occurs, which could be due to (d) clustering of the micelles or (e) increase of aggregation number (number of chains per micelle). These scenarios are based on the DLS results at a temperature of about 20°C (below the T_{CP}), and a 10 g·L^{-1} concentration. Sizes are not to scale.

Chemical Structure of the Hydrophobic Block: PS versus PMMA

Besides evaluating variations in the chemical structure of the thermoresponsive block, the impact of changes in the hydrophobic block was also investigated. For this, PMMA-*b*-PNIPAM copolymers were compared to PS-*b*-PNIPAM copolymers. Poly(methyl methacrylate) (PMMA) and polystyrene (PS) were chosen for this comparison due to their slight difference in polarity:

although both are hydrophobic, PMMA is slightly more polar than PS. Yet, both polymers have similar glass transition temperature (T_g ca. 100°C). This increases the likelihood of similar mobility levels for both PS and PMMA at a given temperature, thus avoiding the so called "frozen chain" condition, if the polymers were investigated below their T_g.[12]

The co-nonsolvency phase curves, that is, the evolution of the cloud point temperature with increasing methanol fractions of PMMA- and PS-based copolymers is compared in Figure 55. The data of a PNIPAM homopolymer is included for reference. The two concentrations (10 and 20 g·L^{-1}) are included here to allow a more direct comparison with the results from literature. The individual light transmittance curves are shown in Figure 59 (reaction indices 13 and 16) and in Annex 7.6 – Figure A 77 (reaction index 9).
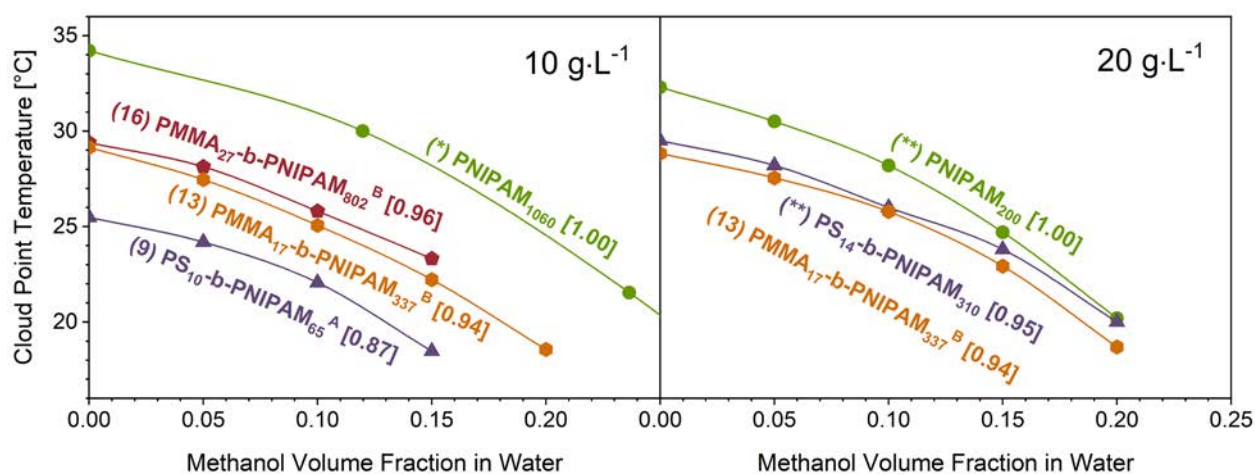
Figure 55. Cloud point temperatures (±1°C) of PNIPAM amphiphilic block copolymers containing PS (▲) and PMMA (⬠, ⬠) hydrophobic blocks, in dependency of methanol fraction in water. Data of PNIPAM homopolymers (●) is included for reference. Measurements performed with solution concentration of 10 g·L^{-1} (left) and 20 g·L^{-1} (right). Reaction indices are given in parenthesis before the sample's name. Weight fraction of PNIPAM in the polymer (w_{PNIPAM}, from SEC) is given in brackets after the sample's name (for homopolymers, end-groups are neglected). (*) Data of PNIPAM$_{1060}$ was redrawn from Costa and Freitas.[15][†] (**) Data of PNIPAM$_{200}$ and PS$_{14}$-b-PNIPAM$_{310}$ was redrawn from Kyriakos et al.[31][‡]

In contrast to what was shown for PNIPMAM and PMMA-*b*-PNIPMAM (see section 4.2.1 - Homopolymers versus Amphiphilic Block Copolymers), both PS-*b*-PNIPAM and PMMA-*b*-PNIPAM copolymers show lower transition temperatures than a PNIPAM homopolymer. Moreover, for both types of copolymers, the reduction of T_{CP} seems to be stronger with lower PNIPAM weight fraction (i.e., increase in PS or PMMA weight fraction). Given the limited variety of samples under evaluation, and the differences in molar mass and PNIPAM weight fractions between the samples, a direct comparison between the effect of PS versus PMMA on the transition temperature will not be conducted. Instead, focus will be on the self-assembly of the samples, specifically PS-*b*-PNIPAM and PMMA-*b*-PNIPAM, that is, reactions index 9 and 13, respectively. A comparison of the hydrodynamic diameter measured for the samples is shown in Figure 56, while the relaxation curves are available in Annex 7.7 - Figure A 81, Figure A 83 and Figure A 84.
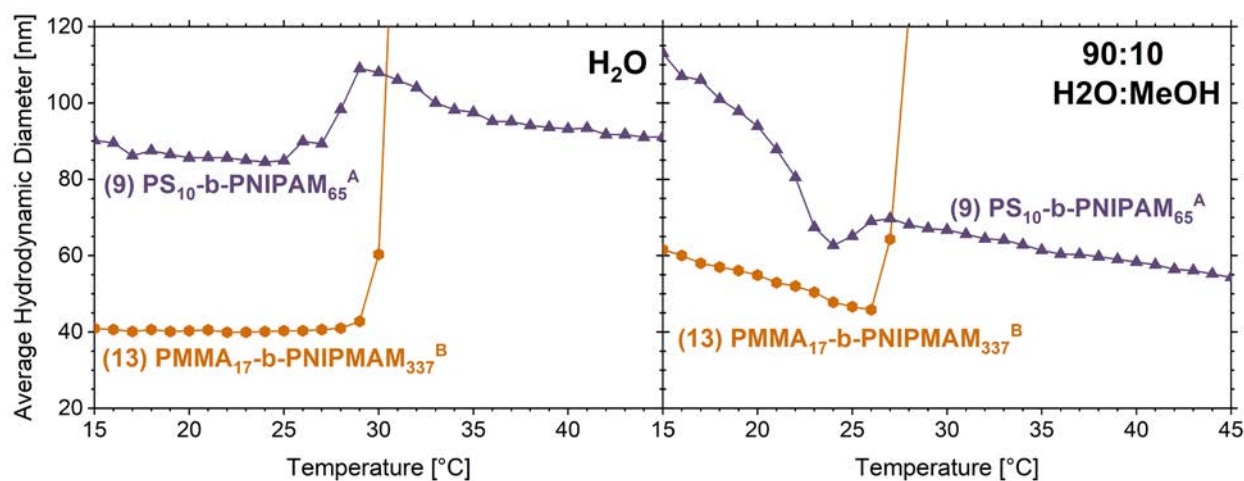
Figure 56. Average hydrodynamic diameter of PMMA$_{17}$-*b*-PNIPAM$_{337}$[B] (● reaction index 13, w_{PNIPAM}^{SEC} 0.94) and PS$_{10}$-*b*-PNIPAM$_{65}$[A] (▲ reaction index 9, w_{PNIPAM}^{SEC} 0.87) in pure water and 90:10 water/methanol (vol.). Results obtained by DLS, with concentration of 10 g·L^{-1}.

In pure water, below the transition temperature, both PMMA$_{17}$-*b*-PNIPAM$_{337}$[B] ($T_{CP} \sim 29.1$°C) and PS$_{10}$-*b*-PNIPAM$_{65}$[A] ($T_{CP} \sim 25.5$°C) show very little hydrodynamic diameter variation upon increase of temperature. At low temperatures (below 20°C), the presence of 10 vol.% methanol causes an increase in D_h for both samples compared to the D_h in pure water. However, as the temperature increases, the D_h of both samples steadily decrease, likely due to contraction of the PNIPAM segment.

In both pure water and water/methanol mixtures, the hydrodynamic diameter of the PS-based copolymer is considerably larger than that of the PMMA-based copolymer, despite its substantially smaller molar mass. As discussed previously, PMMA$_{17}$-*b*-PNIPAM$_{337}$[B] is expected to form

spherical micelles in solution, with a PMMA core and a PNIPAM shell.[260,263,264] Meanwhile, PS-*b*-PNIPAM copolymers have been shown to self-assemble in various different structures, including vesicles ($w_{PNIPAM} \sim 0.48$),[266] large spherical aggregates ($w_{PNIPAM} \sim 0.53$),[267] mixtures of vesicles and spherical micelles ($w_{PNIPAM} \sim 0.63$),[226] spherical micelles ($w_{PNIPAM} \sim 0.63$ to 0.78),[32,266,268,269] mixtures of cylindrical and spherical micelles ($w_{PNIPAM} \sim 0.85$),[226] or unstructured large aggregates ($w_{PNIPAM} \sim 0.88$),[268] depending on molar mass and weight fraction of PNIPAM (w_{PNIPAM}) in the copolymer. Based on these reports, the formation of spherical micelles seems to require a w_{PNIPAM} 0.1 to 0.2 below that of the PS_{10}-*b*-$PNIPAM_{65}{}^{A}$ sample under evaluation here (w_{PNIPAM} 0.87). At a similar w_{PNIPAM} of 0.88, Ke et al. reported the copolymer PS_{65}-*b*-$PNIPAM_{360}$ to form a mixture of spherical and cylindrical structures in pure water (0.06 g·L^{-1}) at 25°C, with mean hydrodynamic diameters (obtained by DLS) around 237 nm and 1 μm, respectively, with overall average around 395 nm.[226] Similarly, at w_{PNIPAM} 0.88, Nuopponen et al. reported the copolymer PS_{50}-*b*-$PNIPAM_{376}$ to form large unstructured aggregates in water, with hydrodynamic diameter around 600 nm at 20°C (0.2 g·L^{-1}).[268]

Although the average hydrodynamic diameter of PS_{10}-*b*-$PNIPAM_{65}{}^{A}$ in water at 25°C (ca. 86 nm) is smaller than the micellar sizes obtained by Ke et al., their copolymer had a greatly larger molar mass than the sample under evaluation here. Considering a bond length of 0.154 nm and a bond angle of 109.5°, the stretched end-to-end distance of a PS_{10}-*b*-$PNIPAM_{65}{}^{A}$ chain is around 19 nm, while for a PS_{65}-*b*-$PNIPAM_{360}$ and a PS_{50}-*b*-$PNIPAM_{376}$, they are around 107 nm. Spherical micelles of these polymers would then have a maximum diameter around 38, 214 and 215 nm, respectively. While these values are somewhat consistent with the spherical micelle diameter reported by Ke et al. (given all experimental uncertainties), the diameters obtained here for PS_{10}-*b*-$PNIPAM_{65}{}^{A}$ are considerably larger than its maximum (fully stretched) spherical micelle size, suggesting that the polymers are not simply self-assembling into micelles, but into larger aggregates. Based on the information provided through the characterization methods available in this study, it is not possible to say whether these large aggregates are a result of several micelles coming together, or simply unstructured large clusters. It is important to highlight, of course, that the concentration evaluated here is considerably higher than that of the evaluations conducted by Ke et al. and Nuopponen et al. This may also contribute to aggregation.

Another interesting characteristic of the PS_{10}-*b*-$PNIPAM_{65}{}^{A}$ seen by DLS, is its behavior when the transition temperature is reached. Differently from the remaining polymers discussed so far, which show extreme aggregation and abrupt increase in hydrodynamic diameters, PS_{10}-*b*-$PNIPAM_{65}{}^{A}$ shows only a minute increase in aggregate D_{h}. Similar behavior was noted by Ke et al,[226] and

may indicate a higher level of repulsion between the aggregates than seen in the homopolymers and PMMA copolymers, likely as a result of the PS core.

These rationalizations are depicted in Figure 57, allowing a visual comparison of both polymers under the effects of temperature and presence of methanol.
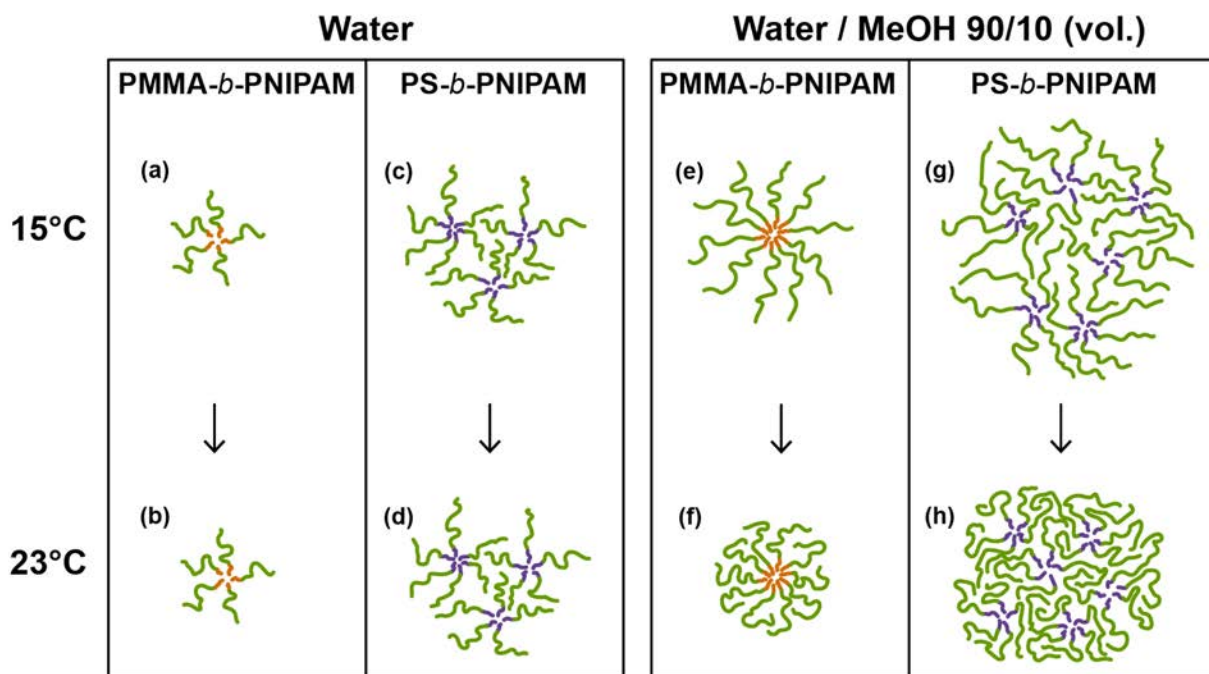
Figure 57. Visual representation of the hypothetical combinatory effects of temperature and methanol cosolvent on the aggregation of PNIPAM copolymers with PMMA and PS hydrophobic blocks. While PMMA$_{17}$-b-PNIPAM$_{337}$[B] tends to assemble into individual micelles, PS$_{10}$-b-PNIPAM$_{65}$[A] tends to form larger clusters in both water and water/methanol. The increase of temperature from 15°C to 23°C has little effect on the copolymers in pure water (a→b and c→d). The presence of 10 vol.% methanol intensifies aggregation for both systems (a→e and c→g). In this solvent mixture, the increase in temperature from 15 to 23°C leads to shrinkage of the aggregates (e→f and g→h), due to lower solvent quality for the PNIPAM block. These scenarios are based on the DLS results below the T_{CP}, with concentration of 10 g·L^{-1}. Sizes are not to scale.

These differences in behavior between PMMA$_{17}$-b-PNIPAM$_{337}$[B] and PS$_{10}$-b-PNIPAM$_{65}$[A], where the former tends to self-assemble into spherical micelles and the latter forms large aggregates, indicate that the chemical structure, presumably through the polarity of the hydrophobic group has a significant impact on the aggregation of PNIPAM. This may serve as an additional tool to tailor the aggregation behavior of the diblock copolymers.

Polymer Architecture and Block Sizes

In section 4.2.1, the transition temperature of various PNIPAM and PNIPMAM amphiphilic block copolymers was briefly discussed (see Table 19 and Figure 49). Here, the behavior of these samples will be evaluated in more detail, and the effects of different block sizes on the resulting thermoresponsivity, co-nonsolvency and aggregation will be examined.

The cloud points of various PNIPAM, PNIPMAM, PS-*b*-PNIPAM, PMMA-*b*-PNIPAM and PMMA-*b*-PNIPMAM polymers in dependence of methanol volume fraction in water are depicted in Figure 58. The individual light transmittance curves are provided in Figure 59 (reaction indices 13, 16, 52, 54 and 56) and in Annex 7.6 – Figure A 76 (reaction indices 59 and 81) and Figure A 77 (reaction index 9).

In accordance with what was shown in Figure 48, the T_{CP} of PNIPMAM is hardly changed by the presence of the hydrophobic PMMA block, or the block size ratio (in the legend of the graph, the PNIPMAM weight fraction in the polymer is given in brackets after the sample's names). Interestingly, however, a significant change on the transition temperatures is seen for PNIPMAM homopolymer with the large hydrophobic CTA **B** end-groups (reaction index 59). The reason for this difference in behavior is not clear, but one can speculate that it is related to the microphase separation that occurs between the PNIPMAM and PMMA blocks in the copolymer. In turn, the PMMA has very little effect on the behavior of the PNIPMAM segments. CTA **B** hydrophobic end-groups, however, may not be large enough to induce a microphase separation, but their hydrophobicity shifts the hydrophobic/hydrophilic balance of PNIPMAM, reducing its transition temperature in pure water. Similarly, as the CTA **B** end-groups do not show co-nonsolvency behavior, their close presence may weaken the co-nonsolvency behavior shown by the PNIPMAM segments, explaining the higher T_{CP} in 0.2 to 0.5 volume fraction of methanol. This hypothesis does not clarify, however, why PNIPAM copolymers, which also microphase separate, still suffer the influence of the hydrophobic PS and PMMA blocks.
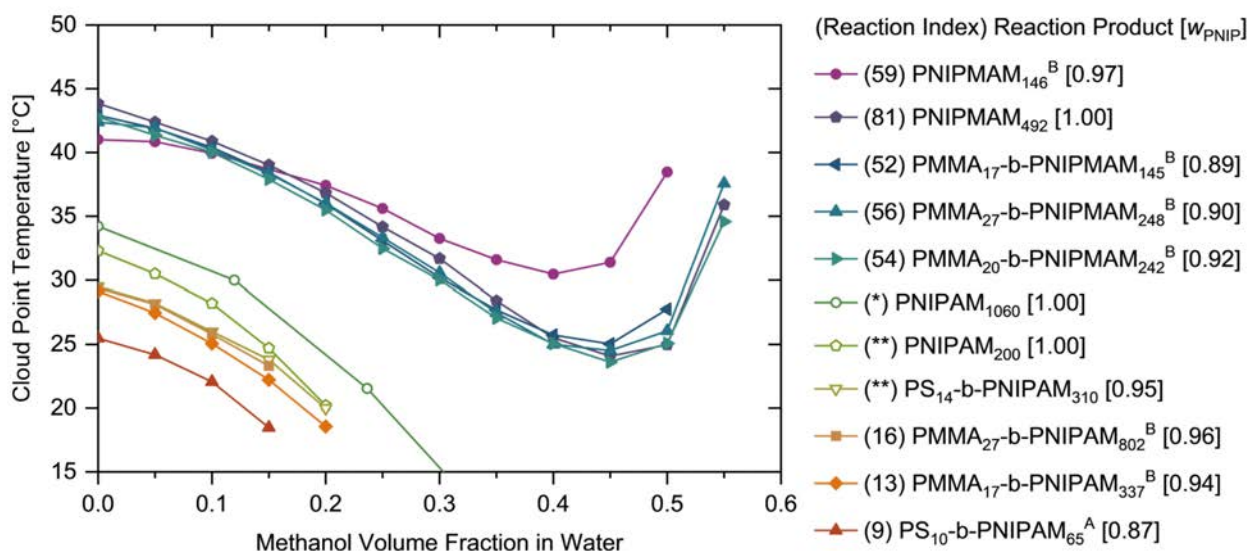
Figure 58. Cloud point temperatures (±1°C) in dependency of methanol volume fraction in water, for PNIPAM and PNIPMAM homopolymers and amphiphilic block copolymers. Unless otherwise stated, measurements were performed with solution concentration of 10 g·L⁻¹. Reaction indices are given in parenthesis before the sample's name. Weight fraction of PNIPAM or PNIPMAM in the polymer (w_{PNIP}, from SEC) is given in brackets after the sample's name (for homopolymers obtained by conventional free radical polymerization, end-groups are neglected). Selected literature data is included for comparison: (*) data of PNIPAM₁₀₆₀ was redrawn from Costa and Freitas[15]† and (**) data of PNIPAM₂₀₀ and PS₁₄-*b*-PNIPAM₃₁₀ (measured with a concentration of 20 g·L⁻¹) was redrawn from Kyriakos et al.[31]‡

Aside from the samples shown in Figure 58, it is also interesting to point out that diblock copolymers PS₁₀-*b*-PNIPAM₈₅^A (reaction index 10, w_{PNIPAM} 0.90) and PMMA₇₅-*b*-PNIPAM₃₆₆^B (index 18, w_{PNIPAM} 0.84), as well as triblock copolymers PS₁₀-*b*-PNIPAM₁₈₀-*b*-PS₁₀^F (index 11, w_{PNIPAM} 0.91) and PS₁₀-*b*-PNIPAM₂₅₀-*b*-PS₁₀^F (index 12, w_{PNIPAM} 0.93) were synthesized, but their cloud points or aggregation could not be evaluated, due to difficulties in obtaining homogeneous solutions of said samples. Rather than fully dissolving in water or forming microscopic assemblies, the samples hydrated, forming gel domains which remained suspended in solution. This behavior did not improve in reduced temperatures (down to 4°C), nor with an increase in the amount of solvent (reduced concentration). Although the T_{CP} of the samples in pure water did seem to be

---

† Reprinted (adapted) from Polymer 43, 22, Ricardo O.R. Costa and Roberto F.S. Freitas, Phase behavior of poly(N-isopropylacrylamide) in binary aqueous solutions, pages 5879-5885, Copyright (2002), with permission from Elsevier.
‡ Reprinted (adapted) with permission from Macromolecules 2014, 47, 19, 6867–6879, Konstantinos Kyriakos, Martine Philipp, Joseph Adelsberger, Sebastian Jaksch, Anatoly V. Berezkin, Dersy M. Lugo, Walter Richtering, Isabelle Grillo, Anna Miasnikova, André Laschewsky, Peter Müller-Buschbaum, and Christine M. Papadakis, Cononsolvency of Water/Methanol Mixtures for PNIPAM and PS b PNIPAM: Pathway of Aggregate Formation Investigated Using Time-Resolved SANS, Copyright (2014) American Chemical Society.

slightly above room temperature, given the visual hydration that occurred, the solutions were not homogenous and translucent enough to yield conclusive turbidimetry or DLS results. As shown in the previous section (Figure 56), PS_{10}-b-$PNIPAM_{65}{}^A$ (reaction index 9, w_{PNIPAM} 0.87) forms relatively large aggregates in water and in 90:10 (vol.) water / methanol, whereas self-assembled spherical micelles are typically obtained for w_{PNIPAM} around 0.63 to 0.78.[32,266,268,269] Similarly, literature reports PS_{50}-b-$PNIPAM_{376}$ (w_{PNIPAM} 0.88) to form large unstructured aggregates in water.[268] Thus, the difficult dissolution seen here for PS_{10}-b-$PNIPAM_{85}{}^A$, PS_{10}-b-$PNIPAM_{180}$-b-$PS_{10}{}^F$ and PS_{10}-b-$PNIPAM_{250}$-b-$PS_{10}{}^F$ is no big surprise, especially for the triblock copolymers, whose tendency to gelation is even stronger, due to the interconnecting effect of the double hydrophobic end blocks.[270,271]

Although PMMA-b-PNIPAM copolymers are reported to form spherical micelles in a much wider range of w_{PNIPAM},[260,263,264,268,272] it is foreseeable that the large hydrophobic block in $PMMA_{75}$-b-$PNIPAM_{366}{}^B$ kinetically "freezes" the chains, hindering their dissolution in water, similarly to what is seen for PS-b-PNIPAM with PS blocks larger than 14 constitutional repeat units.[9] The effect of the PMMA block size on the behavior of PNIPAM in water is made rather clear in Figure 59, where the turbidimetry curves (light transmittance over temperature) of three samples with increasing PMMA block sizes are shown for various solvent mixtures (clearly evidencing the co-nonsolvency behavior as well). As the degree of polymerization (DP_n) of the PMMA block increases from 17 to 27 to 41, the cloud point becomes more "smeared". That is, the transition becomes less sharp, to the point that the T_{CP} of the sample $PMMA_{41}$-b-$PNIPAM_{456}{}^B$ cannot be determined. It is interesting to note that this behavior seems to be more profoundly related to the PMMA block size itself, and less so on the block size ratio.

Also depicted in Figure 59 are the turbidimetry curves of PMMA-b-PNIPMAM samples with increasing PMMA block sizes, where this "smeared cloud point" behavior is not seen, further evidencing the difference in the thermoresponsive behavior between PNIPAM and PNIPMAM-based amphiphilic block copolymers.
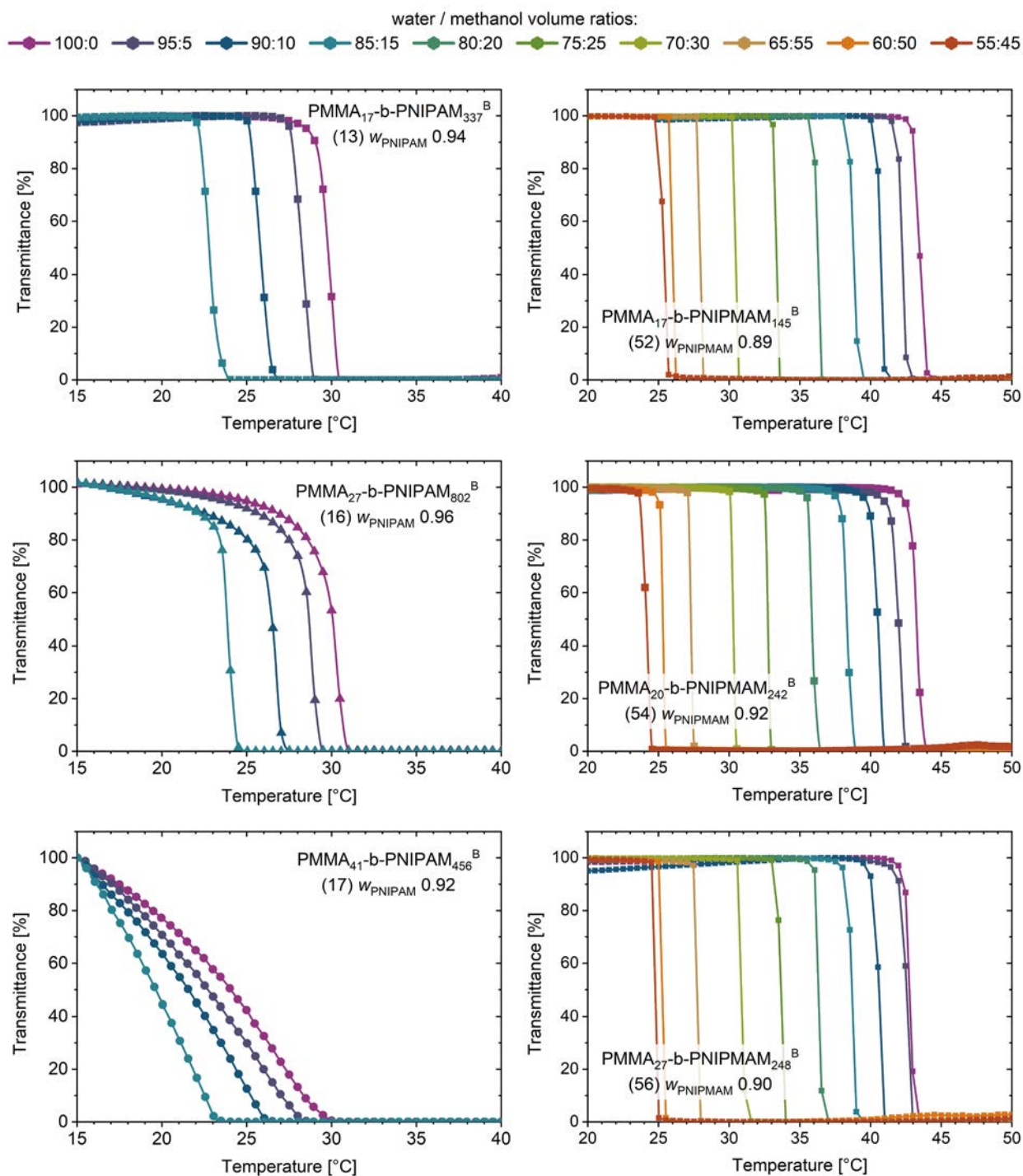
Figure 59. Normalized turbidimetry heating curves for PNIPAM (left) and PNIPMAM (right) PMMA-based amphiphilic diblock copolymers in water/methanol solutions (polymer concentration 10 g·L^{-1}). Reaction indices and weight fraction of the thermoresponsive block (w_{PNIPAM}^{SEC} or $w_{PNIPMAM}^{SEC}$) are given for each sample.

In order to further evaluate the effects of block sizes on the behavior of PNIPAM and PNIPMAM amphiphilic block copolymers in solution, the self-assembly of these samples was also evaluated, using DLS.

Influence of Block Sizes on the Aggregation of PMMA-b-PNIPAM in Solution

The aggregation behavior of PMMA$_{17}$-*b*-PNIPAM$_{337}$^{B} (reaction index 13, w_{PNIPAM}^{SEC} 0.94) has already been discussed in detail in the previous sections and is illustrated in Annex 7.7 - Figure A 81 and Figure A 82. In summary, the sample shows a seemingly monomodal autocorrelation function decay below its transition temperature, both in water, as well as in 90:10 and 80:20 (vol.) water / methanol. In pure water, hydrodynamic diameters hardly vary upon increasing the temperature from 15°C to 29°C (immediately below its transition temperature). A 0.1 volume fraction of methanol in water leads to larger particles at 15°C, which shrink when the temperature is increased from 15°C to 26°C (just below the transition temperature). This seems to indicate that an increased methanol content drives either the clustering of the micelles, or the increase of aggregation number, that is, the number of chains per micelle. Meanwhile, increased temperatures seem to cause contraction of the chains.

The aggregation behavior of PMMA$_{27}$-*b*-PNIPAM$_{802}$^{B} (reaction index 16, w_{PNIPAM}^{SEC} 0.96) in water and water / methanol is depicted in Figure 60a, while the individual relaxation curves are provided in Annex 7.7 - Figure A 85. Increase of temperature from 15°C until just below the cloud point seems to barely induce any changes in the hydrodynamic diameter. However, similar to PMMA$_{17}$-*b*-PNIPAM$_{337}$^{B}, the addition of 0.1 volume fraction of methanol in water leads to a small increase in the D_h of PMMA$_{27}$-*b*-PNIPAM$_{802}$^{B}.
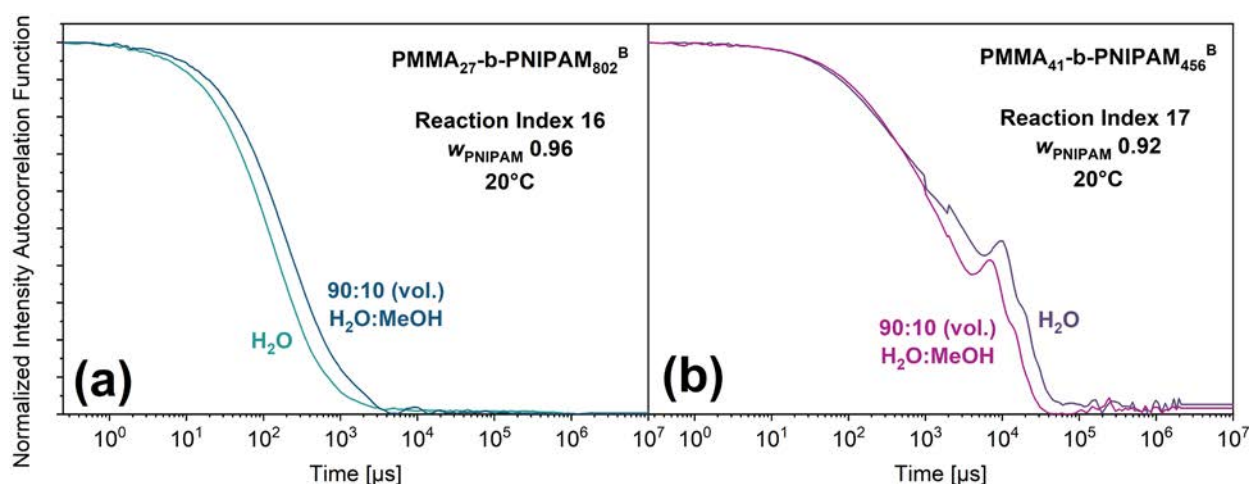
Figure 60. DLS correlograms of (a) PMMA$_{27}$-*b*-PNIPAM$_{802}$^{B} and (b) PMMA$_{41}$-*b*-PNIPAM$_{456}$^{B} in water and 90:10 (vol) water / methanol at 20°C (concentration 10 g·L^{-1}).

Figure 60b depicts the aggregation behavior of PMMA$_{41}$-*b*-PNIPAM$_{456}$^{B} (reaction index 17, w_{PNIPAM}^{SEC} 0.92) in water and water / methanol, while the individual relaxation curves are provided in Annex 7.7 - Figure A 86. In contrast to the fairly monomodal relaxation of PMMA$_{17}$-*b*-PNIPAM$_{337}$^{B} and PMMA$_{27}$-*b*-PNIPAM$_{802}$^{B}, high variability is seen in the relaxation

curves obtained for PMMA$_{41}$-*b*-PNIPAM$_{456}$[B] (reaction index 17, $w_{\text{PNIPAM}}^{\text{SEC}}$ 0.92) in aqueous solution, as well as a markedly multimodal character of the decays. Moreover, for both solvent compositions (water and water / methanol), an artifact in the form of an intensity autocorrelation function peak is seen at ca. 10^4 μs, at temperatures equal and below 24°C (in water) or 26°C (in water / methanol). This artifact was consistently and reproducibly obtained on repeated measurements, and with newly prepared solutions, yet its origin is unclear. Despite these characteristics, when analyzing the evolution of the decay curves of this sample over temperature (Annex 7.7, Figure A 86), the behavior seems to change at around 28 ~ 30°C in pure water, and at around 26°C in water / methanol 90:10 (vol.). Above these temperatures, the decay of the intensity autocorrelation function becomes visually monomodal, and its dispersity is markedly reduced (decay becomes steeper). On the one hand, the transition in pure water is very gradual, and strong variation in the relaxation curves is seen both before and after the change. In water / methanol, on the other hand, the change is very well defined, and the decay times also shifts to considerably lower values, indicating smaller particles, potentially due to collapse of the PNIPAM segments. These sizes then remain relatively constant up to 60°C, where the measurement was stopped. For all other samples discussed thus far, the transition seen in DLS is in quite good agreement with the cloud points from turbidimetry, keeping in mind the lower temperature resolution obtained from DLS, since the measurements are done only every 1°C. If we consider this change in behavior of PMMA$_{41}$-*b*-PNIPAM$_{456}$[B] to indicate its coil-to-globule transition, its transition temperatures would be slightly lower than those seen for PMMA$_{27}$-*b*-PNIPAM$_{337}$[B] and PMMA$_{27}$-*b*-PNIPAM$_{802}$[B].

A comparison of the relaxation curves of PMMA$_{17}$-*b*-PNIPAM$_{337}$[B], PMMA$_{27}$-*b*-PNIPAM$_{802}$[B] and PMMA$_{41}$-*b*-PNIPAM$_{456}$[B] at 20°C, in water and water / methanol, is illustrated in Figure 61. The hydrodynamic diameters obtained from the fit of the relaxation curves of PMMA$_{17}$-*b*-PNIPAM$_{337}$[B] and PMMA$_{27}$-*b*-PNIPAM$_{802}$[B] are shown in Figure 62. Due to their irregularities, an appropriate fit of the curves from PMMA$_{41}$-*b*-PNIPAM$_{456}$[B] could not be achieved.

As expected from its considerably larger chain length, the average D_{h} of PMMA$_{27}$-*b*-PNIPAM$_{337}$[B] (80 to 140 nm) is considerably larger than that of PMMA$_{17}$-*b*-PNIPAM$_{337}$[B] (40 to 60 nm), both in water as well as in water / methanol. Considering a bond length of 0.154 nm and a bond angle of 109.5°, the stretched end-to-end length of a PMMA$_{17}$-*b*-PNIPAM$_{337}$[B] is about 92 nm, while PMMA$_{27}$-*b*-PNIPAM$_{802}$[B] is about 212 nm. Given that even in a good solvent, the chains are likely to adopt a coiled conformation, rather than a stretched one, the hydrodynamic diameters found here would be within realistic micelle sizes for both polymers. This supports the hypothesis that

the chains are indeed self-assembled in the form of individual micelles, rather than aggregated into larger clusters.[260,265]

Interestingly, however, $PMMA_{41}$-b-$PNIPAM_{456}^{B}$ shows enormously larger decay times of the intensity autocorrelation function, indicating much larger aggregates. Given the smaller length of the thermoresponsive water soluble block of $PMMA_{41}$-b-$PNIPAM_{456}^{B}$ compared to $PMMA_{27}$-b-$PNIPAM_{802}^{B}$, this could indicate that $PMMA_{41}$-b-$PNIPAM_{456}^{B}$ aggregates in large clusters, rather than in individual micelles, in both water as well as in the water / methanol mixture.
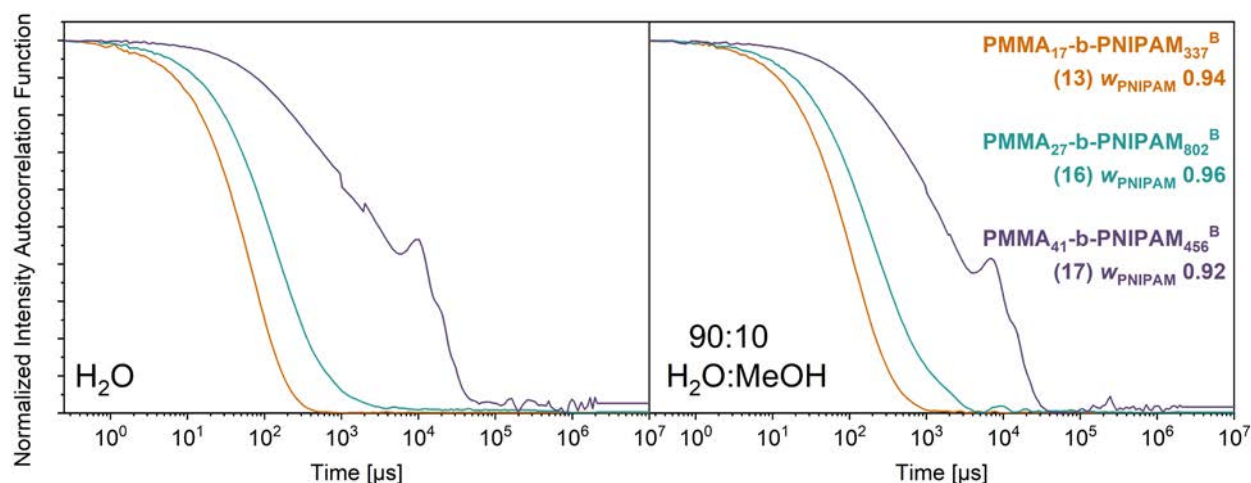
Figure 61. DLS correlograms for PMMA-b-PNIPAM amphiphilic diblock copolymers in water (left) and 90:10 (vol) water / methanol (right) at 20°C (concentration 10 g·L^{-1}). Reaction indices of each sample are given in parenthesis, along with the PNIPAM weight fraction in the copolymer.
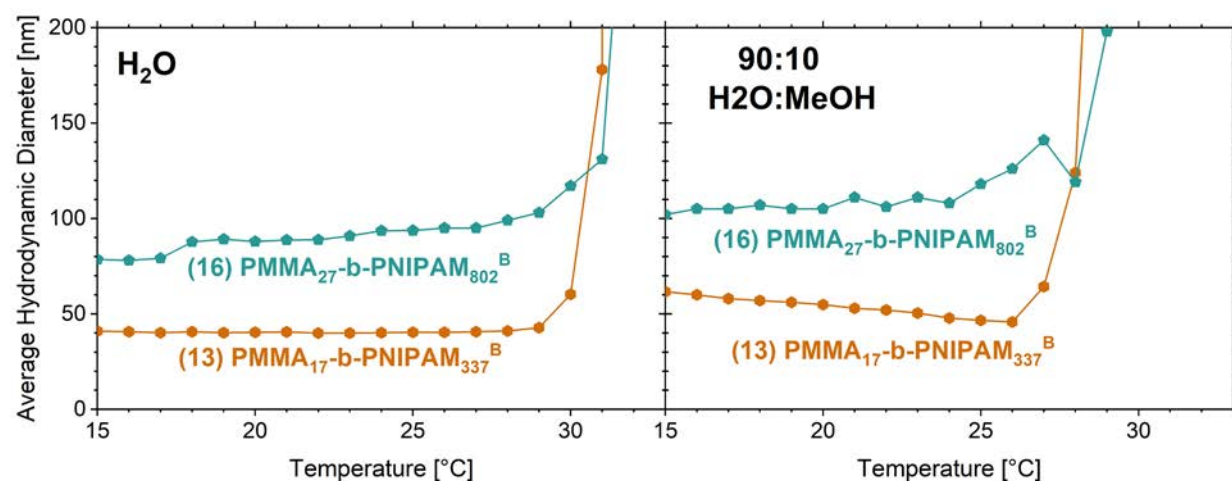
Figure 62. Average hydrodynamic diameter of $PMMA_{17}$-b-$PNIPAM_{337}^{B}$ (● reaction index 13, w_{PNIPAM}^{SEC} 0.94) and $PMMA_{27}$-b-$PNIPAM_{802}^{B}$ (⬟ reaction index 16, w_{PNIPAM}^{SEC} 0.96) in pure water and 90:10 water/methanol (vol.). Results obtained by DLS, with concentration of 10 g·L^{-1}.

Similar to PMMA$_{17}$-*b*-PNIPAM$_{337}$[B], PMMA$_{27}$-*b*-PNIPAM$_{802}$[B] shows an increase in hydrodynamic diameter upon the addition of methanol at low temperatures. However, the D_h seen for PMMA$_{17}$-*b*-PNIPAM$_{337}$[B] in water / methanol decrease upon increasing the temperature, while the D_h of PMMA$_{27}$-*b*-PNIPAM$_{802}$[B] increase. This could indicate that, rather than simply contracting, the increase of temperature drives a further aggregation of the micelles of this sample.

Although PMMA-*b*-PNIPAM copolymers are known to form micelles in a much wider range of PNIPAM weight ratio than, for example, PS-*b*-PNIPAM copolymers,[260] the results presented here show that the aggregation behavior is strongly influenced by the absolute size of the hydrophobic PMMA block, even more so than by the overall molar mass or the PNIPAM content.

Influence of Block Sizes on the Aggregation of PMMA-b-PNIPMAM in Solution

The aggregation behavior of PMMA$_{17}$-*b*-PNIPMAM$_{145}$[B] (reaction index 52, $w_{PNIPMAM}^{SEC}$ 0.89), PMMA$_{20}$-*b*-PNIPMAM$_{242}$[B] (reaction index 54, $w_{PNIPMAM}^{SEC}$ 0.92) and PMMA$_{27}$-*b*-PNIPMAM$_{248}$[B] (reaction index 56, $w_{PNIPMAM}^{SEC}$ 0.90) in water is depicted in Figure 63. The full range of relaxation curves below the transition temperature of each polymer is available in Annex 7.7 – Figure A 79, and Figure A 87.

The results show that the copolymer PMMA$_{17}$-*b*-PNIPMAM$_{145}$[B] aggregates with considerably smaller hydrodynamic diameters than the previously discussed PMMA$_{20}$-*b*-PNIPMAM$_{242}$[B], both of which show a visually monomodal D_h distribution. Given the small difference in the size of the hydrophobic block, it seems plausible that this difference is related to the considerably difference in the length of the hydrophobic block between the two samples, leading to smaller micelle shells for the shorter PNIPMAM block.

PMMA$_{27}$-*b*-PNIPMAM$_{248}$[B], in contrast, clearly shows a multimodal distribution. Due to this multimodality, a suitable fit of the intensity autocorrelation function was not achieved, and therefore, average hydrodynamic sizes cannot provided. While the smaller particle sub-population of this sample seems very similar in relaxation times (and therefore D_h) to that of PMMA$_{20}$-*b*-PNIPMAM$_{242}$[B], larger aggregates are clearly present, as evidenced by the shoulder at high relaxation times. Since the molar mass of PMMA$_{27}$-*b*-PNIPMAM$_{248}$[B] is not considerably bigger than that of PMMA$_{20}$-*b*-PNIPMAM$_{242}$[B], it is not likely that the formation of aggregates is caused by the overall polymer chain length. Moreover, as the $w_{PNIPMAM}^{SEC}$ is in the same range as for the other two samples, it seems that the PMMA block size may cause this larger aggregate formation, similar to what was previously presented for PMMA-*b*-PNIPAM copolymers.

With increase of temperature, all three copolymers show a reduction of hydrodynamic diameter, although to a different degree: while the change is barely seen for PMMA$_{17}$-*b*-PNIPMAM$_{145}$B, it is very evident for PMMA$_{27}$-*b*-PNIPMAM$_{248}$B (see relaxation curves in Annex 7.7 – Figure A 87).
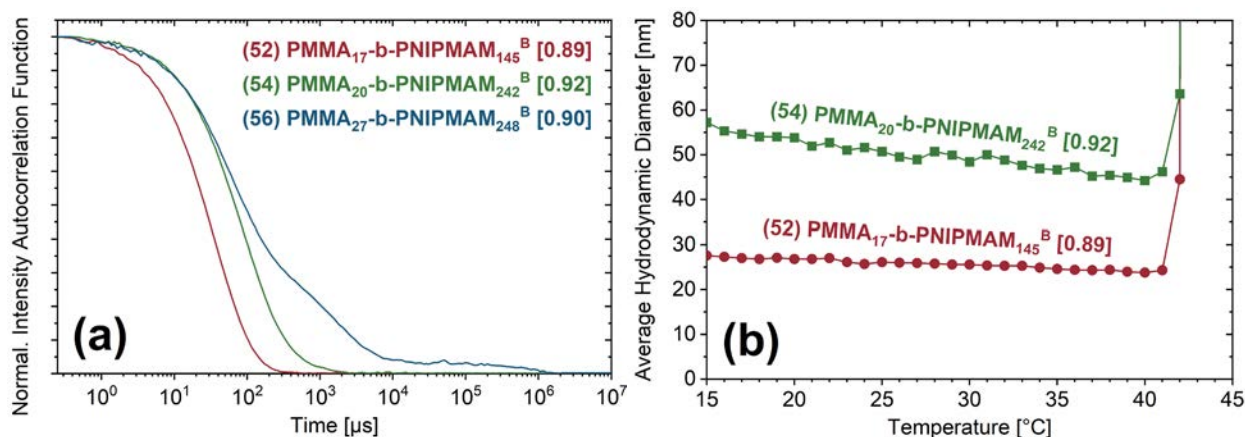
Figure 63. Self-assembly behavior of PMMA-*b*-PNIPMAM amphiphilic diblock copolymers in water (concentration 10 g·L^{-1}): (a) relaxation curves at 20°C and (b) evolution of the average hydrodynamic diameter with temperature. The reaction index of each sample is given in parenthesis, and the PNIPMAM weight fraction in the copolymer ($w_{PNIPMAM}{}^{SEC}$) is given in brackets.

Comparison of Cosolvents

In section 4.1.2, the effect of various cosolvents on the transition temperature of PNIPMAM homopolymers was compared. Here, PMMA-*b*-PNIPMAM amphiphilic block copolymers will be evaluated, and the effect of various cosolvents on the aggregation of these materials in solution will be discussed. For this comparison, three cosolvents were selected: methanol, ethanol, and isopropanol, as these alcohols allow a more direct correlation between the chemical structure of the cosolvent with the effects seen on the behavior of the polymer.

Figure 64 shows the average hydrodynamic diameter of PMMA$_{20}$-*b*-PNIPMAM$_{242}$B (reaction index 54, $w_{PNIPMAM}{}^{SEC}$ 0.92) in aqueous solutions containing up to 50 vol.% of the selected alcohols. Moreover, Figure 65 shows a direct comparison between the three cosolvents, when present in quantities of 10 vol.% in the solution. The intensity autocorrelation functions from which these values originate is provided in Annex 7.7 – Figure A 79 (methanol), Figure A 88 (ethanol) and Figure A 89 (isopropanol).
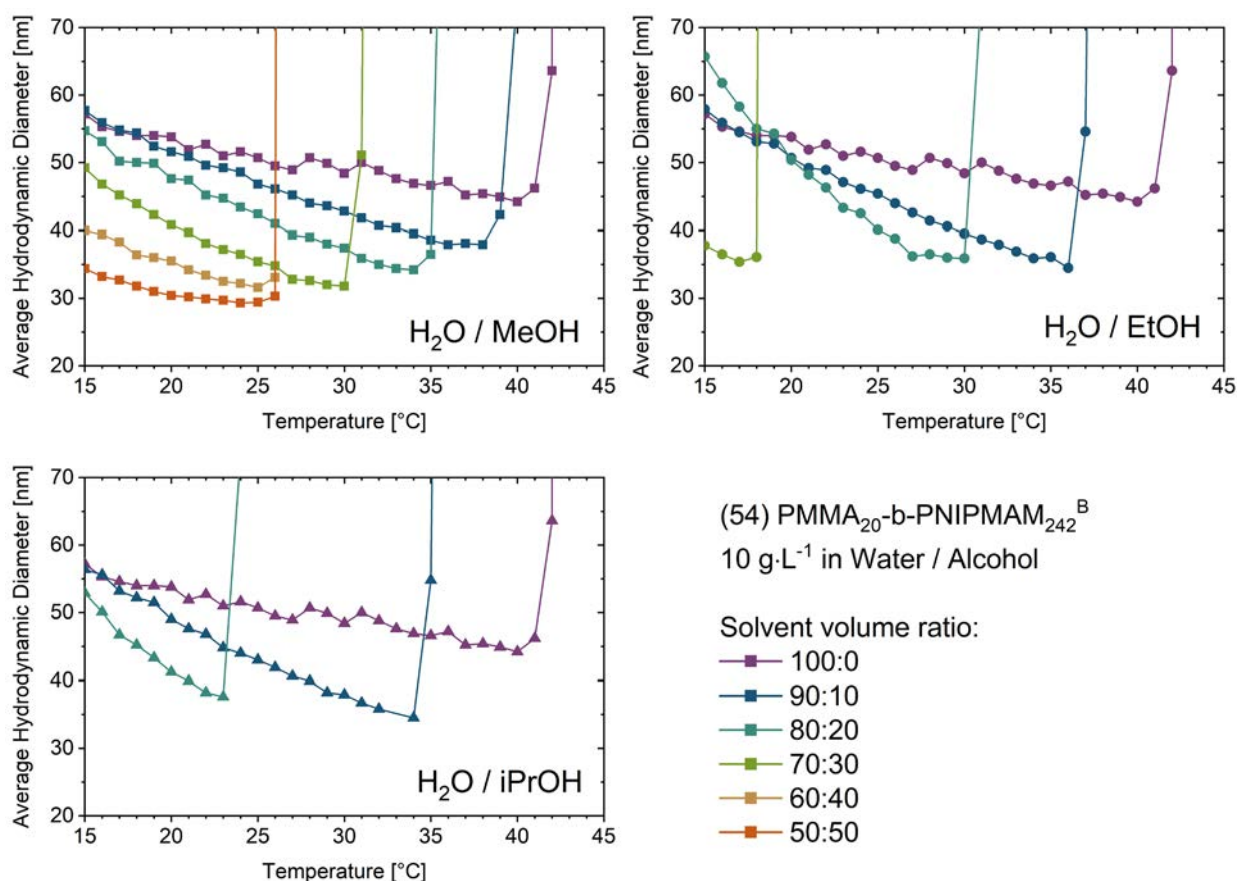
Figure 64. Effect of alcohol content on the hydrodynamic diameter of PMMA$_{20}$-*b*-PNIPMAM$_{242}$^{B} (reaction index 54) in aqueous solutions with methanol, ethanol, and isopropanol as cosolvent. Results obtained by DLS in a concentration of 10 g·L^{-1}.

In section 4.2.1, the effect of methanol content on the self-assembly of PMMA-*b*-PNIPAM in aqueous solutions was presented, pointing out the decreasing hydrodynamic diameters with increasing methanol volume fraction. This decrease of D_h was particularly notable at higher temperatures. Here, this behavior can be seen very clearly, and the same effect is identified for ethanol and isopropanol. However, as particularly evident in Figure 65, the three alcohols affect the D_h to different degrees, which seems inversely proportional to the polarity of the alcohol. That is, the effect of methanol, which is the most polar, is the mildest, whereas isopropanol, the least polar, shows the strongest effect, very much in the same way as the transition temperatures of PNIPAM homopolymers were affected by these three alcohols. This is particularly striking given that, due to the differences in molar mass and density, 10 vol.% of isopropanol represents only around 53% of the number of alcohol molecules that are present in 10 vol.% of methanol. This indicates that considerably less molecules of isopropanol are necessary (in comparison to ethanol and methanol) to impart a much stronger effect on the transition temperature and D_h of PNIPAM copolymers.
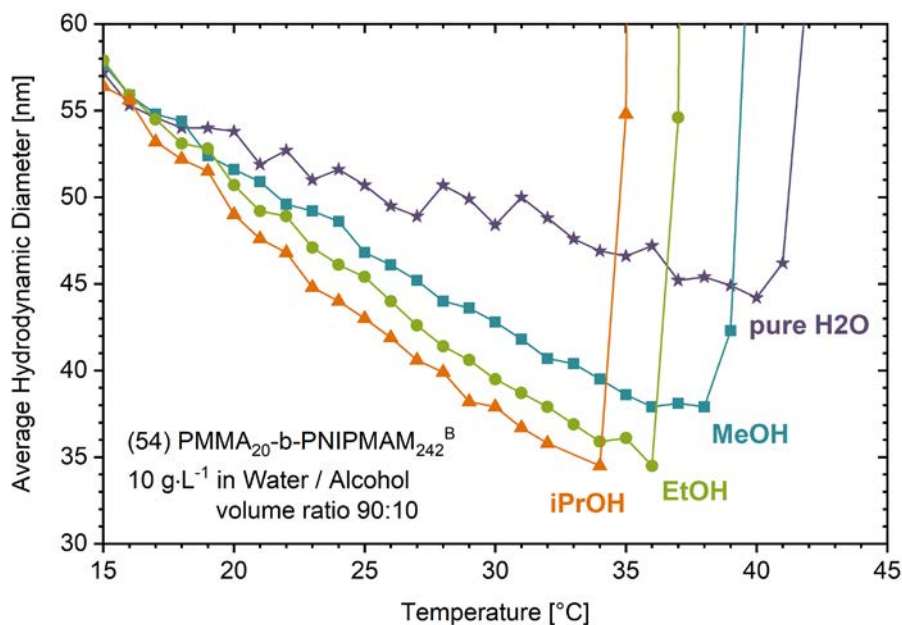
Figure 65. Comparison of alcohol cosolvents on the average hydrodynamic diameters of PMMA$_{20}$-*b*-PNIPMAM$_{242}$^{B} (reaction index 54) in aqueous solution with 10 vol.% of methanol, ethanol, and isopropanol. Results obtained by DLS for a concentration of 10 g·L^{-1}.

One point which is interesting to notice is that throughout all the DLS results presented in this chapter, the data obtained in pure water generally seems to fluctuate more than the data obtained from water/cosolvent mixtures. This phenomenon can be clearly visualized in the average hydrodynamic diameters shown in Figure 64 and Figure 65, and can also be seen when comparing the individual relaxation curves. This can be clearly visualized in Annex 7.7 – Figure A 90, which shows a magnified view of the relaxation curves in water and water/alcohol. On the one hand, the water/alcohol solutions show a uniform shift to shorter relaxation times upon increase of temperature, with rather constant distancing between each curve. In the case of the water solution, on the other hand, there is a greater variability in the distancing between the curves, with a few curves showing small shifts to longer relaxation times, even though a general trend of shift to lower relaxation upon increase of temperature is still seen.

One plausible explanation for this phenomenon is the increased mobility of the PNIPAM and PNIPMAM segments in pure water, whereas the presence of a cosolvent decreases the quality of the solvent mixture, driving the chains to obtain a more compact structure, which is less prone to significant fluctuations in size.

Polymer Concentration

The influence of polymer concentration in solution on the transition temperatures of PNIPMAM homopolymers in pure water was discussed in Section 4.1.1. Here, the impact of concentration on the behavior of amphiphilic block copolymers will be discussed, and how it changes in combination with the co-nonsolvency effect. For this, solutions of PMMA$_{20}$-b-PNIPMAM$_{242}{}^{B}$ (reaction index 54, $w_{PNIPMAM}{}^{SEC}$ 0.92) were prepared in 70:30 (vol.) water / methanol, with polymer concentrations ranging from 1 to 10 g·L^{-1}. These solutions were investigated by dynamic light scattering to evaluate the differences in aggregation, namely hydrodynamic diameters, upon changing the concentration. The results obtained are summarized in Figure 66.

Although no significant variations in the transition temperature could be seen for the various concentrations, the measured D_h does seem to be influenced by the concentration, with increasing diameters detected upon increase of concentration. This is likely due to an increase in the aggregation number (number of polymer chains per micelle). Interestingly, no significant difference was seen between the concentrations of 1 and 3 g·L^{-1}, which could potentially indicate a plateau in the decrease of the aggregation number, potentially due to a threshold concentration for aggregate growth. Alternatively, of course, the similarities between the results with concentrations of 1 and 3 g·L^{-1} could be due to the limit in resolution of the experimental setup.
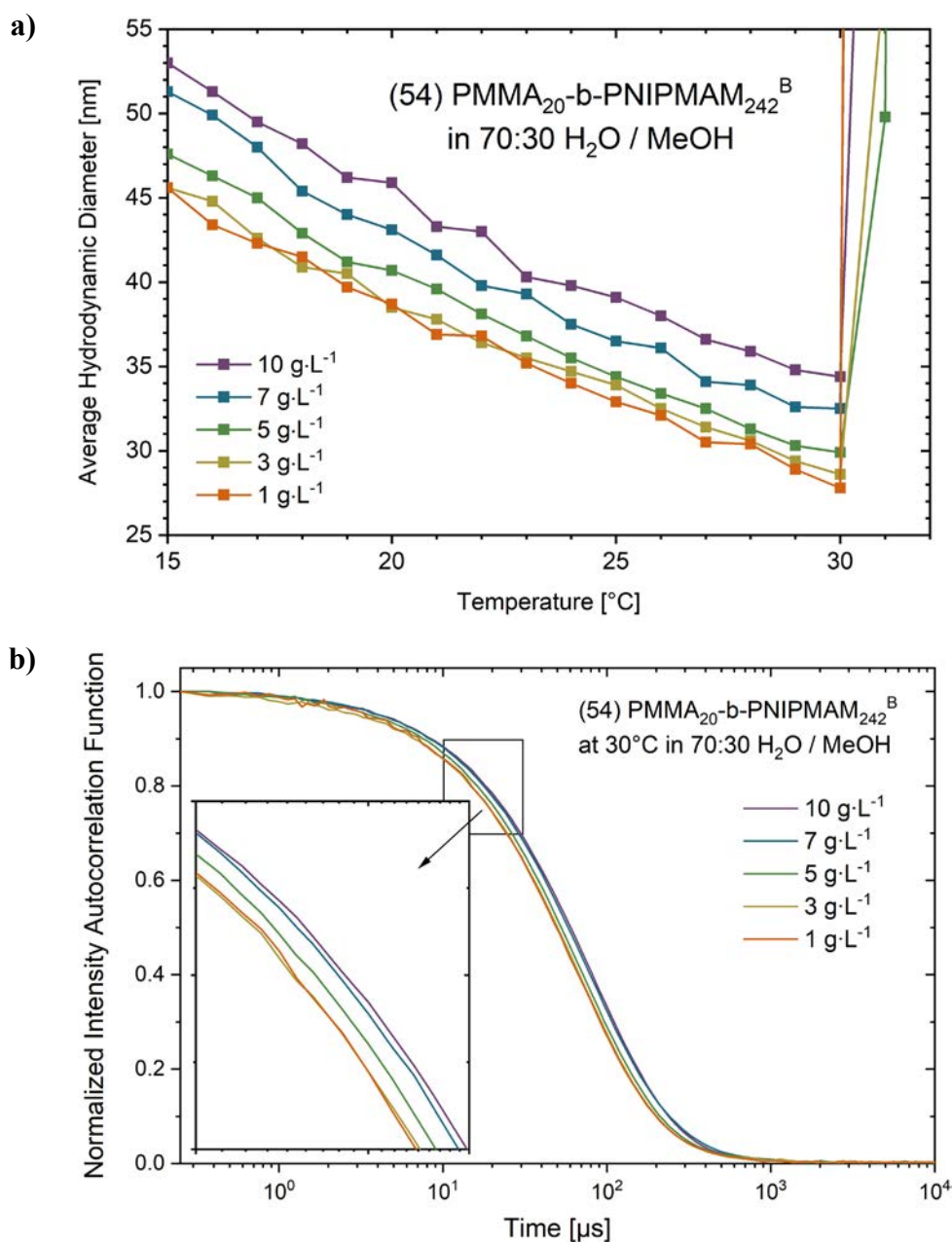
Figure 66. Effect of polymer concentration on the aggregation of PMMA$_{20}$-*b*-PNIPMAM$_{242}$[B] (reaction index 54) in water/methanol 70:30 (vol.), measured by DLS: (a) average hydrodynamic diameter with respect to temperature, (b) normalized intensity autocorrelation function at 30°C (shortly before the phase transition).

5.   Conclusion & Outlook

The goal of this thesis was to synthesize and investigate polymeric systems exhibiting co-nonsolvency, particularly focusing on the behavior of systems other than the classical PNIPAM homopolymers and PS-*b*-PNIPAM block copolymers. To achieve this goal, two main aspects were covered:

(I) the synthesis of homopolymers and copolymers based on PNIPAM, PNIPMAM and PNVIBAM, and (II) the study of their behavior in solution.

On the first aspect, the polymerization of NIPMAM proved considerably more challenging than the well-stablished and straightforward polymerization of NIPAM, both through conventional free radical polymerization (FRP) and even more so through RAFT. Although large molar masses, low dispersities, and high conversions have rarely been reported in literature before, potential issues on the polymerization of NIPMAM had never been concretely discussed either. Here, factors such as initiator, solvent, reaction temperature, and monomer purification method were evaluated. However, the challenges in the polymerization of NIPMAM could not be fully overcome solely by controlling these factors, and are likely caused by a high sensitivity to trace impurities, leading to side-reactions, and generating low monomer conversions, limited molar masses and broad dispersities. Therefore, even though degrees of polymerization DP $\sim$ 1000 with Đ $\sim$ 2.0 may be achieved through FRP, when severely limiting the amount of initiator, the low reproducibility remains an obstacle. When RAFT polymerization is applied, these challenges are heightened. In this case, molar masses are rather limited (DP < 500) and effective control over molar mass distribution is rapidly lost. The low dispersities typically expected of RAFT polymerizations seem achievable only for rather low chain lengths (DP < 100). Based on these findings, it becomes apparent that NIPMAM polymerization results previously reported lay close to the limit of what seems achievable for this monomer through controlled radical polymerization. As a conclusion, although PNIPMAM might be an interesting alternative to the popular PNIPAM and its higher transition temperature may be advantageous to many applications, one must factor the efforts required for its synthesis, and whether alternative, more easily synthesized polymers could be suitable.

In the case of NVIBAM, the vinyl amide equivalent of NIPAM, conventional free radical polymerization was facile and high molar masses could be achieved. Preliminary RAFT experiments, however, showed much room for improvement, even more so when targeting the synthesis of block copolymers with more activated monomers (MAMs) PS and PMMA. Therefore, if block copolymers based on PNVIBAM are desired, it is strongly recommended that a co-

monomer with comparable activity level to NVIBAM be chosen, optimally another LAM, thus significantly reducing the challenge of selecting an appropriate CTA.

The second aspect discussed in this thesis was the thermoresponsive and aggregation behaviors of the synthesized homo- and copolymers in aqueous and mixed aqueous solutions. The extensive evaluation of co-nonsolvency with 9 different cosolvents constitutes the first detailed report on the co-nonsolvency of PNVIBAM, and the most extensive report on the co-nonsolvency of PNIPMAM available in literature. The co-nonsolvency behavior of PNIPMAM and PNVIBAM homopolymers was similar to that of PNIPAM for most of the solvents tested, but some divergences were identified for PNIPMAM. For example, PNIPAM and PNVIBAM both show co-nonsolvency in water / DMF mixtures, although only when a sufficiently large amount of DMF is present: $\geq$ 14 mol.% (41 vol.%) for PNIPAM and $\geq$ 11 mol.% (35 vol.%) for PNVIBAM. PNIPMAM, in contrast, did not show co-nonsolvency behavior in any water / DMF mixture. In the case of DMSO cosolvent, PNIPAM and PNVIBAM show co-nonsolvency already at DMSO contents of 1 ~ 2 mol.% (5 ~ 9 vol.%), whereas PNIPMAM initially shows an increase of cloud point at low DMSO contents, with co-nonsolvency manifesting itself above 6 mol.% (20 vol.%) of DMSO. These divergences are not clearly covered by the current proposed theories to explain co-nonsolvency, evidencing the need for further investigating and understanding of the phenomenon, and evolution of the current theories.

Similarly, the behavior of amphiphilic block copolymers PMMA-b-PNIPMAM in aqueous and mixed aqueous solutions also showed a few divergences compared to that of PMMA-b-PNIPAM. For example, although the cloud point temperature (T_{CP}) of PNIPMAM homopolymers seems to be affected by the polarity and bulkiness of end-groups, the presence and size of a PMMA block did not lead to any difference in T_{CP} compared to the homopolymer. This is not the case of PMMA-*b*-PNIPAM, whose T_{CP} is considerably lower than that of PNIPAM homopolymers.

Overall, the behavior of PNIPAM, PNIPMAM and PNVIBAM, all of which show large solubility gaps across the wide range of cosolvents, is particularly interesting compared to other polymers exhibiting co-nonsolvency, where the phenomenon is seen only for a narrow solvent composition range, and with a small amount of cosolvents. Thus, the wide choice of cosolvents, their higher transition temperatures and the few peculiarities in their behaviors make PNIPMAM and PNVIBAM attractive alternatives to the classical PNIPAM systems.

Notwithstanding the great value of the results obtained, this work is far from comprehensive, and several topics for further investigation have been identified.

Given the preliminary nature of the experiments performed to obtain amphiphilic block copolymers of PNVIBAM, further pursue of these syntheses is recommended (e.g., vinyl pirylat). On the one hand, selecting a less activated (LAM) hydrophobic co-monomer could facilitate the selection of a suitable CTA. On the other hand, if a more activated (MAM) hydrophobic co-monomer is desired, use of a switchable CTA is recommended, as it allows adaptation to the activity level to the respective monomer families. Even in this case, it is recommended that overly activated MAMs, such as MMA, be avoided.

The effects of copolymer architecture on the thermoresponsive, aggregation and co-nonsolvency behavior could also be explored further through the synthesis and characterization of additional triblock copolymers, and star-shaped block copolymers. Suggested examples include PMMA-*b*-PNIPAM-*b*-PMMA, PMMA-*b*-PNIPMAM-*b*-PMMA, (PNIPAM-*b*-PMMA)$_3$ and (PNIPMAM-*b*-PMMA)$_3$. These would naturally require selection and potentially synthesis of suitable CTAs.

Given the limitation of the DLS method, and particularly of the simple setup used in this study, employing other scattering methods, such as small angle neutron scattering (SANS) is also recommended to gain more comprehensive information about the discussed samples.

Another particularly interesting aspect to be evaluated is the effect of mixed solvents on the micellar core. For example, the organic cosolvent may work as a plasticizer, softening the micellar core and increasing chain mobility. This aspect would be particularly important for applications such as drug release, especially when considering that the co-nonsolvency of PNIPAM, PNIPMAM and PNVIBAM does not occur only in water/methanol, but also in the presence of other, more biologically relevant, cosolvents, such as ethanol. Moreover, more powerful scattering methods could provide insights into the effects that the cosolvency behavior of PMMA has on the self-assembly and micelle hydration characteristics of PMMA-*b*-PNIP(M)AM copolymers in mixed aqueous solutions.

6. Materials and Methods

6.1. Chemicals

Materials for the Synthesis and Workup of the Chain Transfer Agents

1-Propylthiol (99%, Merck), triethylamine (99%, Acros), 1-bromoethyl benzene (97%, Sigma Aldrich or TCI), carbon disulfide (>99.9%, Honeywell), H_2SO_4 (95-97%, ChemSolute), HCl (concentrated, ChemSolute), NaOH (≥98.0%, ChemSolute), $MgSO_4$ (100%, VWR Chemicals), ethyl acetate (99.9%, VWR Chemicals) and methyl 2-bromopropionate (98%, Sigma Aldrich) were used as received. 2,2′-(Ethylenedioxy)diethanethiol (95%, Sigma Aldrich) was dried under vacuum overnight before use. Chloroform (≥99.5% stabilized with amylene, Th. Geyer) was distilled and dried over $MgSO_4$ prior to use. Ethanol (≥99.9%, ChemSolute) was dried over $MgSO_4$ prior to use. Water was deionized to a resistivity of 18.2 MΩ × cm using a Milli-Q Plus purification system (Merck Millipore, Darmstadt, Germany). Petroleum ether (boiling range 40-60 °C, VWR Chemicals) was distilled before use.

Materials for the Synthesis and Workup of Monomers

Isopropylamine (99.9%, Fisher Scientific), nitrobenzene (99%, Acros), triethylamine (99%, Acros), tetrahydrofuran (THF, 99.5% extra dry, stabilized with 100 - 250 ppm of BHT, Acros), ethyl acetate (99.9%, VWR Chemicals), NaOH (98.8%, ChemSolute), NaCl (99%, VWR Chemicals), $MgSO_4$ (100%, VWR Chemicals) and CaH_2 (93%, Acros) were used as received. *N*-Vinylformamide (technical grade, kind gift from BASF) was dried over CaH_2 overnight then freshly distilled by Kugelrohr distillation prior to use. Isobutyryl chloride (98%, abcr) was freshly distilled by Kugelrohr distillation prior to use. Methacryloyl chloride (97%, stabilized with ca. 400 ppm of 4-methoxyphenol, Alfa Aesar), diethyl ether (≥99.8%, Th. Geyer) n-hexane (>95.0%, ChemSolute), dichloromethane (DCM, ≥99.5%, Roth) and petroleum ether (boiling range 40-60 °C, VWR Chemicals) were distilled before use. Water was deionized to a resistivity of 18.2 MΩ × cm using a Milli-Q Plus purification system (Merck Millipore, Darmstadt, Germany).

Materials for the Polymerizations and Polymer Workup

Benzene (≥ 99.5%, Carl Roth), 2,2,2-trifluoroethanol (TFE, 99.8% extra pure, Acros), ethanol (≥99.9%, ChemSolute), acetone (≥99%, Merck), trifluorotoluene (TFT, 99+%, Acros), dimethyl-2,2'-azobis(2-methylpropionate) (MAIB, Wako), 2,2'-azobis(2-methylpropionamidine)dihydrochloride (V50, Wako), and 2,2'-azobis(4-methoxy-2,4-dimethylvaleronitrile) (V70, 96%, Wako) were used as received. Diethyl ether (≥99.8%, Th.

Geyer), pentane (≥99%, Roth), and methanol (technical grade, VWR Chemicals) were distilled before use. Methyl methacrylate (MMA, ≥99.0%, stabilized with > 10 ppm hydroquinone monomethyl ether, Merck) and styrene (99.9%, stabilized with 4-tert-butylbrenzcatechin, Merck) were freshly distilled before use. 2,2'-Azobis(isobutyronitrile) (AIBN, >98%, Fluka) and 1,1'-azobis(cyclohexane-1-carbonitrile) (V40, 98%, Aldrich) were crystallized from methanol. *N*-Isopropyl acrylamide (NIPAM, >98%, TCI Chemicals) was crystallized four times from n-hexane. *N*-Isopropyl methacrylamide (NIPMAM, 97%, Aldrich or >98.0% TCI) was recrystallized multiple times from n-hexane and benzene. Alternatively, *N*-isopropyl methacrylamide was synthesized and purified as described in section 6.3.1. *N*-Vinyl isobutyramide (NVIBAM) was synthesized as described in section 6.3.2.

The monofunctional fluorophore-labelled CTA **B** (2-(6-(dimethylamino)-1,3-dioxo-1H-benzo[de]isoquinolin-2(3H)-yl) ethyl 4-cyano-4-(((phenethyl-thio)carbonothioyl)thio)pentanoate, 605.79 g·mol^{-1}) was kindly provided by Viet Hildebrand, who synthesized the CTA as previously described.[157] This CTA was used in this thesis without further purification. The monofunctional dithiocarbamate CTA **D** (cyanomethyl methyl(phenyl)carbamodithioate, 98%) and "universal" CTA **E** (2-cyanobutan-2-yl 4-chloro-3,5-dimethyl-1H-pyrazole-1-carbodithioate, 95%) were purchased from Merck and purified by column chromatography before use (in 1:1 petroleum ether / ethyl acetate (v/v)).

Materials for the Characterizations

N-Methyl-2-pyrrolidone (NMP, 99.5%, Alfa Aesar), lithium bromide (≥99%, Acros), ethyl acetate (99.9%, VWR Chemicals), ethanol (≥99.9%, ChemSolute), isopropanol (100%, VWR Chemicals), acetone (Uvasol, for spectroscopy, Merck), dimethyl sulfoxide (DMSO, >99.0%, TCI), tetrahydrofuran (THF, pure, Merck), deuterated water (D$_2$O, 99.8 atom% D, Armar Chemicals), deuterated acetone (acetone-d6, ≥99.5 atom% D, Armar Chemicals) deuterated chloroform (CDCl$_3$, 99.8 atom% D, Armar Chemicals), and deuterated dichloromethane (DCM, 99.5 atom% D, abcr) were used as received. Methanol (technical grade, VWR Chemicals) was distilled before use. Water was deionized to a resistivity of 18.2 MΩ × cm using a Milli-Q Plus purification system (Merck Millipore, Darmstadt, Germany).

6.2. Chain Transfer Agent (CTA) Synthesis

6.2.1. CTA A: Monofunctional Trithiocarbonate Chain Transfer Agent
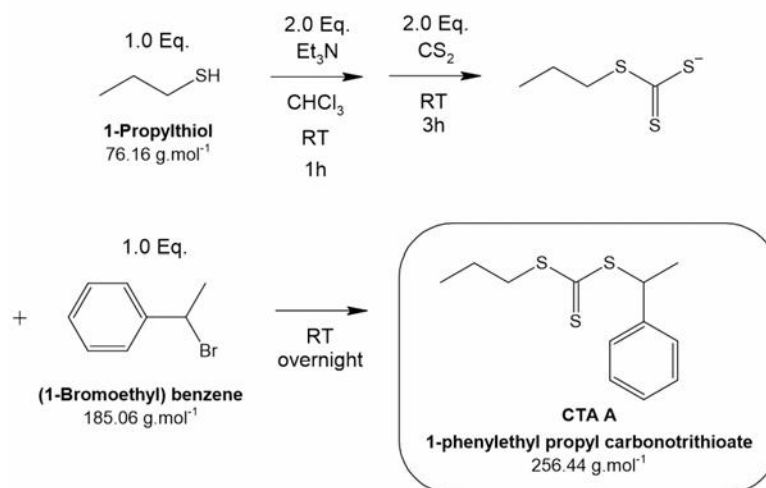
Figure 67. Synthesis of CTA A: 1-phenylethyl propyl carbonotrithioate.

The monofunctional CTA **A** (1-phenylethyl propyl carbonotrithioate, 256.44 g·mol^{-1}) was synthesized following a procedure similar to the literature.[273,274] 1-Propylthiol (2.2 mL, 24.29 mmol) and chloroform (14.4 mL) were placed in a 100 mL 3- neck round bottom flask, equipped with a magnetic stirring bar, dripping funnel and nitrogen inlet. Triethylamine (6.6 mL, 47.48 mmol) was added to the reaction flask, dropwise. After about 1 h, carbon disulfide (2.9 mL, 48.22 mmol) was slowly added to the mixture. After another 3 h, 1-bromoethyl benzene (3.2 mL, 23.45 mmol) was slowly dripped into the mixture. The reaction was stirred overnight at room temperature. The mixture was then washed with water (2x50 mL), 2M aqueous H$_2$SO$_4$ (2x50 mL), and again with water (2x50 mL). The organic phase was then dried with MgSO$_4$, and the solvent was evaporated in a rotary evaporator. The viscous liquid was further purified by column chromatography, in 10:1 petroleum ether / ethyl acetate (v/v), to give 5.74 g of a deep yellow liquid (95% yield, Rf: 0.73 on thin layer chromatography with eluent petroleum ether / ethyl acetate 5:1 v/v).

^{1}H NMR (400 MHz, in Acetone-d6) δ [ppm] = 1.01 (t, *J* = 7.37 Hz, *CH$_3$*-CH$_2$-, 3 H), 1.72 (qt, *J* = 7.31 Hz, CH$_3$-*CH$_2$*-, 2 H), 1.76 (d, *J* = 7.13 Hz, *CH$_3$*-CH<, 3 H), 3.38 (t, *J* = 14.57 Hz, -CH$_2$-S-, 2 H), 5.37 (q, *J* = 7.12 Hz, -CH<, 1 H), 7.30 (m, H aryl meta, 1 H), 7.37 (m, H aryl orto, 2 H), 7.44 (m, H aryl para, 2 H).

^{13}C NMR (100 Hz, in CDCl$_3$) δ [ppm] = 13.52 (*CH$_3$*-CH-), 21.57 (*CH$_3$*-CH< and CH$_3$-*CH$_2$*-) 38.64 (-CH$_2$-S), 50.10 (-CH<), 127.70 (C aryl para), 127.73 (C aryl orto), 128.66 (C aryl meta), 141.19 (>CH=), 223.11 (>C=S).

Elemental analysis (C$_{12}$H$_{16}$S$_3$, *M$_r$* 256.44) = calculated: C 56.20%, H 6.29%, S 37.51%. Found: C 58.23%, H 6.52%, S 39.04%.

UV-vis absorbance maxima in ethyl acetate: λ$_{max}$ = 310 nm, ε$_{310}$ = 16300 L·mol^{-1}·cm^{-1}.

6.2.2. CTA C: Monofunctional Xanthate Chain Transfer Agent
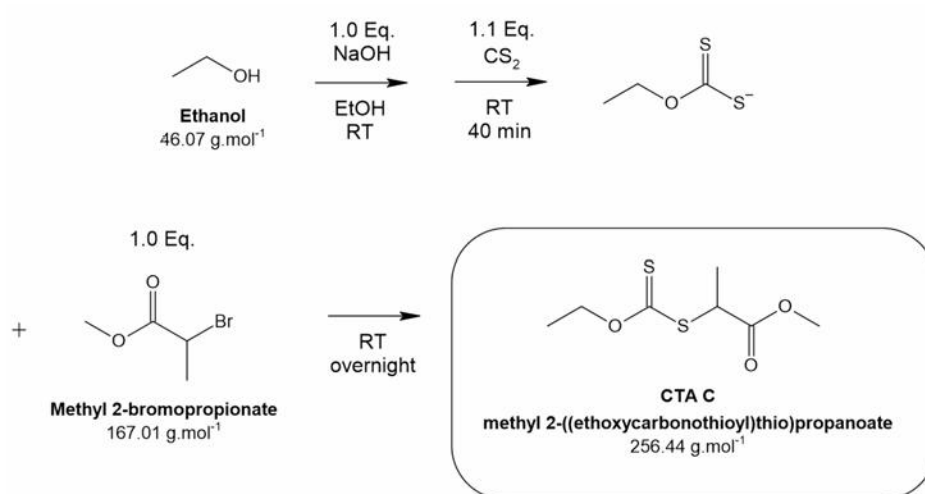
Figure 68. Synthesis of CTA C: methyl 2-((ethoxycarbonothioyl)thio)propanoate.

The monofunctional xanthate CTA **C** (methyl 2-((ethoxycarbonothioyl)thio)propanoate 208.29 g·mol$^-$) was synthesized following a procedure described in literature.[275] Sodium hydroxide (2.02 g, 50.50 mmol) was dissolved in ethanol (100 mL) at room temperature. Carbon disulfide (3.35 mL, 55.70 mmol) was slowly added to the mixture. After about 40 min, methyl 2-bromopropionate (5.6 mL, 50.20 mmol) was added dropwise to the reaction flask. The mixture was stirred overnight at room temperature, after which the solvent was removed in the rotary evaporator. Water (100 mL) was added to the remaining mixture, which was then extracted twice with ethyl acetate (2x80 mL). The combined organic phases were dried over MgSO$_4$, and the solvent was evaporated in a rotary evaporator to yield 9.45 g of the pure product as a pale-yellow liquid (91%, Rf: 0.48 on thin layer chromatography with eluent petroleum ether / ethyl acetate 5:1 v/v).

^{1}H NMR (400 MHz, in CDCl$_3$) δ [ppm] = 1.43 (t, J = 7.12 Hz, CH_3-CH$_2$-, 3 H), 1.58 (d, J = 7.40 Hz, CH_3-CH<, 3 H), 3.76 (s, CH$_3$-O-, 3 H), 4.41 (q, J = 7.39 Hz, -CH<, 1 H), 4.65 (q, J = 7.14 Hz, -CH$_2$-, 2 H).

^{13}C NMR (100 Hz, in CDCl$_3$) δ [ppm] = 13.67 (CH_3-CH-), 16.89 (CH_3-CH<), 47.03 (-CH<), 52.77 (CH$_3$-O-), 70.29 (-CH2-), 171.92 (-CO-), 212.04 (>C=S).

Elemental analysis (C$_7$H$_{12}$O$_3$S$_2$, M_r 208.29) = calculated: C 40.37%, H 5.81%, O 23.04%, S 30.78%. Found: C 40.22%, H 5.74%, N 0.63%, S 30.57%.

UV-vis absorbance maxima in ethyl acetate: λ$_{max}$ = 278 nm, ε$_{278}$ = 10400 L·mol^{-1}·cm^{-1}.

6.2.3. CTA F: Bifunctional Trithiocarbonate Chain Transfer Agent
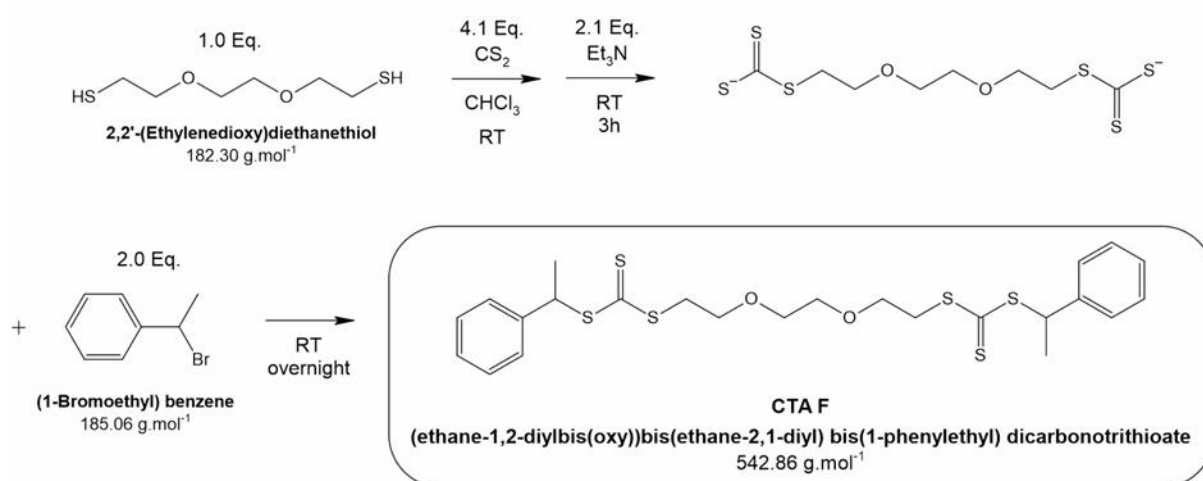
Figure 69. Synthesis of CTA F: (ethane-1,2-diylbis(oxy))bis(ethane-2,1-diyl) bis(1-phenylethyl) dicarbonotrithioate.

The bifunctional CTA F ethane-1,2-diylbis(oxy))bis(ethane-2,1-diyl) bis(1-phenylethyl) dicarbonotrithioate, 542.86 g·mol^{-1}) was synthesized following a procedure similar to that found in literature.[273,274] 2,2′-(Ethylenedioxy)diethanethiol (1.2 mL, 7.37 mmol), carbon disulfide (1.8 mL, 29.93 mmol) and chloroform (6.25 mL) were placed in a 100 mL 3-neck round bottom flask, equipped with a magnetic stirring bar, dripping funnel and nitrogen inlet. Triethylamine (2.2 mL, 15.78 mmol) was then added, over the course of 30 min. After another 3 h, 1-bromoethyl benzene (2.0 mL, 14.65 mmol) was added dropwise, over 10 min. The reaction mixture was stirred overnight at room temperature and then washed with water (20 mL), 0.1 M aqueous HCl (20 mL) and again with water (2x20 mL). The viscous liquid was further purified by column chromatography using 10:1 petroleum ether / ethyl acetate (v/v) was used as eluent. This yielded

a partially purified product which was purified by column chromatography again, using 40:1 petroleum ether / ethyl acetate (v/v) as eluent. Finally, the obtained product was extracted against hexane to give 3.77 g of a viscous deep yellow liquid (94% yield, thin layer chromatography R_f 0.45, with eluent petroleum ether / ethyl acetate 5:1 v/v).

^{1}H NMR (400 MHz, in Acetone-d6) δ [ppm] = 1.76 (d, J = 7.12 Hz, CH_3-, 6 H), 3.59 (s, -O-CH_2-CH_2-O-, 4 H), 3.61 (t, J = 6.02 Hz, -S-CH$_2$-, 4 H), 3.73 (t, J = 6.18 Hz, -S-CH$_2$-CH_2-O-, 4 H), 5.36 (q, J = 7.11 Hz, -CH<, 2 H), 7.30 (m, meta, 2 H), 7.37 (m, orto, 4 H), 7.44 (m, para, 4 H).

^{13}C NMR (100 Hz, in CDCl$_3$) δ [ppm] = 21.40 (CH$_3$-), 36.10 (-S-CH$_2$-), 50.39 (-CH<), 68.66 (-S-CH$_2$-CH_2-O-), 70.09 (-O-CH_2-CH_2-O-), 127.73 (orto), 127.75 (para), 128.68 (meta), 141.07 (>CH=), 222.66 (>C=S).

Elemental analysis (C$_{24}$H$_{30}$O$_2$S$_6$, M_r 542.86) = calculated: C 53.10%, H 5.57%, S 35.43%, O 5.89%. Found: C 52.84%, H 5.51%, S 35.03%.

UV-vis absorbance maxima in ethyl acetate: λ_{max} = 310 nm, ε_{310} = 36700 L·mol^{-1}·cm^{-1}.

6.3. Monomer Synthesis

6.3.1. *N*-Isopropyl methacrylamide (NIPMAM)
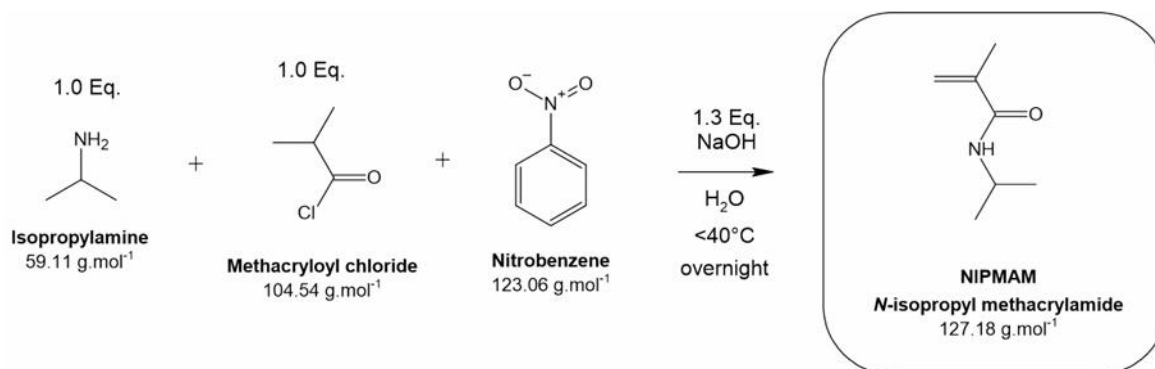
Figure 70. Synthesis of NIPMAM monomer: *N*-isopropyl methacrylamide.

The synthesis of the *N*-isopropyl methacrylamide (NIPMAM) monomer was based on a procedure from literature.[276] Water (500 mL), NaOH (40.0 g, 1.0 mol), isopropylamine (59.00 g, 0.998 mol) and nitrobenzene (ca. 0.3 mL, 3 mmol) were placed in a 1 liter 3-neck round bottom flask, equipped with a magnetic stirring bar, reflux condenser, dripping funnel and thermometer. Methacryloyl chloride (109.22 g, 1.045 mol) was added to the mixture over the course of 30 min, keeping the

temperature of the reaction below 40°C. After 1 h more, additional NaOH (10.00 g, 0.25 mol) was added. The following day, the formed solids were collected by filtration and washed with diethyl ether. The material was then recrystallized twice from n-hexane, then dissolved in dichloromethane and washed against 0.1 N aqueous NaOH. The aqueous phase was extracted repeatedly with dichloromethane. The combined organic phases were washed with H_2O, dried with $MgSO_4$ and the solvent was removed under vacuum to give 72.5 g of NIPMAM as a white solid (57% yield).

^{1}H NMR (400 MHz, in CDCl$_3$) δ [ppm] = 1.17 (d, J = 6.57 Hz, CH_3-CH<, 6 H), 1.93 (dd, J = 1.44, 0.93 Hz, CH3-C=, 3H), 4.10 (dq, J = 7.78, 6.59 Hz, -CH<, 1 H), 5.27 (m broad, =CH$_2$ cis, 1 H), 5.63 (s, =CH$_2$ trans, 1 H), 5.70 (broad, -NH-, 1 H),

6.3.2. *N*-Vinyl isobutyramide (NVIBAM)
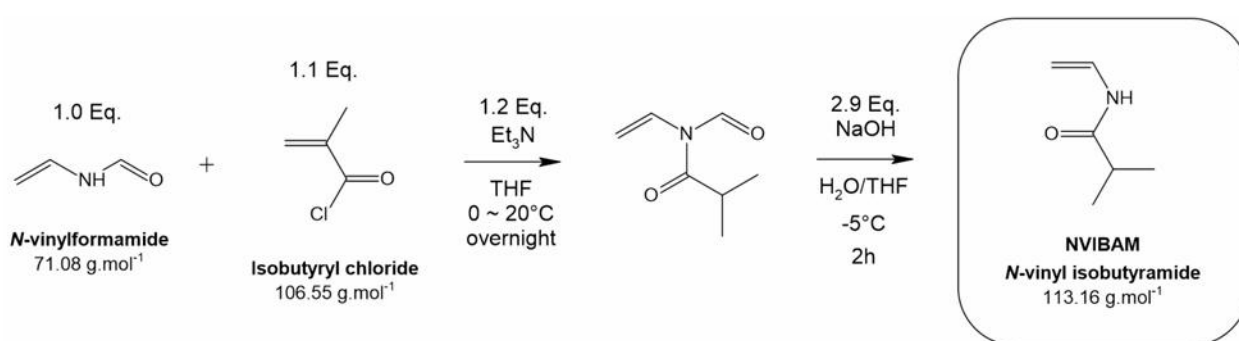
Figure 71. Synthesis of NVIBAM monomer: *N*-vinyl isobutyramide.

The synthesis of the *N*-vinyl isobutyramide (NVIBAM) monomer was done as described by Tu et al.[239] *N*-vinylformamide (28.0 mL, 400.00 mmol), triethylamine (66.9 mL, 480.00 mmol) and tetrahydrofuran (300 mL) were placed in a 500 mL 3-neck round bottom flask, equipped with a magnetic stirring bar, dripping funnel and nitrogen balloon. The mix was cooled to -5 °C in a salt / ice bath. Isobutyryl chloride (48.2 mL, 460.00 mmol) was slowly added, over the course of 1h 30 min, such that the temperature of the mixture stayed below 5°C. The mixture was then stirred overnight at room temperature. The following day, the reaction mixture was again cooled to -5 °C, and 5N aqueous NaOH (240 mL, 1200.00 mmol) was slowly added to the reaction, over the course of 1 h, then further stirred for about 2 h. The aqueous phase was separated and extracted with ethyl acetate (2x100 mL). The organic phases were combined and washed with brine (150 mL). The solvents were evaporated in the rotary evaporator, yielding a viscous dark brown mixture, which was initially purified by column chromatography, with petroleum ether / ethyl acetate 5:1 (v/v) as

eluent. The obtained light-yellow mixture was then recrystallized in n-hexane to give 25.6 g of the pure monomer as a white solid at room temperature (54% yield, thin layer chromatography R_f 0.61, with eluent petroleum ether / ethyl acetate 1:1 v/v).

^{1}H NMR (400 MHz, in acetone-d6) δ [ppm] = 1.10 (d, J = 6.87 Hz, -CH$_3$, 6 H), 2.47 (qq, J = 6.86, 6.86 Hz, -CH<, 1 H), 4.27 (d, J = 8.89 Hz, =CH$_2$ trans, 1 H), 4.62 (d, J = 16.01 Hz, =CH$_2$ cis, 1 H), 6.95 (ddd, J = 16.02, 10.49, 8.92 Hz, =CH-, 1 H), 8.97 (broad, -NH-, 1 H).

^{13}C NMR (100 Hz, in CDCl$_3$) δ [ppm] = 18.75 (-CH$_3$), 34.68 (-CH<), 93.11 (=CH$_2$), 129.58 (=CH-), 205.29 (-NH-).

Elemental analysis (C$_6$H$_{11}$NO, M_r 113.16) = calculated: C 63.69%, H 9.80%, N 12.38%, O 14.14%. Found: C 63.33%, H 10.08%, N 11.94%.

6.4. Polymerizations

6.4.1. Conventional Free Radical Polymerizations

Conventional free radical polymerizations were performed to obtain PNIPMAM and PNVIBAM homopolymers. Typical procedures are presented in the following paragraphs. A complete list of all conventional free radical polymerizations featured in this thesis, along with the specific reaction parameters are given in Table 20 and Table 21.

For the synthesis of PNIPMAM, N-isopropyl methacrylamide (NIPMAM, 1.000 g, 7.8629 mmol) is placed in a round bottom flask equipped with a magnetic stirring bar. Initiator 2,2'-azobis(isobutyronitrile) (AIBN, 0.50 mg, 0.0031 mmol) is added in the form of a 5.00 g·mol^{-1} stock solution in benzene, followed by additional benzene (total 2.66 mL), to achieve an overall monomer concentration of 30 wt.%. The flask is closed with a silicone septum and degassed with Argon for 15 min, after which the flask is immersed in a heated oil bath at 65°C. The reaction is allowed to proceed for 18 h before being quenched by exposure to air and cooling to room temperature. The polymer is dissolved in acetone and precipitated into a 10-fold volume of 2:1 diethyl ether / pentane (v/v). The precipitate is collected by filtration and precipitation is repeated, if necessary, until no residual monomer is present, as evidenced by ^{1}H NMR characterization. Finally, the polymer is dissolved in water and freeze-dried.

Table 20. Reaction conditions and conversion of the conventional free radical polymerizations of PNIPMAM. Unless stated otherwise, all polymerizations were done in a concentration of ca. 30 wt.%.

Index	Sample	Initiator	Solvent	Temp. [°C]	Reaction Time [hh:mm]	Molar Ratio Monomer : Initiator	$m_{monomer}$ [g]	$m_{initiator}$ [mg]	Conv. [%]
19	PNIPMAM$_{264}$	AIBN	benzene [a]	65	24:00	611 : 1	1.23	2.60	57
20	PNIPMAM$_{301}$	AIBN	benzene [a]	65	24:00	611 : 1	1.18	2.50	65
21	PNIPMAM$_{305}$	AIBN	benzene [a]	65	24:00	611 : 1	1.18	2.49	60
22	PNIPMAM$_{295}$	AIBN	benzene [a]	65	24:00	610 : 1	1.20	2.53	74
23	PNIPMAM$_{339}$	AIBN	benzene [a]	65	24:00	611 : 1	1.22	2.57	72
24	PNIPMAM$_{390}$	AIBN	benzene	65	18:30	1202 : 1	0.64	0.69	26
25	PNIPMAM$_{445}$	AIBN	benzene [a]	65	18:00	1203 : 1	0.48	0.51	46
26	PNIPMAM$_{393}$	AIBN	benzene	65	18:10	1201 : 1	0.60	0.64	63
27	PNIPMAM$_{776}$	AIBN	benzene	65	18:05	1203 : 1	0.61	0.65	89
28	PNIPMAM$_{956}$	AIBN	benzene	65	18:05	1194 : 1	0.61	0.65	96
29	PNIPMAM$_{469}$	AIBN	benzene [b]	72	18:00	1201 : 1	0.60	0.64	79
30	PNIPMAM$_{424}$	AIBN	benzene [b]	72	18:30	1198 : 1	0.66	0.71	41
31	PNIPMAM$_{241}$	AIBN	TFE [c]	65	18:00	1196 : 1	0.48	0.52	89
32	-	MAIB	benzene	66	18:00	1201 : 1	0.60	0.91	6
33	-	MAIB	benzene	66	18:00	1201 : 1	0.52	0.78	7
34	-	MAIB	benzene	66	18:25	1199 : 1	0.60	0.91	9
35	PNIPMAM$_{426}$	MAIB	benzene [a]	66	18:00	1202 : 1	0.47	0.71	51
36	PNIPMAM$_{936}$	MAIB	benzene	66	18:20	1632 : 1	0.60	0.66	54
37	-	V40	benzene	88	15:50	1198 : 1	1.00	1.60	0
38	PNIPMAM$_{1154}$	V50	TFE	56	17:50	1194 : 1	0.61	1.08	52
39	PNIPMAM$_{810}$	V50	TFE [c]	56	17:05	1199 : 1	0.61	1.08	66
40	PNIPMAM$_{895}$	V50	TFE	56	18:00	1199 : 1	0.60	1.08	85
41	PNIPMAM$_{201}$	V50	TFE	56	18:00	1202 : 1	0.44	0.78	91
42	-	V70	benzene	30	15:50	1200 : 1	1.00	2.02	0
43	PNIPMAM$_{381}$	V70	ethanol	30	18:15	1200 : 1	0.47	0.95	21
44	PNIPMAM$_{219}$	V70	ethanol	30	17:50	1201 : 1	0.61	1.23	31
45	PNIPMAM$_{682}$	V70	ethanol	30	17:55	1211 : 1	0.61	1.22	35
46	PNIPMAM$_{689}$	V70	ethanol	30	18:00	1200 : 1	0.60	1.21	63
47	-	V70	TFT	30	17:50	1198 : 1	0.90	1.83	0
81	PNIPMAM$_{492}$	AIBN	benzene	65	18:00	360 : 1	2.09	7.50	93

[a] concentration of ca. 25 wt.% | [b] concentration of ca. 34 wt.% | [c] concentration of ca. 20 wt.%

For the synthesis of PNVIBAM, *N*-vinyl isobutyramide (NVIBAM, 8.180 g, 72.2870 mmol) is placed in a round bottom flask equipped with a magnetic stirring bar. Initiator dimethyl-2,2'-azobis(2-methylpropionate) (MAIB, 20.80 mg, 0.0904 mmol) is added in the form of a 5.00 g·mol^{-1} stock solution in benzene, followed by additional benzene (total 23.16 mL), to achieve an overall monomer concentration of 30 wt.%. The flask is closed with a silicone septum and degassed with Argon for 40 min, after which the flask is immersed in a heated oil bath at 66°C. The reaction is allowed to proceed for 1:45 h before being quenched by exposure to air and cooling to room temperature. The polymer is dissolved in acetone and precipitated into a 10-fold volume of pentane. The precipitate is collected by filtration and precipitation is repeated, if necessary, until no residual monomer is present, as evidenced by ^{1}H NMR characterization. Finally, the polymer is dissolved in water and freeze-dried.

Table 21. Reaction conditions and conversion of the conventional free radical polymerizations of PNVIBAM. All polymerizations were done in a concentration of ca. 30 wt.%.

Index	Sample	Initiator	Solvent	Temp. [°C]	Reaction Time [hh:mm]	Molar Ratio Monomer : Initiator	$m_{monomer}$ [g]	$m_{initiator}$ [mg]	Conv. [%]
60	PNVIBAM$_{377}$	AIBN	benzene	65	5:00	600 : 1	3.23	7.82	80
61	PNVIBAM$_{303}$	AIBN	benzene	65	3:30	599 : 1	0.79	1.92	62
62	PNVIBAM$_{340}$	MAIB	Benzene	66	5:20	845 : 1	0.23	0.56	56
63	PNVIBAM$_{287}$	MAIB	benzene	66	4:00	838 : 1	0.29	0.71	42
64	PNVIBAM$_{1069}$	MAIB	benzene	66	1:45	800 : 1	8.81	20.8	78 [a]

(a) Yield is given in lieu of conversion when the latter is not available.

6.4.2. RAFT Polymerizations

Amphiphilic di- and triblock copolymers were synthesized by reversible addition fragmentation chain transfer (RAFT) polymerization in two consecutive steps. First, the short hydrophobic block, either polystyrene (PS) or poly(methyl methacrylate) (PMMA), was synthesized. This oligomer was then used as a macro chain transfer agent (macro-CTA) for the polymerization of the longer thermoresponsive block, either poly(*N*-isopropyl acrylamide) (PNIPAM), poly(*N*-isopropyl methacrylamide) (PNIPMAM) or poly(*N*-vinyl isobutyramide) (PNVIBAM).

Based on the initiating capabilities of the R-group of each of the selected CTAs (see Table 3), CTAs **A**, **C**, **D**, **E** and **F** were used to polymerize PS-based copolymers, while CTAs **B**, **C**, **D**, and

E were used to polymerize PMMA-based block copolymers. Moreover, as previously mentioned, monofunctional CTAs **A**, **B**, **C**, **D** and **E** were used to create diblock copolymers, while bifunctional CTA **F** was used to synthesize triblock copolymers.

Copolymers containing poly(*N*-isopropyl acrylamide) (PNIPAM) and poly(*N*-isopropyl methacrylamide) (PNIPMAM) were synthesized using CTAs **A**, **B** and **F**. Copolymers containing poly(*N*-vinyl isobutyramide) (PNVIBAM), in contrast, were synthesized using CTAs **C**, **D** and **E**, as NVIBAM is a "less activated monomer", thus requiring a less active CTA than to avoid inhibition of the polymerization. Figure 72 depicts schematic representations of all the above-mentioned polymerization steps. Typical procedures for each polymerization steps are described in the following.
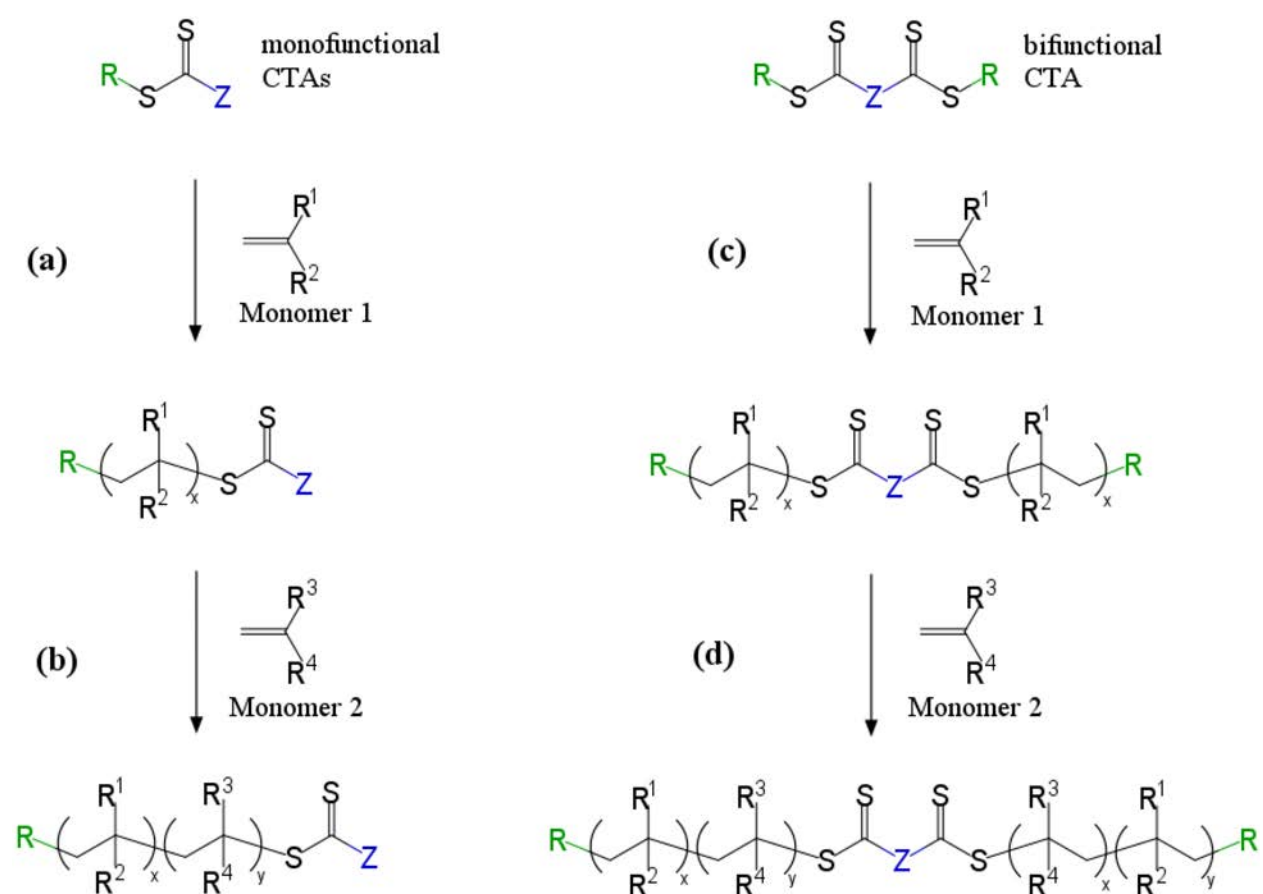
Figure 72. Schematic representation of the consecutive polymerization steps for the synthesis of diblock copolymers [(a)+(b)] and triblock copolymers [(c)+(d)].

Monomer 1 is either styrene (St: R^1 = H, R^2 = phenyl) or methyl methacrylate (MMA: R^1 = CH_3, R^2 = $COOCH_3$) and Monomer 2 is either *N*-isopropyl acrylamide (NIPAM: R^3 = H, R^4 = $CONHCH(CH_3)_2$), *N*-isopropyl methacrylamide (NIPMAM: R^3 = CH_3, R^4 = $CONHCH(CH_3)_2$) or *N*-vinyl isobutyramide (NVIBAM: R^3 = H, R^4 = $NHCOCH(CH_3)_2$). CTAs R-groups (leaving groups) are shown in green, and Z-groups (reactivity modifying groups) are shown in blue.

RAFT Polymerization of Styrene

The synthesis of di- and triblock copolymers with PS hydrophobic block(s) and PNIPAM or PNVIBAM thermoresponsive block was done as depicted in Figure 72. For this, the first step was the polymerization of the hydrophobic block, that is, step (a) in the case of diblock copolymers, or step (c) in case of triblock copolymers. In both cases, the thermally induced polymerization of styrene was done in bulk, without the use of an initiator (self-initiation). The complete list of PS samples discussed in this thesis, and their respective conditions are shown in Table 22. A typical procedure was as follows: freshly distilled styrene (4.7353 g, 45.4664 mmol) and chain transfer agent (ethane-1,2-diylbis(oxy))bis(ethane-2,1-diyl) bis(1-phenylethyl) dicarbonotrithioate (**CTA F**, 667.54 mg, 1.2297 mmol) were placed in a round bottom flask with magnetic stirring bar. The flask was closed with a silicone septum, degassed with argon for 20 min and then immersed in a heated oil bath at 110°C. Small (ca. 0.05 mL) samples were periodically collected from the reaction mixture, under argon, using a syringe to monitor conversion of the monomer. The reaction was not allowed to proceed overnight, and was instead "paused" by freezing to -28°C. As the flask was kept completely closed, the following day the reaction could be restarted and continued by simply reheating to 110°C. Once the desired degree of polymerization had been achieved (ca. 19 h reaction time), the reaction was quenched by exposure to air and cooling to room temperature. The reaction mixture was then dissolved in ca. 4-fold volume of acetone and precipitated in 10-fold volume of methanol. The precipitate was collected by filtration, and the procedure was repeated to eliminate all residual monomer. The polymer was then dissolved in benzene and freeze-dried to give 2.7 g of a pale yellow solid (50% yield).

Table 22. Reaction conditions conversion of the RAFT polymerizations of styrene. Both reactions were done in bulk at 110°C, without addition of an initiator, that is, relying solely on the self-initiation of styrene.

Index	Sample	CTA used	Molar Ratio Styrene : CTA	m_{St} [g]	m_{CTA} [mg]	Reaction Time [hh:mm]	Conversion [%]
1	PS$_{10}$^{A}	A	15.8 : 1	2.97	463	17:30	62
2	PS$_{10}$-*b*-PS$_{10}$^{F}	F	37 : 1	4.74	668	19:30	62
67	PS$_{13}$^{C}	C	9.2 : 1	1.84	400	16:00	40 [a]
66	PS$_{17}$^{C}	C	12.3 : 1	1.85	300	16:00	82 [a]
65	PS$_{28}$^{C}	C	16.0 : 1	9.73	1215	13:00	63
68	PS$_{20}$^{D}	D	7.0 : 1	1.09	334	16:00	83 [a]
69	PS$_{28}$^{D}	D	9.0 : 1	1.27	302	16:00	85
70	PS$_2$^{E}	E	9.2 : 1	1.09	327	17:15	63 [a]

(a) Yield is given in lieu of conversion when the latter is not available.

RAFT Polymerization of Methyl Methacrylate (MMA)

Alternatively to PS, PMMA was also used as hydrophobic block in di- and triblock copolymers containing PNIPAM, PNIPMAM or PNVIBAM as thermoresponsive block. Once again, the first step was the polymerization of the hydrophobic PMMA block (Figure 72 step (a)), for which a typical procedure is described in the following paragraph. The complete list of PMMA reactions discussed in this thesis, and their respective reaction parameters is provided in Table 23.

The chain transfer agent 2-(6-(dimethylamino)-1,3-dioxo-1H-benzo[de]isoquinolin-2(3H)-yl) ethyl 4-cyano-4-((((phenethyl-thio)carbonothioyl)thio)pentanoate (CTA **B**, 550 mg, 0.9079 mmol) is placed in a round bottom flask, equipped with magnetic stirring bar. Freshly distilled methyl methacrylate (MMA, 3.69 g, 36.8558 mmol) is added to it, followed by initiator 2,2'-azobis(isobutyronitrile) (AIBN, 11.301 mg, 0.0688 mmol), in the form of a 5.00 g·mol^{-1} stock solution in benzene. Finally, additional benzene (total 4.6 mL) is added, to achieve an overall concentration of ca. 50 wt.%. A silicone septum is used to close the flask, which is degassed with argon for 15 min, and then immersed in an oil bath pre-heated to 65°C. After 8 h, the reaction is quenched by exposure to air and cooling to room temperature. The reaction mixture is then freeze-dried from benzene two times, thus also removing all residual monomer, to give ca. 2.6 g of the clean copolymer (61% yield).

Table 23. Reaction conditions and obtained conversion of the RAFT polymerizations of MMA. All reactions were done at 65°C, with AIBN initiator and benzene as solvent (concentration ca. 50 wt.%).

Index	Sample	CTA used	Molar Ratio MMA: CTA : AIBN	m_{MMA} [g]	m_{CTA} [mg]	m_{AIBN} [mg]	Reaction Time [h]	Conversion [%]
3	PMMA$_{17}^{B}$	B	39.5 : 1 : 0.08	3.00	460	9.8	8	40 [a]
4	PMMA$_{20}^{B}$	B	40.3 : 1 : 0.08	3.40	511	11.7	24	82 [a]
5	PMMA$_{24}^{B}$	B	40.6 : 1 : 0.08	3.69	550	11.3	8	63
6	PMMA$_{27}^{B}$	B	39.7 : 1 : 0.08	3.01	458	10.0	8	83 [a]
7	PMMA$_{41}^{B}$	B	64.4 : 1 : 0.08	5.24	492	11.2	17	85
8	PMMA$_{75}^{B}$	B	83.7 : 1 : 0.09	6.36	460	10.7	20	63 [a]
71	PMMA$_{279}^{C}$	C	12.8 : 1 : 0.08	1.77	289	18.2	16	97
72	PMMA$_{180}^{D}$	D	12.5 : 1 : 0.08	2.07	367	22.2	16	99
73	PMMA$_{19}^{E}$	E	12.3 : 1 : 0.08	1.34	313	13.8	16	99

(a) Yield is given in lieu of conversion when the latter is not available.

RAFT Polymerization of NIPAM, NIPMAM or PNVIBAM with Macro-CTA

Following the synthesis and workup of the hydrophobic block (PS or PMMA), the thermoresponsive block is then synthesized, as shown in step (b), for diblock copolymers, and step (d) for triblock copolymers, with Monomer 2 being either PNIPAM or PNIPMAM.

In a typical procedure, *N*-isopropyl acrylamide (NIPAM, 9.08 g, 80.2404 mmol) and the PMMA-Macro-CTA (M_n 31.2 kg·mol^{-1} from UV-vis spectroscopy, 1.005 g, 0.3221 mmol) are placed in a round bottom flask equipped with a magnetic stirring bar. Initiator 2,2'-azobis(isobutyronitrile) (AIBN, 6.574 mg, 0.0400 mmol) is added in the form of a 5.00 g·mol^{-1} stock solution in benzene, followed by additional benzene (total 26.8 mL), to achieve an overall concentration of 30 wt.%. The flask is closed with a silicone septum and degassed with argon for 30 min. The flask is then immersed in a pre-heated oil bath at 65°C. After 18 h, the reaction is quenched by exposure to air and cooling to room temperature. The reaction is then diluted with acetone and precipitated in a 10-fold volume of diethyl ether / pentane 3:1. The precipitate is collected by filtration, then dissolved in water and freeze-dried to give ca. 10 g of the clean copolymer (99% yield).

In the case of kinetic studies, polymerizations followed the same procedure described above, whereas small (ca. 0.2 mL) samples were periodically collected from the reaction mixture, under argon, using a syringe.

Table 24. Reaction conditions and obtained conversion of the RAFT polymerizations of PNIPAM. All polymerizations were done in benzene (concentration ca. 30 wt.%) at 65°C, with AIBN initiator.

Index	Sample	Molar Ratio NIPAM : macro-CTA : AIBN	$m_{monomer}$ [g]	m_{CTA} [mg]	$m_{initiator}$ [mg]	Reaction Time [h]	Conv. [%]
9	**PS$_{10}$-*b*-PNIPAM$_{65}$^{A}**	105 : 1 : 0.13	2.99	500	5.2	18	97
10	**PS$_{10}$-*b*-PNIPAM$_{85}$^{A}**	129 : 1 : 0.13	2.16	296	3.1	18	99
11	**PS$_{10}$-*b*-PNIPAM$_{180}$-*b*-PS$_{10}$^{F}**	210 : 1 : 0.12	4.89	458	3.1	18	95
12	**PS$_{10}$-*b*-PNIPAM$_{250}$-*b*-PS$_{10}$^{F}**	284 : 1 : 0.12	4.73	601	4.1	18	98
13	**PMMA$_{17}$-*b*-PNIPAM$_{337}$^{B}**	249 : 1 : 0.17	7.14	660	7.0	18	*92* [a]
14	**PMMA$_{20}$-*b*-PNIPAM$_{554}$^{B}**	262 : 1 : 0.14	11.37	1001	8.7	37	98
15	**PMMA$_{24}$-*b*-PNIPAM$_{379}$^{B}**	249 : 1 : 0.12	9.08	1005	6.6	18	99
16	**PMMA$_{27}$-*b*-PNIPAM$_{802}$^{B}**	552 : 1 : 0.13	8.45	448	2.9	24	98
17	**PMMA$_{41}$-*b*-PNIPAM$_{456}$^{B}**	316 : 1 : 0.14	6.90	907	4.3	24	96
18	**PMMA$_{75}$-*b*-PNIPAM$_{366}$^{B}**	252 : 1 : 0.13	6.98	1987	5.1	22	98

(a) Yield is given in lieu of conversion when the latter is not available.

Table 25. Reaction conditions and obtained conversion of the RAFT polymerizations of PNIPMAM. Unless otherwise stated, all polymerizations were done in a concentration of ca. 30 wt.%.

Index	Sample	Solvent	Initiator	Temp. [°C]	Molar Ratio NIPMAM : (macro-)CTA : AIBN	$m_{monom.}$ [g]	m_{CTA} [mg]	$m_{init.}$ [mg]	Reaction Time [h]	Convers. [%]
48	-	TFE	V50	56	610 : 1 : 0.18	5.04	203	3.16	18	0
49	-	TFE	V50	56	625 : 1 : 0.19	0.555	21.8	0.35	18	0
50	-	TFE	V50	56	638 : 1 : 0.18	0.547	21.03	0.33	18	0
51	-	TFE	AIBN	65	624 : 1 : 0.18	0.659	21.70	0.25	17	0
52	PMMA$_{17}$-*b*-PNIPMAM$_{145}$^{B}	benz.	AIBN	65	551 : 1 : 0.22	17.72	660	9.0	18	97 [a]
53	PMMA$_{20}$-*b*-PNIPMAM$_{146}$^{B}	benz.	AIBN	72	327 : 1 : 0.11	7.03	449	3.2	107	56
54	PMMA$_{20}$-*b*-PNIPMAM$_{242}$^{B}	benz.	AIBN	71	507 : 1 : 0.18	16.02	650	7.36	31	51
55	PMMA$_{24}$-*b*-PNIPMAM$_{443}$^{B}	benz.	AIBN	72	632 : 1 : 0.18	12.25	476	4.54	18	44
56	PMMA$_{27}$-*b*-PNIPMAM$_{248}$^{B}	benz.	AIBN	71	592 : 1 : 0.20	11.06	487	5.0	43	78
57	PMMA$_{41}$-*b*-PNIPMAM$_{153}$^{B}	benz.	AIBN	71	611 : 1 : 0.22	14.36	869	6.54	31	30
58	-	benz.[b]	AIBN	65	302 : 1 : 0.13	9.46	200	5.23	47	28
59	PNIPMAM$_{146}$^{B}	benz.	AIBN	71	271 : 1 : 0.10	5.73	606	2.7	18	58

(a) Yield is given in lieu of conversion when the latter is not available.

(b) Reaction performed with a concentration of 19 wt.%.

Table 26. Reaction conditions and obtained conversion of the RAFT polymerizations of PNVIBAM. All polymerizations were done in benzene (concentration ca. 30 wt.%) at 65°C, with AIBN initiator.

Index	Sample	Molar Ratio NVIBAM : (macro-)CTA : AIBN	$m_{monomer}$ [mg]	m_{CTA} [mg]	$m_{initiator}$ [mg]	Reaction Time [h]	Conv. [%]
74	-	270 : 1 : 0.10	714	4.86	0.38	16	0
75	-	291 : 1 : 0.12	1409	8.90	0.88	16	0
76	PNVIBAM$_{81}$^{D}	271 : 1 : 0.10	974	7.07	0.52	16	10
77	PNVIBAM$_{336}$^{E}	273 : 1 : 0.10	947	8.82	0.50	16	35
78	PS$_{13}$-*b*-PNVIBAM$_{44}$^{C}	268 : 1 : 0.12	949	48.63	0.64	18	10
79	-	271 : 1 : 0.12	901	67.32	0.60	17	0
80	-	277 : 1 : 0.12	1102	75.83	0.72	17	0

6.5. Characterization Methods and Equipment

Nuclear Magnetic Resonance (NMR)

^{1}H NMR spectra were recorded either with a Bruker Avance 300 (300 MHz) or Bruker Avance NEO 400 (400 MHz) spectrometers at ambient temperature in deuterated solvents. For the Macro-CTAs, number-average degrees of polymerization (DP_n) and corresponding number-average molar masses (M_n^{NMR}) were determined from the ^{1}H NMR spectra by end-group analysis, comparing the integrals of a signal characteristic for the constitutional repeat unit of the polymer with a signal group characteristic for the CTA. In the case of the copolymers, the DP_n and corresponding number-average molar masses (M_n^{NMR}) of the second block were determined by comparing the integrals of signals characteristic for the two blocks, assuming that DP_n of the first block in the copolymer was identical to the one of the macro-CTA employed.

Ultraviolet-Visible (UV-Vis) Spectroscopy

UV-vis absorption spectra were measured in ethyl acetate, using a UV-vis-NIR Lambda Spectrometer (PerkinElmer), with quartz cuvettes with optical path length of 10 mm. Number-average molar masses of the polymers (M_n^{vis}) were then calculated by end-group analysis, assuming that every molecule carries exactly one reference end-group moiety, and that its extinction coefficient (ε) is the same in the low molar mass CTA and in the polymers. The absorption band of the trithiocarbonate moiety was used as reference for polymers synthesized

with CTAs **A** and **F**. The absorption band of the naphthalimide chromophore was used as reference for polymers synthesized with CTA **B**. The absorption band of the xanthate moiety was used as reference for polymers synthesized with CTA **C**. And the absorption band of the dithiocarbamate moiety was used as reference for polymers synthesized with CTAs **D** and **E**.

The ε value of the reference moiety was determined by linear regression of the absorbance versus concentration data of the CTA, according to Lambert–Beer's law, shown in Equation (14). The M_n^{vis} values of the polymers were then calculated via Equation (15).

$$\varepsilon = \frac{A}{c \cdot d} \tag{14}$$

$$M_n^{vis} = \frac{\varepsilon \cdot m_o \cdot d}{A \cdot V} \tag{15}$$

where ε is the extinction coefficient (in $L \cdot mol^{-1} \cdot cm^{-1}$), A the absorbance of the sample at λ_{max}, c the molar concentration of the polymer (in $mol \cdot L^{-1}$), d the optical path length of the cuvette (in cm), M_n^{vis} the number-average molar mass (in $g \cdot mol^{-1}$), m_o the mass of the polymer (in g) and V the volume of solvent (in L).

Size-Exclusion Chromatography (SEC)

SEC of the polymers was performed at 25 °C mostly in NMP + 0.5% LiBr as eluent, with a TSP P1000 isocratic pump (Thermo Fisher Scientific, Dreieich, Germany), a Shimadzu RID-6A refractive index detector (Shimadzu Corporation, Kyoto, Japan.), and a PSS GRAM column (7 µm, 8 × 300 mm) (PSS GmbH, Mainz, Germany). The SEC setup was calibrated using narrowly distributed polystyrene or poly(methyl methacrylate) standards, according to the composition of polymer being characterized. PS calibration was used for polymers and oligomers containing PS, while PMMA calibration was used for polymers and oligomers containing PMMA, as well as for PNIPAM, PNIPMAM and PNVIBAM homopolymers.

Dynamic Light Scattering (DLS)

Approximate polymer aggregate sizes in solution were determined using a Malvern High Performance Particle Sizer HPP5002 and Dispersion Technology Software DTS 4.20, in quartz cuvettes with optical path length of 10 mm. Measurements were done with a wavelength of 633 nm and scattering angle θ = 173° (backscattering detection mode), in intervals of 1°C and 2 min equilibration time. The refractive index of the polymers was set as 1.489 (value for PMMA). The temperature-dependent refractive index and viscosity of the solvent mixture was calculated based on its composition (water, methanol, ethanol, isopropanol).

To obtain polymer solutions in mixed solvents (water + cosolvent), the polymer was first dissolved in each of the pure solvents, already in the target concentration (usually 10 g·L^{-1}). These solutions were then combined to obtain the desired proportion of water/cosolvent.

Turbidimetry

Cloud point temperature (T_{CP}) of the polymers was determined with a precision of ±1°C by turbidimetry with a Varian Cary 5000 UV-vis-NIR spectrophotometer, equipped with 6+6 cell Peltier thermostated cell holders, using quartz cuvettes with optical path length of 10 mm. Measurements were performed at a wavelength of 500 nm, with heating and cooling rates of 0.5 K·min^{-1}. Measured transmission values were normalized to the maximum value in each sample's measurement. Cloud points were determined from the heating run, as the onset temperature of the transmission decay.

Polymer solutions in mixed solvents (water + cosolvent) were prepared in the same way as described for Dynamic Light Scattering.

Fourier-Transform Infrared Spectroscopy (FTIR)

A Nicolet Avatar 370 FTIR spectrometer equipped with an ATR Smart Performer element and AMTIR crystal were used to collect the FTIR spectra shown in this thesis.

Elemental Analysis (EA)

Quantitative measurements of the percentages of carbon, hydrogen, nitrogen, and sulfur in the samples were done using a FlashEA 1112 CHNS/O Automatic Elemental Analyzer with MAa2O6R autosampler (Thermo Scientific).

Number-average degrees of polymerization and, respectively, number-average molar mass of the polymers obtained by RAFT were calculated through the carbon-nitrogen and/or carbon-sulfur content ratios. For styrene oligomers, only calculation through the carbon-sulfur ratio was possible, due to the absence of nitrogen in CTAs A and F. For PMMA oligomers, calculation could be done both through the carbon-nitrogen and carbon-sulfur ratios. For copolymers and high molar homopolymers, calculation was done solely through the carbon-nitrogen ratio, due to the small proportion of sulfur atoms in the chain, leading to large inaccuracies.

For homopolymers and oligomers (macro-CTAs), the following equations were used:

$$C/N_{EA} = \frac{\%C_{CTA} \cdot MM_{CTA} + \%C_1 \cdot MM_1 \cdot DP_n^{EA\,1}}{\%N_{CTA} \cdot MM_{CTA} + \%N_1 \cdot MM_1 \cdot DP_n^{EA\,1}} \qquad \textbf{(16)}$$

then

$$DP_n^{EA\ 1} = \frac{MM_{CTA} \cdot (C/N_{EA} \cdot \%N_{CTA} - \%C_{CTA})}{MM_1 \cdot (\%C_1 - C/N_{EA} \cdot \%N_1)} \qquad (17)$$

where C/N_{EA} is the carbon-nitrogen content ratio obtained by elemental analysis, $\%C_{CTA}$ and $\%N_{CTA}$ are the calculated carbon and nitrogen contents of the CTA, MM_{CTA} is the molar mass of the CTA, $\%C_1$ and $\%N_1$ are the calculated carbon and nitrogen contents of each constitutional repeat unit of the homopolymer in question, MM_1 is the molar mass of each constitutional repeat unit of the homopolymer, and $DP_n^{EA\ 1}$ is the degree of polymerization of the homopolymer. For carbon-sulfur ratio calculations, the same equations were used, with nitrogen contents being exchanged by sulfur contents.

Subsequently, the degree of polymerization of the second block ($DP_n^{EA\ 2}$) could then be calculated through the following equations:

$$C/N_{EA} = \frac{\%C_{CTA} \cdot MM_{CTA} + \%C_1 \cdot MM_1 \cdot DP_n^{EA\ 1} + \%C_2 \cdot MM_2 \cdot DP_n^{EA\ 2}}{\%N_{CTA} \cdot MM_{CTA} + \%N_1 \cdot MM_1 \cdot DP_n^{EA\ 1} + \%N_2 \cdot MM_2 \cdot DP_n^{EA\ 2}} \qquad (18)$$

then

$$DP_n^{EA\ 2} = \frac{C/N_{EA} \cdot \%N_{CTA} \cdot MM_{CTA} + C/N_{EA} \cdot \%N_1 \cdot MM_1 \cdot DP_n^{EA\ 1} - \%C_{CTA} \cdot MM_{CTA} - \%C_1 \cdot MM_1}{MM_2 \cdot (\%C_2 - \%N_{CTA} \cdot C/N_{EA})} \qquad (19)$$

where $\%C_2$ and $\%N_2$ are the calculated carbon and nitrogen contents of each constitutional repeat unit of the second block, and MM_2 is the molar mass of each constitutional repeat unit of the second block.

Differential Scanning Calorimetry (DSC)

DSC measurements were performed with a Mettler-Toledo DSC822e device, under N_2 atmosphere (20 mL·min^{-1}) in temperatures ranging from 0 to 230 °C, in 4 heating-cooling cycles. Heating and cooling rate was 10 K·min^{-1} on the first and second cycles and 30 K·min^{-1} on the third and fourth cycles. Glass transition temperatures were derived from the second heating curve, at the mid-point (half height) of the transition step.

Thermogravimetric Analysis (TGA)

TGA was conducted using a Mettler-Toledo TGA/SDTA851e apparatus, under N_2 atmosphere (20 mL·min^{-1}) in temperature ranging from 25 °C to 900 °C, with a heating rate of 10 K·min^{-1}.

7. Annexes

7.1. NMR Spectra

Chain Transfer Agents
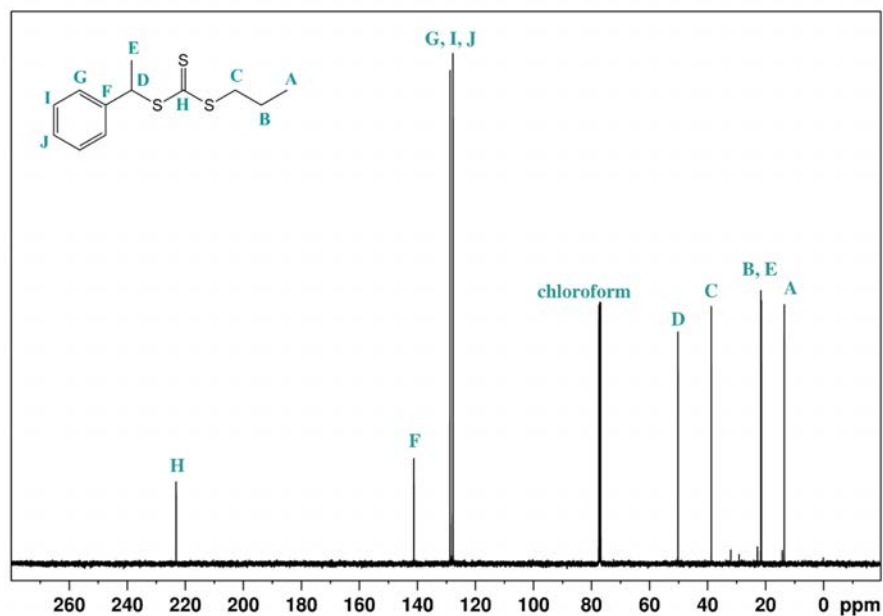
Figure A 1. ^{13}C APT NMR spectrum of CTA A, in CDCl$_3$.
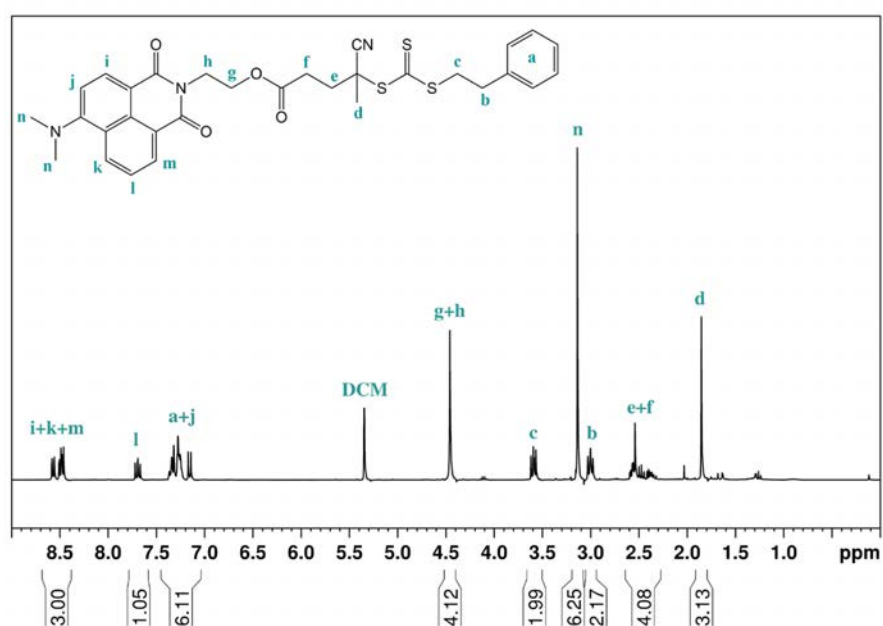
Figure A 2. ^{1}H NMR spectrum of CTA B, in DCM-d$_2$.
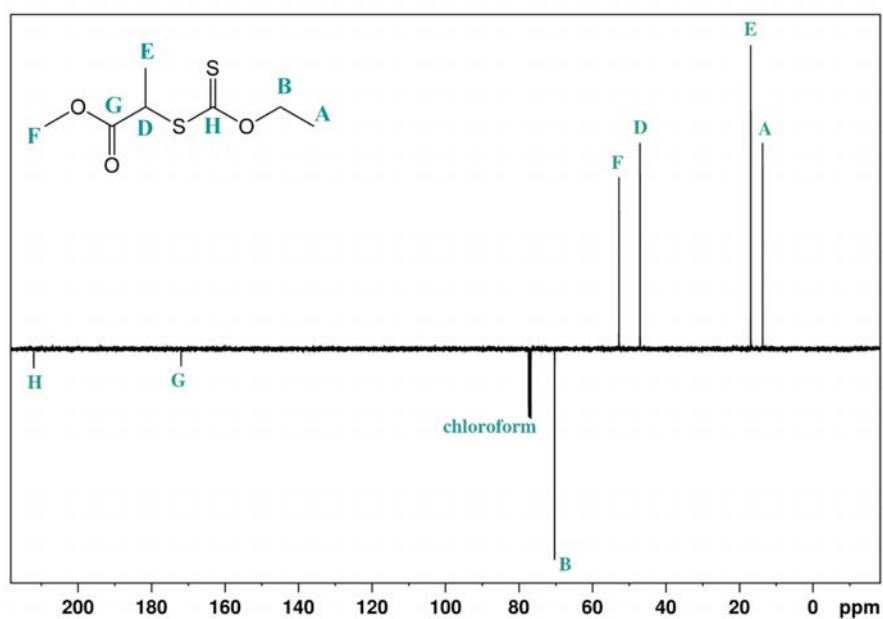
Figure A 3. ^{13}C APT NMR spectrum of CTA C, in CDCl$_3$.
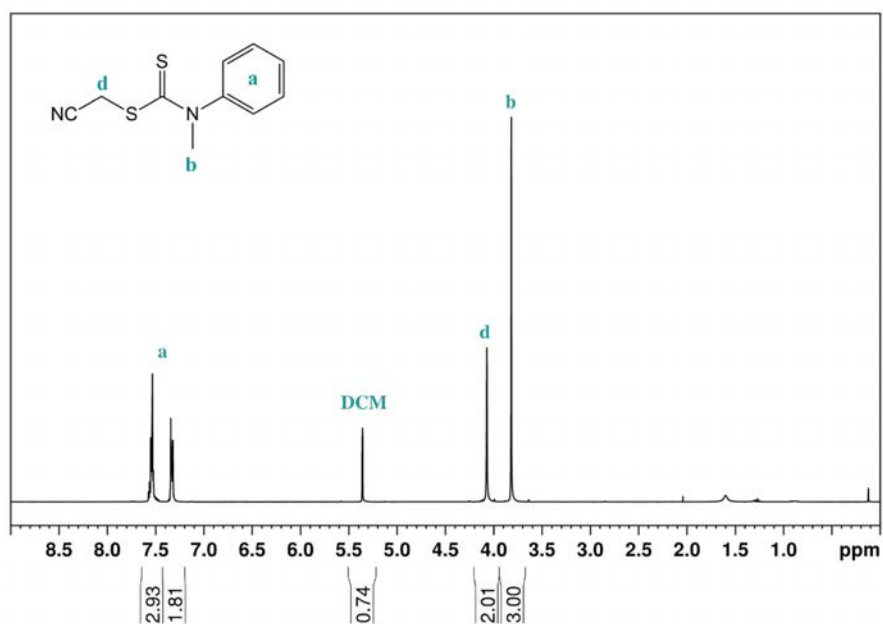
Figure A 4. ^{1}H NMR spectrum of CTA D, in DCM-d$_2$.
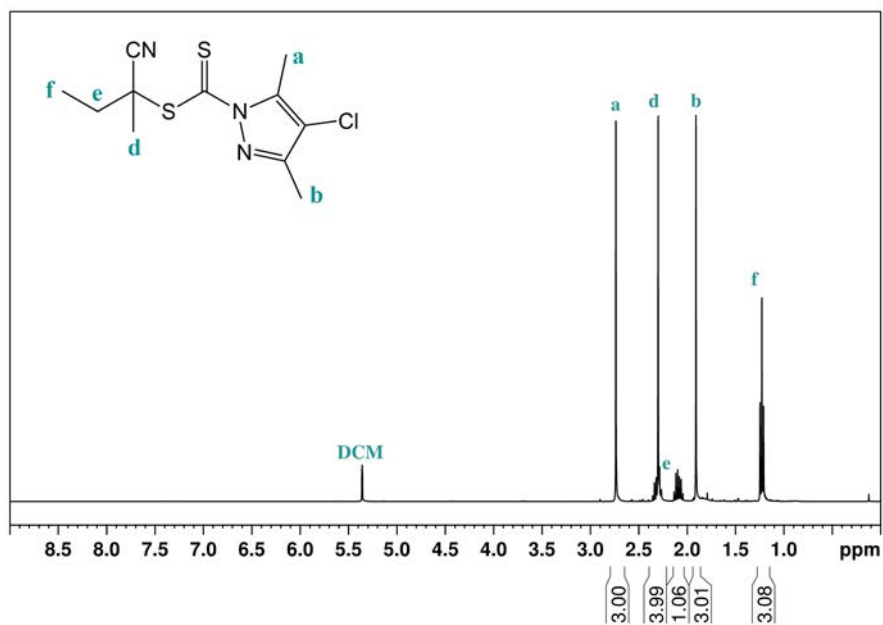
Figure A 5. ^{1}H NMR spectrum of CTA E, in DCM-d$_2$.
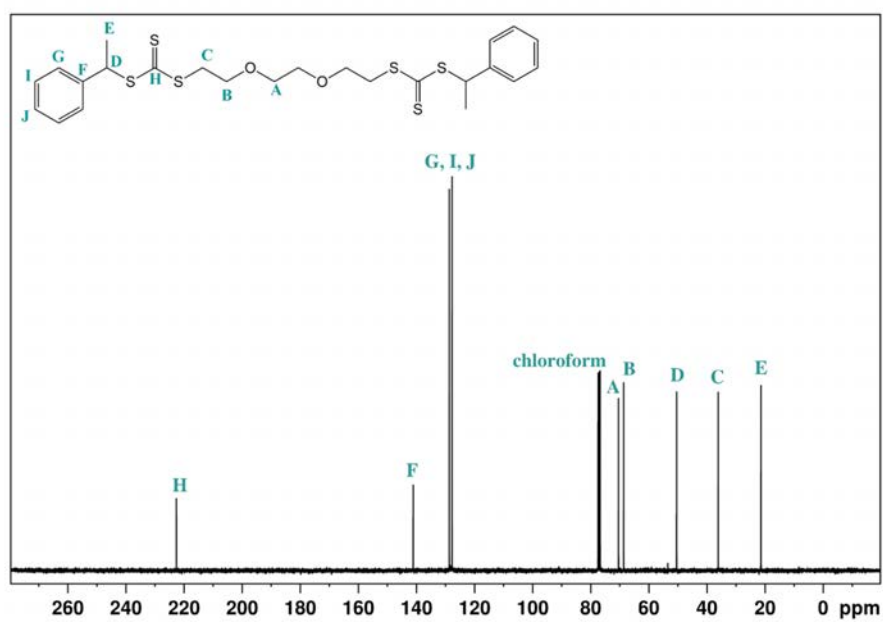
Figure A 6. ^{13}C APT NMR spectrum of CTA F, in CDCl$_3$.

Monomers
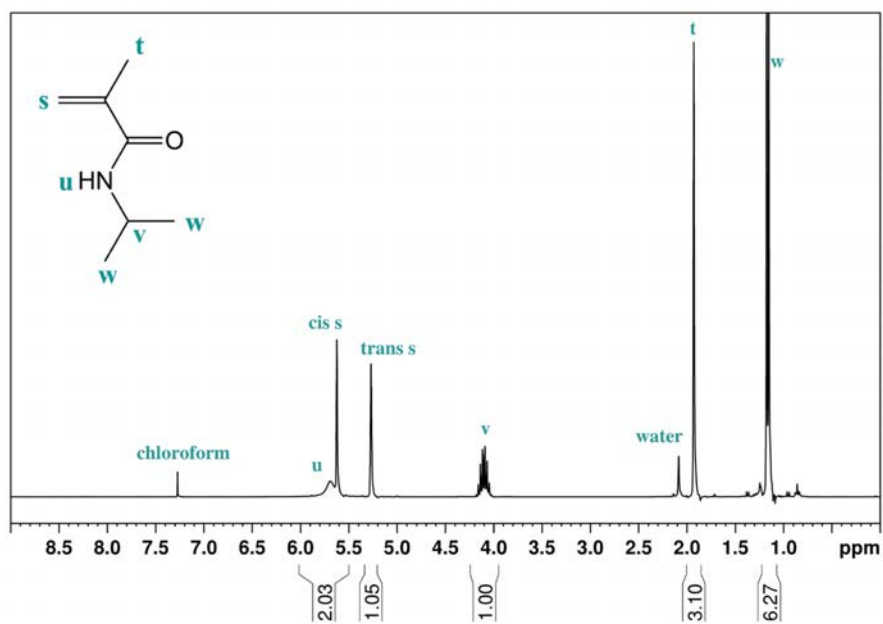
Figure A 7. ^{1}H NMR spectrum of NIPMAM monomer in CDCl$_3$.
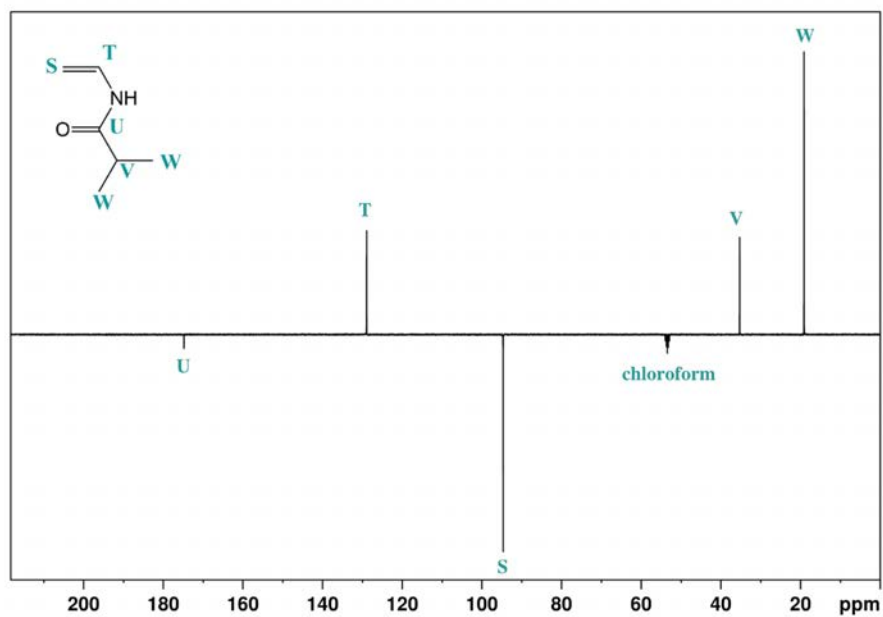
Figure A 8. ^{13}C APT NMR spectrum of NVIBAM monomer, in CDCl$_3$.
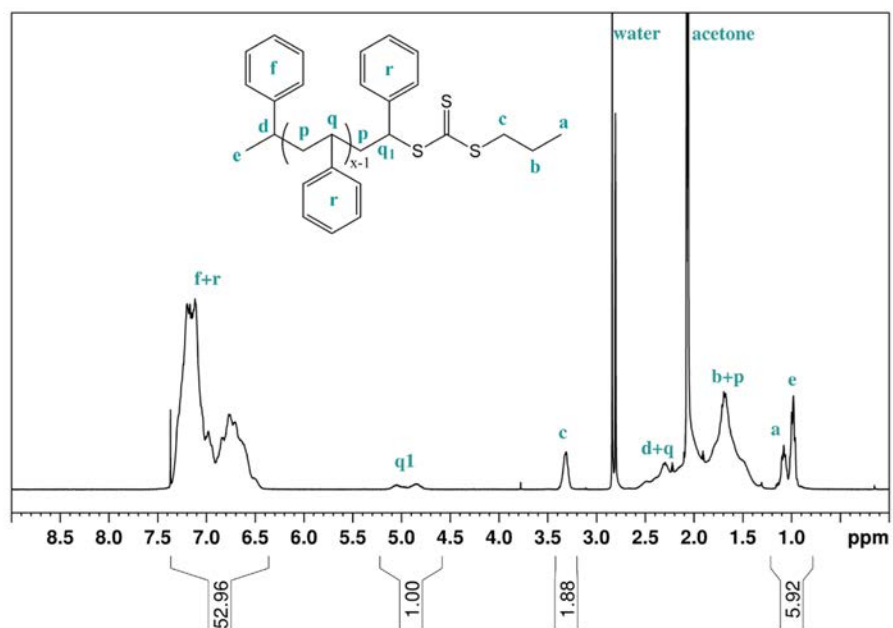
Figure A 9. ^{1}H NMR spectrum of PS_{10}^A (reaction index 1) in acetone-d_6.
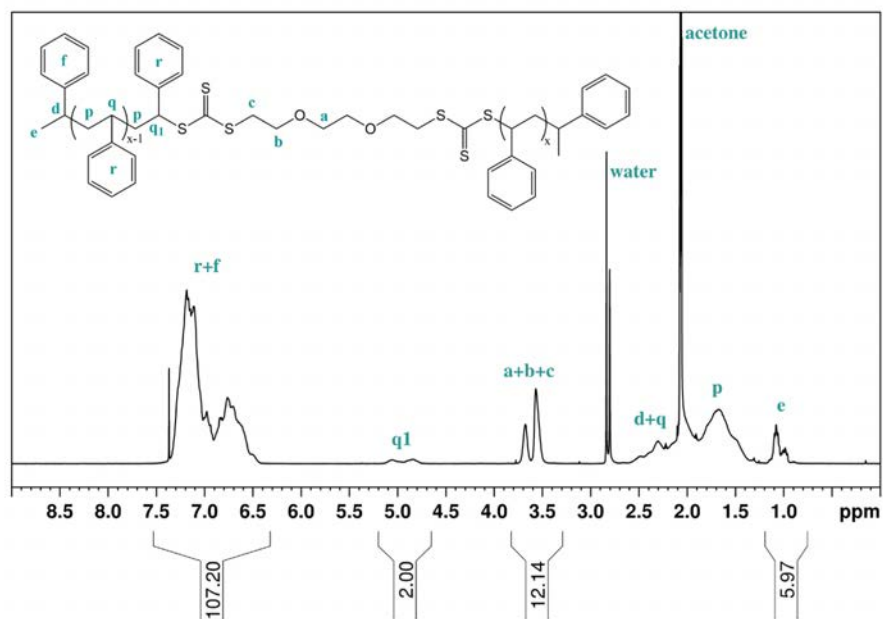
Figure A 10. ^{1}H NMR spectrum of PS_{10}-b-PS_{10}^F (reaction index 2) in acetone-d_6.
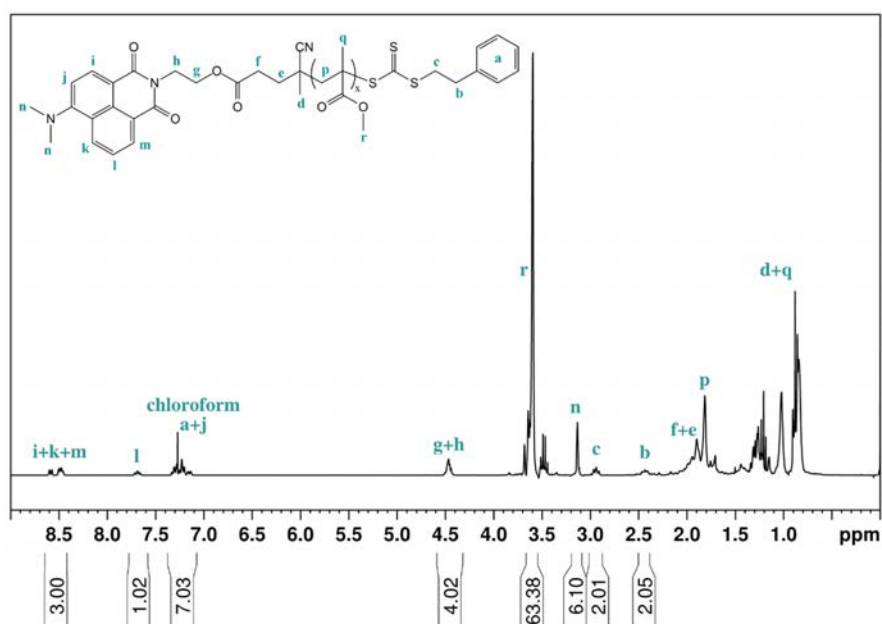
Figure A 11. ^{1}H NMR spectrum of PMMA$_{17}$^{B} (reaction index 3) in CDCl$_3$.
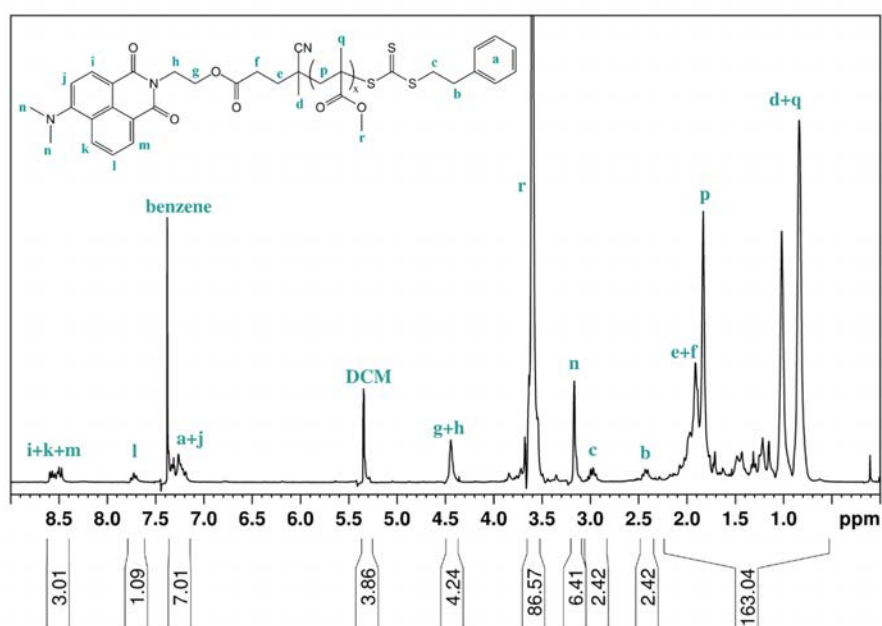
Figure A 12. ^{1}H NMR spectrum of PMMA$_{20}$^{B} (reaction index 4) in DCM-d$_2$.
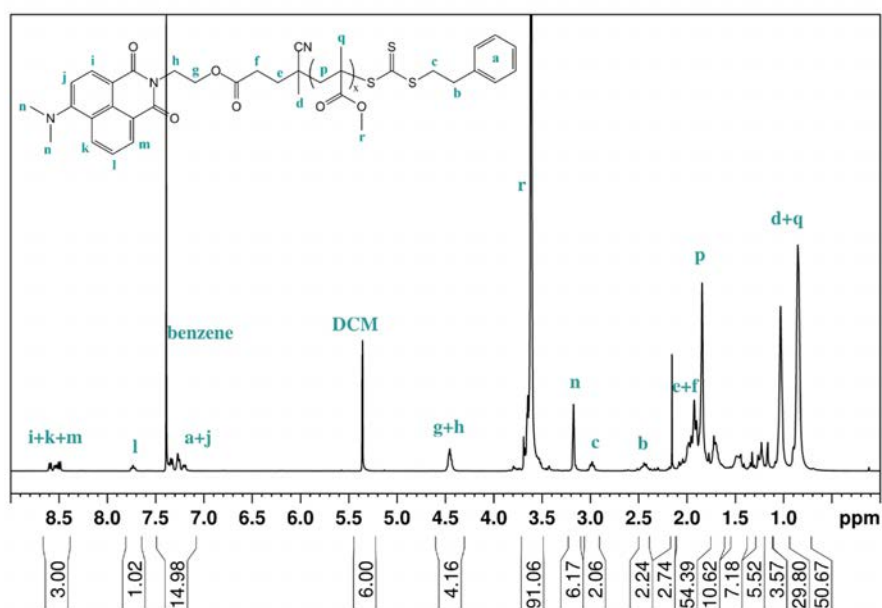
Figure A 13. ^{1}H NMR spectrum of PMMA$_{24}$^{B} (reaction index 5) in DCM-d$_{2}$.
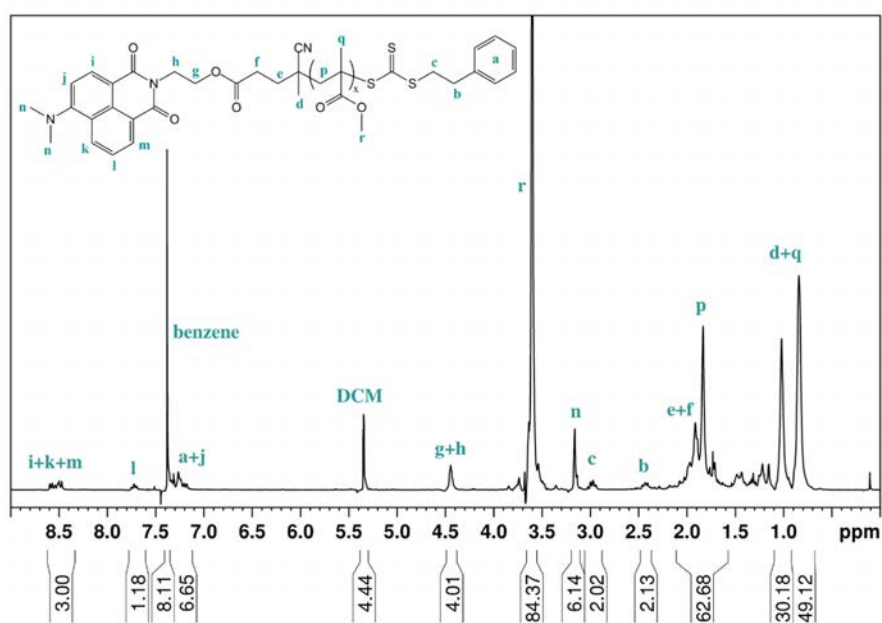
Figure A 14. ^{1}H NMR spectrum of PMMA$_{27}$^{B} (reaction index 6) in DCM-d$_{2}$.
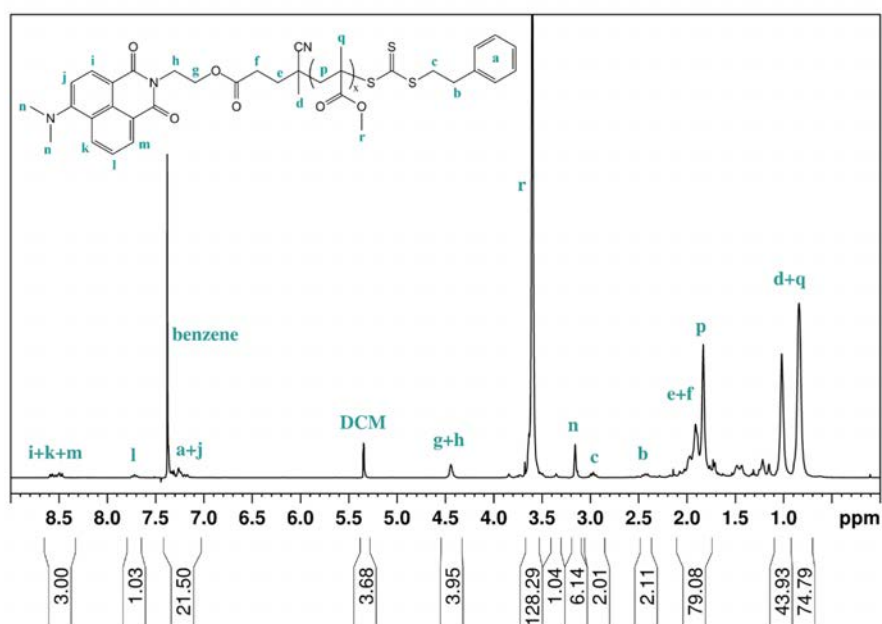
Figure A 15. ^{1}H NMR spectrum of PMMA$_{41}$[B] (reaction index 7) in DCM-d$_2$.
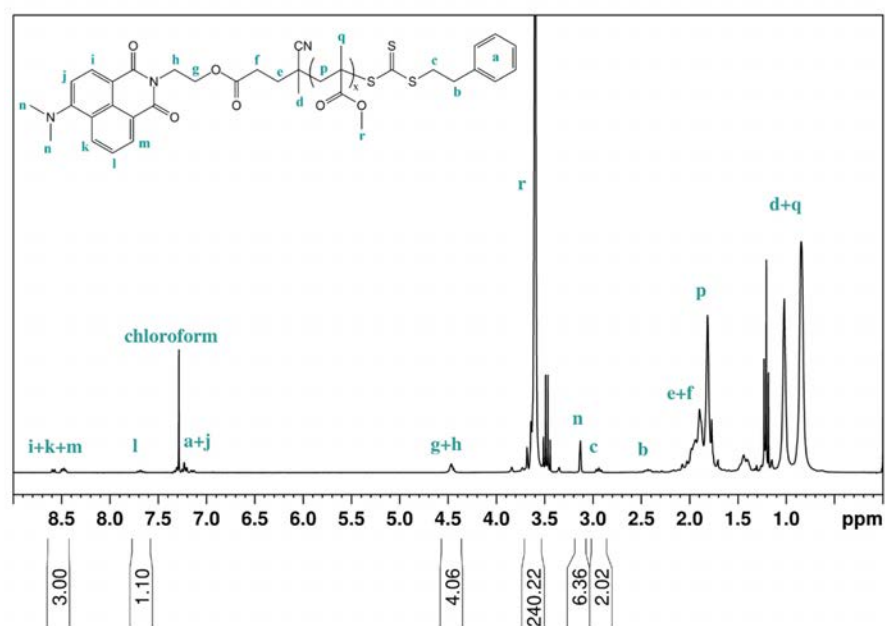
Figure A 16. ^{1}H NMR spectrum of PMMA$_{75}$[B] (reaction index 8) in CDCl$_3$.
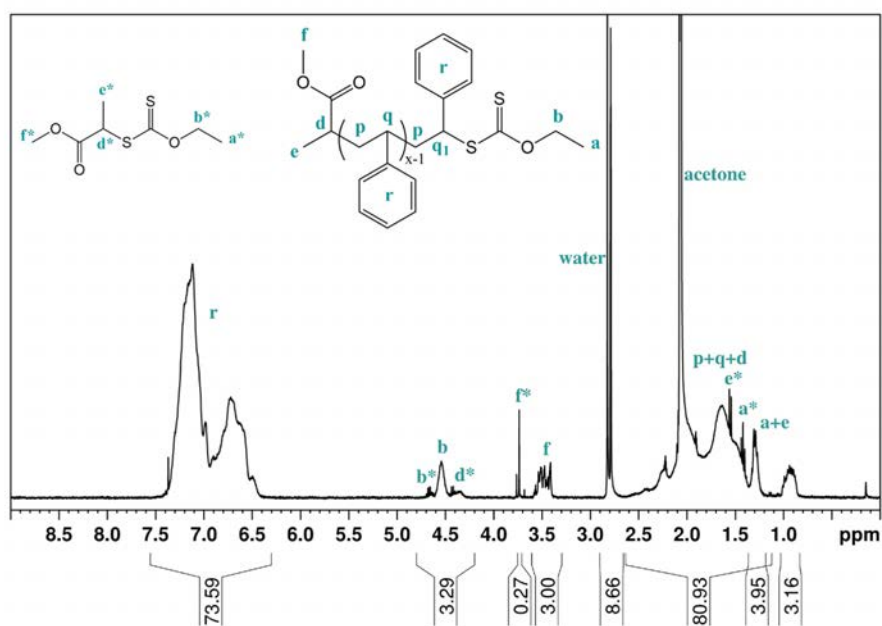
Figure A 17. ^{1}H NMR spectrum of PS_{13}^C (reaction index 65) in acetone-d_6.
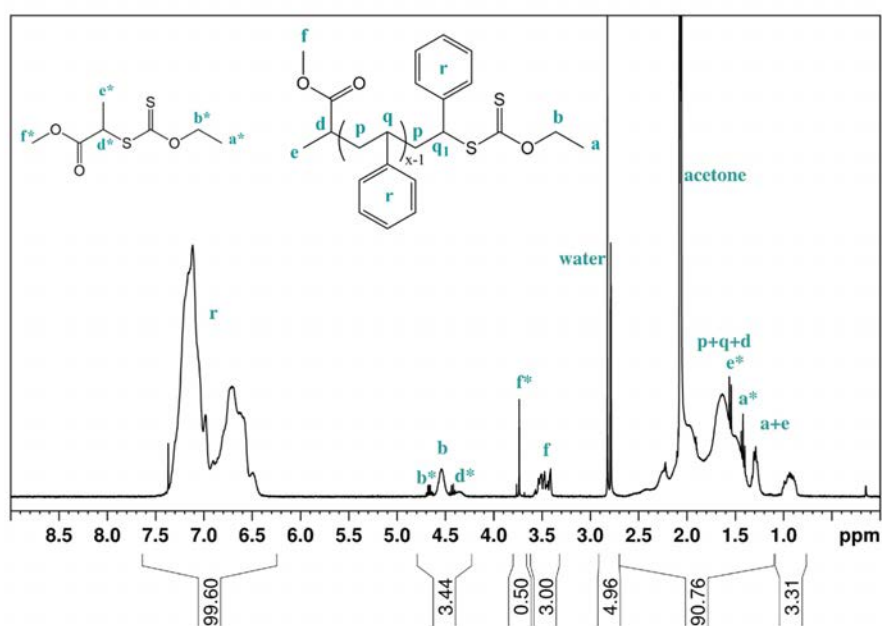
Figure A 18. ^{1}H NMR spectrum of PS_{17}^C (reaction index 66) in acetone-d_6.
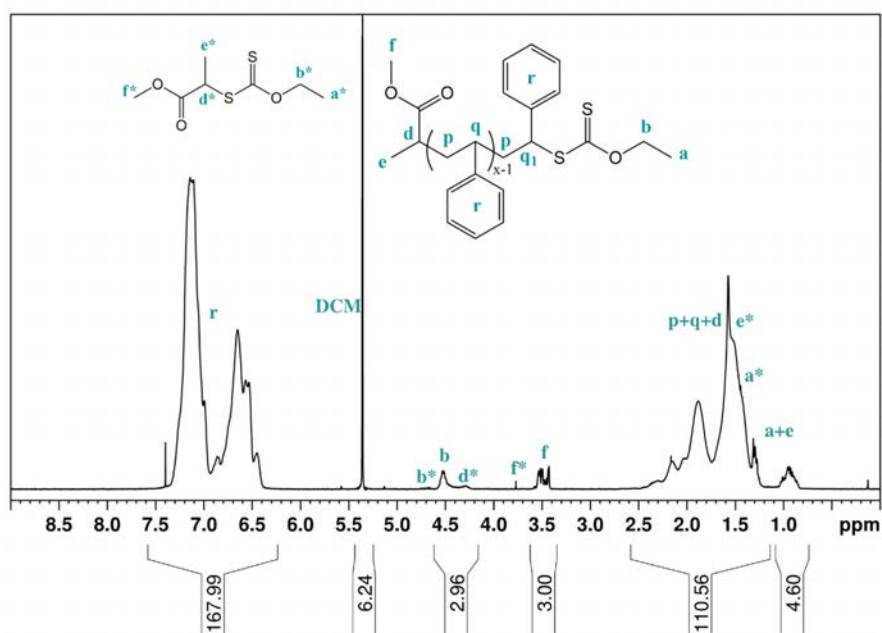
Figure A 19. ^{1}H NMR spectrum of PS$_{28}^C$ (reaction index 67) in DCM-d$_2$.
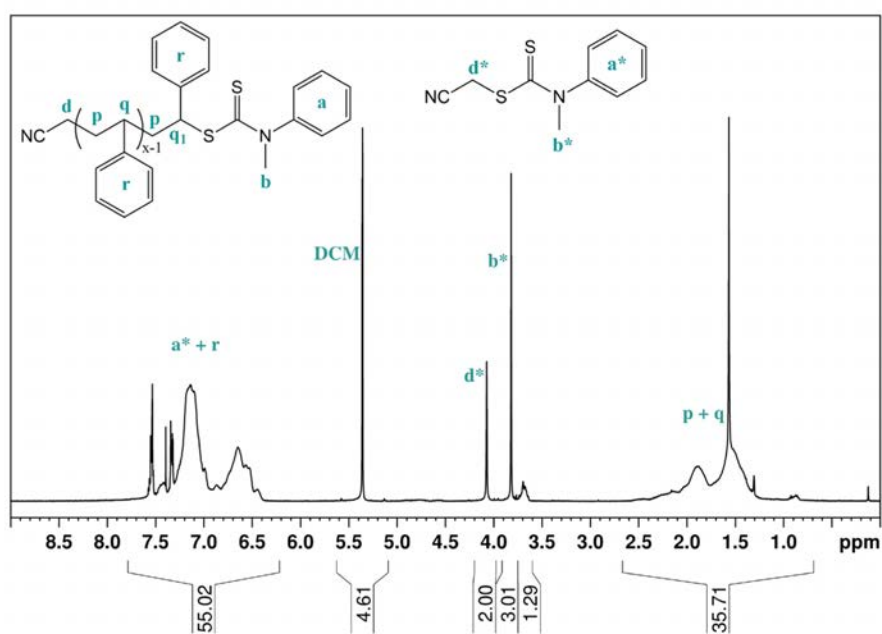
Figure A 20. ^{1}H NMR spectrum of PS$_{20}^D$ (reaction index 68) in DCM-d$_6$.
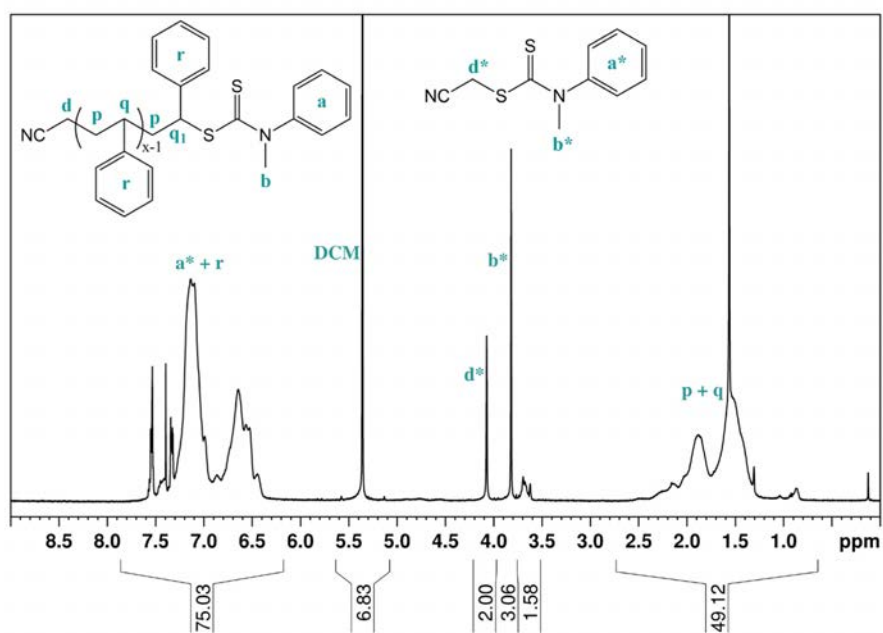
Figure A 21. ^{1}H NMR spectrum of PS_{28}^D (reaction index 69) in DCM-d$_2$.
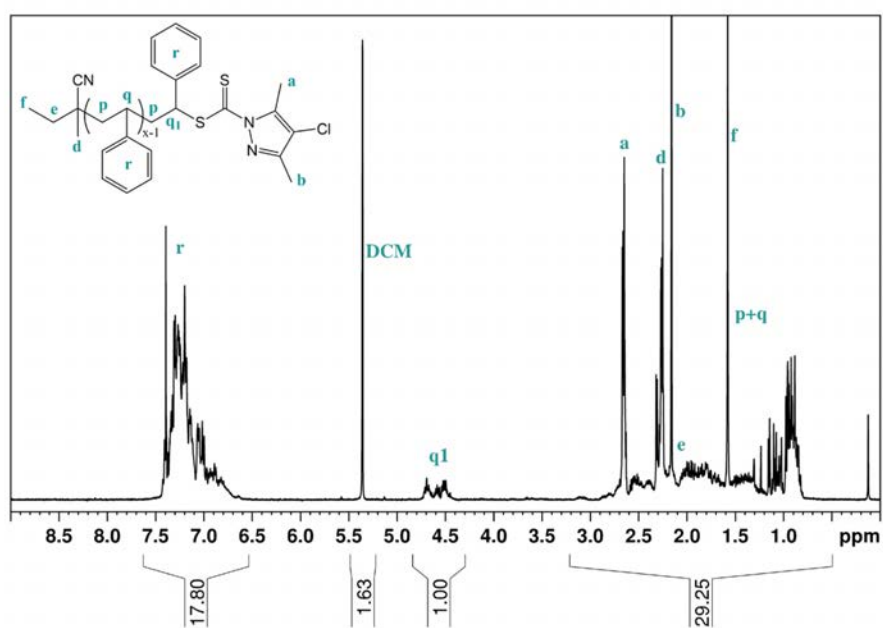
Figure A 22. ^{1}H NMR spectrum of PS_2^E (reaction index 70) in DCM-d$_2$.
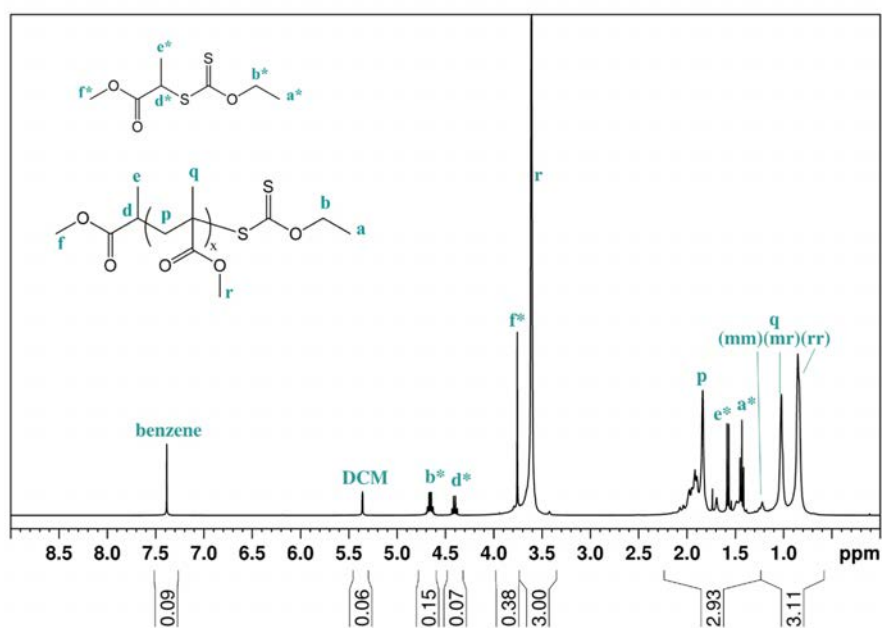
Figure A 23. ^{1}H NMR spectrum of PMMA$_{279}$^{C} (reaction index 71) in DCM-d$_2$.
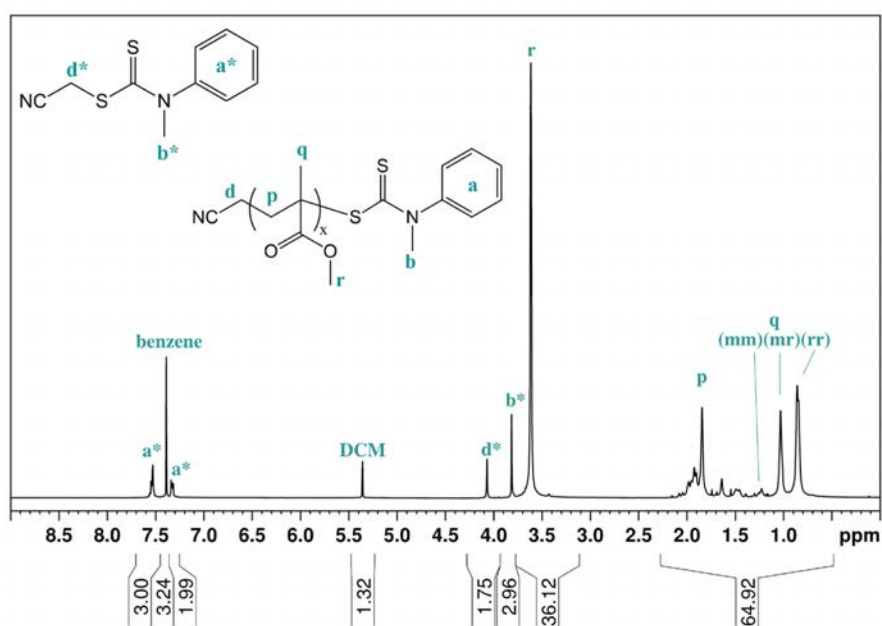
Figure A 24. ^{1}H NMR spectrum of PMMA$_{180}$^{D} (reaction index 72) in DCM-d$_2$.
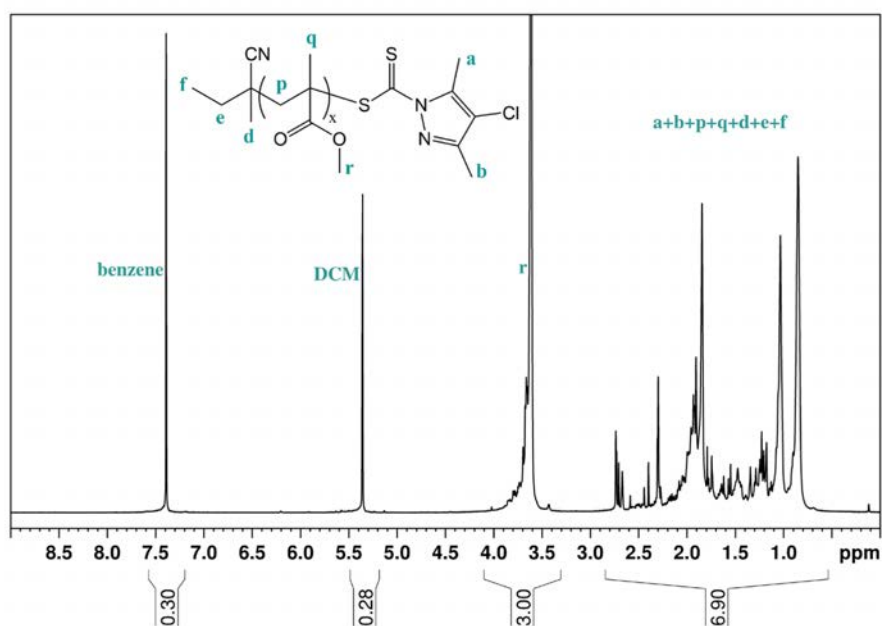
Figure A 25. ^{1}H NMR spectrum of PMMA$_{19}^E$ (reaction index 73) in DCM-d$_2$.

PNIPAM Copolymers
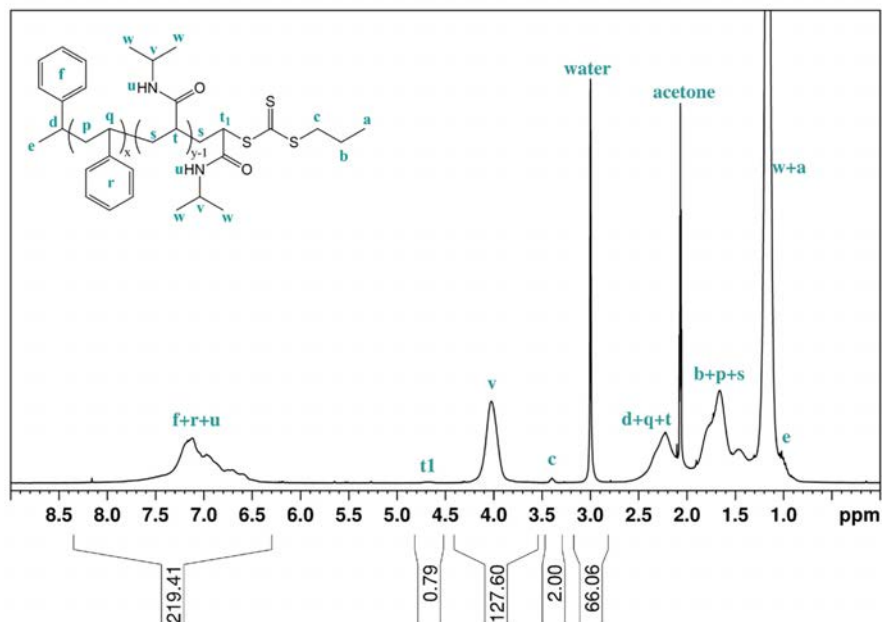
Figure A 26. ^{1}H NMR spectrum of PS$_{10}$-b-PNIPAM$_{65}^A$ (reaction index 9) in acetone-d6.
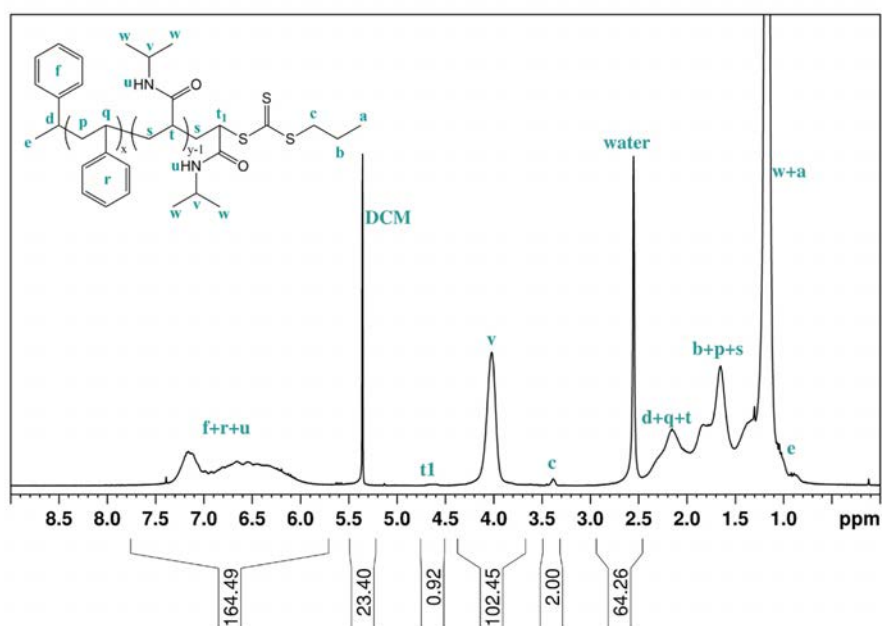
Figure A 27. ^{1}H NMR spectrum of PS$_{10}$-b-PNIPAM$_{85}^A$ (reaction index 10) in DCM-d$_2$.
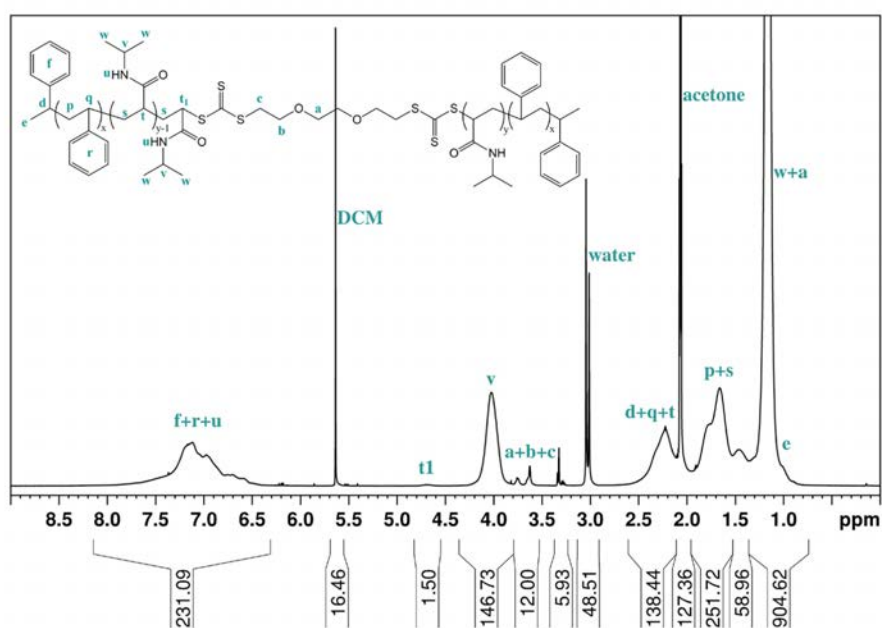
Figure A 28. ^{1}H NMR spectrum of PS$_{10}$-b-PNIPAM$_{180}$-b-PS$_{10}^F$ (reaction index 11) in acetone-d6.
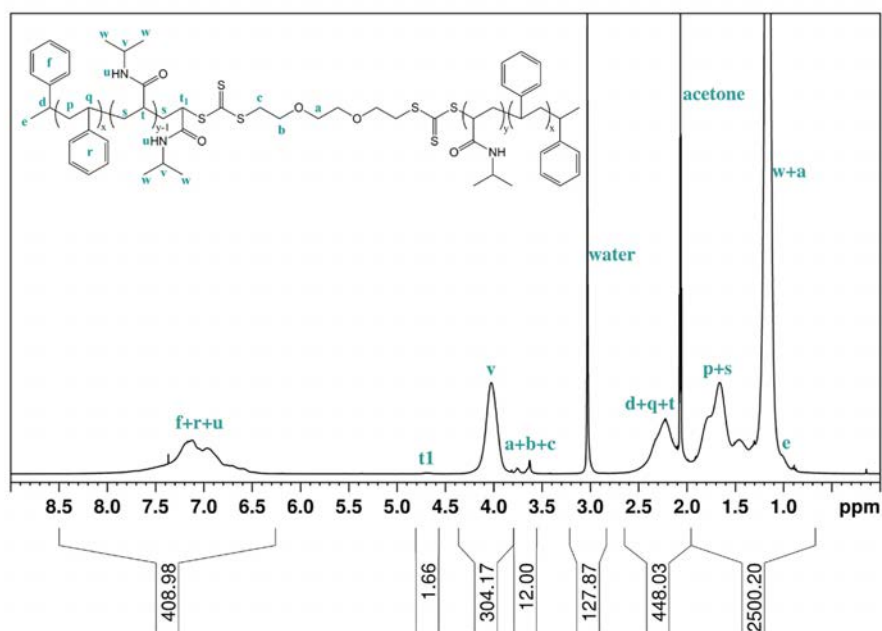
Figure A 29. ^{1}H NMR spectrum of PS$_{10}$-*b*-PNIPAM$_{250}$-*b*-PS$_{10}^F$ (reaction index 12) in acetone-d6.
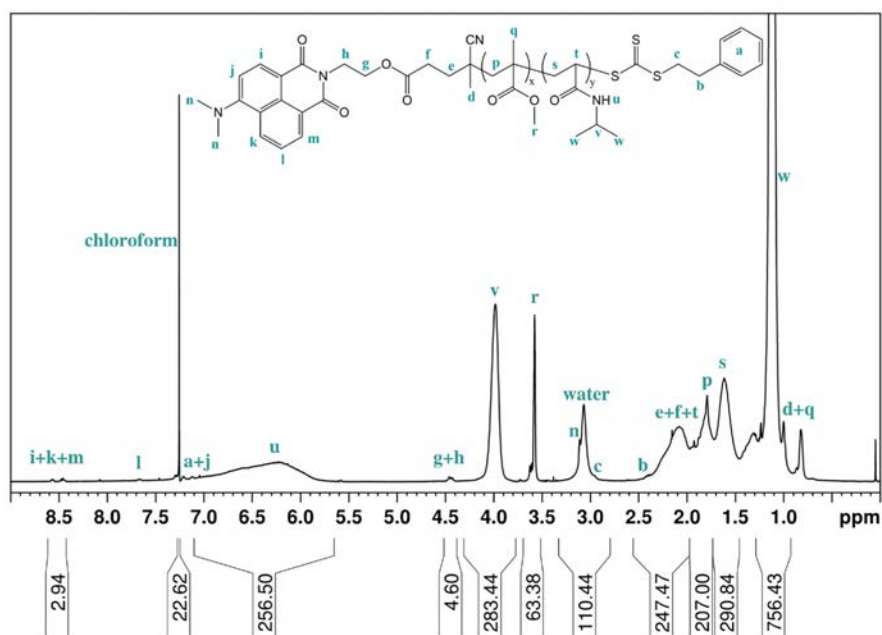
Figure A 30. ^{1}H NMR spectrum of PMMA$_{17}$-*b*-PNIPAM$_{337}^B$ (reaction index 13) in CDCl$_3$.
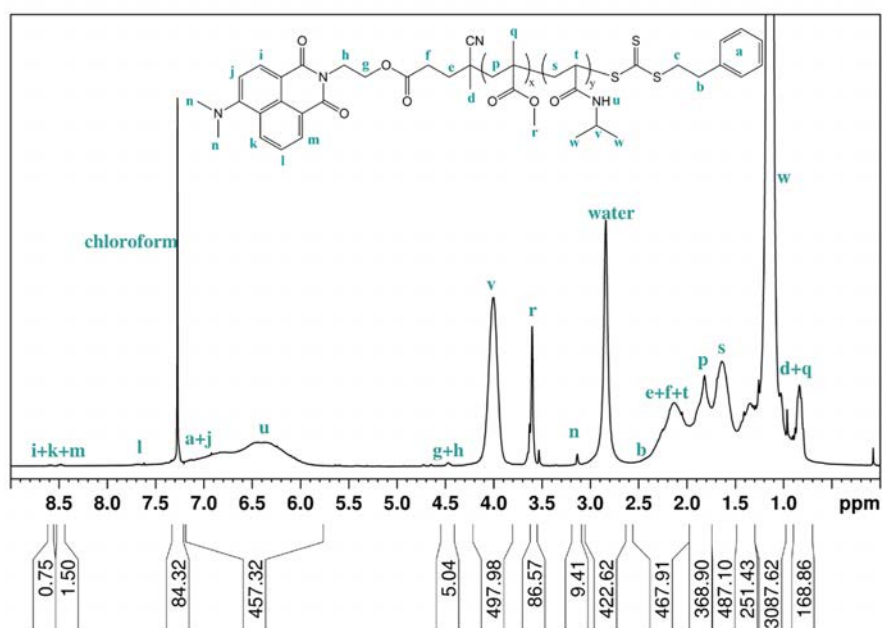
Figure A 31. ^{1}H NMR spectrum of PMMA$_{20}$-*b*-PNIPAM$_{554}$^{B} (reaction index 14) in CDCl$_3$.
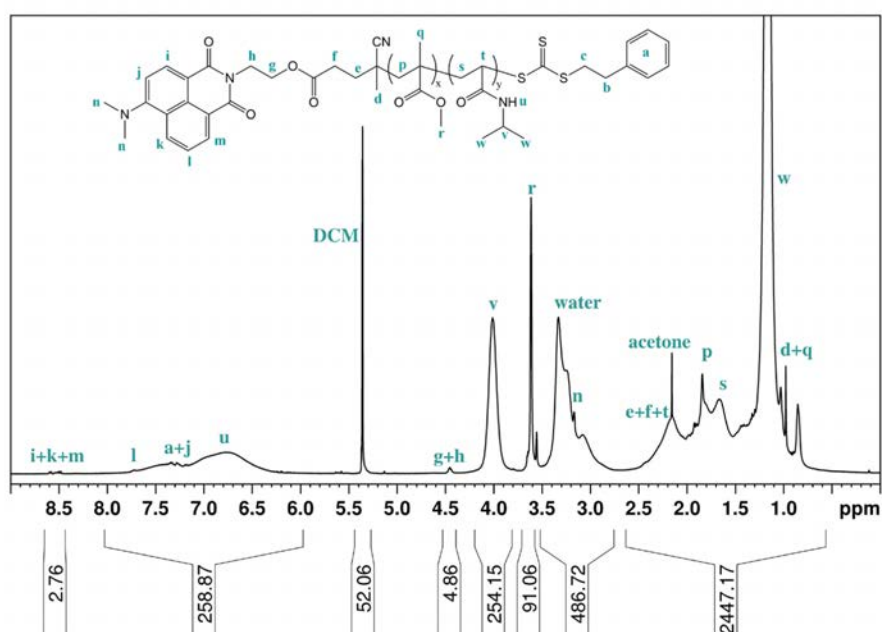
Figure A 32. ^{1}H NMR spectrum of PMMA$_{24}$-*b*-PNIPAM$_{379}$^{B} (reaction index 15) in DCM-d$_2$.
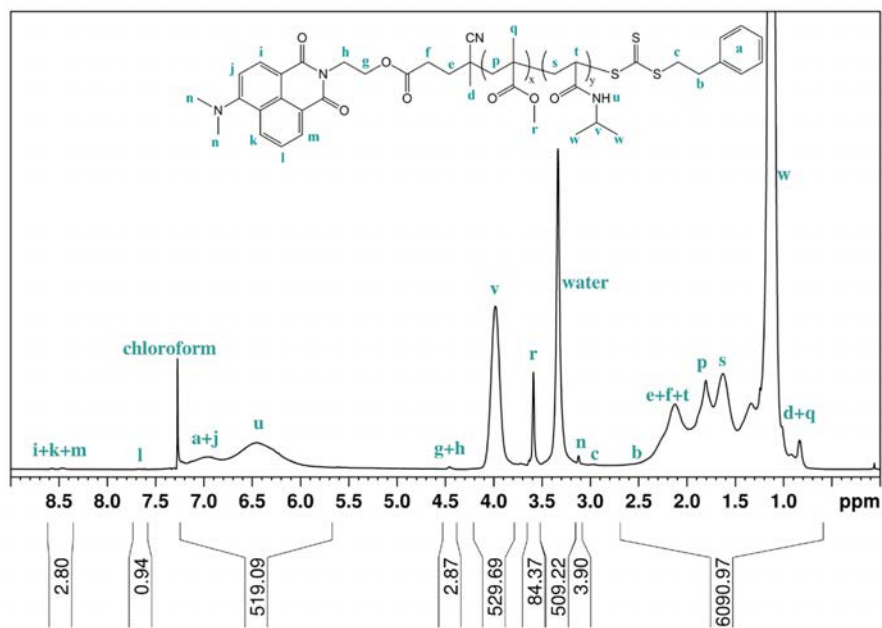
Figure A 33. ^{1}H NMR spectrum of PMMA$_{27}$-*b*-PNIPAM$_{802}$^{B} (reaction index 16) in CDCl$_3$.
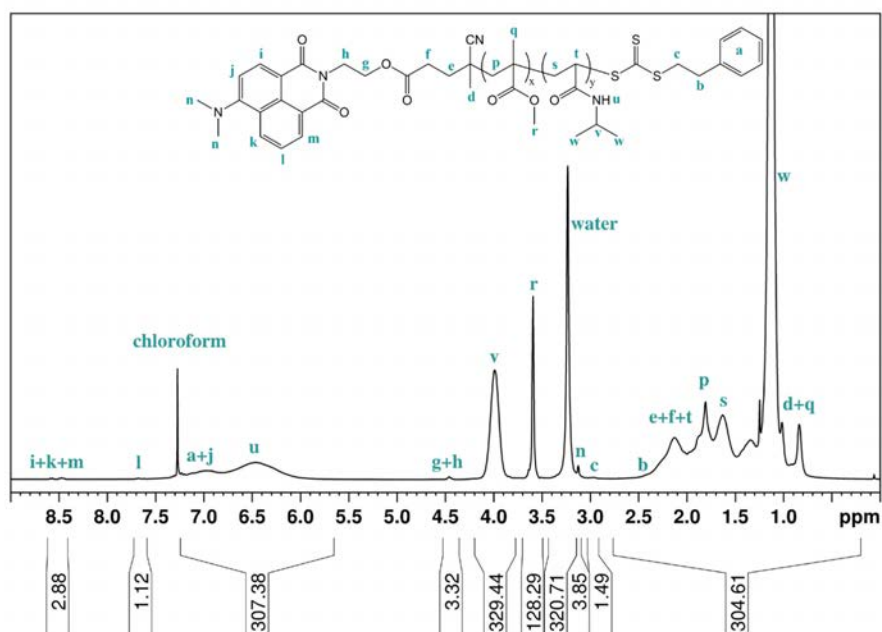
Figure A 34. ^{1}H NMR spectrum of PMMA$_{41}$-*b*-PNIPAM$_{456}$^{B} (reaction index 17) in CDCl$_3$.
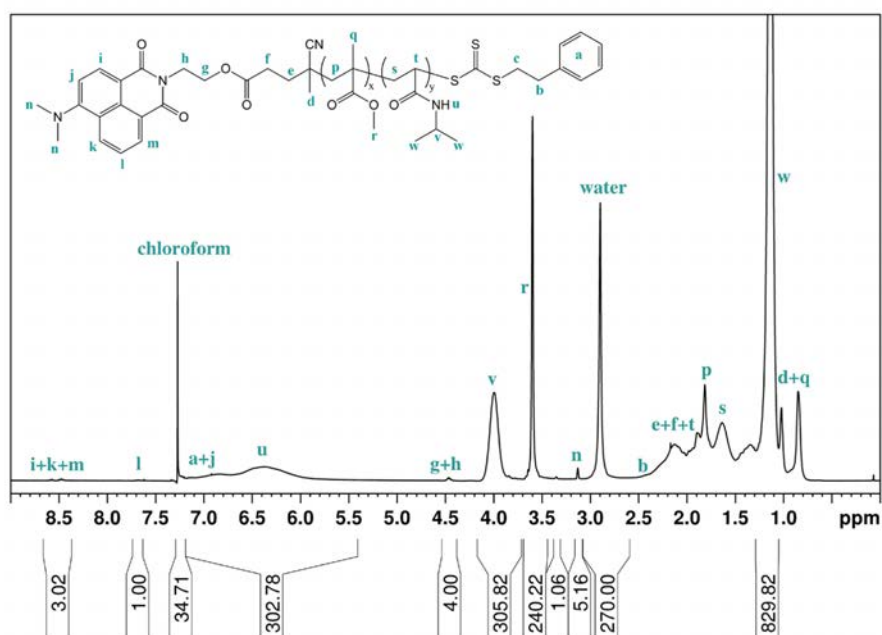
Figure A 35. ^{1}H NMR spectrum of PMMA$_{75}$-*b*-PNIPAM$_{366}^{B}$ (reaction index 18) in CDCl$_3$.

PNIPMAM Homopolymers and Copolymers
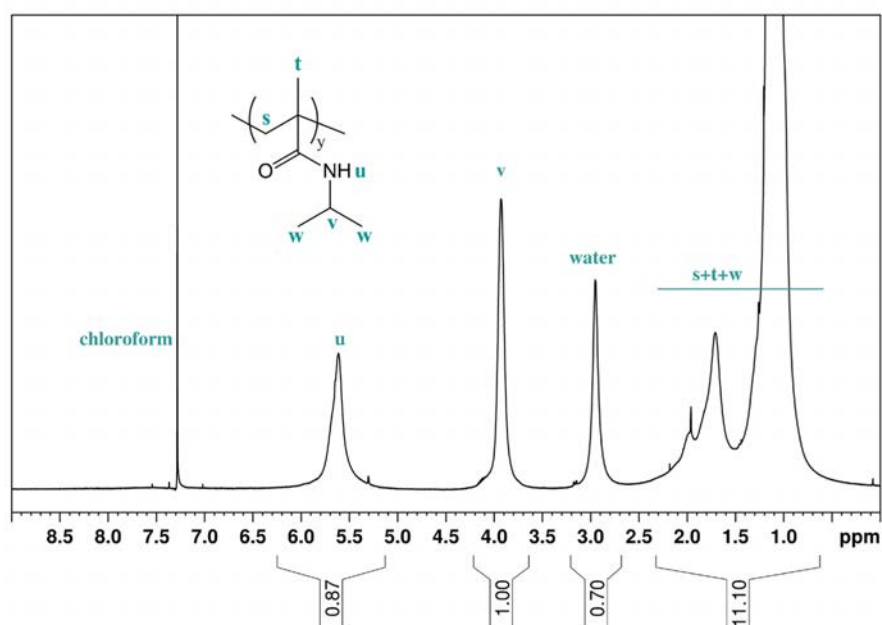
Figure A 36. ^{1}H NMR spectrum of PNIPMAM$_{682}$ (reaction index 45) in CDCl$_3$.
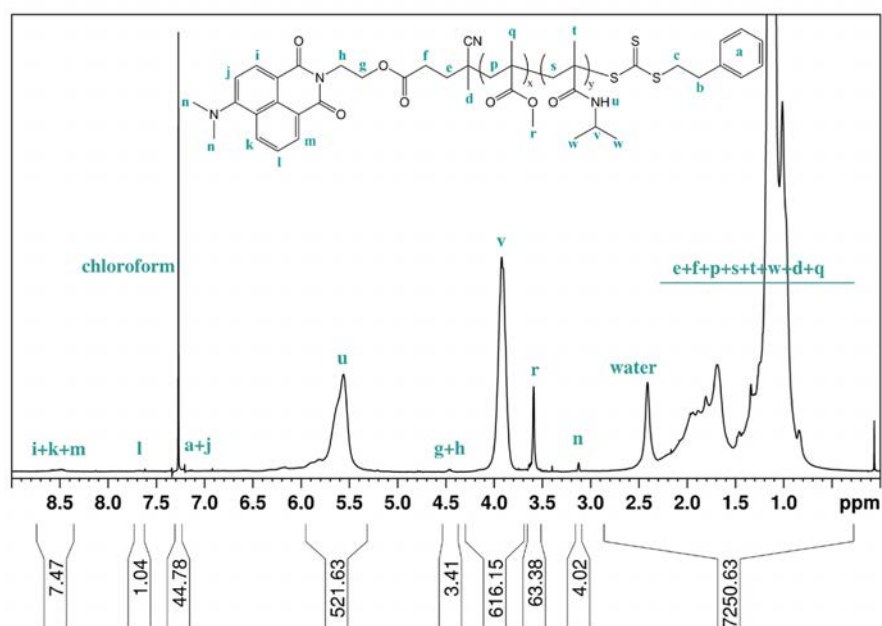
Figure A 37. ^{1}H NMR spectrum of PMMA$_{17}$-*b*-PNIPMAM$_{145}$^{B} (reaction index 52) in CDCl$_3$.
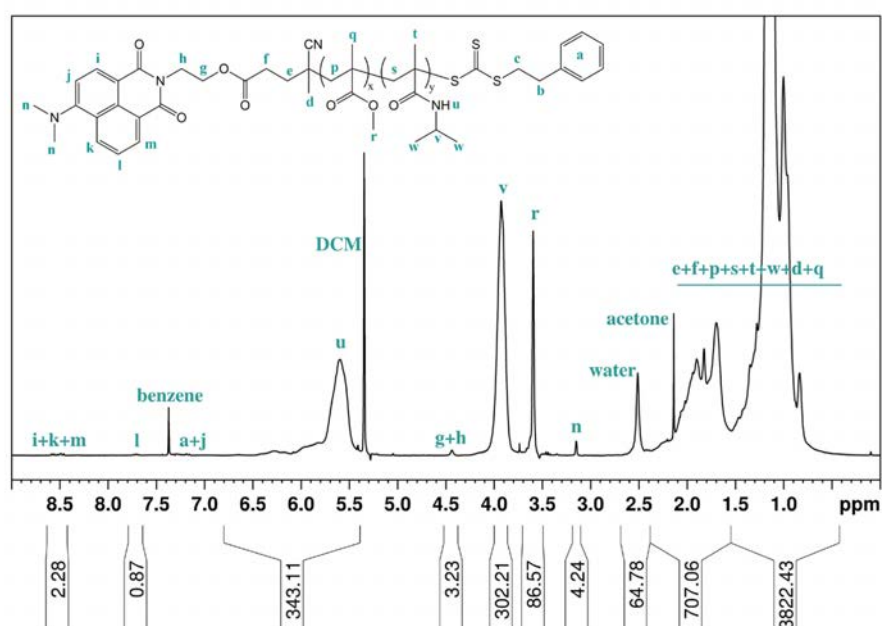
Figure A 38. ^{1}H NMR spectrum of PMMA$_{20}$-*b*-PNIPMAM$_{146}$^{B} (reaction index 53) in DCM-d$_2$.
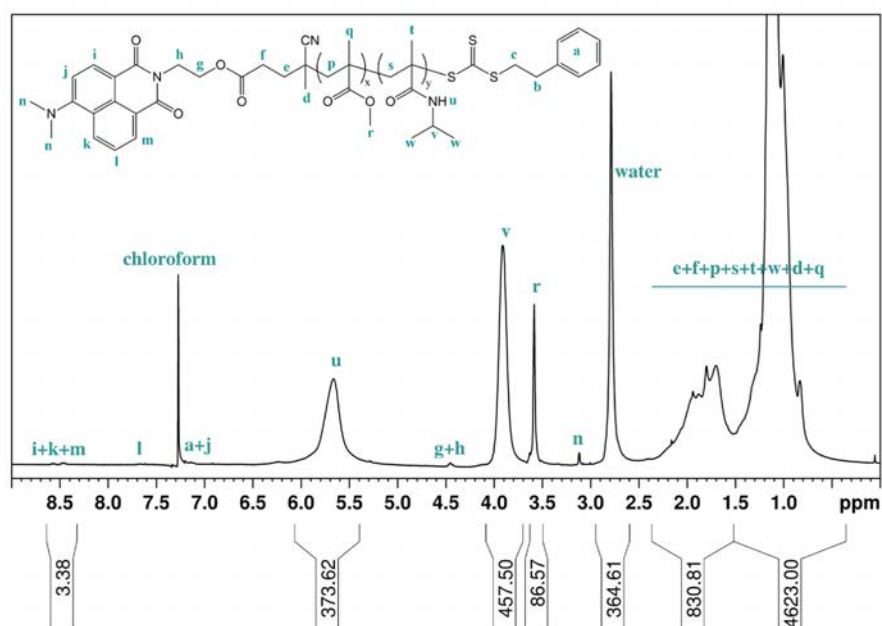
Figure A 39. ^{1}H NMR spectrum of PMMA$_{20}$-*b*-PNIPMAM$_{242}{}^B$ (reaction index 54) in CDCl$_3$.
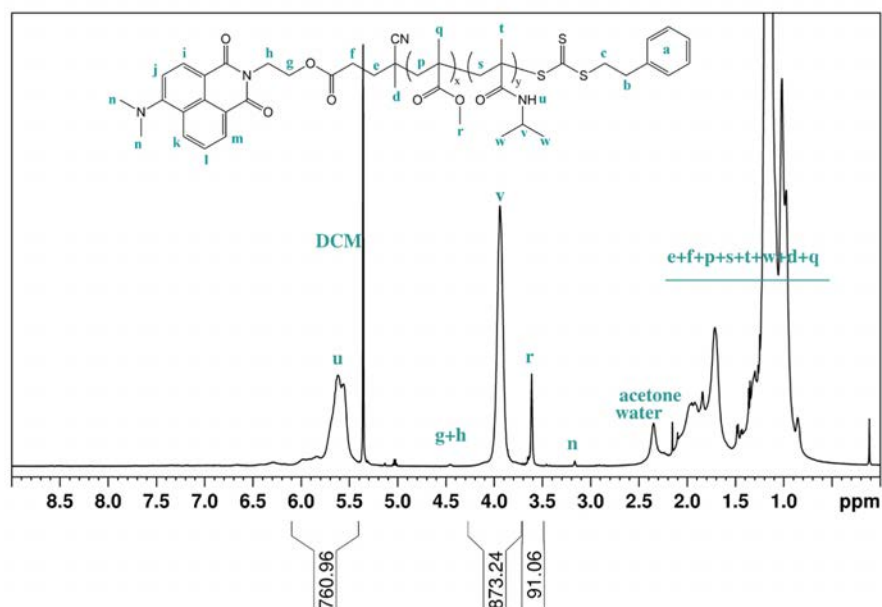
Figure A 40. ^{1}H NMR spectrum of PMMA$_{24}$-*b*-PNIPMAM$_{443}{}^B$ (reaction index 55) in DCM-d$_2$.
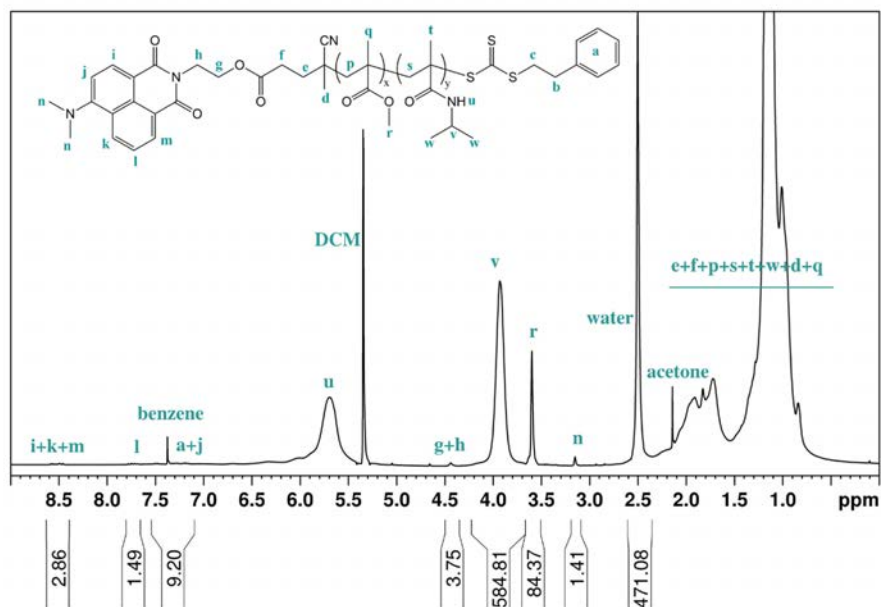
Figure A 41. ^{1}H NMR spectrum of PMMA$_{27}$-*b*-PNIPMAM$_{248}$^{B} (reaction index 56) in DCM-d$_2$.
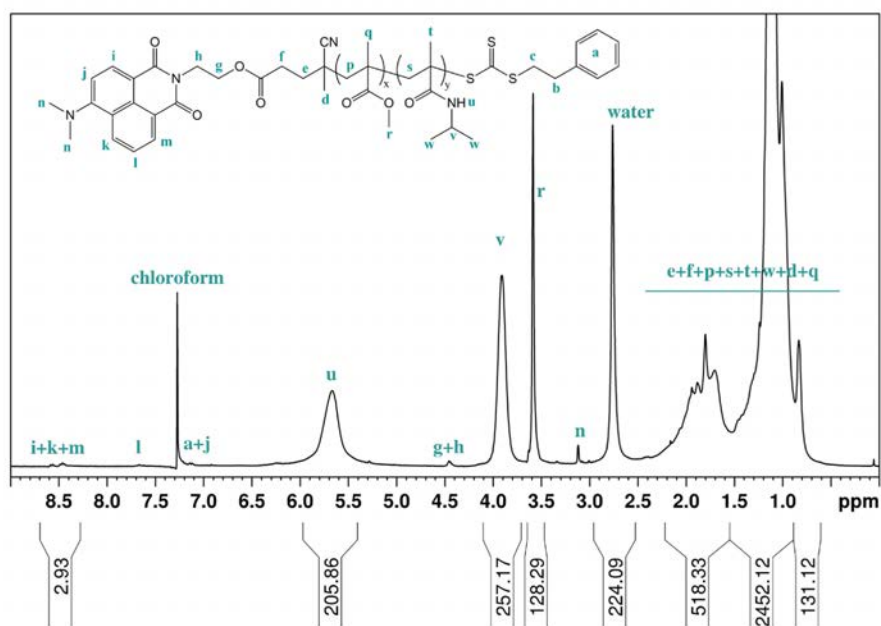
Figure A 42. ^{1}H NMR spectrum of PMMA$_{41}$-*b*-PNIPMAM$_{153}$^{B} (reaction index 57) in CDCl$_3$.
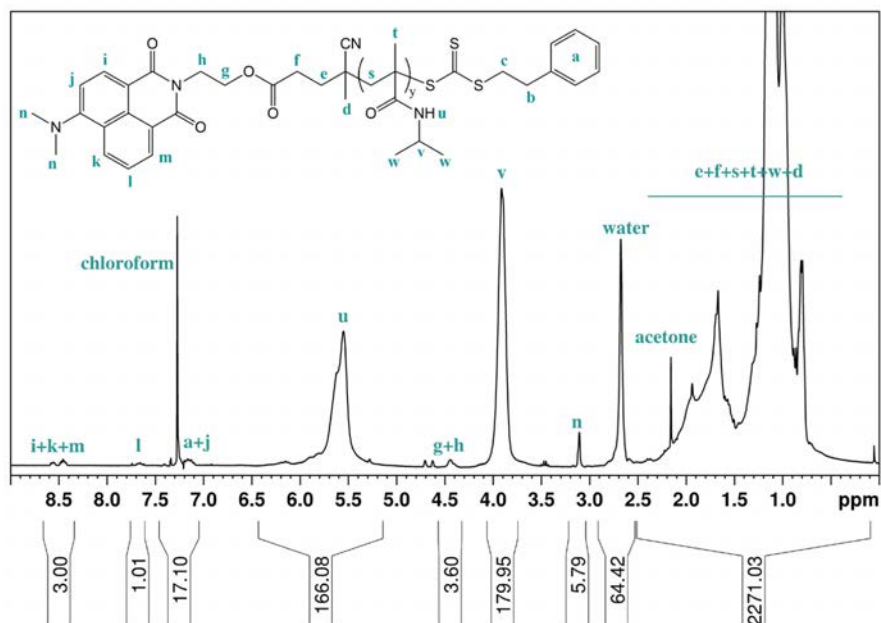
Figure A 43. ^{1}H NMR spectrum of PNIPMAM$_{146}$^{B} (reaction index 59) in CDCl$_{3}$.

PNVIBAM Homopolymers and Copolymers
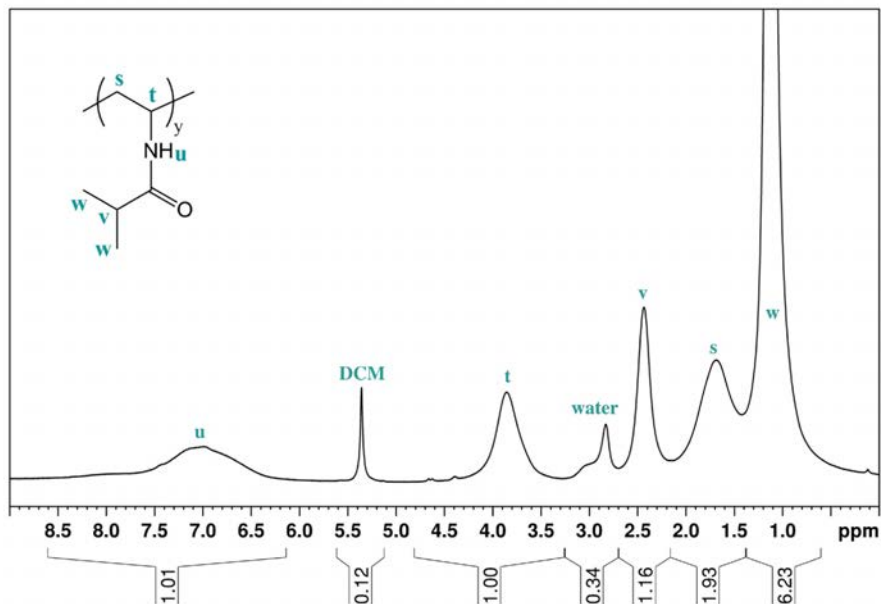
Figure A 44. ^{1}H NMR spectrum of PNVIBAM$_{377}$ (reaction index 60) in DCM-d$_{2}$.
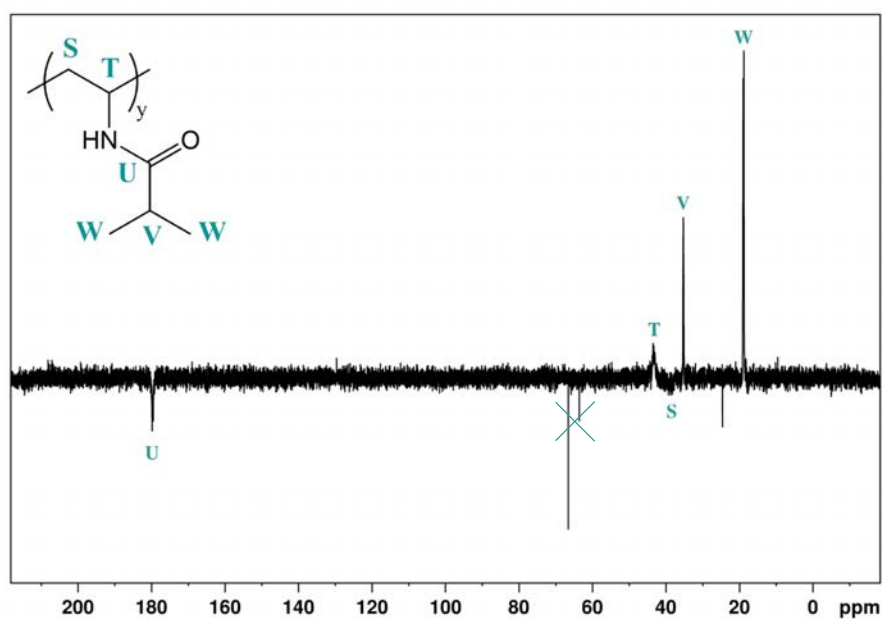
Figure A 45. ^{13}C NMR spectrum of PNVIBAM$_{377}$ (reaction index 60) in D$_2$O. Signals at about 25 ppm, 64 ppm and 67 ppm could not be assigned to any carbon in the structure of the copolymer and are expected to belong to low molar mass impurities, which are overrepresented in the ^{13}C spectrum due to the difference in relaxation times between low molar mass compounds and macromolecules.
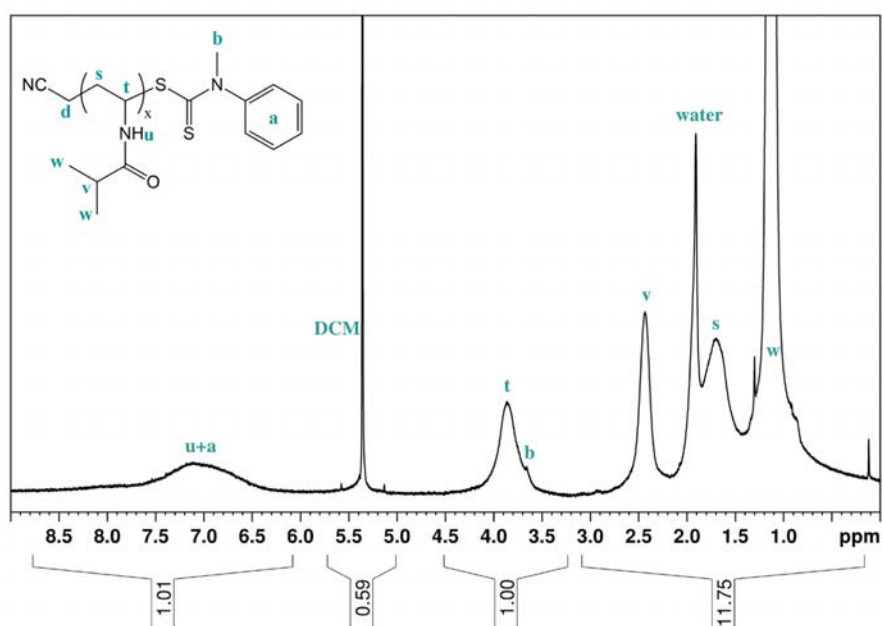
Figure A 46. ^{1}H NMR spectrum of PNVIBAM$_{81}^{D}$ (reaction index 76) in DCM-d$_2$.
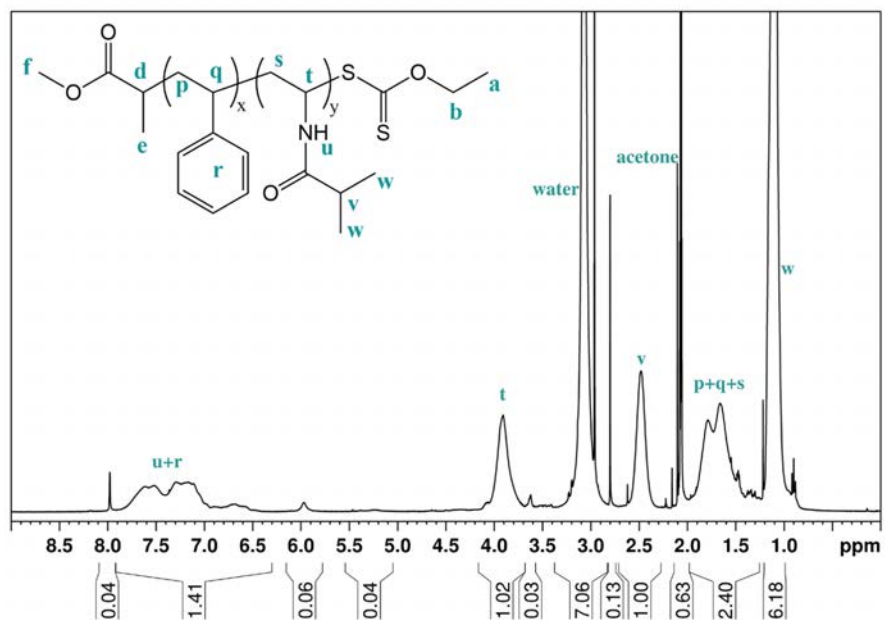
Figure A 47. ^{1}H NMR spectrum of PS$_{13}$-*b*-PNVIBAM$_{44}^C$ (reaction index 78) in acetone-d$_6$.

7.2. UV-Vis Absorption Spectra
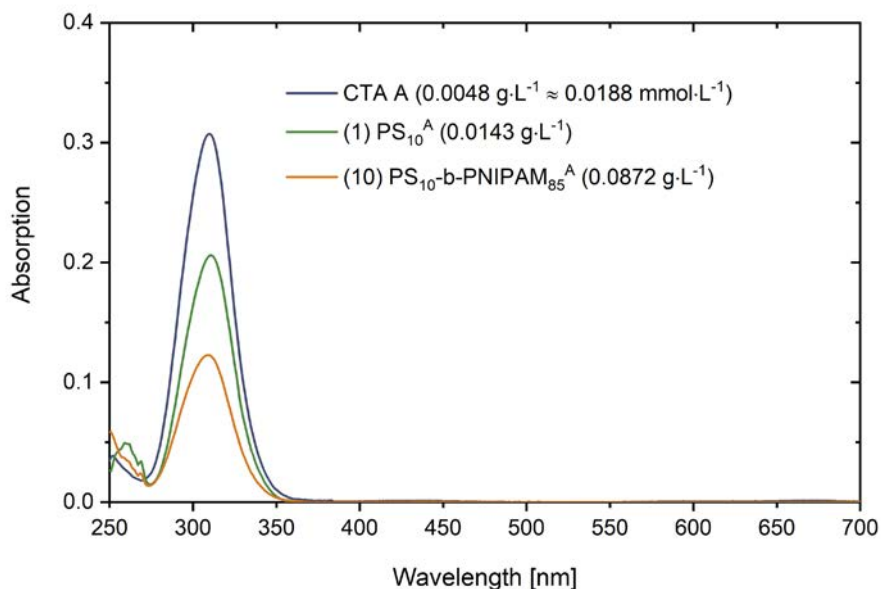
Figure A 48. UV-vis absorbance spectra of the chain transfer agent CTA A, the $PS_{10}{}^A$ macro-CTA (reaction index 1) and the PS_{10}-*b*-$PNIPAM_{85}{}^A$ diblock copolymer (reaction index 10), all in ethyl acetate.
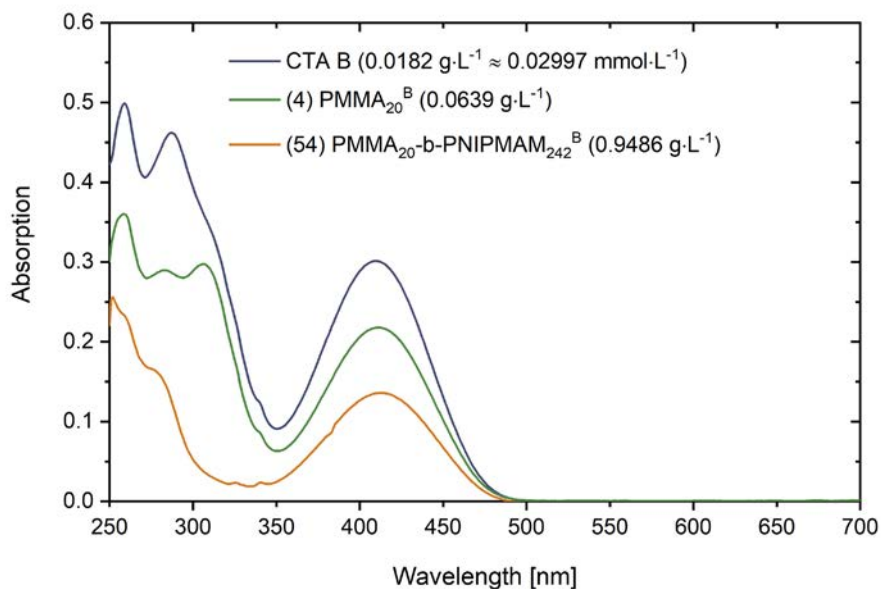
Figure A 49. UV-vis absorbance spectra of the chain transfer agent CTA B, the $PMMA_{20}{}^B$ macro-CTA (reaction index 4) and the $PMMA_{20}$-*b*-$PNIPMAM_{242}{}^B$ diblock copolymer (reaction index 54), all in ethyl acetate.
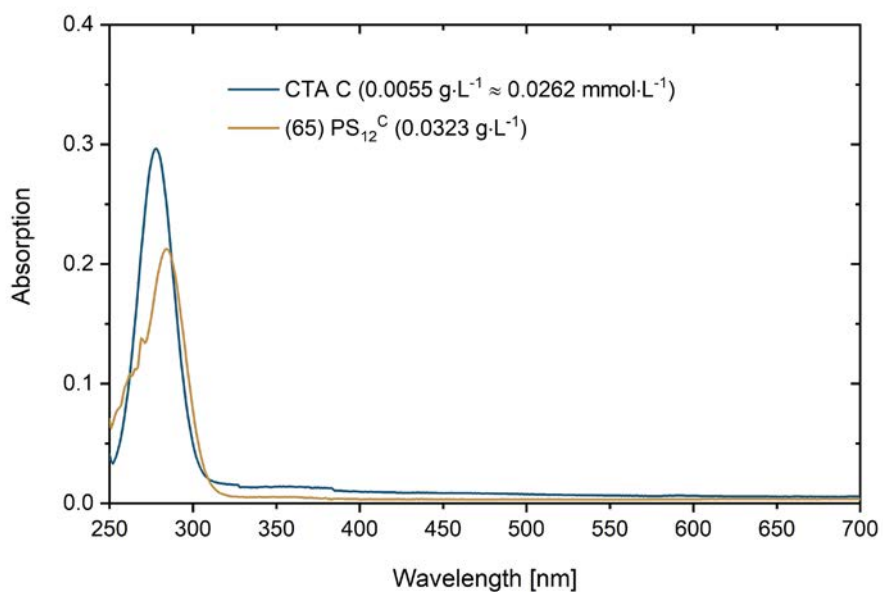
Figure A 50. UV-vis absorbance spectra of the chain transfer agent CTA C and the PS_{13}^{C} macro-CTA (reaction index 65), both in ethyl acetate.
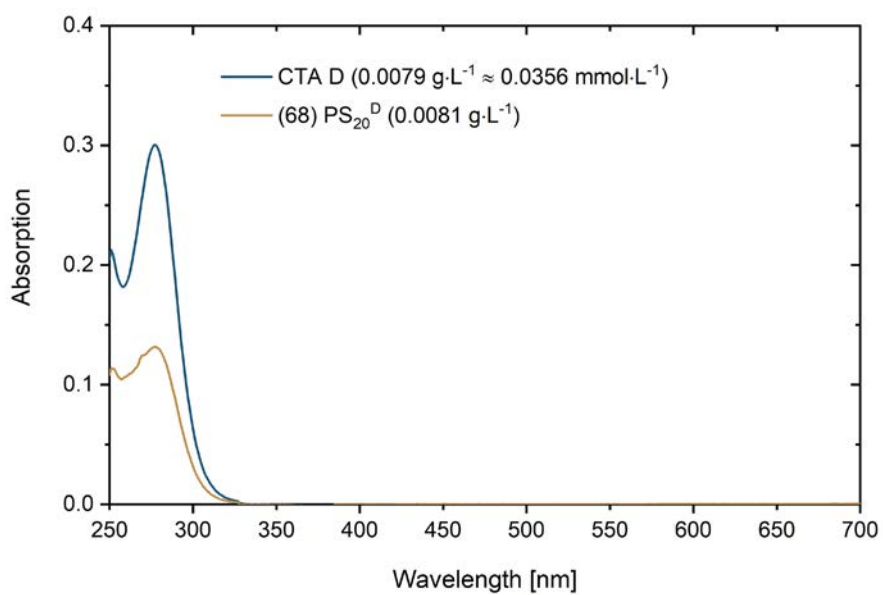
Figure A 51. UV-vis absorbance spectra of the chain transfer agent CTA D and the PS_{20}^{D} macro-CTA (reaction index 68), both in ethyl acetate.
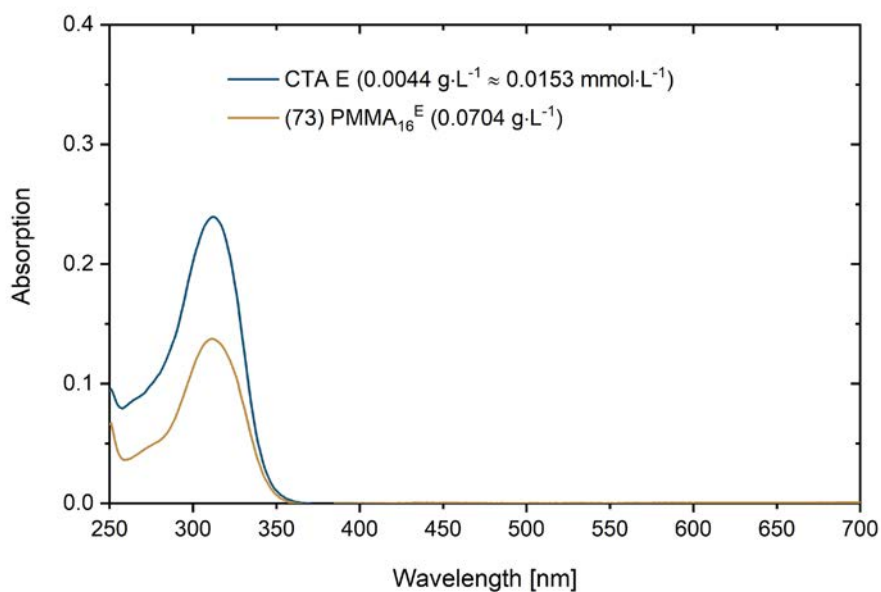
Figure A 52. UV-vis absorbance spectra of the chain transfer agent CTA E and the $PMMA_{19}{}^{E}$ macro-CTA (reaction index 73), both in ethyl acetate.
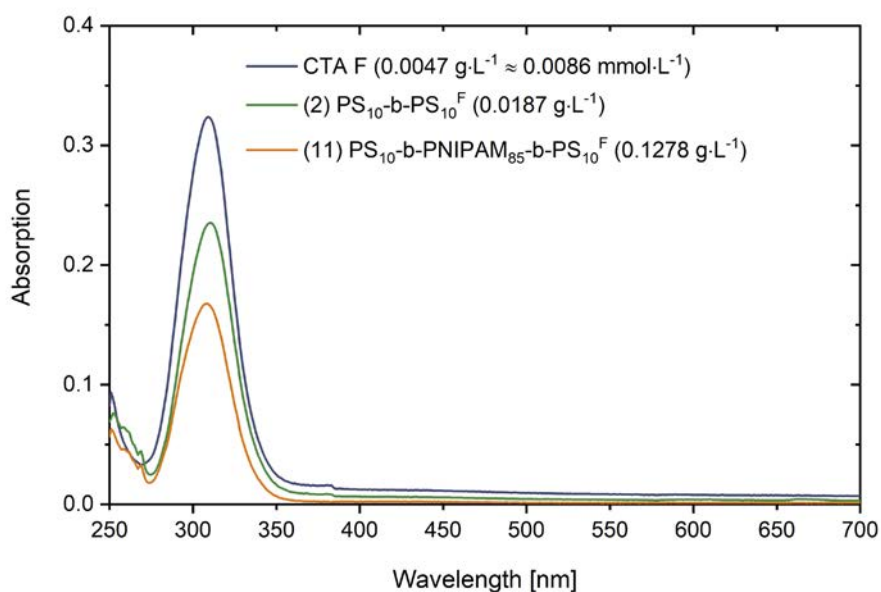
Figure A 53. UV-vis absorbance spectra of the chain transfer agent CTA F, the PS_{10}-*b*-$PS_{10}{}^{F}$ macro-CTA (reaction index 2) and the PS_{10}-*b*-$PNIPAM_{180}$-*b*-$PS_{10}{}^{F}$ triblock copolymer (reaction index 11), all in ethyl acetate.

7.3. SEC Elugrams
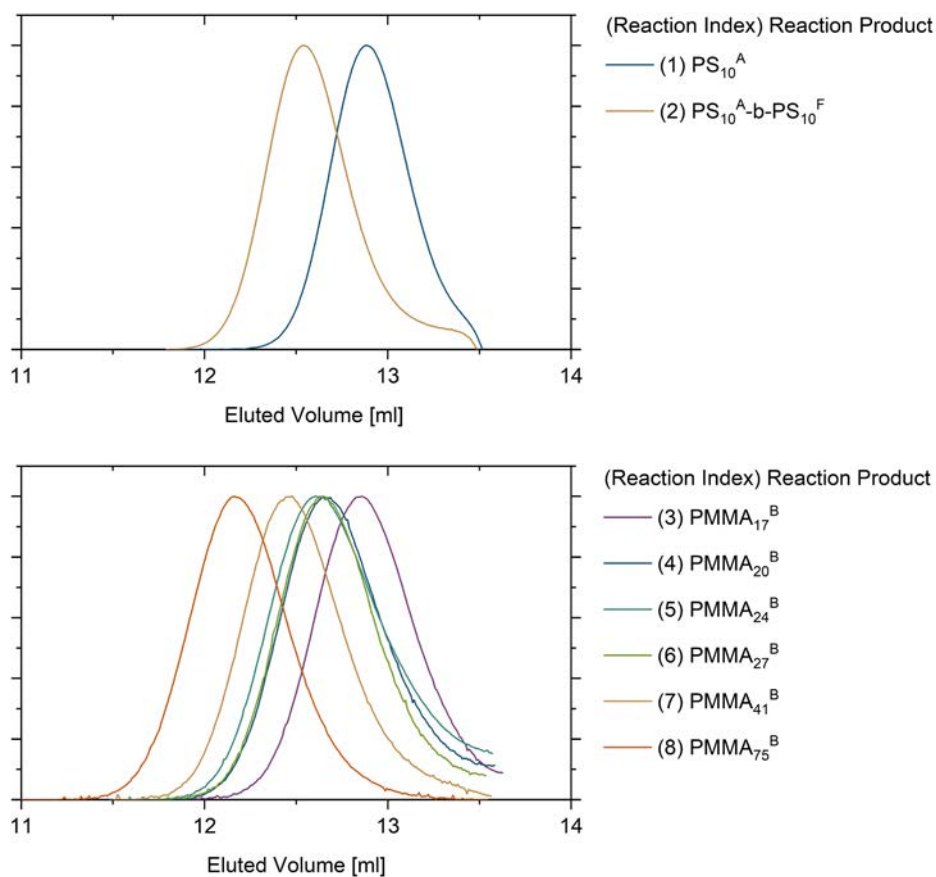
Figure A 54. SEC elugrams of all PS (top) and PMMA (bottom) macro-CTAs obtained with CTAs designed for the polymerization of more activated monomers (MAMs). All SEC were measured in NMP. The curves have been normalized.
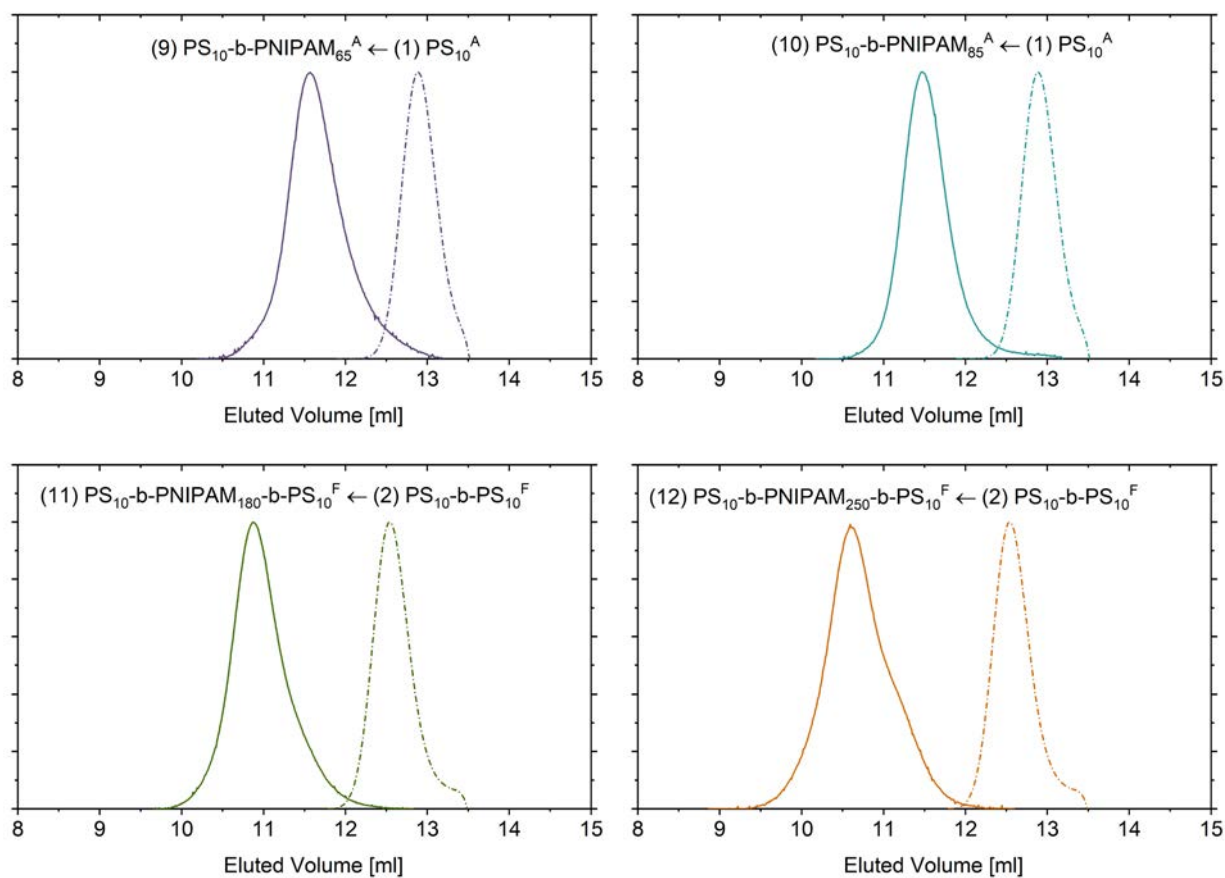
Figure A 55. SEC elugrams of all PS/PNIPAM diblock and triblock copolymers, along with the PS mono- and bifunctional macro-CTAs used as precursor for their synthesis. All SEC were measured in NMP. The curves have been normalized. The reaction indices are shown in parenthesis before the name of each reaction product.
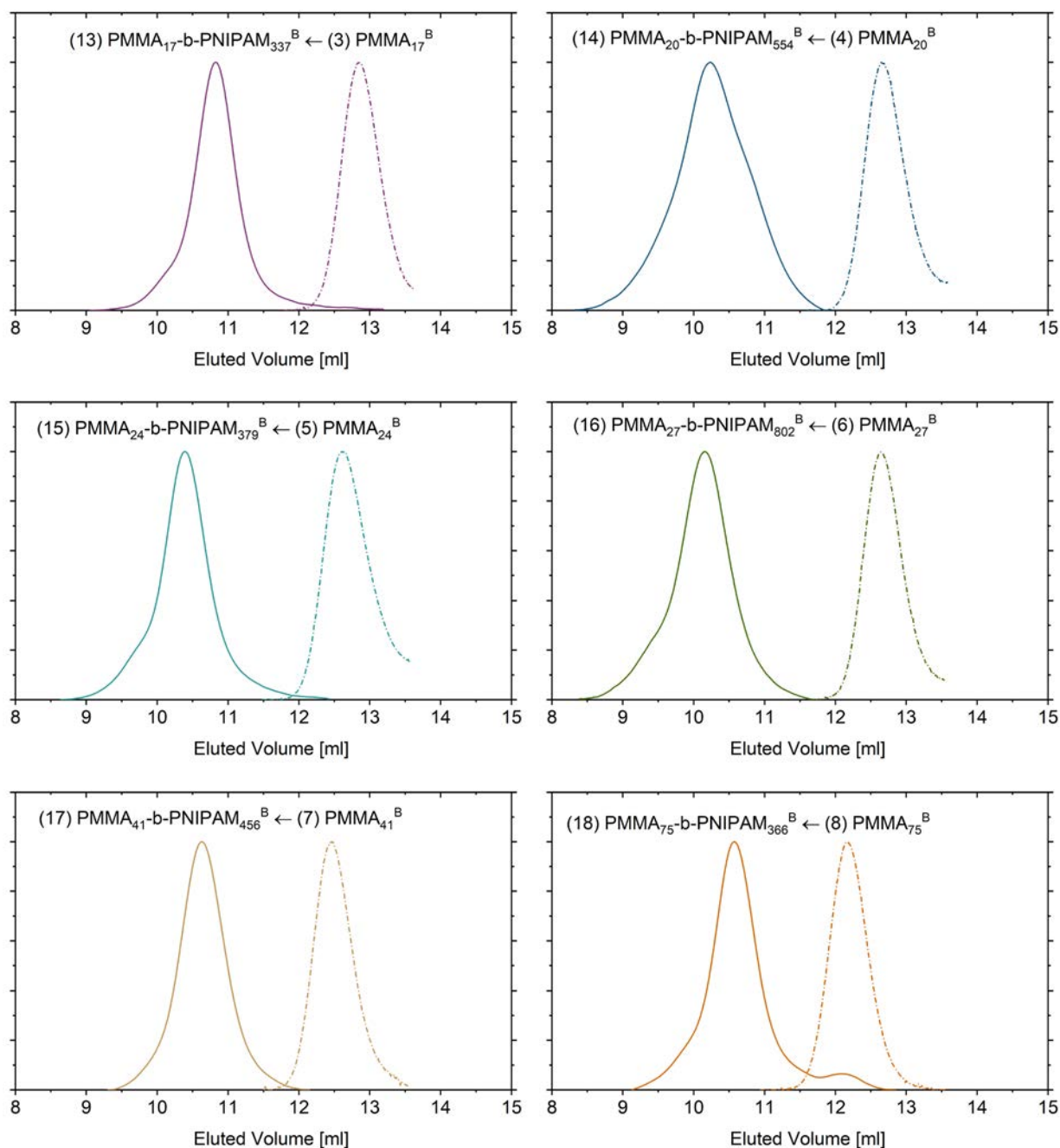
Figure A 56. SEC elugrams of all PMMA-*b*-PNIPAM copolymers, along with the PMMA monofunctional macro-CTAs used as precursor for their synthesis. All SEC were measured in NMP. The curves have been normalized. The reaction indices are shown in parenthesis before the name of each reaction product.
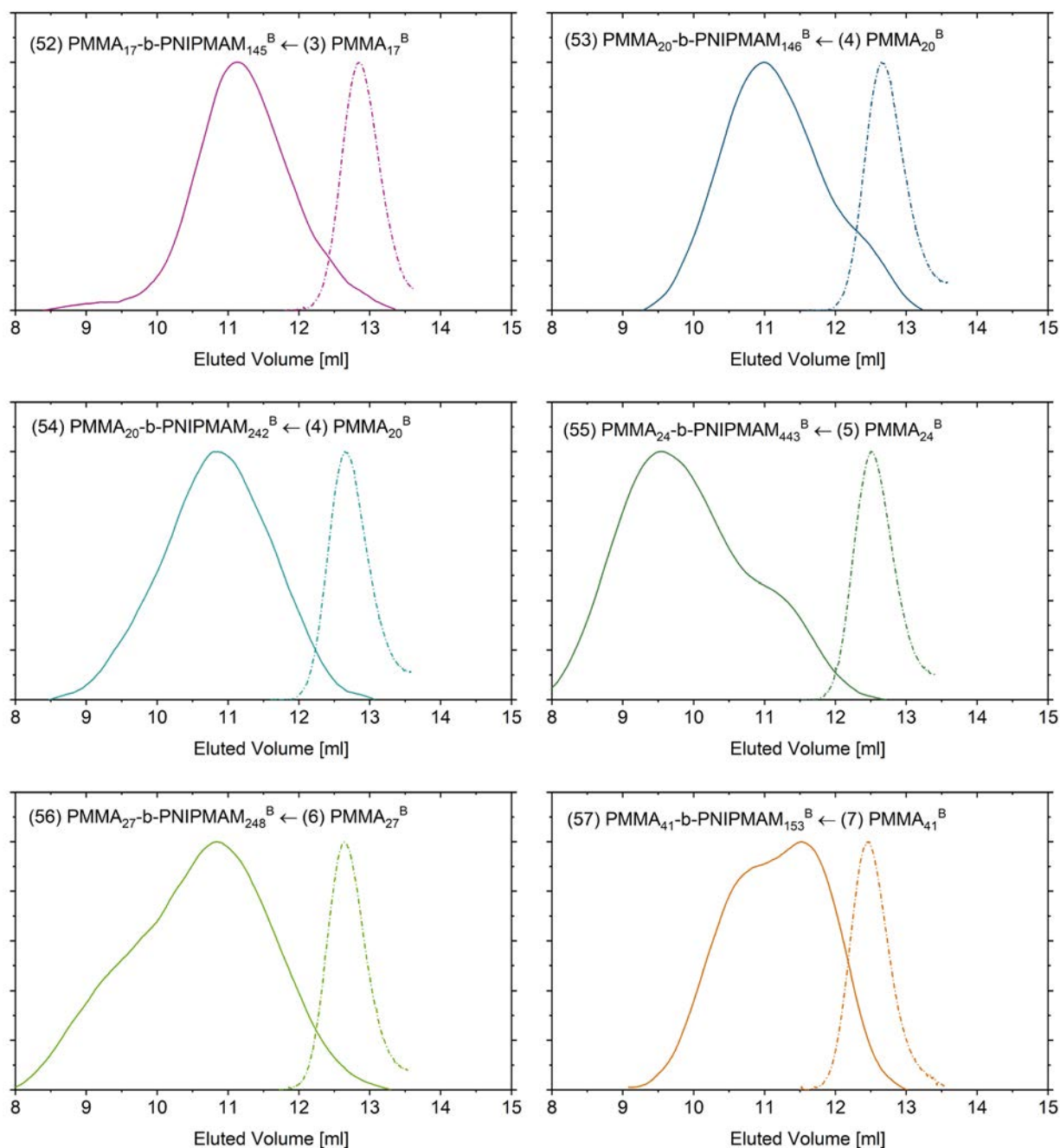
Figure A 57. SEC elugrams of all PMMA-*b*-PNIPMAM copolymers, along with the PMMA macro-CTAs used as precursor for their synthesis. All SEC were measured in NMP. The curves have been smoothed and normalized.
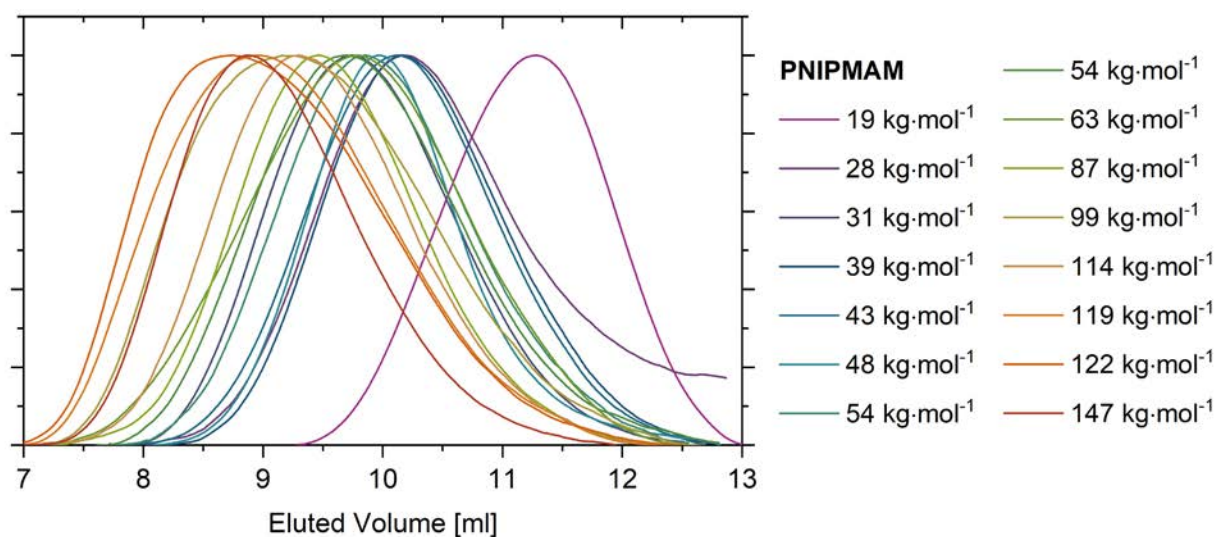
Figure A 58. SEC elugrams of PNIPMAM homopolymers with various molar masses, as described in section 4.1.1. All SEC were measured in NMP. The curves have been smoothed and normalized.
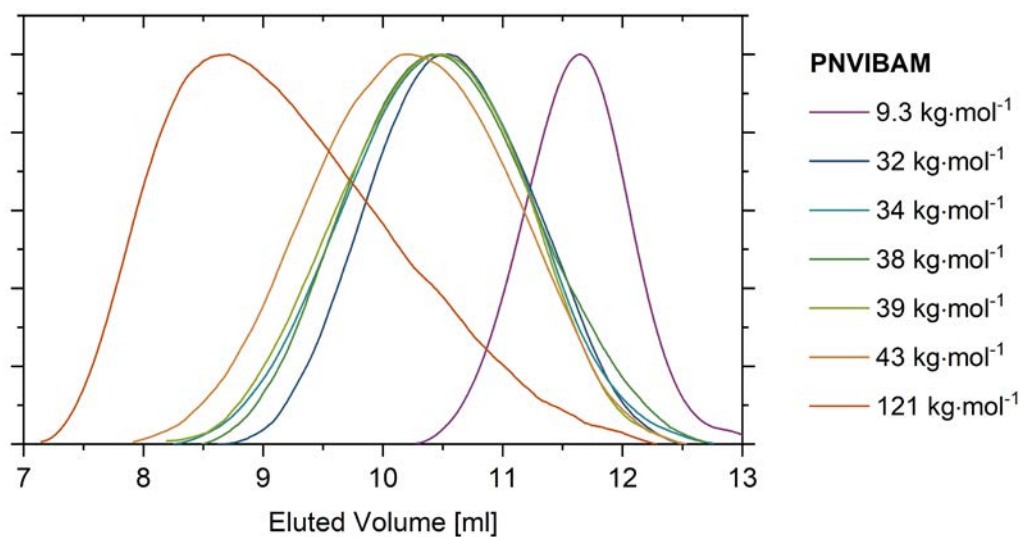
Figure A 59. SEC elugrams of PNVIBAM homopolymers with various molar masses, as described in section 4.1.1. All SEC were measured in NMP. The curves have been smoothed and normalized.
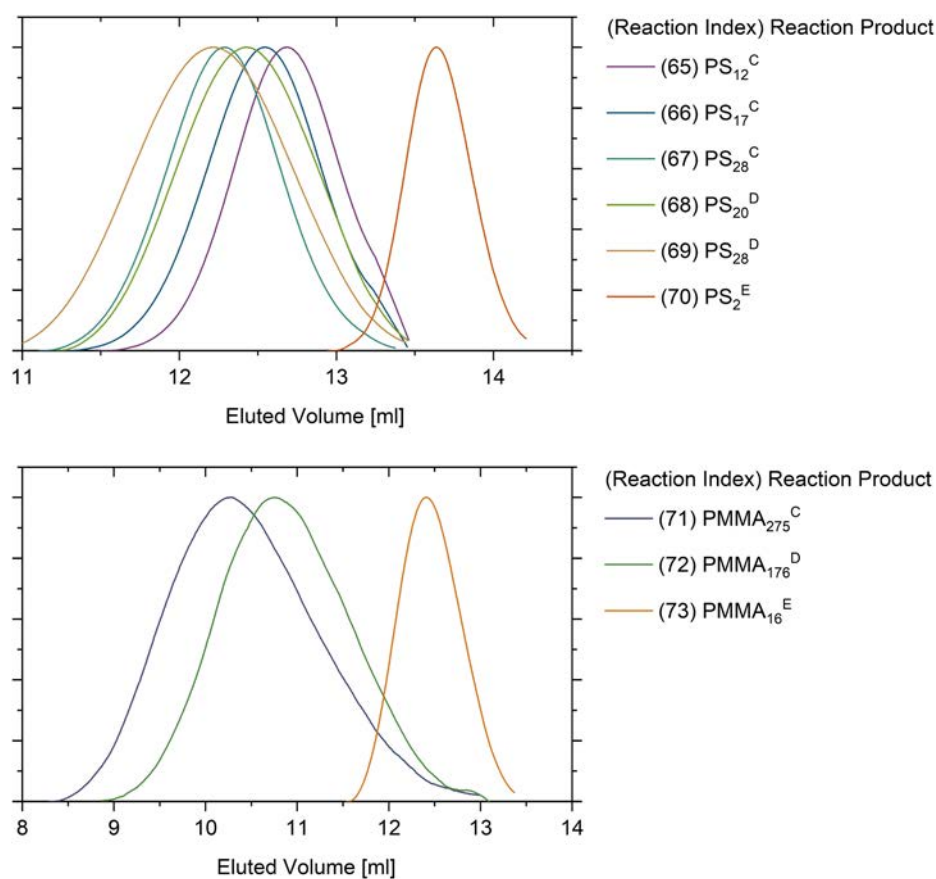
Figure A 60. SEC elugrams of all PS (top) and PMMA (bottom) macro-CTAs obtained with CTAs designed for the polymerization of less activated monomers (LAMs). All SEC were measured in NMP. The curves have been smoothed and normalized.
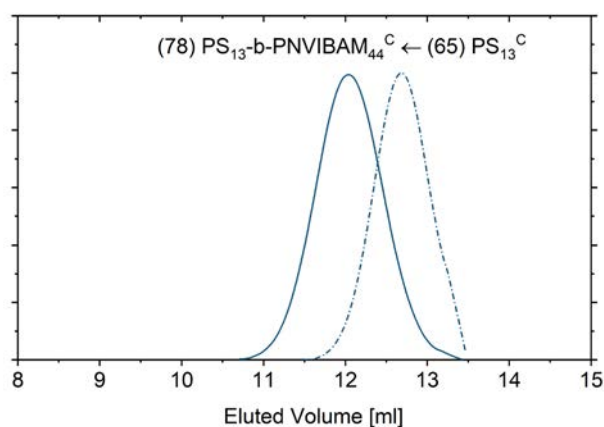
Figure A 61. SEC elugrams of PS₁₃-*b*-PNVIBAM₄₄ᶜ copolymer and PS₁₃ᶜ macro-CTA precursor used for its polymerization. All SEC were measured in NMP. The curves have been smoothed and normalized.
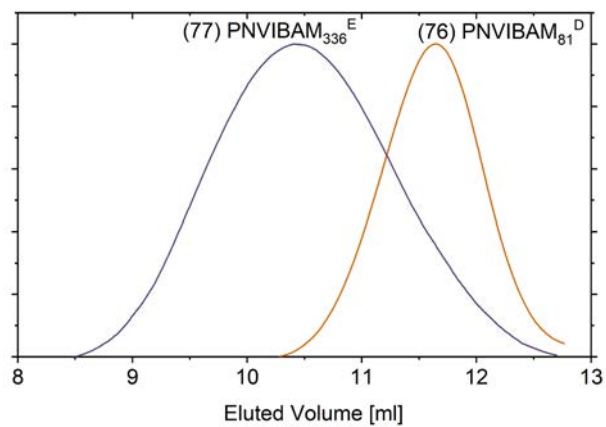
Figure A 62. SEC elugrams of PNVIBAM homopolymers, obtained by RAFT using CTAs D and E. All SEC were measured in NMP. The curves have been smoothed and normalized.

7.4. FTIR Transmittance Spectra
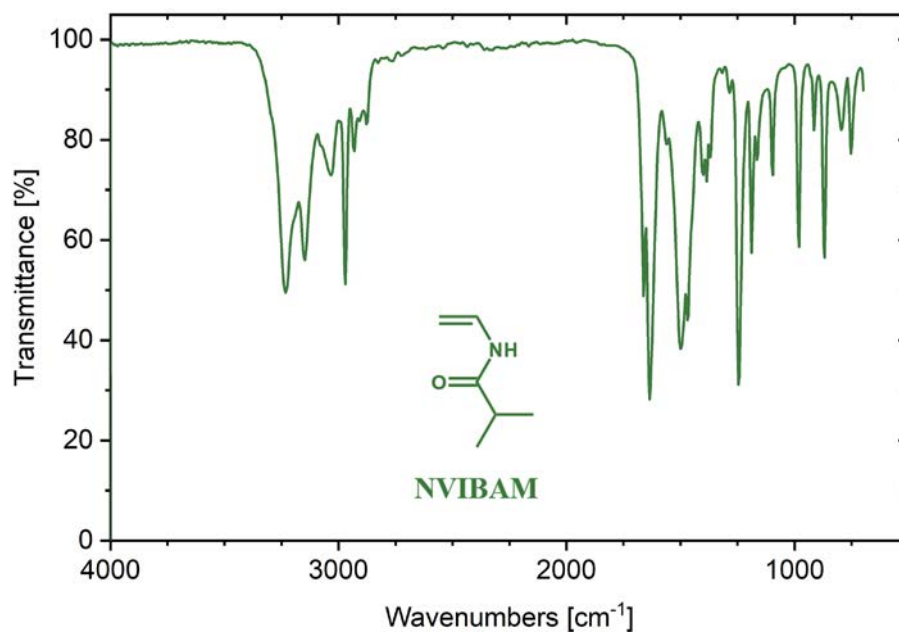
Figure A 63. FTIR transmittance spectra of NVIBAM monomer.
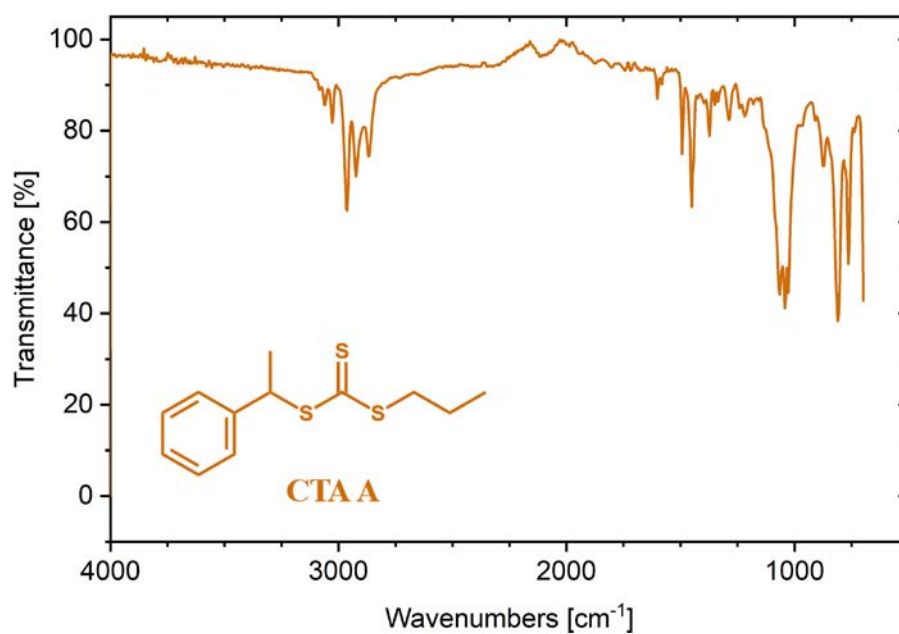
Figure A 64. FTIR transmittance spectra of CTA A.
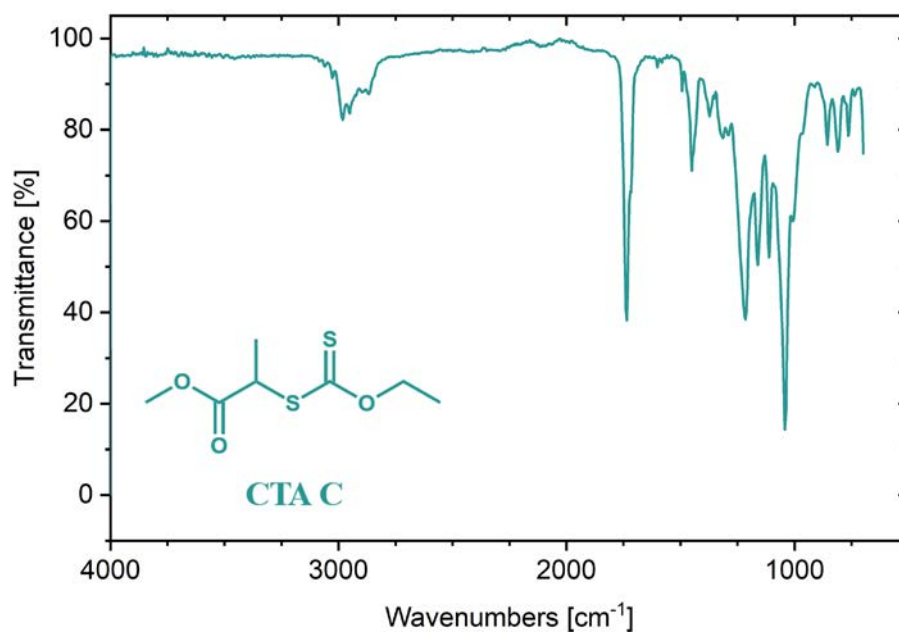
Figure A 65. FTIR transmittance spectra of CTA C.
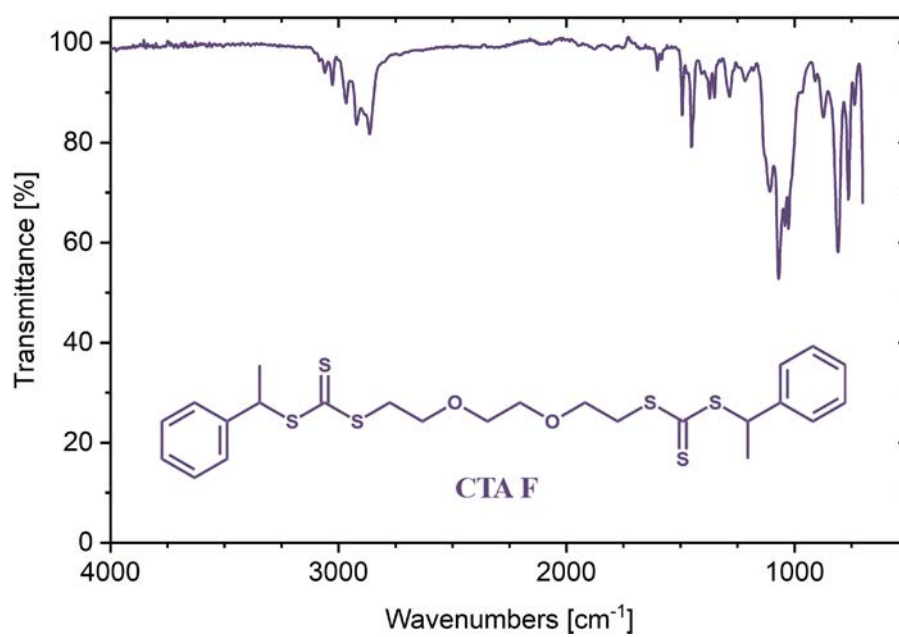
Figure A 66. FTIR transmittance spectra of CTA F.

7.5. DSC & TGA Thermograms
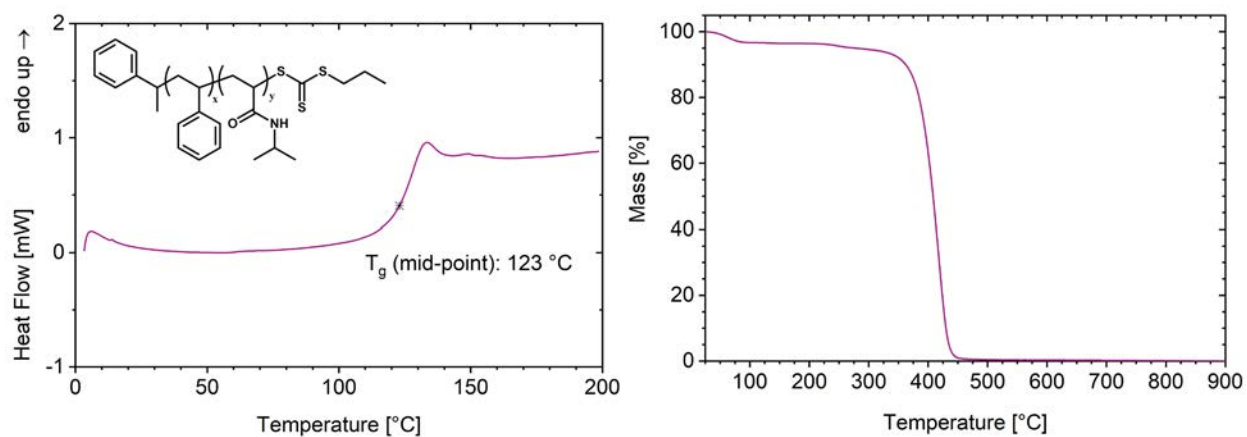
Figure A 67. DSC (on the left, second heating cycle) and TGA (on the right) thermograms (10 K·min^{-1}) of the copolymer PS$_{10}$-b-PNIPAM$_{65}$^{A} (reaction index 9).
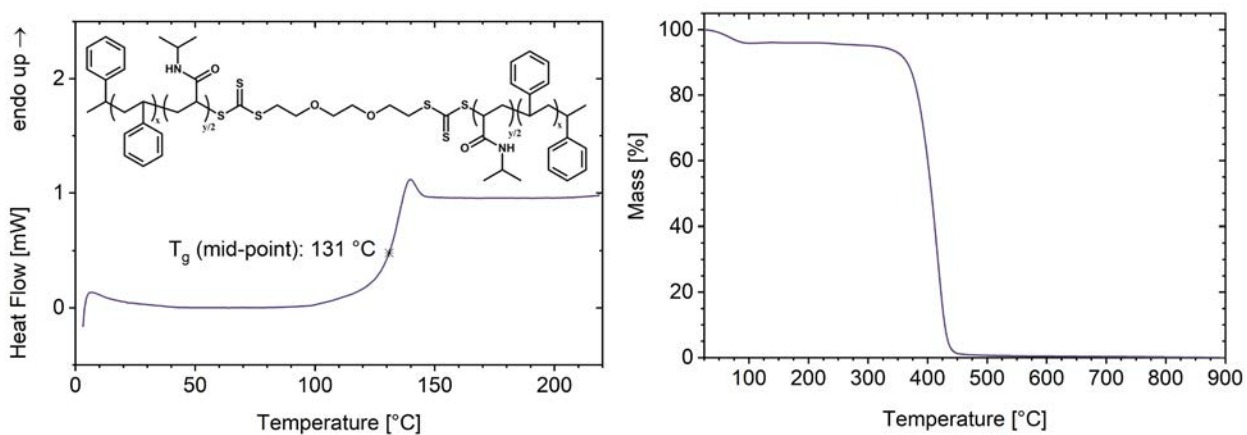
Figure A 68. DSC (on the left, second heating cycle) and TGA (on the right) thermograms (10 K·min^{-1}) of the copolymer PS$_{10}$-b-PNIPAM$_{250}$-b-PS$_{10}$^{F} (reaction index 12).
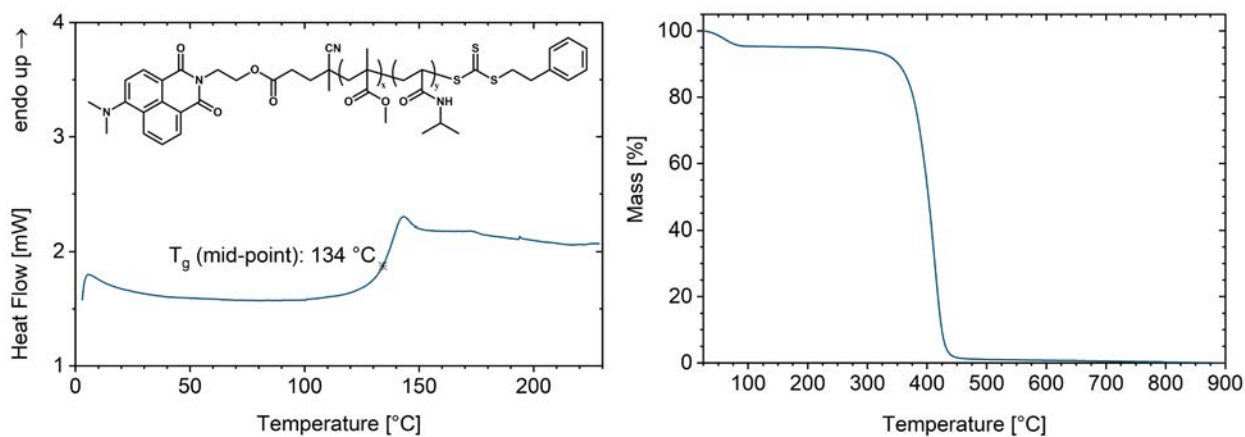
Figure A 69. DSC (on the left, second heating cycle) and TGA (on the right) thermograms (10 K·min⁻¹) of the copolymer PMMA$_{17}$-*b*-PNIPAM$_{337}$^{B} (reaction index 13).
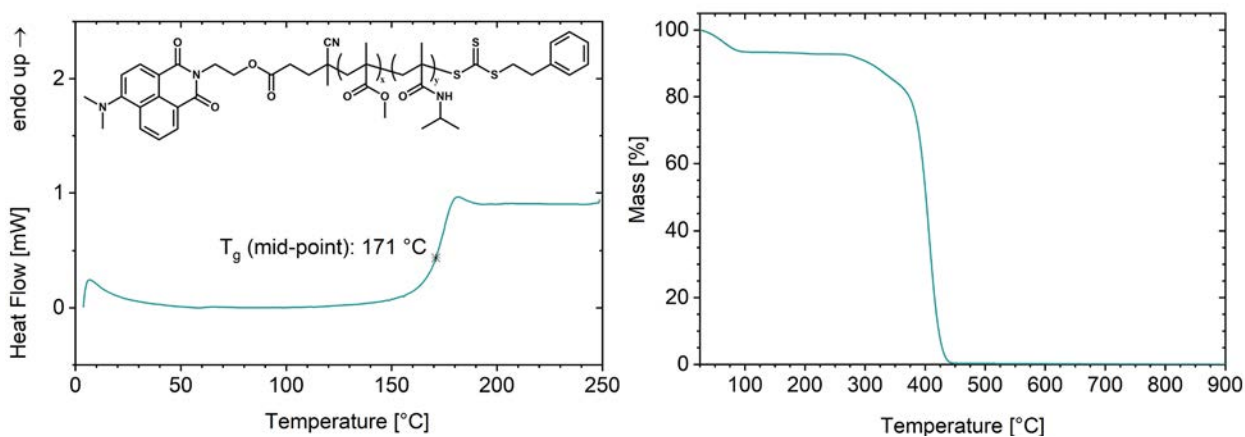
Figure A 70. DSC (on the left, second heating cycle) and TGA (on the right) thermograms (10 K·min⁻¹) of the copolymer PMMA$_{20}$-*b*-PNIPMAM$_{242}$^{B} (reaction index 54).
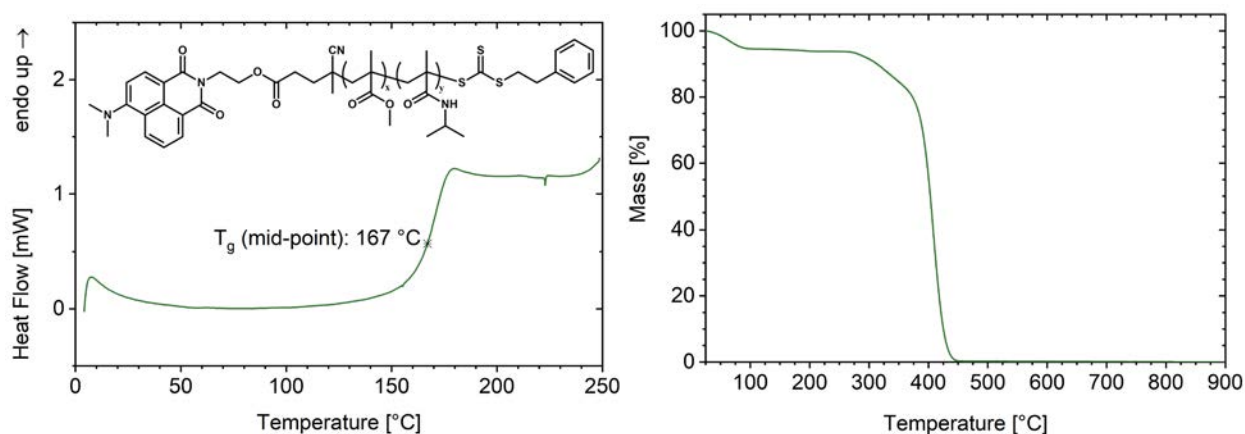
Figure A 71. DSC (on the left, second heating cycle) and TGA (on the right) thermograms (10 K·min⁻¹) of the copolymer PMMA$_{41}$-*b*-PNIPMAM$_{153}$^{B} (reaction index 57).
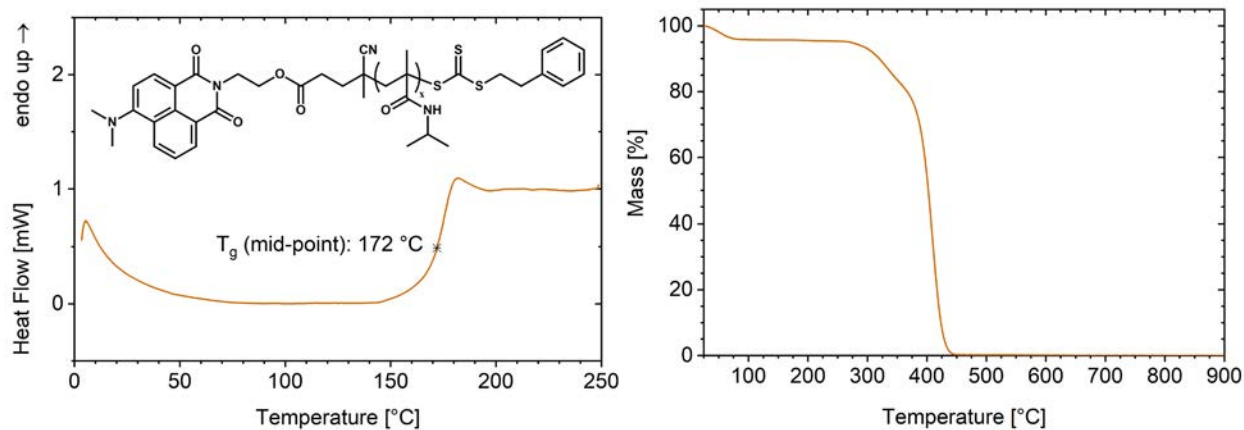
Figure A 72. DSC (on the left, second heating cycle) and TGA (on the right) thermograms (10 K·min^{-1}) of the homopolymer PNIPMAM$_{146}$^{B} (reaction index 59).
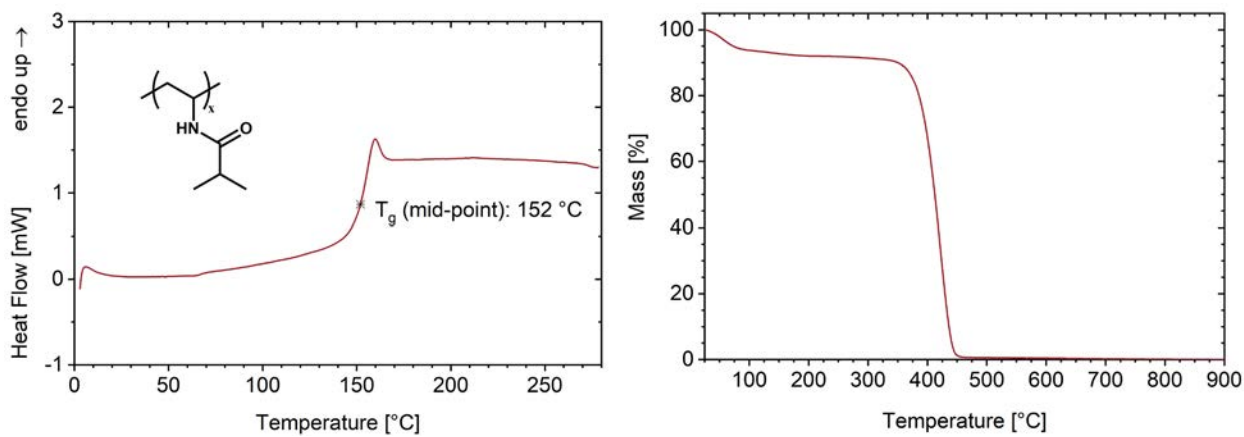
Figure A 73. DSC (on the left, second heating cycle) and TGA (on the right) thermograms (10 K·min^{-1}) of the homopolymer PNVIBAM$_{377}$ (reaction index 60).

7.6. Light Transmittance Curves (Turbidimetry)
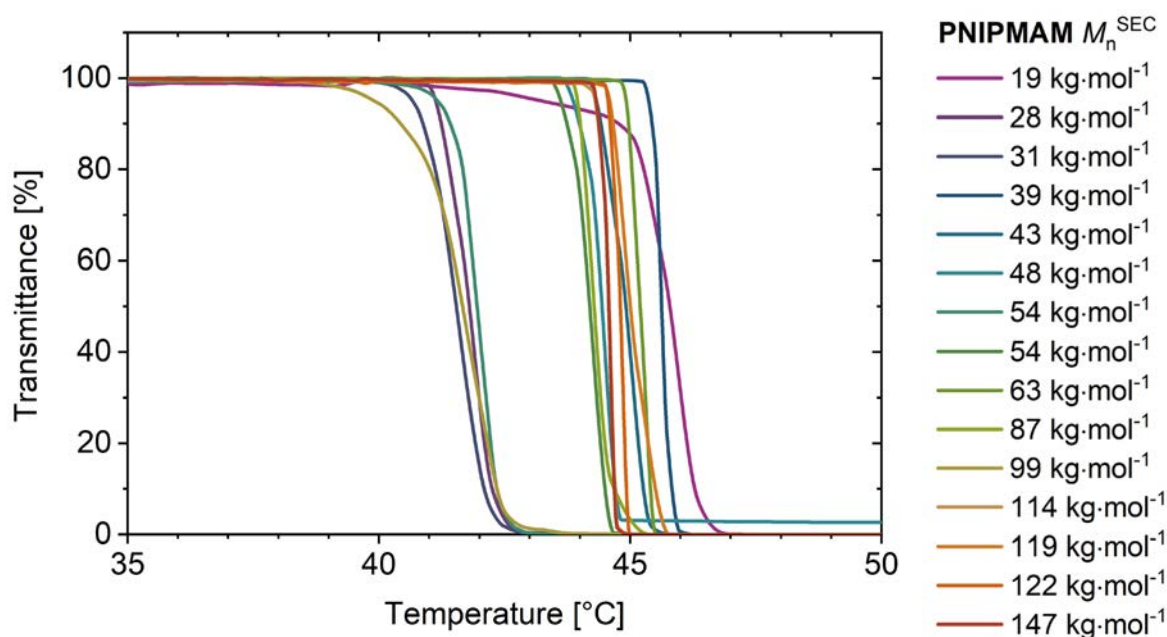
Figure A 74. Normalized turbidimetry heating curves of PNIPMAM homopolymers of different number-average molar masses, measured in water with concentration of 10 g·L^{-1} (see Table 17 and Figure 41, page 104).
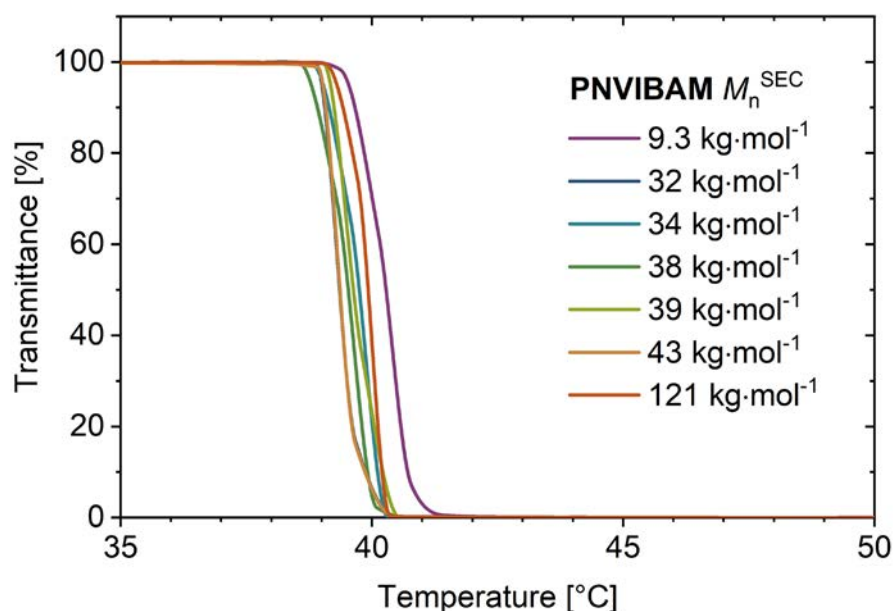
Figure A 75. Normalized turbidimetry heating curves of PNVIBAM homopolymers of different number-average molar masses, measured in water with concentration of 10 g·L^{-1} (see Table 18 and Figure 42, page 106).
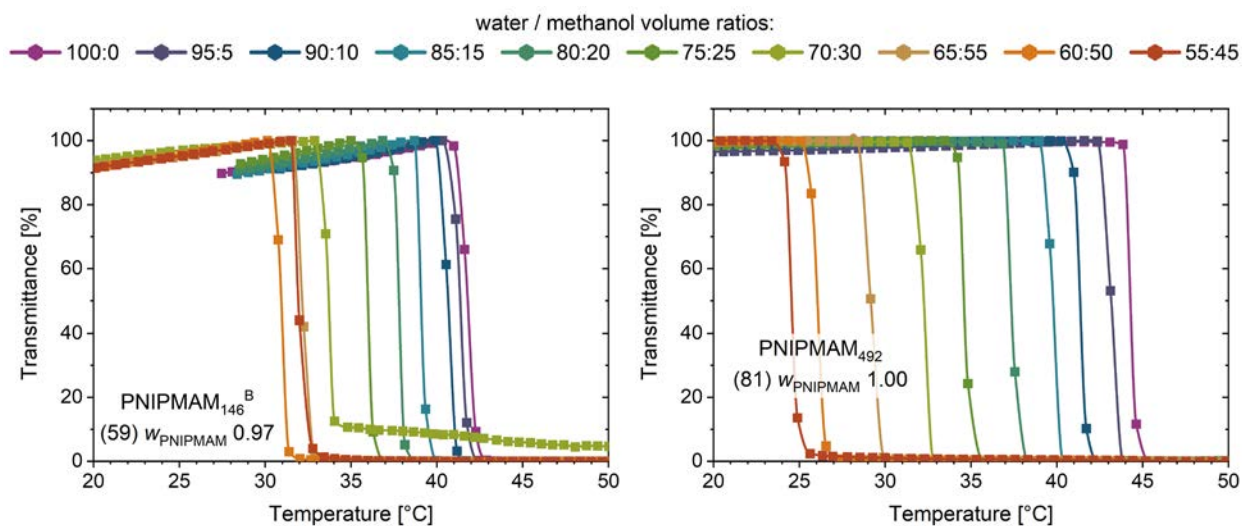
Figure A 76. Normalized turbidimetry heating curves for PNIPMAM homopolymers in water/methanol solutions (polymer concentration 10 g·L^{-1}). Reaction indices are given in parenthesis for each sample.
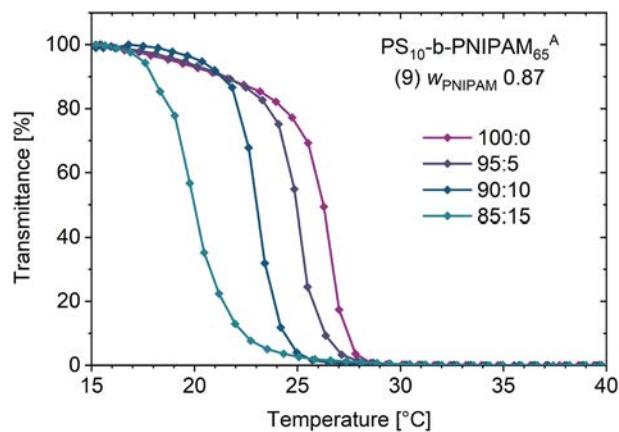
Figure A 77. Normalized turbidimetry heating curves for PS$_{10}$-b-PNIPAM$_{65}$^{A} (reaction index 9) in water/methanol solutions (polymer concentration 10 g·L^{-1}).

7.7. DLS: Relaxation Curves & Supplementary Data
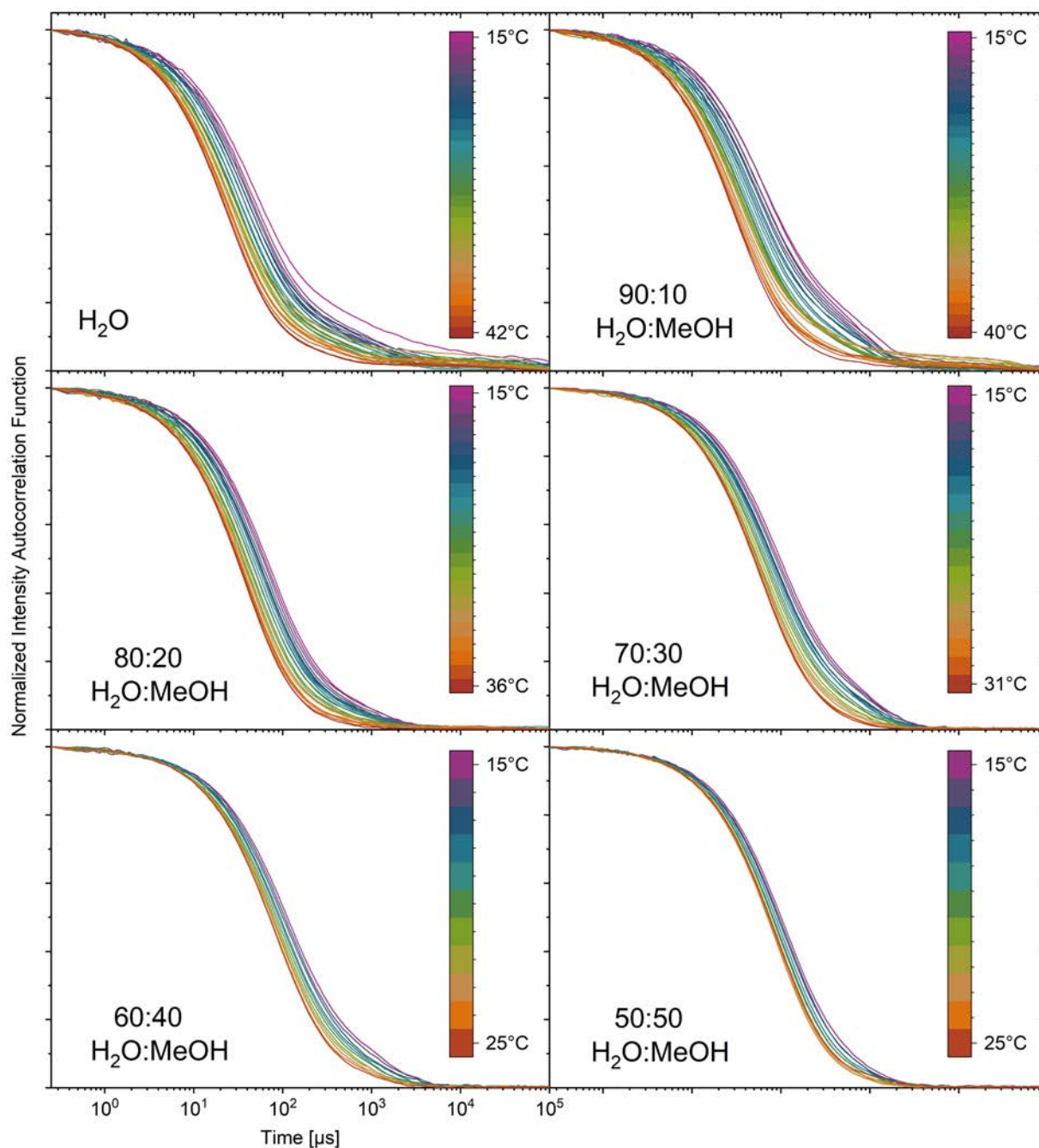
Figure A 78. Normalized intensity autocorrelation function of PNIPMAM$_{492}$ (reaction index 81) in water/methanol solutions (10 g·L^{-1}) with varying volume fractions of methanol, in temperatures ranging from 15°C until immediately below the transition temperature of each system.
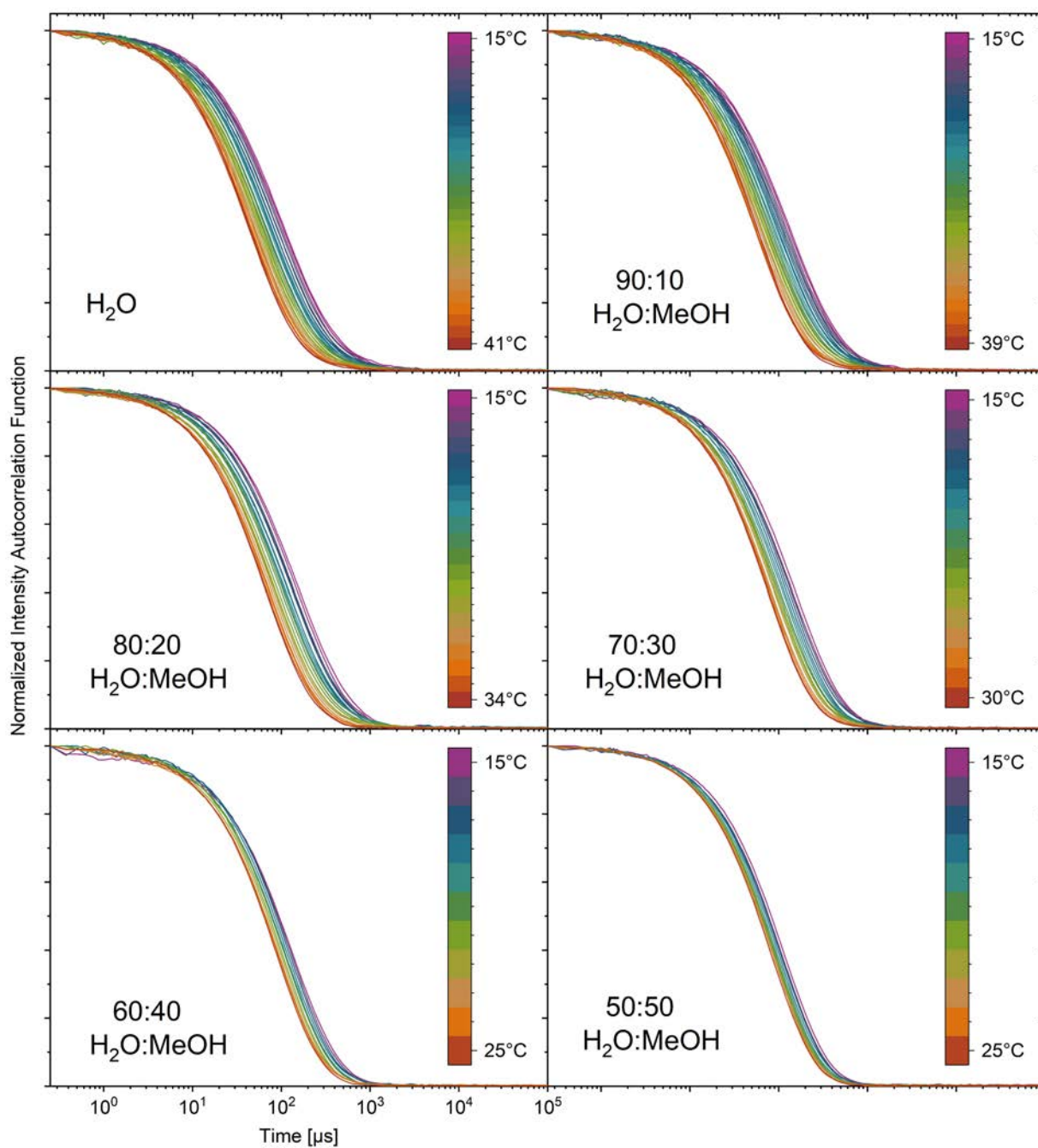
Figure A 79. Normalized intensity autocorrelation function of PMMA$_{20}$-*b*-PNIPMAM$_{242}$^{B} (reaction index 54, $w_{PNIPMAM}^{SEC}$ 0.92) in water/methanol solutions (10 g·L^{-1}) with varying volume fractions of methanol, in temperatures ranging from 15°C until immediately below the transition temperature of each system.
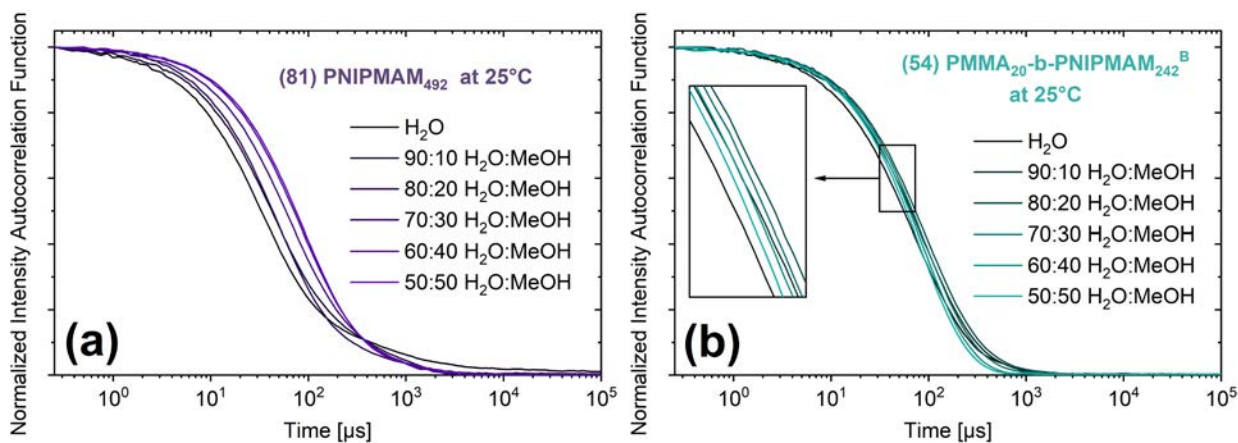
Figure A 80. Normalized intensity autocorrelation function of (a) PNIPMAM$_{492}$ (reaction index 81), and (b) PMMA$_{20}$-*b*-PNIPMAM$_{242}$^{B} (reaction index 54, $w_{PNIPMAM}^{SEC}$ 0.92) in water / methanol solutions (10 g·L^{-1}) with varying volume fractions of methanol, at 25°C, i.e. below the cloud point of all systems.
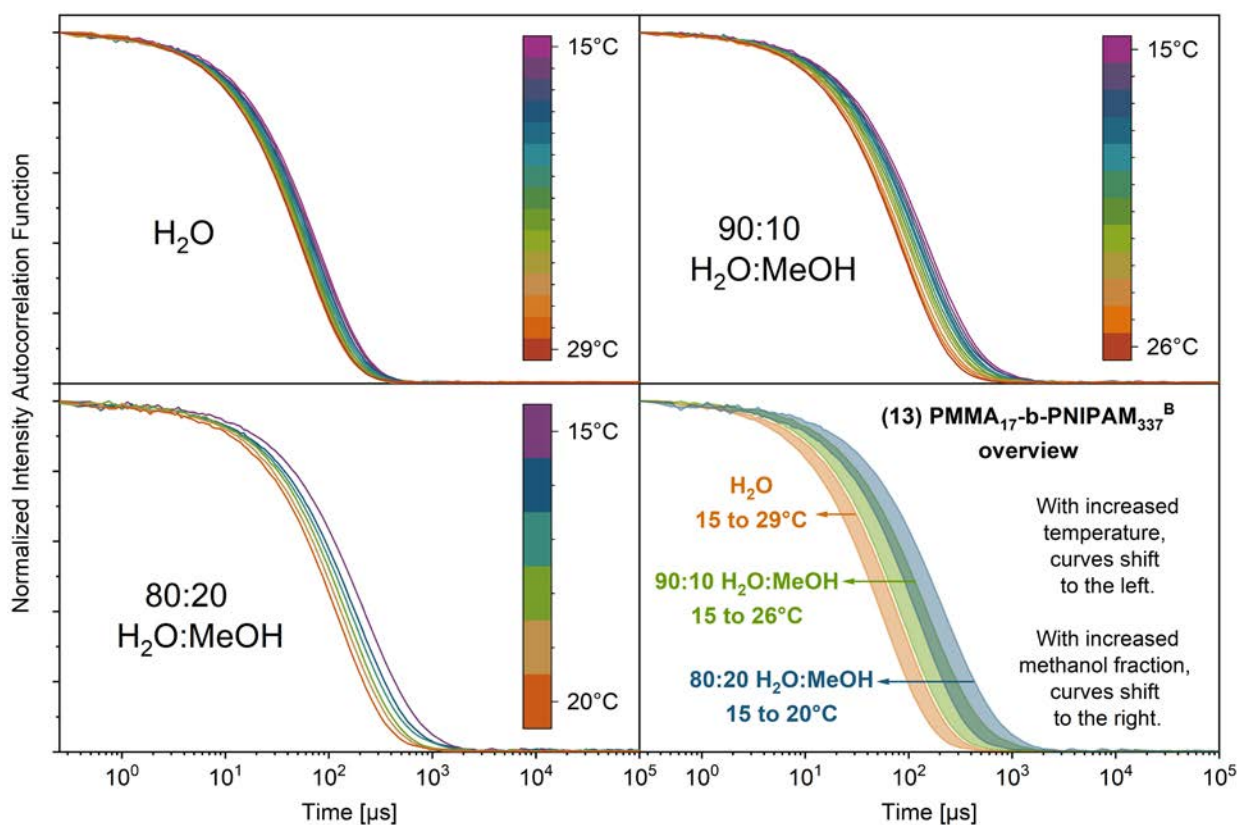
Figure A 81. Normalized intensity autocorrelation function of PMMA$_{17}$-*b*-PNIPAM$_{337}$^{B} (reaction index 13, w_{PNIPAM}^{SEC} 0.94) in water and water / methanol solutions (10 g·L^{-1}) with varying volume fractions of methanol, at temperatures ranging from 15°C to immediately below the cloud point of each system.
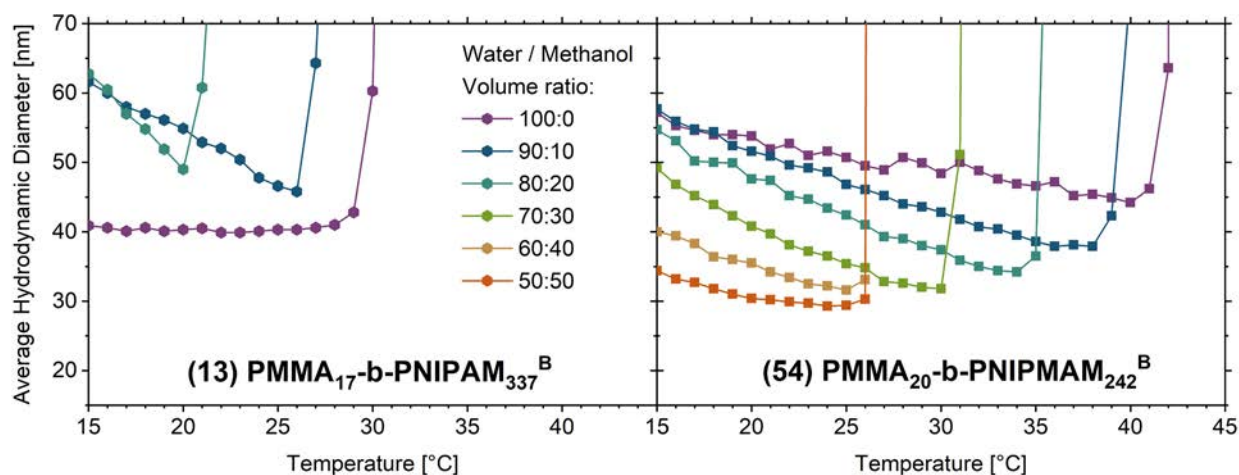
Figure A 82. Effect of methanol volume fraction on the aggregate size of PMMA$_{17}$-*b*-PNIPAM$_{337}$^{B} (reaction index 13, w_{PNIPAM}^{SEC} 0.94) and PMMA$_{20}$-*b*-PNIPMAM$_{242}$^{B} (reaction index 54, $w_{PNIPMAM}^{SEC}$ 0.92) solutions. Results obtained by DLS, with a polymer concentration in solution of 10 g·L^{-1}.
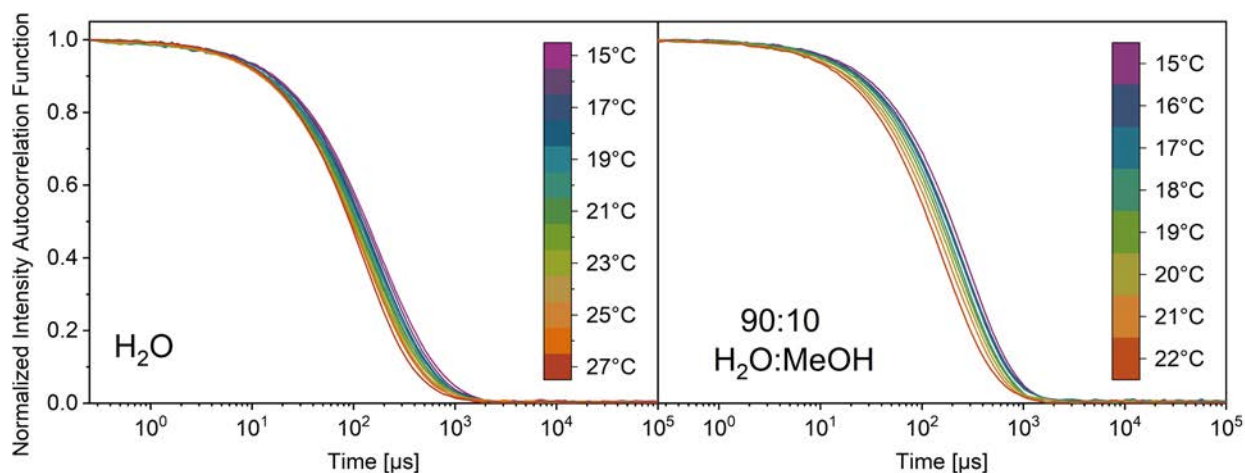
Figure A 83. Normalized intensity autocorrelation function of PS$_{10}$-*b*-PNIPAM$_{65}$^{A} (reaction index 9, w_{PNIPAM}^{SEC} 0.87) in water and 90:10 (vol.) water / methanol solutions (10 g·L^{-1}), at temperatures ranging from 15°C to immediately below the cloud point of each system.
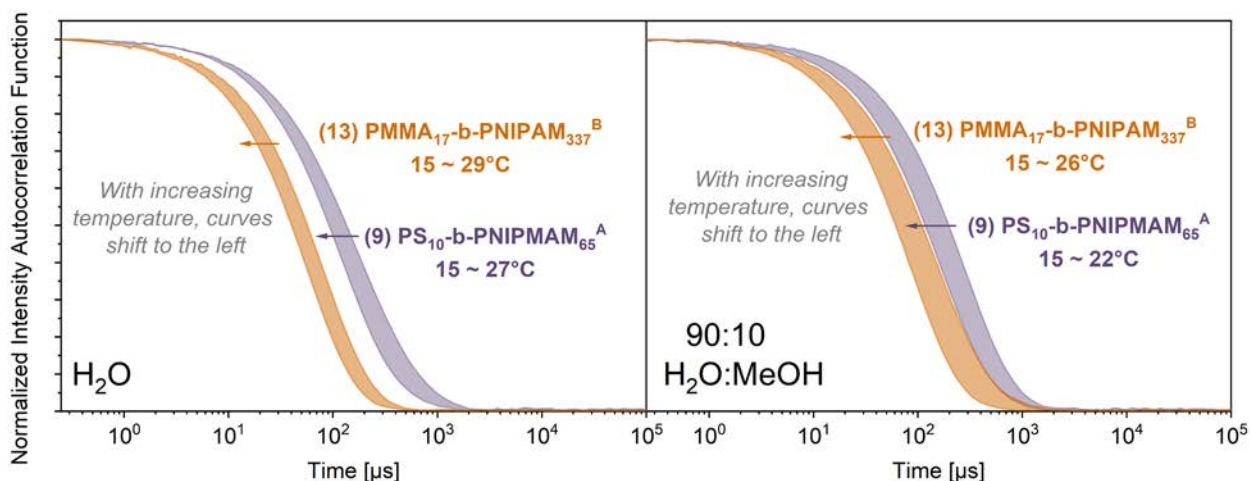
Figure A 84. Effect of temperature on the intensity autocorrelation function of **PMMA$_{17}$-*b*-PNIPAM$_{337}$^{B}** (reaction index 13, $w_{\text{PNIPAM}}^{\text{SEC}}$ 0.94) and **PS$_{10}$-*b*-PNIPAM$_{65}$^{A}** (reaction index 9, $w_{\text{PNIPAM}}^{\text{SEC}}$ 0.87) in water and water/methanol solutions, from 15°C until immediately below the transition temperature of each sample. Results obtained by DLS, with concentration of 10 g·L^{-1}.
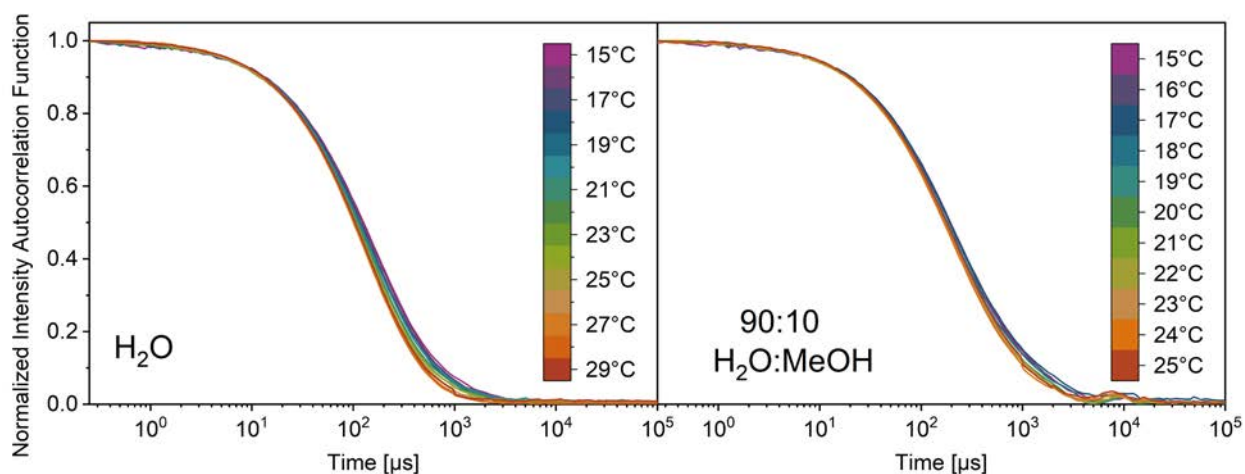
Figure A 85. Normalized intensity autocorrelation function of PMMA$_{27}$-*b*-PNIPAM$_{802}$^{B} (reaction index 16, $w_{\text{PNIPAM}}^{\text{SEC}}$ 0.96) in water and 90:10 (vol.) water / methanol solutions (10 g·L^{-1}), at temperatures ranging from 15°C to immediately below the cloud point of each system.
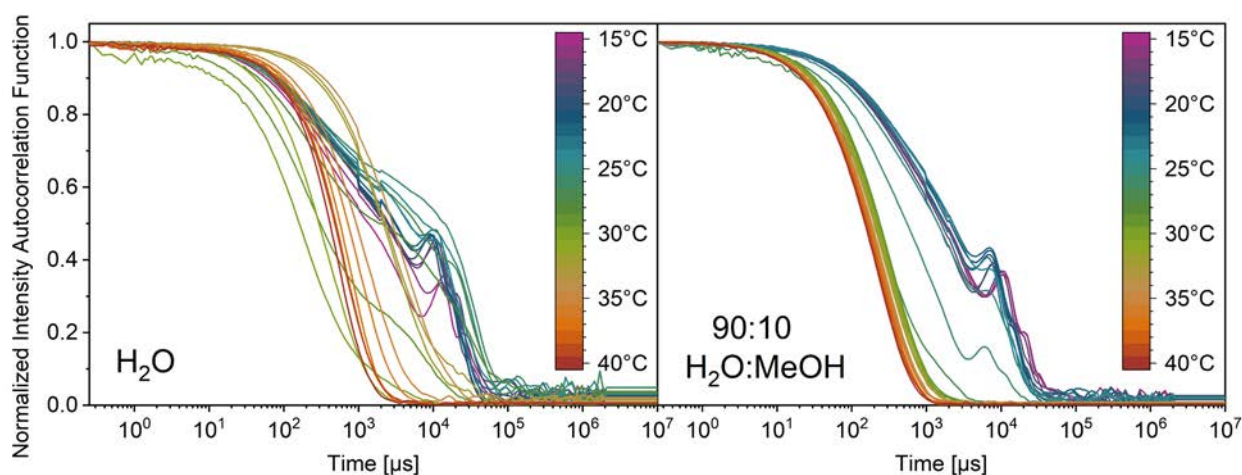
Figure A 86. Normalized intensity autocorrelation function of PMMA$_{41}$-*b*-PNIPAM$_{456}$^{B} (reaction index 17, w_{PNIPAM}^{SEC} 0.92) in water and 90:10 (vol.) water / methanol solutions (10 g·L^{-1}), at temperatures ranging from 15 to 40°C.
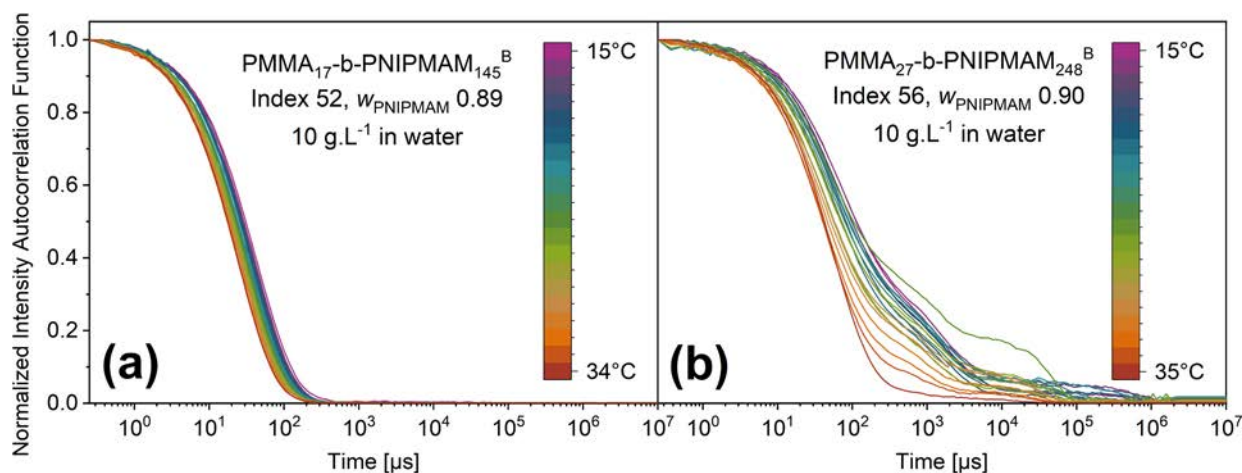
Figure A 87. Normalized intensity autocorrelation function of (a) PMMA$_{17}$-*b*-PNIPMAM$_{145}$^{B} (reaction index 52, $w_{PNIPMAM}^{SEC}$ 0.92) and (b) PMMA$_{27}$-*b*-PNIPMAM$_{248}$^{B} (reaction index 56, $w_{PNIPMAM}^{SEC}$ 0.90) in aqueous solutions (10 g·L^{-1}), at temperatures ranging from 15°C to immediately below the cloud point of each system.
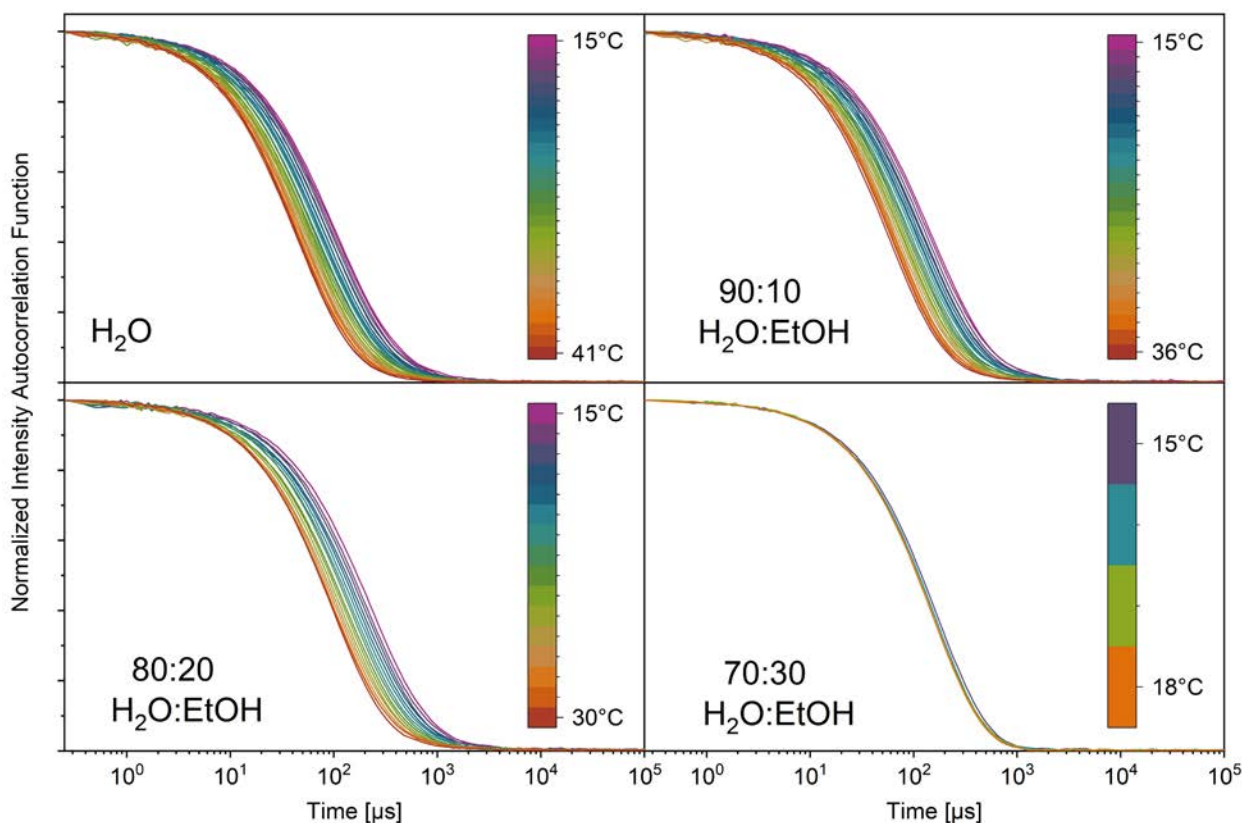
Figure A 88. Normalized intensity autocorrelation function of PMMA$_{20}$-*b*-PNIPMAM$_{242}$^{B} (reaction index 54, $w_{PNIPMAM}^{SEC}$ 0.92) in water/ethanol solutions (10 g·L^{-1}) with varying volume fractions of ethanol, in temperatures ranging from 15°C until immediately below the transition temperature of each system.
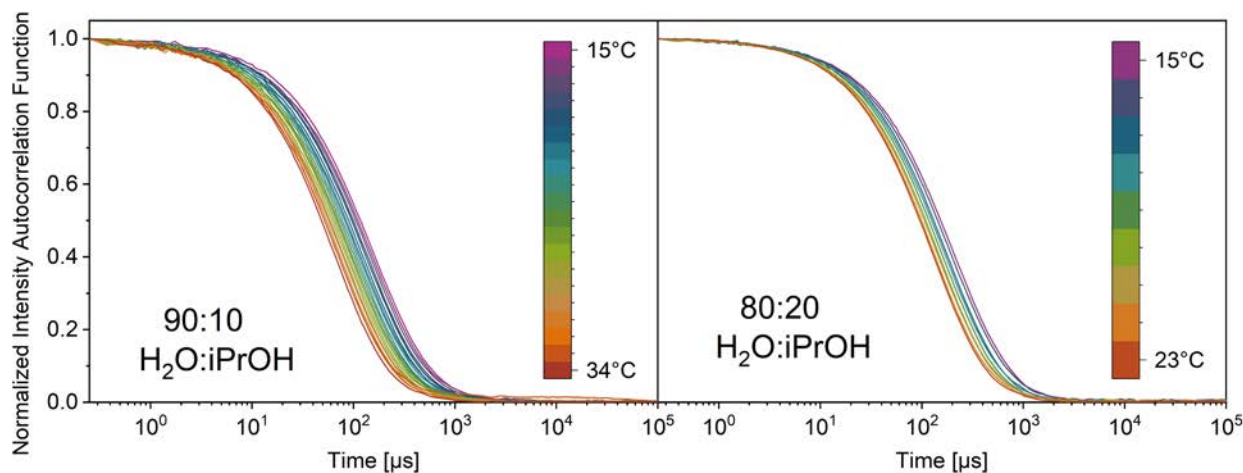
Figure A 89. Normalized intensity autocorrelation function of PMMA$_{20}$-*b*-PNIPMAM$_{242}$^{B} (reaction index 54, $w_{PNIPMAM}^{SEC}$ 0.92) in water/isopropanol solutions (10 g·L^{-1}) with varying volume fractions of isopropanol, in temperatures ranging from 15°C until immediately below the transition temperature of each system.
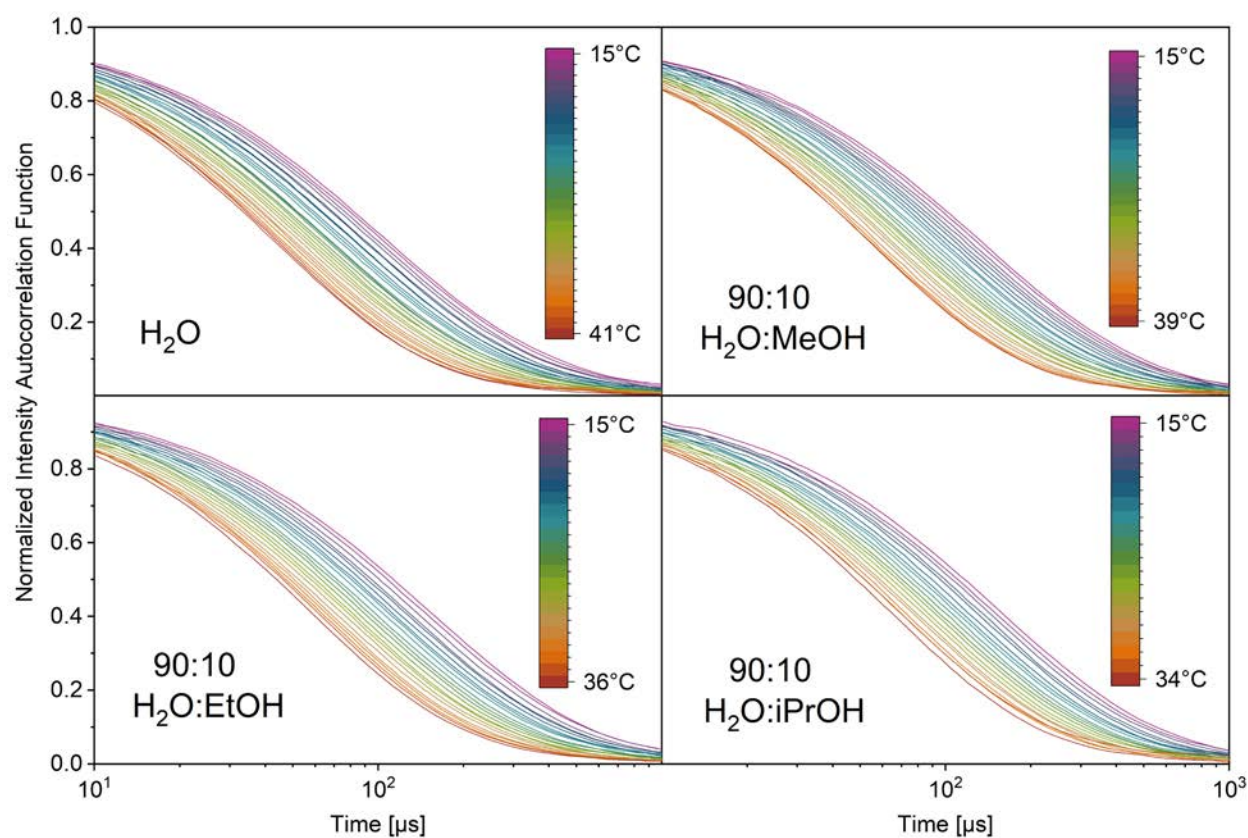
Figure A 90. Normalized intensity autocorrelation functions of PMMA$_{20}$-*b*-PNIPMAM$_{242}$^{B} (reaction index 54, $w_{PNIPMAM}^{SEC}$ 0.92) in pure water and 90:10 (vol.) water/alcohol solutions (10 g·L^{-1}), in temperatures ranging from 15°C until immediately below the transition temperature of each system. Smaller axis ranges are shown, for facilitated visualization of the variability between the curves of each system.

8. List of Figures

Figures on Main Text

Figures in Annexes

9. List of Tables

10. References

[1] Aguilar, M.R., San Román, J. (eds.). Smart polymers and their applications. Amsterdam: WP Woodhead Publ./Elsevier, 2014.

[2] Ebara, M. et al. Smart Biomaterials. Tokyo: Springer Japan, 2014.

[3] Kumar, A; Srivastava, A; Galaev, I.Y., Mattiasson, B. *Prog. Polym. Sci.* **2007,** *32(*10), 1205–1237.

[4] Lodge, T. *Microchimica Acta* **1994,** *116*, 1–31.

[5] Kreuzer, L.P. et al. *Macromolecules* **2021,** *54(*3), 1548–1556.

[6] Cowie, J., Arrighi, V. Polymers: Chemistry and Physics of Modern Materials, 3rd ed. Hoboken: CRC Press, 2007.

[7] Winnik, M.A., Yekta, A. *Curr. Opin. Colloid Interface Sci.* **1997,** *2(*4), 424–436.

[8] Choucair, A., Eisenberg, A. *Eur. Phys. J. E* **2003,** *10(*1), 37–44.

[9] Laschewsky, A; Müller-Buschbaum, P., Papadakis, C.M. *Progress in Colloid and Polymer Science* **2013,** *140*, 15–34.

[10] Mai, Y., Eisenberg, A. *Chem. Soc. Rev.* **2012,** *41(*18), 5969–5985.

[11] Zhao, C; Ma, Z., Zhu, X.X. *Prog. Polym. Sci.* **2019,** *90*, 269–291.

[12] Aseyev, V; Tenhu, H., Winnik, F.M. Non-ionic thermoresponsive polymers in water. In: Müller, A.H.E., Borisov, O., editors. Self Organized Nanostructures of Amphiphilic Block Copolymers II, vol. 242. Berlin Heidelberg: Springer, 2010. pp. 29–89.

[13] Wolf, B.A., Willms, M.M. *Makromol. Chem.* **1978,** *179(*9), 2265–2277.

[14] Schild, H.G; Muthukumar, M., Tirrell, D.A. *Macromolecules* **1991,** *24(*4), 948–952.

[15] Costa, R.O., Freitas, R.F. *Polymer* **2002,** *43(*22), 5879–5885.

[16] Zhang, G., Wu, C. *J. Am. Chem. Soc.* **2001,** *123(*7), 1376–1380.

[17] Pang, J; Yang, H; Ma, J., Cheng, R. *J. Phys. Chem. B* **2010,** *114(*26), 8652–8658.

[18] Tanaka, F; Koga, T; Kojima, H., Winnik, F.M. *Macromolecules* **2009,** *42(*4), 1321–1330.

[19] Tanaka, F; Koga, T., Winnik, F.M. *Progress in Colloid and Polymer Science* **2009,** *136*, 1–8.

[20] Walter, J; Sehrt, J; Vrabec, J., Hasse, H. *J. Phys. Chem. B* **2012,** *116(*17), 5251–5259.

[21] Hao, J; Cheng, H; Butler, P; Zhang, L., Han, C.C. *J. Chem. Phys.* **2010,** *132(*15), 154902.

[22] Sun, S., Wu, P. *Macromolecules* **2010,** *43(*22), 9501–9510.

[23] Ivanov, P., Tsvetanov, C. *Bulg. Chem. Commun.* **2017,** *49*B, 145–150.

[24] Uyama, H., Kobayashi, S. *Chem. Lett.* **1992,** *21(*9), 1643–1646.

[25] Pooch, F; Teltevskij, V; Karjalainen, E; Tenhu, H., Winnik, F.M. *Macromolecules* **2019,** *52(*17), 6361–6368.

[26] Lambermont-Thijs, H.M.L; van Kuringen, H.P.C; van der Put, J.P.W; Schubert, U.S., Hoogenboom, R. *Polymers* **2010,** *2(*3), 188–199.

[27] Meyer, M; Antonietti, M., Schlaad, H. *Soft Matter* **2007,** *3(*4), 430–431.

[28] Ko, C.-H. et al. *Macromolecules* **2020,** *53(*16), 6816–6827.

[29] Suwa, K; Wada, Y; Kikunaga, Y; Morishita, K; Kishida, A., Akashi, M. *J. Polym. Sci. A* **1997,** *35(*9), 1763–1768.

[30] Chen, C.-W; Tano, D., Akashi, M. *Colloid Polym. Sci.* **1999,** *277*, 488–493.

[31] Kyriakos, K. et al. *Macromolecules* **2014,** *47(*19), 6867–6879.

[32] Adelsberger, J. et al. *Colloid Polym. Sci.* **2011,** *289*, 711–720.

[33] Shipp, D.A. *Polym. Rev.* **2011,** *51(*2), 99–103.

[34] Keddie, D.J. *Chem. Soc. Rev.* **2014,** *43(*2), 496–505.

[35] Keddie, D.J; Moad, G; Rizzardo, E., Thang, S.H. *Macromolecules* **2012,** *45(*13), 5321–5342.

[36] Viet Hildebrand. Twofold Switchable Block Copolymers Based on New Polyzwitterions. Dissertation. Potsdam, Germany, 2016.

[37] Liu, G; Zhou, W; Zhang, J., Zhao, P. *J. Polym. Sci. A* **2012,** *50(*11), 2219–2226.

[38] Barner-Kowollik, C. et al. *J. Polym. Sci. A* **2006,** *44(*20), 5809–5831.

[39] Elias, H.-G. An introduction to polymer science, 1st ed. Weinheim: VCH, 1997.

[40] Gennes, P.-G. de. Scaling concepts in polymer physics. Ithaca, NY: Cornell Univ. Press, ca. 2005.

[41] Brazel, C.S., Rosen, S.L. Fundamental principles of polymeric materials, 3rd ed. Hoboken, N.J: John Wiley & Sons Inc, 2012.

[42] Seiffert, S. Physical Chemistry of Polymers: A Conceptual Introduction. Berlin, Boston: De Gruyter, 2020.

[43] Hamley, I.W. Introduction to Soft Matter: Synthetic and Biological Self-Assembling Materials, 2nd ed. Hoboken: John Wiley & Sons Incorporated, 2007.

[44] Painter, P.C., Coleman, M.M. Fundamentals of Polymer Science: An Introductory Text, Second Edition, 2nd ed. Boca Raton: Routledge, 1997.

[45] Miller-Chou, B.A., Koenig, J.L. *Prog. Polym. Sci.* **2003,** *28(*8), 1223–1270.

[46]   Venkatram, S; Kim, C; Chandrasekaran, A., Ramprasad, R. *J. Chem. Inf. Model.* **2019,** *59(*10), 4188–4194.

[47]   Hansen, C.M. (ed.). Hansen solubility parameters: A user's handbook, 2nd ed. Boca Raton: Taylor & Francis, 2007.

[48]   Brandrup, J. (ed.). Polymer handbook, 4th ed. New York, NY: Wiley, 1999.

[49]   Ben-Naim, A. Molecular theory of water and aqueous solutions: Part I: Understanding water. Singapore, Hackensack, N.J: World Scientific Pub. Co, 2009.

[50]   Riess, G. *Prog. Polym. Sci.* **2003,** *28(*7), 1107–1170.

[51]   Matyjaszewski, K. *Science* **2011,** *333(*6046), 1104–1105.

[52]   Amado, E., Kressler, J. *Soft Matter* **2011,** *7(*16), 7144.

[53]   Ratcliffe, L.P.D; Derry, M.J; Ianiro, A; Tuinier, R., Armes, S.P. *Angew. Chem. Int. Ed.* **2019,** *58(*52), 18964–18970.

[54]   Förster, S., Antonietti, M. *Adv. Mater.* **1998,** *10(*3), 195–217.

[55]   Discher, D.E., Eisenberg, A. *Science* **2002,** *297(*5583), 967–973.

[56]   Hayward, R.C., Pochan, D.J. *Macromolecules* **2010,** *43(*8), 3577–3584.

[57]   Chassenieux, C; Nicolai, T., Benyahia, L. *Curr. Opin. Colloid Interface Sci.* **2011,** *16(*1), 18–26.

[58]   Bovey, F. Macromolecules: Introduction to Polymer Science. Oxford: Elsevier Science, 1979.

[59]   Halperin, A; Kröger, M., Winnik, F.M. *Angew. Chem. Int. Ed.* **2015,** *54(*51), 15342–15367.

[60]   van Krevelen, D.W., Nijenhuis, K.t. Properties of polymers: Their correlation with chemical structure ; their numerical estimation and prediction from additive group contributions, 4th ed. Amsterdam: Elsevier, 2009.

[61]   Hoogenboom, R. et al. *Chem. Commun.* **2009**, 5582–5584.

[62]   Zhang, Q; Schattling, P; Theato, P., Hoogenboom, R. *Eur. Polym. J.* **2015,** *62*, 435–441.

[63]   Hoogenboom, R; Becer, C.R; Guerrero-Sanchez, C; Hoeppener, S., Schubert, U.S. *Aust. J. Chem.* **2010,** *63(*8), 1173.

[64]   Can, A; Hoeppener, S; Guillet, P; Gohy, J.-F; Hoogenboom, R., Schubert, U.S. *J. Polym. Sci. A* **2011,** *49(*17), 3681–3687.

[65]   Kempe, K; Neuwirth, T; Czaplewska, J; Gottschaldt, M; Hoogenboom, R., Schubert, U.S. *Polym. Chem.* **2011,** *2(*8), 1737.

[66]   Hoogenboom, R. et al. *Soft Matter* **2009,** *5(*19), 3590.

[67]   Lambermont-Thijs, H.M.L; Heuts, J.P.A; Hoeppener, S; Hoogenboom, R., Schubert, U.S. *Polym. Chem.* **2011,** *2(*2), 313–322.

[68]   Zhang, Q., Hoogenboom, R. *Prog. Polym. Sci.* **2015,** *48*, 122–142.

[69]   Can, A. et al. *Eur. Polym. J.* **2015,** *69*, 460–471.

[70]   Bharadwaj, S; Niebuur, B.-J; Nothdurft, K; Richtering, W; van der Vegt, N.F., Papadakis, C.M. *Soft Matter* **2022,** *18(*15), 2884–2909.

[71]   Mukae, K. et al. *Colloid Polym. Sci.* **1994,** *272*, 655–663.

[72]   Pagonis, K., Bokias, G. *Polym. Int.* **2006,** *55(*11), 1254–1258.

[73]   Hofmann, C.H; Plamper, F.A; Scherzinger, C; Hietala, S., Richtering, W. *Macromolecules* **2012,** *46(*2), 523–532.

[74]   Michailova, V.I. et al. *J. Phys. Chem. B* **2018,** *122(*22), 6072–6078.

[75]   Yong, H; Bittrich, E; Uhlmann, P; Fery, A., Sommer, J.-U. *Macromolecules* **2019,** *52(*16), 6285–6293.

[76]   Yong, H; Merlitz, H; Fery, A., Sommer, J.-U. *Macromolecules* **2020,** *53(*7), 2323–2335.

[77]   Raftopoulos, K.N. et al. *Soft Matter* **2020,** *16(*36), 8462–8472.

[78]   Geiger, C. et al. *Macromolecules* **2021,** *54(*7), 3517–3530.

[79]   Geiger, C. et al. *Adv. Eng. Mater.* **2021,** *23(*11), 2100191.

[80]   Hofmann, C.H; Grobelny, S; Erlkamp, M; Winter, R., Richtering, W. *Polymer* **2014,** *55(*8), 2000–2007.

[81]   Osaka, N., Shibayama, M. *Macromolecules* **2012,** *45(*4), 2171–2174.

[82]   Oliveira, T.E. de; Netz, P.A; Mukherji, D., Kremer, K. *Soft Matter* **2015,** *11(*44), 8599–8604.

[83]   Niebuur, B.-J; Lohstroh, W; Ko, C.-H; Appavou, M.-S; Schulte, A., Papadakis, C.M. *Macromolecules* **2021,** *54(*9), 4387–4400.

[84]   Nandi, A.K; Sen, U.K; Bhattacharyya, S.N., Mandal, B.M. *Eur. Polym. J.* **1983,** *19(*4), 283–286.

[85]   Fernández-Piérola, I., Horta, A. *Polym. Bull.* **1980,** *3*, 273–278.

[86]   Winnik, F.M; Ringsdorf, H., Venzmer, J. *Macromolecules* **1990,** *23(*8), 2415–2416.

[87]   Pagonis, K., Bokias, G. *Polymer* **2004,** *45(*7), 2149–2153.

[88]   Liu, B; Wang, J; Ru, G; Liu, C., Feng, J. *Macromolecules* **2015,** *48(*4), 1126–1133.

[89]   Hiroki, A; Maekawa, Y; Yoshida, M; Kubota, K., Katakai, R. *Polymer* **2001,** *42(*5), 1863–1867.

[90] Matsuda, Y; Kobayashi, M; Annaka, M; Ishihara, K., Takahara, A. *Polym. J.* **2008,** *40*, 479–483.

[91] Edmondson, S; Nguyen, N.T; Lewis, A.L., Armes, S.P. *Langmuir* **2010,** *26(*10), 7216–7226.

[92] Takahashi, N; Kanaya, T; Nishida, K., Kaji, K. *Polymer* **2003,** *44(*15), 4075–4078.

[93] Young, T.-H., Chuang, W.-Y. *J. Membr. Sci.* **2002,** *210(*2), 349–359.

[94] Djokpé, E., Vogt, W. *Macromol. Chem. Phys.* **2001,** *202(*5), 750–757.

[95] Fujishige, S; Kubota, K., Ando, I. *J. Phys. Chem.* **1989,** *93(*8), 3311–3313.

[96] Netopilík, M; Bohdanecký, M; Chytrý, V., Ulbrich, K. *Macromol. Rapid Commun.* **1997,** *18(*2), 107–111.

[97] Alenichev, I; Sedláková, Z., Ilavský, M. *Polym. Bull.* **2007,** *58*, 191–199.

[98] Spěváček, J; Starovoytova, L; Hanyková, L., Kouřilová, H. *Macromol. Symp.* **2008,** *273(*1), 17–24.

[99] Kouřilová, H; Hanyková, L., Spěváček, J. *Eur. Polym. J.* **2009,** *45(*10), 2935–2941.

[100] Zuo, T. et al. *Macromolecules* **2019,** *52(*2), 457–464.

[101] Chen, C.-W; Takezako, T; Yamamoto, K; Serizawa, T., Akashi, M. *Colloids Surf. A* **2000,** *169*1-3, 107–116.

[102] Sato, T; Miyoshi, T., Seno, M. *J. Polym. Sci. A* **2000,** *38(*3), 509–515.

[103] Zhang, G., Wu, C. *J. Am. Chem. Soc.* **2001,** *123(*7), 1376–1380.

[104] Bischofberger, I; Calzolari, D.C; Los Rios, P. de; Jelezarov, I., Trappe, V. *Sci. Rep.* **2014,** *4*, 4377.

[105] Okada, Y., Tanaka, F. *Macromolecules* **2005,** *38(*10), 4465–4471.

[106] Tanaka, F; Koga, T; Kojima, H; Xue, N., Winnik, F.M. *Macromolecules* **2011,** *44(*8), 2978–2989.

[107] Tanaka, F; Koga, T., Winnik, F.M. *Phys. Rev. Lett.* **2008,** *101(*2), 28302.

[108] Pica, A., Graziano, G. *Phys. Chem. Chem. Phys.* **2016,** *18(*36), 25601–25608.

[109] Dalgicdir, C; Rodríguez-Ropero, F., van der Vegt, N.F. *J. Phys. Chem. B* **2017,** *121(*32), 7741–7748.

[110] Rodríguez-Ropero, F; Hajari, T., van der Vegt, N.F. *J. Phys. Chem. B* **2015,** *119(*51), 15780–15788.

[111] Tavagnacco, L; Zaccarelli, E., Chiessi, E. *J. Mol. Liq.* **2020,** *297*, 111928.

[112] Grinberg, V.Y. et al. *Macromolecules* **2020,** *53(*24), 10765–10772.

[113] Heyda, J; Muzdalo, A., Dzubiella, J. *Macromolecules* **2013,** *46(*3), 1231–1238.

[114] Mukherji, D; Marques, C.M., Kremer, K. *Nature Commun.* **2014,** *5*, 4882.

[115] Zhu, P.-W., Chen, L. *Phys. Rev. E* **2019,** *99(*2), 22501.

[116] Park, G., Jung, Y. *Soft Matter* **2019,** *15(*39), 7968–7980.

[117] Mukherji, D. et al. *Soft Matter* **2016,** *12(*38), 7995–8003.

[118] Bharadwaj, S., van der Vegt, N.F. *Macromolecules* **2019,** *52(*11), 4131–4138.

[119] Furyk, S; Zhang, Y; Ortiz-Acosta, D; Cremer, P.S., Bergbreiter, D.E. *J. Polym. Sci. A* **2006,** *44(*4), 1492–1501.

[120] Aoshima, S., Kanaoka, S. Synthesis of Stimuli-Responsive Polymers by Living Polymerization: Poly(N-Isopropylacrylamide) and Poly(Vinyl Ether)s. In: Aoshima, S. et al., editors. Wax Crystal Control - Nanocomposites - Stimuli-Responsive Polymers, vol. 210. Berlin, Heidelberg: Springer Berlin Heidelberg, 2007. pp. 169–208.

[121] Kitayama, T; Shibuya, W., Katsukawa, K. *Polym. J.* **2002,** *34*, 405–409.

[122] Ishizone, T., Ito, M. *J. Polym. Sci. A* **2002,** *40(*23), 4328–4332.

[123] Matyjaszewski, K., Spanswick, J. *Mater. Today* **2005,** *8(*3), 26–33.

[124] Odian, G., Odian, G.G. Principles of polymerization, 4th ed. Hoboken, NJ: Wiley-Interscience, 2004.

[125] FUJIFILM Wako Chemicals Europe GmbH. Oil soluble Azo initiators: AIBN. [April 15, 2022]; Available from: https://specchem-wako.fujifilm.com/europe/en/oil-soluble-azo-initiators/AIBN.htm.

[126] FUJIFILM Wako Chemicals Europe GmbH. Oil soluble Azo initiators: V-601. [April 15, 2022]; Available from: https://specchem-wako.fujifilm.com/europe/en/oil-soluble-azo-initiators/V-601.htm.

[127] FUJIFILM Wako Chemicals Europe GmbH. Oil soluble Azo initiators: V-40. [April 15, 2022]; Available from: https://specchem-wako.fujifilm.com/europe/en/oil-soluble-azo-initiators/V-40.htm.

[128] FUJIFILM Wako Chemicals Europe GmbH. Water soluble Azo initiators: V-50. [April 15, 2022]; Available from: https://specchem-wako.fujifilm.com/europe/en/water-soluble-azo-initiators/V-50.htm.

[129] FUJIFILM Wako Chemicals Europe GmbH. Oil soluble Azo initiators: V-70. [April 15, 2022]; Available from: https://specchem-wako.fujifilm.com/europe/en/oil-soluble-azo-initiators/V-70.htm.

[130] Mayo, F.R. *J. Am. Chem. Soc.* **1968,** *90(*5), 1289–1295.

[131] Khuong, K.S; Jones, W.H; Pryor, W.A., Houk, K.N. *J. Am. Chem. Soc.* **2005,** *127(*4), 1265–1277.

[132] Buzanowski, W.C; Graham, J.D; Priddy, D.B., Shero, E. *Polymer* **1992,** *33(*14), 3055–3059.

[133] Moad, G; Rizzardo, E., Thang, S.H. *Aust. J. Chem.* **2005,** *58(*6), 379.

[134] Ring, W; Mita, I; Jenkins, A.D., Bikales, N.M. *Pure Appl. Chem.* **1985,** *57(*10), 1427–1440.

[135] Garnier, S; Laschewsky, A., Storsberg, J. *Tenside Surf. Det.* **2006,** *43(*2), 88–102.

[136] Chiefari, J. et al. *Macromolecules* **1998,** *31(*16), 5559–5562.

[137] Perrier, S; Takolpuckdee, P; Westwood, J., Lewis, D.M. *Macromolecules* **2004,** *37(*8), 2709–2717.

[138] Perrier, S. *Macromolecules* **2017,** *50(*19), 7433–7447.

[139] Willcock, H., O'Reilly, R.K. *Polym. Chem.* **2010,** *1(*2), 149–157.

[140] Moad, G; Chong, Y.K; Postma, A; Rizzardo, E., Thang, S.H. *Polymer* **2005,** *46(*19), 8458–8468.

[141] Moad, G; Rizzardo, E., Thang, S.H. *Aust. J. Chem.* **2006,** *59(*10), 669.

[142] Moad, G; Rizzardo, E., Thang, S.H. *Aust. J. Chem.* **2009,** *62(*11), 1402.

[143] Moad, G; Rizzardo, E., Thang, S.H. *Aust. J. Chem.* **2012,** *65(*8), 985.

[144] Moad, G. *Macromol. Chem. Phys.* **2014,** *215(*1), 9–26.

[145] Moad, G. *J. Polym. Sci. A* **2019,** *57(*3), 216–227.

[146] Destarac, M; Taton, D; Zard, S.Z; Saleh, T., Six, Y. On the Importance of Xanthate Substituents in the MADIX Process. In: Patil, A., editor. Polymers for personal care and cosmetics: Based on an international symposium on "Polymers for Cosmetics and Personal Care" held at the 244th National ACS meeting in Philadelphia on August 22, 2012, vol. 854. Washington, DC, Oxford: ACS American Chemical Soc; Oxford Univ. Press, 2013. pp. 536–550.

[147] Chiefari, J; Mayadunne, R.T.A; Moad, G; Rizzardo, E., Thang, S.H. Polymerization process with living characteristics and polymers made therefrom. E.I. Du Pont De Nemours And Company, Commonwealth Scientific And Industrial Research Organization, WO1999031144A1, 24.06.1999.

[148] Destarac, M; Charmot, D; Franck, X., Zard, S.Z. *Macromol. Rapid Commun.* **2000,** *21(*15), 1035–1039.

[149] Mayadunne, R.T.A; Rizzardo, E; Chiefari, J; Chong, Y.K; Moad, G., Thang, S.H. *Macromolecules* **1999,** *32(*21), 6977–6980.

[150] Gardiner, J. et al. *Polym. Int.* **2017,** *66(*11), 1438–1447.

[151] Gardiner, J; Martinez-Botella, I; Tsanaktsidis, J., Moad, G. *Polym. Chem.* **2016,** *7(*2), 481–492.

[152] Zeng, R; Chen, Y; Zhang, L., Tan, J. *Macromolecules* **2020,** *53(*5), 1557–1566.

[153] Mellot, G; Beaunier, P; Guigner, J.-M; Bouteiller, L; Rieger, J., Stoffelbach, F. *Macromol. Rapid Commun.* **2019,** *40(*2), e1800315.

[154] Herfurth, C; Molina, P.M. de; Wieland, C; Rogers, S; Gradzielski, M., Laschewsky, A. *Polym. Chem.* **2012,** *3(*6), 1606–1617.

[155] Bivigou-Koumba, A.M; Kristen, J; Laschewsky, A; Müller-Buschbaum, P., Papadakis, C.M. *Macromol. Chem. Phys.* **2009,** *210(*7), 565–578.

[156] Skrabania, K; Miasnikova, A; Bivigou-Koumba, A.M; Zehm, D., Laschewsky, A. *Polym. Chem.* **2011,** *2(*9), 2074–2083.

[157] Hildebrand, V; Laschewsky, A., Zehm, D. *J. Biomater. Sci. Polym. Ed.* **2014,** *25*14-15, 1602–1618.

[158] Huang, C.-F; Hsieh, Y.-A; Hsu, S.-C., Matyjaszewski, K. *Polymer* **2014,** *55(*23), 6051–6057.

[159] Zehm, D; Laschewsky, A; Liang, H., Rabe, J.P. *Macromolecules* **2011,** *44(*24), 9635–9641.

[160] Higashi, N; Matsubara, S; Nishimura, S., Koga, T. *Materials* **2018,** *11(*3), 424.

[161] Ding, Z; Wang, C; Feng, G., Zhang, X. *Polymers* **2018,** *10(*3), 283.

[162] Kokufuta, M.K; Sato, S., Kokufuta, E. *Colloid Polym. Sci.* **2012,** *290*, 1671–1681.

[163] Kano, M., Kokufuta, E. *Langmuir* **2009,** *25(*15), 8649–8655.

[164] Guo, Z; Zhu, W; Xiong, Y., Tian, H. *Macromolecules* **2009,** *42(*5), 1448–1453.

[165] Dybal, J; Trchová, M., Schmidt, P. *Vibrat. Spectrosc.* **2009,** *51(*1), 44–51.

[166] Uchiyama, S; Matsumura, Y; Silva, A.P. de, Iwai, K. *Anal. Chem.* **2003,** *75(*21), 5926–5935.

[167] Salmerón Sánchez, M; Hanyková, L; Ilavský, M., Monleón Pradas, M. *Polymer* **2004,** *45(*12), 4087–4094.

[168] Starovoytova, L; Spěváček, J; Hanyková, L., Ilavský, M. *Polymer* **2004,** *45(*17), 5905–5911.

[169] Suito, Y; Isobe, Y; Habaue, S., Okamoto, Y. *J. Polym. Sci. A* **2002,** *40(*14), 2496–2500.

[170] ITO S. *Kobunshi Ronbunshu* **1989,** *46(*7), 437–443.

[171] Ruiz-Rubio, L; Vilas, J.L; Rodríguez, M., León, L.M. *Polym. Degrad. Stab.* **2014,** *109*, 147–153.

[172] Kouřilová, H; Spěváček, J., Hanyková, L. *Polym. Bull.* **2013,** *70,* 221–235.

[173] Tang, Y; Ding, Y., Zhang, G. *J. Phys. Chem. B* **2008,** *112(*29), 8447–8451.

[174] Kirsh, Y.E; Yanul, N., Popkov, Y.M. *Eur. Polym. J.* **2002,** *38(*2), 403–406.

[175] Tiktopulo, E.I; Uversky, V.N; Lushchik, V.B; Klenin, S.I; Bychkova, V.E., Ptitsyn, O.B. *Macromolecules* **1995,** *28(*22), 7519–7524.

[176] Chtryt, V., Ulbrich, K. *J. Bioact. Compat. Polym.* **2001,** *16(*6), 427–440.

[177] Meersman, F; Wang, J; Wu, Y., Heremans, K. *Macromolecules* **2005,** *38(*21), 8923–8928.

[178] Kubota, K; Hamano, K; Kuwahara, N; Fujishige, S., Ando, I. *Polym. J.* **1990,** *22,* 1051–1057.

[179] Duracher, D; Elaïssari, A., Pichot, C. *J. Polym. Sci. A* **1999,** *37(*12), 1823–1837.

[180] Fomenko, A; Pospíšil, H; Sedláková, Z; Pleštil, J., Ilavský, M. *Phys. Chem. Chem. Phys.* **2002,** *4(*18), 4360–4367.

[181] Tirumala, V.R; Ilavsky, J., Ilavsky, M. *J. Chem. Phys.* **2006,** *124(*23), 234911.

[182] Dainton, F.S., Sisley, W.D. *Trans. Faraday Soc.* **1963,** *59(*0), 1369–1376.

[183] Natarajan, L.V., Santappa, M. *J. Polym. Sci. A-1* **1968,** *6(*12), 3245–3257.

[184] Manickam, S.P; Subbaratnam, N.R., Venkatarao, K. *J. Polym. Sci. Polym. Chem. Ed.* **1980,** *18(*6), 1679–1684.

[185] Montaudo, G; Librando, V; Caccamese, S., Maravigna, P. *J. Am. Chem. Soc.* **1973,** *95(*19), 6365–6370.

[186] Montaudo, G; Maravigna, P; Caccamese, S., Librando, V. *J. Org. Chem.* **1974,** *39(*18), 2806–2809.

[187] Okamoto, Y., Yuki, H. *J. Polym. Sci. Polym. Chem. Ed.* **1981,** *19(*10), 2647–2650.

[188] Schrooten, J; Lacík, I; Stach, M; Hesse, P., Buback, M. *Macromol. Chem. Phys.* **2013,** *214(*20), 2283–2294.

[189] Akashi, M; Nakano, S., Kishida, A. *J. Polym. Sci. A* **1996,** *34(*2), 301–303.

[190] Suwa, K; Morishita, K; Kishida, A., Akashi, M. *J. Polym. Sci. A* **1997,** *35(*15), 3087–3094.

[191] Suwa, K; Wada, Y; Kishida, A., Akashi, M. *J. Polym. Sci. A* **1997,** *35(*16), 3377–3384.

[192] Kunugi, S; Takano, K; Tanaka, N; Suwa, K., Akashi, M. *Macromolecules* **1997,** *30(*15), 4499–4501.

[193] Suwa, K; Yamamoto, K; Akashi, M; Takano, K; Tanaka, N., Kunugi, S. *Colloid Polym. Sci.* **1998,** *276,* 529–533.

[194] Chen, C.-W; Arai, K; Yamamoto, K; Serizawa, T., Akashi, M. *Macromol. Chem. Phys.* **2000,** *201(*18), 2811–2819.

[195] Yamamoto, K; Serizawa, T; Muraoka, Y., Akashi, M. *J. Polym. Sci. A* **2000,** *38(*19), 3674–3681.

[196] Kishida, A; Kikunaga, Y., Akashi, M. *J. Appl. Polym. Sci.* **1999,** *73(*13), 2545–2548.

[197] Kunugi, S; Tada, T; Yamazaki, Y; Yamamoto, K., Akashi, M. *Langmuir* **2000,** *16(*4), 2042–2044.

[198] Yamamoto, K; Serizawa, T; Muraoka, Y., Akashi, M. *Macromolecules* **2001,** *34(*23), 8014–8020.

[199] Kunugi, S; Tada, T; Tanaka, N; Yamamoto, K., Akashi, M. *Polym. J.* **2002,** *34*, 383–388.

[200] Yamamoto, K; Imamura, Y; Nagatomo, E; Serizawa, T; Muraoka, Y., Akashi, M. *J. Appl. Polym. Sci.* **2003,** *89(*5), 1277–1283.

[201] Kunugi, S; Kameyama, K; Tada, T; Tanaka, N; Shibayama, M., Akashi, M. *Braz. J. Med. Biol.* **2005,** *38(*8), 1233–1238.

[202] Serizawa, T; Chen, M.-Q., Akashi, M. *J. Polym. Sci. A* **1998,** *36(*14), 2581–2587.

[203] Kunugi, S; Yamazaki, Y; Takano, K; Tanaka, N., Akashi, M. *Langmuir* **1999,** *15(*12), 4056–4061.

[204] Chen, C.-W; Tano, D., Akashi, M. *J. Colloid Int. Sci.* **2000,** *225(*2), 349–358.

[205] Tachaboonyakiat, W; Ajiro, H., Akashi, M. *J. Appl. Polym. Sci.* **2016,** *133*, 43852.

[206] Yoshida, H; Furumai, H., Ajiro, H. *Langmuir* **2022,** *38(*17), 5269–5274.

[207] Ruiz-Rubio, L; Lizundia, E; Vilas, J.L; León, L.M., Rodríguez, M. *Thermochim. Acta* **2015,** *614*, 191–198.

[208] Polymer Source Inc. Poly(N-vinyl isobutyramide). [May 01, 2022]; Available from: https://www.polymersource.ca/index.php?route=product/category&path=2_2183_15_166_1099&subtract=1&categorystart=A-1.1.5.3&serachproduct=.

[209] Zhang, Q; Weber, C; Schubert, U.S., Hoogenboom, R. *Mater. Horiz.* **2017,** *4(*2), 109–116.

[210] Kawaguchi, T; Kojima, Y; Osa, M., Yoshizaki, T. *Polym. J.* **2008,** *40*, 455–459.

[211] Xia, Y; Burke, N.A., Stöver, H.D. *Macromolecules* **2006,** *39(*6), 2275–2283.

[212] Qiu, X; Koga, T; Tanaka, F., Winnik, F.M. *Sci. China Chem.* **2013,** *56(*1), 56–64.

[213] Boutris, C; Chatzi, E.G., Kiparissides, C. *Polymer* **1997,** *38(*10), 2567–2570.

[214] Schönemann, E. et al. *Biomacromolecules* **2021,** *22(*4), 1494–1508.

[215] van Durme, K; van Assche, G., van Mele, B. *Macromolecules* **2004,** *37(*25), 9596–9605.

[216] Hildebrand, V; Laschewsky, A., Wischerhoff, E. *Polym. Chem.* **2016,** *7(*3), 731–740.

[217] Nakano, S. et al. *J. Chem. Phys.* **2011,** *135(*11), 114903.

[218] Shi, F; Han, Z; Li, J; Zheng, B., Wu, C. *Macromolecules* **2011,** *44(*4), 686–689.

[219] Russo, P.S; Streletzky, K.A; Gorman, A; Huberty, W., Zhang, X. Characterization of polymers by dynamic light scattering. In: Malik, M.I., editor. Molecular Characterization of Polymers: A Fundamental Guide. San Diego: Elsevier, 2021. pp. 441–498.

[220] Lehner, D; Lindner, H., Glatter, O. *Langmuir* **2000,** *16(*4), 1689–1695.

[221] He, W.-N; Xu, J.-T; Du, B.-Y; Fan, Z.-Q., Sun, F.-L. *Macromol. Chem. Phys.* **2012,** *213(*9), 952–964.

[222] He, W.-N; Xu, J.-T; Du, B.-Y; Fan, Z.-Q., Wang, X. *Macromol. Chem. Phys.* **2010,** *211(*17), 1909–1916.

[223] Guérin, G; Raez, J; Manners, I., Winnik, M.A. *Macromolecules* **2005,** *38(*18), 7819–7827.

[224] Huang, H. et al. *J. Am. Chem. Soc.* **2006,** *128(*11), 3784–3788.

[225] Du, B; Mei, A; Yin, K; Zhang, Q; Xu, J., Fan, Z. *Macromolecules* **2009,** *42(*21), 8477–8484.

[226] Ke, X.-X; Wang, L; Xu, J.-T; Du, B.-Y; Tu, Y.-F., Fan, Z.-Q. *Soft Matter* **2014,** *10(*28), 5201–5211.

[227] Chu, B. Laser Light Scattering: Basic Principles and Practice. Oxford: Elsevier Science, 1974.

[228] Carvalho, P.M; Felício, M.R; Santos, N.C; Gonçalves, S., Domingues, M.M. *Front. Chem.* **2018,** *6*, 237.

[229] Stetefeld, J; McKenna, S.A., Patel, T.R. *Biophys. Rev.* **2016,** *8(*4), 409–427.

[230] Afroze, F; Nies, E., Berghmans, H. *J. Mol. Struct.* **2000,** *554(*1), 55–68.

[231] Spěváček, J. Application of NMR Spectroscopy to Study Thermoresponsive Polymers. In: Khutoryanskiy, V.V., Georgiou, T.K., editors. Temperature-Responsive Polymers: Chemistry, Properties, and Applications: John Wiley and Sons Inc, 2018. pp. 225–247.

[232] Larsson, A; Kuckling, D., Schönhoff, M. *Colloids Surf. A* **2001,** *190*1-2, 185–192.

[233] Grillo, I. Small-angle neutron scattering and applications in soft condensed matter. In: Borsali, R., Pecora, R., editors. Soft Matter Characterization. Netherlands: Springer, 2008. pp. 723–782.

[234] Saini, A; Thomas, K.R.J; Huang, Y.-J., Ho, K.-C. *J. Mater. Sci. Mater. Electron.* **2018,** *29(*19), 16565–16580.

[235] Li, J.-J; Zhou, Y.-N., Luo, Z.-H. *Ind. Eng. Chem. Res.* **2014,** *53(*47), 18112–18120.

[236] Nuopponen, M; Kalliomäki, K; Laukkanen, A; Hietala, S., Tenhu, H. *J. Polym. Sci. A* **2008,** *46(*1), 38–46.

[237] Vishnevetskaya, N.S. et al. *Macromolecules* **2017,** *50(*10), 3985–3999.

[238] Choi, H; Shirley, H.J; Hume, P.A; Brimble, M.A., Furkert, D.P. *Angew. Chem. Int. Ed.* **2017,** *129(*26), 7528–7532.

[239] Tu, S., Zhang, C. *Org. Process Res. Dev.* **2015,** *19(*12), 2045–2049.

[240] Yang, Z.-F; Xu, C; Zheng, X., Zhang, X. *Chem. Commun.* **2020,** *56(*17), 2642–2645.

[241] Pinschmidt, R.K. *J. Polym. Sci. A* **2010,** *48(*11), 2257–2283.

[242] Destarac, M; Brochon, C; Catala, J.-M; Wilczewska, A., Zard, S.Z. *Macromol. Chem. Phys.* **2002,** *203(*16), 2281–2289.

[243] Chong, Y.K. et al. *Macromolecules* **2003,** *36(*7), 2256–2272.

[244] Moad, C.L; Moad, G; Rizzardo, E., Thang, S.H. *Macromolecules* **1996,** *29(*24), 7717–7726.

[245] Tilottama, B; Manojkumar, K; Haribabu, P.M., Vijayakrishna, K. *J. Macromol. Sci. A* **2022,** *59(*3), 180–201.

[246] van Nieuwenhove, I; Maji, S; Dash, M; van Vlierberghe, S; Hoogenboom, R., Dubruel, P. *Polym. Chem.* **2017,** *8(*16), 2433–2437.

[247] Pan, X; Guo, X; Choi, B; Feng, A; Wei, X., Thang, S.H. *Polym. Chem.* **2019,** *10(*16), 2083–2090.

[248] Lang, X; Patrick, A.D; Hammouda, B., Hore, M.J. *Polymer* **2018,** *145*, 137–147.

[249] Ohnsorg, M.L; Ting, J.M; Jones, S.D; Jung, S; Bates, F.S., Reineke, T.M. *Polym. Chem.* **2019,** *10(*25), 3469–3479.

[250] Xia, Y; Yin, X; Burke, N.A., Stöver, H.D. *Macromolecules* **2005,** *38(*14), 5937–5943.

[251] Xu, S; Trujillo, F.J; Xu, J; Boyer, C., Corrigan, N. *Macromol. Rapid Commun.* **2021,** *42(*18), 2100212.

[252] Schild, H.G., Tirrell, D.A. *J. Phys. Chem.* **1990,** *94(*10), 4352–4356.

[253] Gomes de Azevedo, R; Rebelo, L; Ramos, A.M; Szydlowski, J; Sousa, H.C. de, Klein, J. *Fluid Phase Equilib.* **2001,** *185*1-2, 189–198.

[254] Poschlad, K., Enders, S. *J. Chem. Thermodyn.* **2011,** *43(*3), 262–269.

[255] Rzaev, Z.M; Dinçer, S., Pişkin, E. *Prog. Polym. Sci.* **2007,** *32(*5), 534–595.

[256] Wu, C., Wang, X. *Phys. Rev. Lett.* **1998,** *80(*18), 4092–4094.

[257] Wu, C., Zhou, S. *Macromolecules* **1995,** *28(*24), 8381–8387.

[258] Kubota, K; Fujishige, S., Ando, I. *J. Phys. Chem.* **1990,** *94(*12), 5154–5158.

[259] Gorelov, A.V; Du Chesne, A., Dawson, K.A. *Physica A* **1997,** *240*3-4, 443–452.

[260] Ko, C.-H. et al. *Macromolecules* **2021,** *54(*1), 384–397.

[261] Zhang, G., Wu, C. *Phys. Rev. Lett.* **2001,** *86(*5), 822–825.

[262] Pang, J; YANG, H.U; Ma, J., Cheng, R. *J. Theor. Comput. Chem.* **2011,** *10(*03), 359–370.

[263] Tang, T. et al. *Macromol. Chem. Phys.* **2006,** *207(*19), 1718–1726.

[264] Kelarakis, A; Tang, T; Havredaki, V; Viras, K., Hamley, I.W. *J. Colloid Int. Sci.* **2008,** *320(*1), 70–73.

[265] Ko, C.-H. et al. *Macromolecules* **2021,** *54(*12), 5825–5837.

[266] Zhang, W; Zhou, X; Li, H; Fang, Y., Zhang, G. *Macromolecules* **2005,** *38(*3), 909–914.

[267] Kessel, S; Urbani, C.N., Monteiro, M.J. *Angew. Chem. Int. Ed.* **2011,** *50(*35), 8082–8085.

[268] Nuopponen, M; Ojala, J., Tenhu, H. *Polymer* **2004,** *45(*11), 3643–3650.

[269] Cao, M; Nie, H; Hou, Y; Han, G., Zhang, W. *Polym. Chem.* **2019,** *10(*3), 403–411.

[270] Laschewsky, A. et al. Stars and Blocks: Tailoring Polymeric Rheology Modifiers for Aqueous Media by Controlled Free Radical Polymerization. In: Patil, A., editor. Polymers for personal care and cosmetics: Based on an international symposium on "Polymers for Cosmetics and Personal Care" held at the 244th National ACS meeting in Philadelphia on August 22, 2012, vol. 1148. Washington, DC, Oxford: ACS American Chemical Soc; Oxford Univ. Press, 2013. pp. 125–143.

[271] Adelsberger, J. et al. *Macromolecules* **2010,** *43(*5), 2490–2501.

[272] Wei, H; Zhang, X.-Z; Zhou, Y; Cheng, S.-X., Zhuo, R.-X. *Biomaterials* **2006,** *27(*9), 2028–2034.

[273] Postma, A; Davis, T.P; Evans, R.A; Li, G; Moad, G., O'Shea, M.S. *Macromolecules* **2006,** *39(*16), 5293–5306.

[274] Lv, C; He, C., Pan, X. *Angew. Chem. Int. Ed.* **2018,** *130(*30), 9574–9577.

[275] Li, J. et al. *Polym. Chem.* **2020,** *11(*15), 2724–2731.

[276] Knebel, J; Karnbrock, W., Kerscher, V. Method for producing N-isopropyl(meth)acrylamideUS 9,512,062 B2, Dec. 6, 2016.

List of Publications

Papers

1. **Self-Assembled Micelles from Thermoresponsive Poly(methyl methacrylate)-*b*-poly(*N*-isopropylacrylamide) Diblock Copolymers in Aqueous Solution**

   Chia-Hsin Ko, Cristiane Henschel, Geethu P. Meledam, Martin A. Schroer, Peter Müller-Buschbaum, André Laschewsky, and Christine M. Papadakis

   Macromolecules **2021** *54* (1), 384-397

   DOI: 10.1021/acs.macromol.0c02189

2. **PMMA-*b*-PNIPAM Thin Films Display Cononsolvency-Driven Response in Mixed Water/Methanol Vapors**

   Christina Geiger, Julija Reitenbach, Lucas P. Kreuzer, Tobias Widmann, Peixi Wang, Robert Cubitt, Cristiane Henschel, André Laschewsky, Christine M. Papadakis, and Peter Müller-Buschbaum

   Macromolecules **2021** *54* (7), 3517-3530

   DOI: 10.1021/acs.macromol.1c00021

3. **Co-Nonsolvency Effect in Solutions of Poly(methyl methacrylate)-*b*-poly(*N*-isopropylacrylamide) Diblock Copolymers in Water/Methanol Mixtures**

   Chia-Hsin Ko, Cristiane Henschel, Geethu P. Meledam, Martin A. Schroer, Renjun Guo, Luka Gaetani, Peter Müller-Buschbaum, André Laschewsky, and Christine M. Papadakis

   Macromolecules **2021** *54* (12), 5825-5837

   DOI: 10.1021/acs.macromol.1c00512

4. **Ternary Nanoswitches Realized with Multiresponsive PMMA-*b*-PNIPMAM Films in Mixed Water/Acetone Vapor Atmospheres**

   Christina Geiger, Julija Reitenbach, Cristiane Henschel, Lucas P. Kreuzer, Tobias Widmann, Peixi Wang, Gaetano Mangiapia, Jean-François Moulin, Christine M. Papadakis, André Laschewsky, Peter Müller-Buschbaum

   Advanced Engineering Materials **2022** *23* (11), 2100191

   DOI: 10.1002/adem.202100191

5. **Poly(sulfobetaine)-Based Diblock Copolymer Thin Films in Water/Acetone Atmosphere: Modulation of Water Hydration and Co-nonsolvency-Triggered Film Contraction**

Peixi Wang, Christina Geiger, Lucas P. Kreuzer, Tobias Widmann, Julija Reitenbach, Suzhe Liang, Robert Cubitt, Cristiane Henschel, André Laschewsky, Christine M. Papadakis, and Peter Müller-Buschbaum

Langmuir **2022** *38* (22), 6934-6948

DOI: 10.1021/acs.langmuir.2c00451

Posters

1. **Thermoresponsive Block Copolymers from One-Pot Sequential RAFT Polymerizations and their Self-Assembly in Aqueous Solution**

Michelle Hechenbichler, Cristiane Henschel, Christoph Herfurth, André Laschewsky, Benjamin von Lospichl, Michael Gradzielski

14th European Detergents Conference (EDC), part of the SEPAWA Congress

Berlin (Germany), October 10th, 2018

Poster awarded with the Best Poster Prize

2. **Self-assembly and Co-nonsolvency of Hydrophobic / Thermoresponsive Block Copolymers**

Cristiane Henschel, Chia-Hsin Ko, André Laschewsky, Christine M. Papadakis

Macromolecular Colloquium Freiburg

Freiburg (Germany), February 20th, 2019

3. **Self-assembly and Co-nonsolvency of Hydrophobic / Thermoresponsive Block Copolymers**

Cristiane Henschel, Chia-Hsin Ko, André Laschewsky, Christine M. Papadakis

Institutsfest from the Institute of Chemistry at Universität Potsdam

Potsdam (Germany), June 12th, 2019

Poster awarded with the Best Poster Prize

4. **Self-assembly and Co-nonsolvency of Hydrophobic / Thermoresponsive Block Copolymers**

   Cristiane Henschel, Chia-Hsin Ko, André Laschewsky, Christine M. Papadakis

   Tag der Chemie, organized by NordostChemie, Freie Universität Berlin, Humboldt Universität zu Berlin, IGAFA, Technische Universität Berlin and Universität Potsdam

   Berlin (Germany), July 11th, 2019

5. **Self-assembly and Co-nonsolvency of Amphiphilic Thermoresponsive Block Copolymers**

   Cristiane Henschel, Chia-Hsin Ko, André Laschewsky, Christine M. Papadakis

   1st PhD and PostDoc Conference of ProMatLeben Polymere, by the Bundesministerium für Bildung und Forschung (BMBF)

   Berlin (Germany), August 3rd, 2019

6. **"Schizophrenic" Micellar Self-organization of Twofold Switchable Zwitterionic Block Copolymers**

   Cristiane Henschel, Viet Hildebrand, André Laschewsky, Noverra M. Nizardo, Peter Müller-Buschbaum, Christine M. Papadakis, Natalya S. Vishnevetskaya

   Polydays Conference 2019, from the Berlin-Brandenburg Association of Polymer Science, organized by the Institute of Biomaterial Science of the Helmholtz-Zentrum Geesthacht (HZG) and Humboldt Universität zu Berlin.

   Berlin (Germany), August 11th, 2019

7. **Self-assembly and Co-nonsolvency of Thermoresponsive Amphiphilic Diblock Copolymers**

   Cristiane Henschel, Chia-Hsin Ko, André Laschewsky, Christine M. Papadakis

   15th European Detergents Conference (EDC), part of the SEPAWA Congress

   Berlin (Germany), October 23rd, 2019

Statement of Originality

I hereby declare that this thesis is the product of my own work. It has not been previously submitted

to any other university and it has been prepared independently and exclusively with the specified

resources. All the assistance received in preparing this thesis and the sources used have been

acknowledged.

Potsdam, July 27th 2022

Cristiane Henschel

Acknowledgments

First and foremost, I would like to thank Prof. Dr. André Laschewsky, who from the very beginning of my PhD has been an example of immense knowledge and kind heart. Thank you for always looking out for us and making sure to pass on as much knowledge as possible, not only on polymer chemistry, but on topics ranging from the history of the German language to politics and football. I cannot put into words the admiration I have for you, and I will really miss our long conversations.

I would also like to acknowledge the remaining of the AKL team, especially Michelle Hechenbichler, for helping turn an engineer into a chemist, for improving my German, and for always being honest and open. This experience would not have been the same without you. My gratitude also goes to Dr. Dirk Schanzenbach, for all the assistance on new reactions, for the endless TGA and DSC measurements, and for all those "last measurements", that kept on coming. A thank you is also due to Alejandro Martinez Guajardo, for being a great office mate, and for letting me play my Spotify playlists on repeat in the lab all pandemic long. I must also acknowledge Alejandro, Kayly Madeline Rominger, Helena Fehrmann, Ekin Sehit and Dr. Dirk Schanzenbach for the PS and PMMA polymerizations performed for me. Finally, a thank you to Johannes Martin for the various MS measurements, and for being a great team member, even if officially was not part of the team.

My deepest appreciation also goes to Christoph Herfurth, who was always ready to save my day with a nice coffee, cookies, and some friendly words, share your knowledge, and give me some tips on how to tackle all those reactions that refused to work (and there were quite a few of those). Above all, knowing that a friend was just down the hall made the last 4 years extremely joyful.

I am also extremely grateful to Prof. Böker and all the remaining colleagues from the Fraunhofer IAP and from the Institute of Chemistry in the University of Potsdam, for allowing me to conduct my work at your facilities, and for making my time there so enjoyable. I would also like to acknowledge Sascha Prentzel for the numerous SEC measurements of my samples.

In addition, I must acknowledge the several people that have provided me with wonderful scientific exchanges and helped me grow during my PhD: Prof. Helmut Schlaad, Prof. Joachim Koetz,